Nanofilled Epoxy Adhesive for Structural Aeronautic Materials

Luigi Vertuccio

Unione Europea

UNIVERSITÀ DEGLI
STUDI DI SALERNO

FONDO SOCIALE EUROPEO

Programma Operativo Nazionale 2000/2006
"Ricerca Scientifica, Sviluppo Tecnologico, Alta Formazione"
Regioni dell'Obiettivo 1 – Misura III.4
"Formazione superiore ed universitaria"

Department of Industrial Engineering

Ph.D. Course in Industrial Engineering
(XV Cycle-New Series, XXIX Cycle)

Nanofilled Epoxy Adhesive for Structural Aeronautic Materials

Supervisor
Prof. Liberata Guadagno

Ph.D. student
Luigi Vertuccio

Scientific Referees
Prof. Maria Rossella Nobile
Ing.. Salvatore Russo (Leonardo-Finmeccanica)

Ph.D. Course Coordinator
Prof. Ernesto Reverchon

Year 2015/2016

Publication list related to the Ph.D. research activity

International research paper

1) U. Vietri, L. Guadagno, M. Raimondo, L. **Vertuccio**, K. Lafdi, Nanofilled epoxy adhesive for structural aeronautic materials, Composites Part B: Engineering 61 (2014) 73-83.
2) L. Guadagno, M. Raimondo, V. Vittoria, L. **Vertuccio**, C. Naddeo, S. Russo, B. De Vivo, P. Lamberti, G. Spinelli, V. Tucci, Development of epoxy mixtures for application in aeronautics and aerospace, RSC Advances 4 (2014) 15474-15488.
3) L. Guadagno, M. Raimondo, L. **Vertuccio**, M. Mauro, G. Guerra, K. Lafdi, B. De Vivo, P. Lamberti, G. Spinelli, V. Tucci, Optimization of graphene-based materials outperforming host epoxy matrices, RSC Advances 5 (2015) 36969-36978.
4) L. **Vertuccio**, S. Russo, M. Raimondo, K. Lafdi, L. Guadagno, Influence of carbon nanofillers on the curing kinetics of epoxy-amine resin, RSC Advances 5 (2015) 90437-90450.

International conferences

4th ICEAF International Conference of Engineering Against Failure 24-26 June 2015 Skiathos, Greece.
1) Effect of carbon nanotubes on adhesive properties of structural materials - U. Vietri, L. **Vertuccio**, M. Raimondo, S. Russo, L. Guadagno
2) Epoxy Mixture at Low Moisture Content for Aeronautic Application - L. **Vertuccio**, V. Vittoria, C. Naddeo, M. Raimondo, S. Russo, L. Guadagno.

International Patent:

EP 2873682 (A1) "Epoxy resin with low humidity content" European patent application, **May 2015**. Università di Salerno (L. Guadagno, M. Raimondo, V. Vittoria, L. **Vertuccio**, C. Naddeo, P. Lamberti , V. Tucci). Alenia Aeronautica S.p.A. (G. Iannuzzo, S. Russo)

Submitted paper

"**Influence of Carbon Nanoparticles/Epoxy Matrix interaction on Mechanical, Electrical and Transport Properties of Structural Advanced Materials**" L. Guadagno, C. Naddeo, M. Raimondo, G. Barra, L. **Vertuccio**, S. Russo, K. Lafdi, V. Tucci, G. Spinelli, P. Lamberti. (Nanotechnology) (**Accepted 10 January 2017**)

Ph.D. Schools Participation:

1st SUMMER SCHOOL- POLIGRID "Realizing the Full Value of Centralized and Distributed Energy Resources in Microgrids" Dipartimento di Ingegneria Industriale dell'Università di Salerno" July 14th – 18th 2014

GRICU PhD NATIONAL SCHOOL 2014 "Risk Analysis: Fundamentals and Applications" Ferrara Polo Tecnologico Università di Ferrara September 15th – 19th 2014

GRICU PhD NATIONAL SCHOOL 2015 "Biological and bioprocess engineering" University of Padova September 7th – 11th 2015

Participation to training course:

Training course about the preparation of international research projects (Horizon 2020). Teacher: Ing. Francesco Salvato, (Alenia Aermacchi). 13 and 20 March 2015 frontal lessons; June 22, 2015 discussion of the developed research proposal

Other publications during Ph.D. course

International research paper

1) G. Barra, F. De Nicola, B. De Vivo, L. Egiziano, L. Guadagno, P. Lamberti, M. Raimondo, G. Spinelli, V. Tucci, L. **Vertuccio**, U. Vietri, R. Volponi, Enhanced electrical properties of carbon fiber reinforced composites obtained by an effective infusion process, 2014 IEEE 9th Nanotechnology Materials and Devices Conference, NMDC 2014, 2014, pp. 88-91.
2) B. De Vivo, L. Guadagno, P. Lamberti, M. Raimondo, G. Spinelli, V. Tucci, L. **Vertuccio**, V. Vittoria, Temperature effects on the electrical properties of multiphase polymer composites, AIP Conference Proceedings, 2014, pp. 362-365.
3) B. De Vivo, P. Lamberti, G. Spinelli, V. Tucci, L. **Vertuccio**, V. Vittoria, Simulation and experimental characterization of polymer/carbon nanotubes composites for strain sensor applications, Journal of Applied Physics 116 (2014).
4) V. Romano, C. Naddeo, L. Guadagno, L. **Vertuccio**, Thermal conductivity of epoxy nanocomposites filled with MWCNT and hydrotalcite clay: A preliminary study, AIP Conference Proceedings, 2014, pp. 410-413.
5) L. Guadagno, M. Raimondo, U. Vietri, G. Barra, L. **Vertuccio**, R. Volponi, G. Cosentino, F. De Nicola, A. Grilli, P. Spena, Development of multifunctional carbon fiber reinforced composites (CFRCs) - Manufacturing process, AIP Conference Proceedings, 2014, pp. 461-464.
6) B. De Vivo, P. Lamberti, R. Raimo, V. Tucci, L. **Vertuccio**, L. Beneduce, Effects of thermo-electrical aging on the properties of epoxy-based nanocomposites for motor insulation, Proceedings - SDEMPED 2015: IEEE 10th International Symposium on Diagnostics for Electrical Machines, Power Electronics and Drives, 2015, pp. 226-231.
7) L. **Vertuccio**, V. Vittoria, L. Guadagno, F. De Santis, Strain and damage monitoring in carbon-nanotube-based composite under cyclic strain, Composites Part A: Applied Science and Manufacturing 71 (2015) 9-16.

8) L. Guadagno, M. Raimondo, U. Vietri, L. **Vertuccio**, G. Barra, B. De Vivo, P. Lamberti, G. Spinelli, V. Tucci, R. Volponi, G. Cosentino, F. De Nicola, Effective formulation and processing of nanofilled carbon fiber reinforced composites, RSC Advances 5 (2015) 6033-6042.
9) L. Guadagno, U. Vietri, M. Raimondo, L. **Vertuccio**, G. Barra, B. De Vivo, P. Lamberti, G. Spinelli, V. Tucci, F. De Nicola, R. Volponi, S. Russo, Correlation between electrical conductivity and manufacturing processes of nanofilled carbon fiber reinforced composites, Composites Part B: Engineering 80 (2015) 7-14.
10) V. Romano, C. Naddeo, L. Guadagno, L. **Vertuccio**, Thermal conductivity of epoxy resins filled with MWCNT and hydrotalcite clay: Experimental data and theoretical predictive modeling, Polymer Composites 36 (2015) 1118-1123.
11) L. Egiziano, P. Lamberti, G. Spinelli, V. Tucci, L. Guadagno, L. **Vertuccio**, Electrical properties of multiphase composites based on carbon nanotubes and an optimized clay content, AIP Conference Proceedings, 2016.
12) P. Lamberti, B. De Vivo, G. Spinelli, V. Tucci, L. Guadagno, M. Raimondo, L. **Vertuccio**, Analysis of the Effects of Hydrotalcite Inclusion on the Temperature-Sensing Properties of CNT-Epoxy Nanocomposites, IEEE Sensors Journal PP (2016).
13) P. Lamberti, G. Spinelli, V. Tucci, L. Guadagno, M. Raimondo, L. **Vertuccio**, Morphological and electrical properties of epoxy-based composites reinforced with exfoliated graphite, AIP Conference Proceedings, 2016.
14) P. Lamberti, G. Spinelli, V. Tucci, L. Guadagno, L. **Vertuccio**, S. Russo, Investigation on strain sensing properties of carbon-based nanocomposites for structural aircraft applications, AIP Conference Proceedings, 2016.
15) V. Romano, C. Naddeo, L. **Vertuccio**, K. Lafdi, L. Guadagno, Thermal investigation of tetrafunctional epoxy resin filled with different carbonaceous nanostructures, AIP Conference Proceedings, 2016.
16) G. Gorrasi, V. Bugatti, L. Tammaro, L. **Vertuccio**, G. Vigliotta, V. Vittoria, Active coating for storage of Mozzarella cheese packaged under thermal abuse, Food Control 64 (2016) 10-16.
17) G. Gorrasi, L. **Vertuccio**, Evaluation of zein/halloysite nano-containers as reservoirs of active molecules for packaging applications: Preparation and analysis of physical properties, Journal of Cereal Science 70 (2016) 66-71.
18) L. **Vertuccio**, L. Guadagno, G. Spinelli, P. Lamberti, V. Tucci, S. Russo, Piezoresistive properties of resin reinforced with carbon nanotubes for health-monitoring of aircraft primary structures, Composites Part B: Engineering 107 (2016) 192-202.

International conferences

AIP Conference Proceedings 7th International Conference on Times of Polymers (TOP) and Composites 2014; Ischia; Italy; 22 June 2014 through 26 June 2014;

1) Development of multifunctional carbon fiber reinforced composites (CFRCs) - Manufacturing process - Guadagno, L., Raimondo, M. , Vietri, U., Barra, G., **Vertuccio**, L., Volponi, R., Cosentino, G., De Nicola, F., Grilli, A., Spena, P. - Volume 1599, 2014, Pages 461-464
2) Temperature effects on the electrical properties of multiphase polymer composite-De Vivo B., Guadagno L., Lamberti P., Raimondo M., Spinelli G., Tucci V., **Vertuccio** L., Vittoria, V.- Volume 1599, 2014, Pages 362-365
3) Thermal conductivity of epoxy nanocomposites filled with MWCNT and hydrotalcite clay: A preliminary study. Romano V., Naddeo C., Guadagno L., **Vertuccio** L., Volume 1599, 2014, Pages 410-413

4th ICEAF International Conference of Engineering Against Failure 24-26 June 2015 Skiathos, Greece.

1) Incorporation of ZrO2 and CB4 fillers into epoxy resins for enhancing the hydrophobic behaviour - Valeria Bugatti, Luigi **Vertuccio**, Libero Sesti Osseo, Andrea Sorrentino, Salvatore Russo, Vittoria Vittoria, Liberata Guadagno.
2) Strain-dependent Electrical and Mechanical Properties of Carbon Nano Tubes-Loaded Epoxy Resin - B. De Vivo, P. Lamberti, R. Raimo, G. Spinelli, V. Tucci , L. **Vertuccio**
3) Thermal and Spectroscopic Characterization of Aeronautical Epoxy Composites filled with Carbonaceous Nanoparticles - M. Raimondo, L. Guadagno, C. Naddeo, L. **Vertuccio**, K. Lafdi

GM 2016 Graphene and related Materials: properties and applications - International Conference, **Paestum, Salerno (Italy) May 23-27, 2016**

Graphene-based multifunctional epoxy resin for high performance aeronautic structures. M. Raimondo, L. Guadagno, C. Naddeo, L. **Vertuccio**, L. Bonnaud, O. Murariu, Ph. Dubois.

International Conference "Times of Polymers e Composites from Aerospace to Nanotechnology 19-23 June 2016 Ischia, Italy.
1) Investigation on Strain Sensing Properties of Carbon-based Nanocomposites for Structural Aircraft Applications. P. Lamberti, G. Spinelli, V. Tucci, L. Guadagno, L. Vertuccio, S. Russo
2) Electrical Properties of Multiphase Composites based on Carbon Nanotubes and an Optimized Clay Content. L. Egiziano, P. Lamberti, G. Spinelli, V. Tucci, L. Guadagno, L. **Vertuccio**
3) Morphological and Electrical Properties of Epoxy-based Composites Reinforced with Exfoliated Graphite. P. Lamberti, G. Spinelli, V. Tucci, L. Guadagno, M. Raimondo, L. **Vertuccio**
4) Thermal Investigation of Tetrafunctional Epoxy Resin Filled with Different Carbonaceous Nanostructures. Vittorio Romano, Carlo Naddeo, Luigi **Vertuccio**, Khalid Lafdi, Liberata Guadagno

International Patent

EP2271706 B1 "Epoxy resin based composition and method for the curing thereof" –- 21-09-2016. Università di Salerno (V. Vittoria, L. Guadagno, A. Sorrentino, M. Raimondo, C. Naddeo, **L. Vertuccio**) G. Alenia Aeronautica S.p.A (G.Iannuzzo, S. Russo, E. Calvi.)

Italian Patent

Title : **Nuovo catalizzatore per reazioni di metatesi in ambienti ad elevata reattività**
Filing of patent: **14.09.2015** N.: **102015000051271**

Title : **Metodo di monitoraggio di un materiale composito**
Filing of patent: **27.04.2016** N.: **102016000042740**

Submitted paper

"**Experimental Evaluation and Modelling of Thermal Conductivity of Tetrafunctional Epoxy Resin Containing Different Carbon Nanostructures**" Vittorio Romano, Carlo Naddeo, Luigi **Vertuccio**, Khalid Lafdi, Liberata Guadagno

Index

Figures Index

Tables Index

Abstract

The focus of this study is to design new nano-modified epoxy adhesives using carbon nanofillers such as carbon nanotubes, carbon nanofibers and exfoliated graphite. Kinetic analysis, transport properties, dynamic mechanical properties and electrical properties have shown to be a powerful means for understanding molecular structure and phase composition of the formulated nanocomposites. Kinetic analysis, performed by using an advanced iso-conversional method and the Kamal's model-diffusion controlled respectively, has shown which, in epoxy resin, based on the tetrafunctional epoxy precursor N,N′-tetraglycidyl methylene dianiline-(TGMDA) hardened with 4,4-diaminodiphenyl sulfone (DDS), the introduction of the diluent decreases particularly the activation energy of secondary amine-epoxy reaction. The inclusion in the resin of one-dimensional fillers does not lead to big differences in the curing kinetics behaviour with respect to the raw epoxy. An increase in the activation energy is found in the case of highly exfoliated graphite. It is likely due to a reduction of free molecular segments of the epoxy network entrapped inside self-assembly structures. Transport properties have shown that, using a non-stoichiometric amount of hardener, the chemical structure of epoxy mixture exhibits unique properties concerning the water sorption for which the Equilibrium Concentration of Water is reduced up to a maximum of 30%. Dynamic mechanical analysis have shown that the nanoparticles are responsible of a more mobile phase, in the structure of the resin, determining an additional glass transition at lower temperature with respect to the main glass transition temperature. The fraction of the more mobile phase is strictly related to the amount and nature of the nanofiller and to the amount of the hardener, in fact, using a non-stoichiometric amount of hardener, also the electrical properties are improved further. The adhesive formulations based on epoxy/nanostructured carbon forms are used to obtain both adhesive and adherents to order to evaluate the adhesion properties with different joint configurations (tensile butt joint and single lap joint). The inclusion of carbon nanofillers inside the epoxy adhesive caused a significant

improvement in the bond strength of the joints, changing the failure mode of joints in single lap joint shear tests.
Finally, the conductive adhesive carbon nanotubes based, have been modified, by introduction of an elastomer, to order to obtain high performance in the configuration lap shear strength (LSS) with adherents in carbon fiber reinforced plastics (CFRP) used in aeronautic field. A correct combination of elastomer and carbon nanotubes, has allowed obtaining a conductive adhesive with high performance.

Chapter One

1. Topic and aim

This chapter underlines the reason why the necessity of the conductive adhesives in the structural aeronautic materials, are of critical importance. Moreover, the aims of the thesis and the research activities planned in order to reach the aims are described.

1.1 Topic

The adhesively bonded joints, in which an adhesive is placed between the surfaces of adherents and chemically cured, are increasingly being pursued as alternatives to mechanical joints in aerospace and other engineering applications and provide many advantages over conventional mechanical fasteners. The advantages are lower weight, lower fabrication cost, and improved damage tolerance(J.Bishopp, 2011). While electrically conductive adhesives (ECAs) also exist and are used in the electronics industry, conventional ECAs require 25–30% by volume (80% by weight) of conductive filler(S, 2011). Due to this high loading of filler, most commonly silver particles, only a small portion of the shear strength is retained and existing ECAs are not suitable for aerospace structural applications. As such, while structural adhesives are already common on aircraft, riveting is still the only current solution for electrical bonding. This technique is unfavourable due to the resulting corrosion risks and damage to carbon fiber reinforced plastics (CFRP), as well as the additional holes and the weight of the rivets. Development of conductive adhesives with good structural bonding capability is required in order to address these challenges and achieve both structural and electrical adhesive bonding of aircraft structures. In order to obtained this, many researchers has focused their research toward the development of new multifunctional adhesives for structural applications, based on appropriate epoxy resin nano-modified by carbon nano-forms, able to hinder the insulator properties of resin if employed beyond their Electrical Percolation Threshold (EPT)(Billias and Borders, 1984, Meguid and Sun, 2004b, Gkikas et al., 2012c, Vietri et al., 2014, Guadagno et al., 2015d, Jakubinek et al., 2015a). CNTs are known as materials with very remarkable electronic, thermal, optical, mechanical, spectroscopic and chemical properties, which have been attributed to the bonding structure of the CNTs(Yakobson and Avouris, 2001, Qian et al., 2002, Reich et al., 2008, Hollertz et al., 2011). The epoxy resins are reactive monomers, which are commonly cured with amine to form thermosetting polymers. If the epoxy is cured with an aromatic amine of sufficient functionality, the result is a highly cross-linked network with relatively high stiffness, glass transition temperature (T_g) and chemical resistance. Unfortunately, Epoxy resins are brittle materials that have fracture energies some two orders of magnitude lower than modern thermoplastics and other high performance materials(Rezaifard et al., 1993). In order to remain competitive as the materials of choice for many applications such as adhesives and composite matrices, the epoxies are modified to improve their fracture toughness. The techniques that allow the tailoring of the resin properties are in the forefront of scientific research. These techniques have the target in maximizing the dissipated energy through either the plastic deformation of the

matrix, e.g. the inclusion of elastomers which increase the resin toughness (Pearson and Yee, 1989), or the modification of the crack initiation and propagation process e.g. ceramic modified polymers that inhibit interlaminar crack propagation(Gkikas et al., 2012a). An additional problem is that the bonded structures are difficult and expensive to repair. (The adhesives used in the original construction are usually high-temperature-curing resins, room temperature curing adhesives are available, but they are not as strong as desired and they do not have a sufficiently high heat-distortion temperature to be used in critical applications on higher-performance aircraft. However, it is seldom possible to use high-temperature-curing adhesives in on-site repairs so the repair facility must either replace large sections of wing, fuselage, or engine structure or "make-do" with the low-performance, low-temperature-curing adhesives. Research and development should be undertaken to develop new adhesive systems able to overcome current limitations of aeronautic adhesive such as:

- Electrical insulating properties
- High Water sorption
- Debonding
- Poor mechanical properties and fatigue resistance
- Durability
- Flammability
- Processing temperature

1.2 Aims of this thesis

The aim of the research project is the development of new, conductive, structural high performance adhesives to be used for the bonding of structural parts. The attention will be mainly focused on adhesion between composites but metals and hybrid configurations will not be neglected. Specifically, epoxy based formulations will be loaded with nanostructured forms of carbon to impart specific properties able to simultaneously enhance functional and structural characteristics of aeronautic adhesives. The main functionalities which will be brought to the adhesive via the nanocomposite strategy are:

1. electrical conductivity (at least 10^{-2} S/m at low electrical percolation threshold - less than 2% by weight of conductive nanoparticles);
2. enhancement of the mechanical properties such as tensile strength, elastic modulus, toughness;
3. adhesion strength enhancement;
4. low water vapour sorption (lower equilibrium concentration of water);

5. chemical resistance
6. durability of adhesive in severe environmental condition

The main concept underpinning the research project is the exploitation of new nanofilled polymeric composites, integrating electrical conductivity properties with durable structural-mechanical functions (multifunctional materials) for the production of new high performance structural adhesives. The new products must be able to overcome the current limitations and specifically the difficulty of their application and their costs. In fact, currently the use of adhesive in aeronautic application, is limited due to doubts about their reliability of long-term bonding, which may deteriorate after been subjected to fatigue cycles or environmental aging (Relative humidity, UV radiation, thermal gradients, pollution). This has led to the introduction fail-secure devices that in many cases are very disadvantageous in terms of weight, application and costs. Other relevant aspects limiting the use of the adhesives are related to their processes under conditions of high temperature and pressure. Moreover, an assessment of the repeatability of the processes together with the refinement of non-destructive testing are fundamental needs for standard certification issues. The use of different types of adhesives (for example paste) that can polymerize also at lower temperatures (preferably at room temperature) while the structural characteristics are maintained, could decisively promote the spread up of the adhesively bonded structures. The introduction of conductive nanocharges in structural adhesive for composite and metal structures is a potential way to obtain multifunctional adhesives able to meet these requirements and to integrate simultaneously the structural mechanical functions with properties of electrical conductivity. It is worth noting that there are some specific functionalities on the nano-charges that can act as catalysts for the curing mechanisms, allowing high curing degree even at relatively low temperatures. In addition, the higher thermal conductivity, due to the presence of the nanocharges, also favours the efficiency of the curing process with the benefit of energy-saving. The appropriate selection and elaboration of the polymer matrix composition, the nanofiller type and the incorporation techniques will allow obtaining tailored multifunctional properties of the resulting nanocomposites which could not be achieved by conventional materials or composites. Therefore, in this proposal, multifunctional nano-structured polymeric composites will be developed on the basis of polymer matrices characterized by original formulations and the combined use of innovative nanofillers suitably incorporated within the matrices by optimized approaches. The possibility to manipulate the material structures at nano-scale allows, indeed, the realizations of new conductive systems able to overcome the previously described limitations. The development of the specific nanocomposite materials will be structured according to following main research activities:

1. Identification of the functional requirements
2. Formulation and fabrication of the adhesive nanocomposites
3. Characterizations of the structural and physical properties
4. Processing and demonstrator production; Adhesion tests, electrical continuity
5. Validation of results

1.2.1 Identification of the functional requirements

Based on the analysis of the state of the art, the specific functional requirements for the various nanocomposites will be fixed. Epoxy matrices with variable cross-link density and chain flexibility will be considered to extend the range of applicability of mechanical and thermal stresses. Hybrid nanocomposites incorporating appropriately elastomers and nano-structured forms of carbon (CNT, graphene) will be also developed.

1.2.2 Formulation and fabrication of the different nanocomposites

The epoxy matrix formulation will be the matrix to be loaded with the nanocharges. Further activities will be developed from a detailed analysis of oxidized and reduced graphene layers (GNP), CNT, CNF, to be used as nanofillers to impact electrical conductivity (with no additional weight and properties of the electrical continuity allowing the elimination of the inter-panel jumper cabling) and to improve the adhesion between the substrates. Nanostructured forms of carbon (CNFs, Graphene, and CNTs) will be loaded inside the epoxy matrix in order to have two main effects on the adhesion mechanisms:

1) Improvement of the interactions at the interface between the adhesive and the adherent.
2) Making of an appropriate conductive epoxy based matrix.

The addition of other nanoparticles, molecules and different hardeners (reactive diluents, elastomer) will be studied to improve other characteristic of the adhesives, such as the flame resistance, the viscosity at the application temperature, resistance to the moisture, cure temperature. The (eventual) synergic effect of these particles together with the nanostructured forms of carbon, on the mechanical properties, curing temperature and viscosity and process parameters will be evaluated.

1.2.3 Characterizations of the structural and physical properties

The planned activities include morphological and structural analysis aimed at studying the polymer-filler interactions using, SEM and TEM, FTIR and Raman spectroscopy, X-ray Diffraction (XRD) small angle X-Ray scattering (SAXS), and thermomechanical analysis. Thermo-mechanical characterizations will be carried out to determine the properties at different temperatures and to assess the viscoelastic behaviour in order to control the final properties of the adhesives. Nanofilled adhesive formulations will be studied at all hierarchical scales of organization, mastering the phenomena involved in phase transitions and structural development (e.g. solidification, vitrification, formation of nanostructured phases, gelation) as well as the interfacial interactions. A special effort will be devoted to the evaluation of the electrical transport. Thermomechanical behavior and its evolution with time will be considered as well as thermostability. Water sorption and durability will be also evaluated. Physical and chemical characteristics of epoxy resin are modified as a result of water absorption. The physical change arises mainly from the plasticization effect of absorbed water, with the direct result of decreased glass transition temperature. Water absorption may change the epoxy structures and thus impart adverse effects on properties like the mechanical properties of the material.

1.2.4 Processing and demonstrator production; Adhesion tests, electrical continuity

A test campaign allowing the characterization according to the aeronautic standard will be performed. Composite substrates on which the adhesive will be applied to evaluate the adhesion properties and electrical continuity will be specifically prepared. Composites components will undergo treatments to increase their surface roughness. The specimens will be prepared in sizes appropriate to perform the tests in accordance with international standards and regulation (ASTM).

1.2.5 Validation of the results

Validation of the nanofilled adhesive will be focused on the authentication of mechanical properties of both the adhesive and typical joints configurations used in aeronautics. Validation activities will be in compliance with the aerospace standards and airworthiness regulations.

Chapter Two

2. State of art

This chapter is going to give, on the one hand, a general overview on the world of adhesives, highlighting the drawbacks related to the adhesion in a joint, on the other hand, it describes how the use of nanoparticles, can overcome these drawbacks.

2.1 Introduction

Polymeric materials that fall within the classifications of thermoplastics, thermosetting resins, elastomeric compounds, and natural adhesives (animal glue, casein, starch, and resin) may serve adhesive functions. Polymeric adhesives may be used to join a large variety of material combinations: metal-metal, metal-plastic, metal-composite, composite-composite, plastic-plastic, metal-ceramic, and so on. The primary drawback is the service temperature limitation. Organic polymers maintain their mechanical integrity only at relatively low temperatures, and strength decreases rapidly with increasing temperature. Even though the inherent strength of the adhesive may be much less than that of the adhered materials, nevertheless, a strong joint may be produced if the adhesive layer is thin and continuous. If a good joint is formed, the adhered material may fracture or rupture before the adhesive. Polymers are attractive materials and usually offer the following advantages:

(a) weight,
(b) cost,
(c) moisture and chemical resistance,
(d) toughness,
(e) abrasive resistance,
(f) strength,
(g) appearence,
(h) insulation (both thermal and electrical),
(i) formability,
(j) machinability.

Polymeric materials, unlike metals, do not respond elastically to stress and undergo permanent deformation under sustained loading. The term viscoelastic describes the behaviour of plastics when subject to stress. After the application of an initial load, the polymeric structure will move in response to the applied stress. The stress-strain curve for plastics change with time. When compared with metals, polymeric materials lack stiffness and their physical properties are temperature-dependent. Service experience with adhesive bonded structures has been extremely varied, with some components providing excellent service and others failing or requiring extensive maintenance over a comparatively short service lifetime. The deficient adhesively bonded components have performed so badly when compared to conventionally fastened structures that they have been considered representative of the generic lack of reliability of bonded structures, leading to an overall poor acceptance of the technology. Adhesively bonded joints offer essential advantages in comparison with other joining methods, such as higher joint stiffness and superior fatigue performance (Flinn et al., 1989). For

this reason, the number of adhesive bonding applications in various industries is steadily growing. Typical examples of beneficial applications of the adhesive bonding technology are in the construction of aircraft, rail vehicles and in the automobile industry. Since the nature of the bonding is dependent on the atomic arrangement and chemical properties of the molecular conformation, chemical constitution and diffusivity of elements in each constituent, it follows that the interface between the different substrates has the specific properties. As a result of theoretical considerations and extensive practical testing, the following recommendations (Flinn et al., 1989) are made to achieve satisfactory joints: (a) *Suitable surface pretreatment*. Surface preparation is, perhaps, the most important process step governing the quality of an adhesive bond (Molitor et al., 2001); not only is a clean bond surface in the conventional sense required, but fresh cleaning to avoid adsorbed gases is often useful. Activated inert gases are sometimes used. (b) *Adhesive choice*. The adhesive should wet the adhered and solidify under production conditions of time, temperature, and pressure. Often the desired production conditions narrow the choice of adhesive. Some thermoplastic and thermosetting polymers are used as adhesives. Following forms of adhesives are available: liquids, pastes, and solids. (c) *Joint Design*. Adhesive joints are generally more resistant to shearing, compressive, and tensile stresses than they are to stress systems due to peeling. For example, it is easier to remove adhesive tape from a surface by peeling than by any other method of applying stress. (d) *Service condition*. Polymers as adhesives generally have higher thermal epansion (i.e., the coefficient of expansion) than metals and ceramics. Furthermore, their expansion coefficients are not truly constants; that is, the polymers expand markedly in a nonlinear way with temperature. Epoxy resins have coefficient of linear expansion values between 50×10^{-6} and 100×10^{-6} K^{-1} while polyester show values between 100×10^{-6} and 200×10^{-6} K (Baldan, 2004). Small compositional changes can have a marked influence on polymer expansion characteristics. If severe temperature changes are to be encountered, this effect and the required accommodations of the adhesive must be considered. Weathering and solvents that may be encountered in service are also important considerations.

2.2 Adhesives, adhesion theories and surface pre-treatment

An adhesive is defined as a polymeric substance with viscoelastic behaviour, capable of holding adherents together by surface attachment to produce a joint with a high shear strength. Some thermoplastic and thermosetting polymers are used as adhesives. They are tough, strong, and reliable, and can be applied almost any combination of materials. In thousands of years people have used natural adhesives (glues) made from animal sources. Many of the early natural

adhesives are still used. These include starch and protein-based formulations such as hydrolyzed collagen from animal hides, hooves, and bones and casein from milk. However, with advances in polymers in recent years, synthetic adhesives with superior characteristics have appeared. As new adhesive formulations based on synthetic polymers (often the same polymers used in other applications) continue to be developed, the range of applications for adhesives has expanded dramatically (see for example (Shields, 2013, Landrock and Ebnesajjad, 2008, Wake, 1987)). One important aspects of this rapidly growing field is that thermosets, thermoplastics, and elastomers have all found applications as adhesives, and so-called alloys have been developed in which more than one type of polymer is used. Adhesively bonded joints between various substrates have the following advantages (Strong, 2008, Brazel and Rosen, 2012, Niebel et al., 1989):

(a) the capability of joining dissimilar materials without regard to galvanic corrosion.
(b) Bonding very thin sections to heavy sections without distortion.
(c) Joining heat-sensitive alloys.
(d) Producing bonds with unbroken surfaces.
(e) Bonding small adherents. For example, it is hard to imagine welding abrasive grains to a paper backing to make sandpaper, or bolting the grains together to make a grinding wheel.
(f) Adhesive bonds have lower stress concentrations than mechanical joints; in the adhesive joining of large adherents, resulting in low stresses, and holes (necessary for riveting or bolting), which invariably act as stress concentrators in the adherents, are eliminated, thus lowering the possibility of adherent failure.
(g) In addition to joining, adhesives may also act as seals against the penetration of fluids. In the case of corrosive fluids, this, coupled with the absence of holes, where corrosion usually gains an initial foothold, can reduce corrosion problems.

Adhesive bonded joints weigh less than mechanically bonded joints; in terms of weight, it does not take much adhesive to join much larger adherents. As a result, it is not surprizing that many of the newer high-performance adhesives were originally developed for aerospace applications.

(a) Adhesive bonding has less sensitivity to cyclic loading.
(b) Adhesive bonds permit smooth external surfaces at the joint.
(c) Adhesive joining may offer economic advantages, often by reducing the hand labour necessary for other bonding techniques.

Surface preparation is, perhaps, the most important process step governing the quality of an adhesive bond. Structural adhesive bonding of joints is achieved either by mechanical interlocking of the polymer with the adherent surface or chemical bonding of the polymer molecules with the metal oxide (Molitor et al., 2001). To improve bond strength and durable adhesive joint between different substrates, surface preparation is a necessary pre-treatment prior to adhesive bonding. Certain bonding techniques provide adequate static strength, but have little durability when exposed to hot moisture environments, while others are susceptible to debonding in the presence of harsh environmental conditions, i.e., fuels, oils and cleaning solvents commonly encountered in industry such in aircraft application (Molitor et al., 2001). In addition, the nature of the surface treatment prior to bonding is found to be a major influence in the control of this effect (Brewis, 1992). Surface pre-treatment increases the bond strength by altering the substrate surface in a number of ways including (Molitor et al., 2001):

(a) increasing surface tension,
(b) increasing surface roughness
(c) changing surface chemistry.

By increasing surface roughness, an increase in surface area occurs which allows the adhesive to flow in and around the irregularities on the surface to form a mechanical bond (Molitor et al., 2001). Changing surface chemistry may result in the formation of a chemical bond e.g., between the polymer molecules in the polymer matrix composite and the metal oxide layer on the other adherent layer (Brockmann et al., 1986, Venables, 1984, Baldan, 2004, Molitor et al., 2001). As a result, the nature of the surface will also influence the stability of the joint. When exposed to hot/humid environmental conditions, a polymeric adhesive/ polymer interface is much more stable than the equivalent polymeric adhesive/metal interface. A well-chosen polymeric adhesive/polymer interface is unlikely to fail because of the environmental-induced stress due to the nature of the bond formed (Molitor et al., 2001). On the other hand, the durability of a polymeric adhesive/metal joint is not as stable. Early studies in the 1960s revealed that these joints did not perform well in hot/wet conditions with frequent occurrence of short-term interfacial bond failure. Hart-Smith (Baldan, 2004) has studied the interfaces in bonded, co-bonded, and co-cured composite structures using a peel-ply durability test coupon in order to assess durability of these materials. The composite structures fail during the service, even though they appeared to have been manufactured correctly, according to the short-term quality control coupons tested at the time of initial fabrication. The issue is not one of structural overloading. The interface between the adhesive and the composite surfaces simply disbonds without the trace of either material ever having adherent to

the other. What appears to be a common element in many of these problems is contamination introduced by the use of a “released” peel ply without subsequent thorough abrasion of the bonding surfaces. Another common but unrelated contributor to premature interfacial failures is some form of pre-bond moisture. Moisture can be present in an undried laminate cured long before it was bonded, as condensation on the surface of adhesive film not stored or thawed out properly, or absorbed within adhesive film, which had been left out too long in the lay-up room. Water absorbed by the nylon filaments before the original laminates are cured with the peel ply in place is also identified as a contributing problem. The cause of such weak bonds should be acknowledged as processing errors. This is that such weaknesses are invariably undetected by conventional non-destructive testing (NDT) techniques such as ultrasonic inspections, suggesting to some that the parts might not be detective after all. It took almost a decade to acknowledge the criticality of surface preparation for metal-bonded structures (Baldan, 2004).

2.3 Adhesives classification

In adhesive bonding, a non-metallic material (i.e., adhesive) is used to create a joint between two surfaces. The actual adhesives span a wide range of material types and forms, including (a) thermoplastic resins, (b) thermosetting resins, (c) artificial elastomers, and (d) even some ceramics. They can be applied as drops, beads, pellets, tapes, or coatings (films) and are available in the form of liquids, pastes, gels, and solids. The adhesive systems are classified on the following basis:

(a) organic chemistry,
(b) intended applications,
(c) high-temperature composites as adherents.

With such a range of possibilities, the selection of the best adhesive for the task at hand can often be quite challenging. Adhesive systems on the basis of organic chemistry are categorized into five different systems that accomplish the objectives (Brazel and Rosen, 2012):

(a) solvent-based adhesives,
(b) latex adhesives,
(c) pressure-sensitive adhesives,
(d) hot-melt,
(e) reactive adhesives.

Whereas intended applications range (DeGarmo et al., 1997) from
(a) load-bearing (structural adhesives)

(b) light-duty holding (non-structural or fixturing adhesives,
(c) sealing (the forming of liquid or gas-tight joints).

Commonly used structural (i.e., load-bearing) adhesives include (DeGarmo et al., 1997)

(a) epoxies,
(b) cyanoacrylates,
(c) anaerobics,
(d) acrylics,
(e) urethanes,
(f) silicones,
(g) high-temperature adhesives,
(h) hot melts.

For these materials, the bond can be stressed to a high percentage of its maximum load, for extended periods, without failure. Because of fatigue considerations, whenever possible, it is preferable to bond rather than mechanically fasten composite structures. For this reason, the increased usage of high-temperature resin-matrix systems for composite materials has necessitated the development of compatible and equally heat stable adhesive systems. Therefore, the adhesives used for bonding the composite materials can be classified as (Baldan, 2004):

(a) high-temperature epoxy,
(b) epoxy-phenolic,
(c) condensation-reaction polyimide,
(d) addition-reaction polyimide,
(e) bismaleimide adhesives (Politi, 1985, Baldan, 2004).

Epoxies are a broad family of polymer materials characterized by the presence of epoxy groups in their molecular structure. Although high-molecular-weight linear epoxies are often used as thermoplastics, they are most often used as thermosetting materials that cross-link to form a three-dimensional non-melting matrix. The thermosetting epoxies are the oldest, most common, and most diverse of the adhesive systems, and can be used to join most engineering materials, including metal, glass, composite, and ceramic. Just as epoxies are the most common matrix for advanced composites, epoxy adhesives are also the most common. Epoxy adhesives can be either one-stage (curing agent already mixed in) or two-stage where the user mixes in the curing agent just before use. The form of the one-stage material is most often a sheet, very much like a prepreg without the reinforcement, or in a paste. Both room temperature and elevated temperature curing systems are used, although many times the

room temperature curing adhesives require post-curing to develop good mechanical properties at elevated temperatures. Cure times can range from a few minutes for simple no critical parts to more than 12 h for large, critical-performance parts (Strong, 2008). All adhesives are sensitive to the surface conditions of the materials to be joined. However, epoxies are more sensitive than other adhesive materials in the case of metal. They have the following advantages:

(a) strong, versatile adhesives that can be designed to offer high adhesion,
(b) good tensile and shear strength,
(c) high rigidity,
(d) good chemical resistance,
(e) excellent bonding,
(f) good creep resistance,
(g) easy curing with little shrinkage
(h) good tolerance to elevated temperatures.

Various epoxies can be used (DeGarmo et al., 1997) over the temperature range −51 to 260◦C. After curing at room temperature, shear strengths can be (DeGarmo et al., 1997) as high as 35 to 70 MPa. The heat is used as the curing agent for single component epoxies. Majority of the epoxies, however, are two-component blends involving (a) a resin and (b) a curing agent, plus (c) possible additives such as accelerators, plasticizers, and fillers that serve to enhance cure rate, flexibility, peel resistance, impact resistance, or other characteristics. Heat may again be used to drive or accelerate the cure. Epoxy adhesives based on multifunctional resins (Baldan, 2004) are available which exhibit excellent strength retention at temperatures up to about 225◦C. Where long-term aging is required, epoxies are generally limited to applications requiring continuous service at temperatures no higher than 175◦C. The adherents involved are most commonly aluminium alloys and epoxy-matrix composite structures. However, these adhesives have the following disadvantages:

(a) the relatively low peel strength, and flexibility,
(b) the bond strength is sensitive to moisture and surface contamination,
(c) often brittle at low temperatures,
(d) the rate of curing is comparatively slow,
(e) relatively high resin cost.

Sufficient strength for structural applications is generally achieved in 8 to 10 h, with full strength often requiring 2 to 7 days (DeGarmo et al., 1997). The new epoxy adhesives developed for use on aerospace industry have excellent strength retention at temperatures up to 215◦C. Strength then drops (Baldan,

2004) rather sharply to 6.9 MPa at 260◦C. After 3000 h aging at 215◦C, the adhesive retains approximately 80% of its original lap shear strength (Baldan, 2004).

2.4 Bonding mechanisms in adhesively bonded joints

It is important to control the interfaces between the adhesive and substrates. To do so, it is necessary to understand all the different possible bonding mechanisms, one or more of which may be acting at any given instant. Despite the wide use of adhesives, a good deal of controversy surrounds the nature of the bond. There are following bonding mechanisms or types existing in the literature, which are particularly useful in explaining certain phenomena associated with adhesive bonding (Baldan, 2004, Flinn et al., 1989):

(a) physical bonding,
(b) chemical bonding,
(c) diffusion or inter-diffusion theory,
(d) mechanical bonding or mechanical interlock theory.

It is beneficial to summarize these bonding mechanisms because they indicate procedures commonly followed for optimal bonding.

2.4.1 Physical bonding

Physical bonding involves weak, secondary or van der Waals forces, dipolar interactions, hydrogen bonding and other low energy forces (Baldan, 2004). The bond energy in such physical bonding is approximately 8–16 kJ/mol (Baldan, 2004). Physical bonding contains the following bonding types:

(a) the absorption theory,
(b) the electrostatic attraction theory.

2.4.1.1 The absorption theory

This theory states that to be successful, an adhesive must wet the surface to be bonded (called the adherent). This theory has led to the development of materials with lower surface tension than that of the adherent (Flinn et al., 1989). Supporting this theory is the fact that epoxy wets steel and provides a

good bond, whereas it does not wet the olefins PE, PP, and PTFE and does not bond them.

2.4.1.2 The electrostatic attraction theory

This theory postulates that as a result of the interaction of the adhesive and the adherent, an electrostatically charged double layer of ions develops at the interface. In another words, forces of attraction occur between two surfaces when one surface carries a net positive charge and the other surface a net negative charge as in the case of acid-base interactions and ionic bonding (Baldan, 2004) (see Figure 2.1a). The fact that electrical discharges are observed when an adhesive is peeled from a substrate is cited as evidence of these attractive forces (Flinn et al., 1989). A difference in electrostatic charge between constituents at the interface may contribute to the force of attraction bonding. The strength of the interface will depend on the charge density. This attraction is unlikely to make a major contribution to the final bond strength of the interface. The bonding of this type will explain why silane finishes are especially effective for certain acidic or neutral reinforcements like glass, silica and alumina, but are less effective with alkaline surfaces like magnesium, asbestos and calcium carbonate (Baldan, 2004).

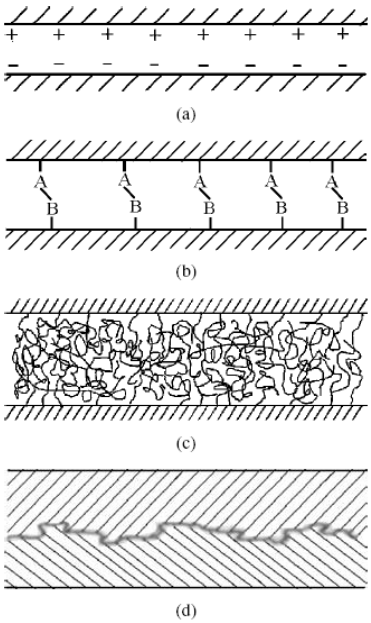

Figure 2. 1 *Types or mechanisms of bonding (Baldan, 2004): (a) Bond formed by electrostatic attraction, (b) Chemical bond formed between groups A on*

one surface and group B on the other surface, (c) bond formed by molecular entanglement following interdiffusion, and (d) mechanical bond formed when a liquid polymer wets a rough solid surface.

2.4.2 Chemical bonding

A chemical bond is formed between a chemical grouping on the adhesive surface and a compatible chemical group in the adherent (Figure 2.1b). The strength of the chemical bond depends on the number and type of bonds and interface failure must involve bond breakage. The processes of bond formation and breakage are in some form of thermally activated dynamic equilibrium (Baldan, 2004). The chemical bonding theory is the oldest and best known of all bonding theories. The nature of the chemical bonding is the key to the physical and chemical behaviour of matter. Atomic or molecular transport, by diffusional processes, is involved in chemical bonding. Solid solution and compound formation may occur at the interface, resulting a reaction zone with a certain thickness. This encompasses all types of covalent, ionic, and metallic bonding. Chemical bonding involves primary forces and the bond energy in the range of approximately 40–400 kJ/mol (Baldan, 2004). For example, a chemical reaction at the interface is of particular interest for polymer matrix composites because it offers the major explanation for the use of coupling agents on glass fibers and probably the surface oxidative treatments on carbon fibers for application with most thermoset and amorphous thermoplastic matrices. Surface treatments often involve chemicals, which produce surfaces with different chemical compositions and oxides. These morphological changes influence the nature of the chemical bonds. Subsequently, a relationship exists between chemical composition of the surface and the bond durability (Molitor and Young, 2002, Baldan, 2004).

2.4.3 Diffusion or inter-diffusion theory

This bonding mechanism is applicable to cases in which the adhesive contains a solvent for the adherent (Flinn et al., 1989). A type of bonding similar to diffusion bonding in metals develops, and molecules pass across the interface. This diffusion can obliterate the mechanical plane of the interface and its weakness. It is possible to form a bond between two polymer surfaces by the diffusion of the polymer molecules on one surface into the molecular network of the other surface, as illustrated schematically in Figure 2.1c. The bond strength will depend on the amount of molecular entanglement and the number of molecules involved. The phenomena of inter-diffusion has been called auto-adhesion in relation to adhesives. A bond between two surfaces may be formed by inter-diffusion of atoms or molecules across the surface. As an example, the bond strength in polymer matrix composites will depend on the

amount of molecular entanglement, the number of molecules involved and the strength of the bonding between molecules. Inter-diffusion may be promoted by the presence of solvents and the amount of diffusion will depend on the molecular conformation, constituents involved and the ease of molecular motion. For example, bonding between glass fibers and polymer resins through silane coupling agents by other than chemical bonding can be explained by inter-diffusion and interpenetrating network (IPN) formation at the interface region (Ishida, 1988, De Gennes, 1985, Baldan, 2004). The interface region thus formed has a substantial thickness, and its chemical, physical and mechanical properties are different from those of the bulk fiber and of the matrix (Tsai et al., 1990, Garton and Daly, 1985, Baldan, 2004). In metal matrix composites, inter-diffusion is also necessary for proper reaction between elements of each constituent to take place. However, inter-diffusion here may not always be beneficial because undesirable compounds are often formed, particularly when the oxide films present on the fibers are completely disrupted under extremely high temperature and pressure in a solid state process (Whatley and Wawner, 1985). To prevent or reduce the interaction it is necessary to apply an effective diffusion barrier in the form of a coating on the fiber. The selection of an appropriate diffusion barrier relies on a detailed knowledge of the nature of the interaction, which is specific to each other. It is generally agreed that the highest strength is achieved when, upon stressing, the fracture occurs in the body of the adherent or within the adhesive, not at the interface. The weak boundary layer theory holds that for an adhesive to perform satisfactorily, the weak boundary layer should be eliminated. For example, in case of metals with a scaly oxide layer, failure has a coherent oxide layer. Similarly, in the case of polyethylene, a weak, low-molecular-weight additive is present throughout the structure, and this leads to a weak interface. In both cases the potentially weak layers can be removed by surface treatments (Flinn et al., 1989).

2.4.4 Mechanical bonding or mechanical interlock theory

Some bonding may occur purely by the mechanical interlocking of two surfaces as illustrated in Figure 2.1d .This theory points out that surfaces on a micro scale are very rough (Flinn et al., 1989). Therefore, when a liquid adhesive is placed between two surfaces, it penetrates the crevices and pores and then solidifies. Thus, a cement interlocks with the surface layers on both sides and provides a mechanical bond. The fact that fresh, roughened surfaces provide the best bond support this theory. Simple mechanical keying or interlocking effects between two surfaces can lead to a considerable degree of bonding. In general, mechanical bonding is a low-energy bond vis a vis a chemical bond, i.e., the strength of a mechanical bonding is lower than that of

a chemical bond (Baldan, 2004). Pure mechanical bonding alone is not enough in most cases. However, mechanical interlock bonding could add, in the presence of reaction bonding, to the overall bonding. Mechanical bonds involve solely mechanical interlocking at the surface. The strength of this interface is unlikely to be very high in transverse tension, but the strength in shear may be significant dependent on the degree of roughness. However, mechanical bonding is efficient in load transfer when the applied force is parallel to the interface (Baldan, 2004). In addition to the simple geometrical aspects of mechanical bonding, there are many internal or residual stresses in composite materials, which develop during fabrication process due to matrix shrinkage and differential thermal expansion between fiber and matrix. Among these stresses, the residual clamping stress on the fiber provides a major bonding at the interface of many ceramic matrix composites, which plays a decisive role in controlling the fracture resistance of these materials. Roughness or an increase in the surface are results in increased mechanical interlocking of the adhesive to the adherent. It has been shown that as a result of the high stability of the fresh oxide layer to moisture degradation, good durable bonds can be achieved (Pilato and Michno, 1994).

2.5 Surface pre-treatments for polymers, polymer composites and metallic materials substrates

Good surface pre-treatment is achieved by one or a combination of the following (Schweizer and Curro, 1987): (a) the production of a surface free from contaminants, (b) the production of a macro/microscopically rough surface, (c) the production of a fresh stable oxide layer, and the chemical composition of the oxide. Surface treatments enable the nature of the chemical groups present at the surface to be modified and they may be used to modify the topography. Depending on the treatment used, the modification may be carried out without changing the bulk properties of the polymer. The alterations to the polymer may come under many different forms, as stated by Lennon *et al.* (Lennon et al., 1999):

(a) removal of the weak cohesion layer, or of the pollution present at the surface,
(b) introduction of new or an increased number of chemical functions,
(c) increase the roughness of the surface.

All these parameters can contribute to an improvement of the wet ability and/or of the adhesive properties of the surface. However, the efficiency of a surface treatment depends on the nature of the substrate and on the depth of treatment. There is often a compromise between the functionalization and the

degradation of the surface. There are many methods available to pre-treat polymers and metallic alloys substrates. These include both physical and chemical surface pre-treatments. With the former, material with low cohesive strength is removed and the topography may be changed. With chemical methods, a number of changes may occur, namely,

(a) removal of weak material,
(b) roughening,
(c) the introduction of functional groups into the polymer.

The methods used to pre-treat a polymer or metallic material surface are highly varied. More specifically, they can be (Lennon et al., 1999, Baldan, 2004):

(a) chemical or electrochemical,
(b) mechanical,
(c) thermal,
(d) photochemical,
(e) plasma.

Over the last 25 years, the possibility of using electrochemical methods to pre-treat polymers has been examined (Baldan, 2004). Many chemical treatments involve oxidative methods but reagents usually used with fully fluorinated polymers e.g., sodium in liquid ammonia, are powerful reducing agents. It is possible to provide both powerful reducing and oxidising conditions using electrochemical methods. In previous article, (Baldan, 2004) it was discussed the pre-treatments of polymers. In general, the methods that have been shown to be effective with plastics are considerably different from those that are effective with elastomers (Table 2.1). Typical composite surface treatments include traditional abrasion/solvent cleaning techniques for thermoset composites, while thermoplastic composites require surface chemistry and surface topographical changes to ensure strong and durable bond strengths. However, to increase strength and durability a more intimate bond is necessary; to achieve this the following conditions should be met (Baldan, 2004):

(a) increasing surface tension,
(b) increasing surface roughness,
(c) changing the surface chemistry.

Clearly, not all the methods listed for plastics, or elastomers, are effective with all plastics or all elastomers. For example, physical methods such as abrasion are not effective with polyethylene (PE). It is normally necessary to

chemically modify PE to achieve good adhesion, for example with a corona discharge. A key difference between plastics and elastomers is that the latter generally contain large quantities of cohesively weak additives.

Table 2. 1 *Examples of surface pre-treatments for plastics or elastomers substrates (Baldan, 2004)*

Plastics	Elastomers
Abrasion	Abrasion
Solvent cleaning	Solvent cleaning
Corona[a]	Conc. sulphuric acid[a]
Flame[a]	Trichloroisocyanuric acid[a]
Plasma[a]	Halogen gases[a]
Active gases[a]	
Specific reagents[a]	

[a]Expected to cause chemical modifications to substrate surfaces.

These are often present, in substantial quantities, on the surface and if they can not be absorbed by the adhesive used, poor bond strengths will result. For those elastomers, which contain a substantial quantity of functional groups, e.g., nitrile rubber, a physical method that removes any weak layers may be sufficient to provide good adhesion. However, with elastomers, which possess few functional groups, it may be necessary to remove any weak layers and chemically modify the elastomers. It may not be necessary to remove the weak layer if this is chemically modified to make it compatible with the adhesive used so that the layer can be absorbed. Selection of surface pre-treatments for polymers depends on several factors (Baldan, 2004) including:

(a) cost,
(b) safety,
(c) environmental impact,
(d) effectiveness,
(e) stability of the treated surface in service.

In some cases it will be necessary to pre-treat 3 dimensional objects while in other cases it may be required that one side of a sheet is treated. A variety of surface pre-treatments have been used with various degrees of success to increase surface tension, increase surface roughness, change surface chemistry, and thereby increase bond strength and durability of polymer composite adhesive joints and are shown (Molitor et al., 2001) in Table 2.2.

Table 2. 2 *Showing the effects of various surface pre-treatments methods on the surface tension, surface roughness, surface chemistry, bond strength and durability of the polymer composites (Molitor et al., 2001)*

Treatment type	Material	Nature of treatment	Surface tension	Surface roughness	Surface chemistry	Bond strength	Durability
(1) Abrasion and solvent wipe	Thermoset and thermoplastic	Remove mold release		Y		Increased found for thermosets	Good for thermosets
(2) Grit blasting	Thermoset and thermoplastic	Remove mold release		Y		Increased found for thermosets	Good for thermosets
(3) Acid etch	Thermoset and thermoplastic	Etch[a]	Y		Y	Slight increase	Poor
(4) Peel-ply	Thermoset	Remove mold release		Y		Increase	Good
(5) Tear-ply	Thermoset	Remove mold release				Increase	Good
(6) Corona discharge	Thermoplastic	Oxidising	Y		Y	Double	Good (90 days)
(7) Plasma treatment	Thermoplastic	Ablation and/or oxidation[a]	Y	Y	Y	Increase	Good (90 days)
(8) Flame treatment	Thermoplastic	Oxidasing[a]	Y			Increase	
(9) Laser treatment	Thermoset and thermoplastic	Ablation and or oxidation		Y	Y	Increase	More research is necessary

[a]Depends on polymer matrix material.

Wetting of the adherents by the adhesive is critical for the formation of secondary bonds in the absorption theory (Baldan, 2004). It has been theoretically verified that for complete wetting (i.e., for a contact angle θ equal to zero) the surface energy of the adhesive must be lower than the surface energy of the adherent (Gutowski et al., 1986). For thermoplastic composites, the primary aim of the surface treatment is to increase the surface energy of the adherent as much as possible. Surface treatments (Molitor et al., 2001):

(a) decrease water contact angle,
(b) increase surface tension,
(c) increase bond strength.

The researchers (Sancaktar, 1995, Harper-Tervet and Neff, 1983, Davies et al., 1997, Arnold et al., 1997, Critchlow and Brewis, 1995, Baldan, 2004) have used many different titanium alloys as substrates in the past; however Ti-6V-4Al is the most widely used one in the aerospace industry (Molitor et al., 2001). Durability studies of T-6Al-4V reveal that surface preparations that produce no roughness (macro or micro) yield the poorest bond durability. Those that produce significant macro-roughness but little micro-roughness yield moderate to good durability. Finally, those that produce significant micro-roughness yield the best durability (Table 2.3A). Table 2.3B gives the six surface pre-treatment procedures and their effects for titanium alloys. The surface pre-treatments used for polymeric and metallic materials are highly varied (see for example Tables 2.2 and 2.3), and can be conveniently classified

(see for example (Broad et al., 1999, Lennon et al., 1999, Molitor and Young, 2002, Harris and Beevers, 1999, Baldan, 2004, Molitor et al., 2001) into:

(a) mechanical,
(b) chemical,
(c) electrochemical,
(d) thermal,
(e) photochemical,
(f) plasma.

The followings are surface pre-treatment methods used for polymeric materials:

(a) abrasion/solvent cleaning,
(b) grit blasting,
(c) peel-ply (or tear films),
(d) tear-ply,
(e) acid etching,
(f) corona discharge treatment,
(g) plasma treatment,
(h) flame treatment,
(i) laser treatment,
(j) silver electrolytic pre-treatment process.

Whereas for metallic materials such as titanium alloys the following methods are used to surface pre-treat them:

(a) Abrasion and grit blasting,
(b) VAST (Vought Abrasive Surface Treatment),
(c) Acid etchants,
(d) Alkaline peroxide etch,
(e) Phosphate fluoride process,
(f) Modified phosphotate fluoride process,
(g) TURCO 5578, (viii) DAPCOtreat,
(h) Pasajell 107 Treatment,
(i) Electrochemical reactions,
(j) Chromic acid anodization,
(k) Sodium hydroxide anodisation,
(l) Catodically deposited aluminum oxide,
(m) Plasma Treatment,
(n) Sol/Gel Methods,
(o) Primers,
(p) γ -APS,

(q) Laser.

Table 2. 3 *A) Showing the effects of various surface pretreatment methods on the surface roughness, oxide layer, bond strength, and durability of titanium alloys (Molitor et al., 2001); B) Showing the procedures applied and their surface modification effects of selected surface pre-treatment methods for titanium alloys substrates (Molitor and Young, 2002)*

Treatment type	Alloy	Nature of treatment	Surface roughness	Oxide layer (nm)	Bond strength	Durability
Abrasion and solvent wipe	Ti-6Al-4V	Remove mold release	Macro		Poor	Poor
Grit blasting	Ti-6Al-4V	Remove mold release	Macro		Increase	Adequate
VAST	Ti-6Al-4V	Remove mold release	Macro		Good	Poor
Acid etch	Ti-6Al-4V	Etch	Micro		Adequate poor	Poor
Alkaline etch	Ti-6Al-4V	Etch	Micro	60–200	Good	Good
Phosphate-fluoride	T-6Al-4V	Etch	None	20	Adequate	Poor
Modified phosphate-fluoride	Ti-6Al-4V	Etchant and oxidation	None	8	Adequate	Better than phosphate-fluoride
TURCO	Ti-6Al-4V	Oxidising	Macro	17.5	Adequate	Adequate
DAPCOtreat	Ti-6Al-4V		Macro	6	Increase	Good
Pasajell	Ti-6Al-4V	Oxidising	Macro	10–20	Adequate	Adequate
Chromic acid anodisation	Ti-6Al-4V	Oxidising	Micro	40–140	High	Excellent
NaOH anodisation	Ti-6Al-4V	Oxidising	Micro	80–90	High	Excellent
Cathodically deposited Al_2O_3		Oxidising			Adequate	Adequate
Plasma spray	Ti-6Al-4V	Ablation and oxidation	Micro	130	High	Excellent
Sol gel	Ti-6Al-4V	Coupling and oxidation			High	Good
Laser treatment	Ti-6Al-4V	Ablation and oxidation	Macro		High	Poor

A

Surface treatment	Procedure	Surface effect
Surface modification by excimer laser	Produced using a wavelength of 308 nm wit XeCl. The focal length was 100 mm and the fluence produced was 77 J/cm^2.	Riblets or wavelike structures were produced on the surface which were approximately 40 μm deep with 100 μm period
Surface cleaning by excimer laser	Produced using a wavelength of 308 nm with XeCl. The focal lenght was 150 mm and the fluence produced was 2.8 J/cm^2.	A homogenised area of ~4 mm^2 was produced. Each irradiated zone was overlapped in both x and y directions.
Plasma spray	The titanium specimens were heated to 100°C in an oven to remove moisture, grit blasted with 180/220 Al_2O_3 grit, rinsed with a cleaner and subsequently dried. Plasma spraying was applied by spraying Hamdry 6506. TiO_2 powder.	A TiO_2 coating of thickness 50 μm was producded.
Pasa Jell 107	Pasa Jell 107 was applied to grit blasted samples. It was applied for 12–15 min. After which it was rinsided with deionised water at room temperature. The specimens were subsequently dried and sprayed with a thin layer of the primer Redux 101 using a De Vilbiss suction feed cup spray gun, type JGA.	Etched the existing oxide film
Sodium hydroxide anodisation	Performed as described by Ingram and Ramani [149]. The samples were degreased in methylthylketone (MEK) for 10 min, pickled by in 15% volume of 70% nitric acid, 3% by volume of 50% hydrofluoric acid at room temperature for 30 s. They were subsequently rinsed in 2 baths of agitated deionised water for 5 min. Anodisation was performed in a 5 M NaOH electrolyte at 10 V for 20–30 min. Upon removal from the solution, the samples were rinsed for 5 min in running water. The samples were allowed to dry and sprayed with a thin layer of the primer Redux 101 using a spray gun.	Cleaned and created a fresh oxide film
Chromic acid anodisation	Performed as described by Arnold *et al.* [150]. The samples were degreased in MEK for 10 min, pickled in 15% by volume of 70% nitric acid, 3% by volume of 50% hydrofluoric acid at RT for 30 s. They were subsequently rinsed in 2 baths of agitated deionised water for 5 min. Anodisation was performed in an electrolyte containing 5% CrO_3 and 0.1% NH_4HF_2 at RT. The voltage was applied after the specimens were immersed in the solution and increased from 2 to 10 V at a rate of 2 V/min. The voltage held constant for 20 min. Upon removal from the solution, the samples were rinsed in the agitated deionised water and subsequently rinsed for for 5 min in running water. The samples were allowed to dry and sprayed with a thin layer of the primer Redux 101 using a spray gun.	Cleaned and created a fresh oxide

B

The various surface pre-treatment methods used for polymeric materials and titanium alloys, and the qualitative descriptions of their effects on the surface tension, surface roughness, bonding strengths and durability of the these materials are presented (Molitor et al., 2001) in Tables 2.2 and 2.3. Both thermoset and thermoplastic composite materials have been bonded to titanium with varying degrees of success (Baldan, 2004). However, it is noted that thermoplastic materials are inherently more difficult to bond (Baldan, 2004). Carbon-fiber-reinforced polymer composite material has been widely used as the adherent in the past (Baldan, 2004). Although glass-fiber-reinforced composite material has a much lower modulus than carbon fiber, bond integrity tends to be dominated by the characteristics of the matrix, rather than the fiber and for this reason the research conducted on fiber composite is also relevant to studies involving glass-fiber (Molitor et al., 2001). Thermoset polyester or epoxy composites can have a resin-rich surface layer, which can cause particular problems in bonding (Molitor et al., 2001). The reason for this is that most of them contains a gel coat at the surface, or if the latter has not been deliberately created, the surface layer usually contains a higher proportion of resin as opposed to the interior. Both the gel coat and the resin-rich surface layer are very brittle and can subsequently fail catastrophically when overload. Highly compliant adhesives are a particularly good choice, as they spread the applied load over a large area and hence reduce the stress borne by the surface of the composite.

2.6 Factors affecting the durability of adhesively bonded joints

The formation of a suitable surface chemistry is the most important step in the surface preparation process because the integrity of this surface directly influences the durability of the adhesive bond (Baldan, 2004). To study the ability of surface pre-treatments to promote adhesion and to protect the surface against corrosion, it is usually necessary to run accelerated aging test to differentiate the surface treatment quality. Aging tests run under normal conditions of temperature and humidity after the curing of the adhesive may not provide results allowing a clear ranking of different surface pre-treatments adhesion promoter, and anti-corrosion protector abilities. To do so, adhesively bonded samples have to be exposed to severe conditions of temperature and humidity. As pointed out by Lapique and Redford (Lapique and Redford, 2002), when aging tests are run to evaluate the quality of surface pre-treatments, changes in the mechanical properties of the adhesive should also be taken into account. They may affect the stress transfer from the adhesive layer to the interface and modify the results of the mechanical testing. In order to analyze correctly such experiments, the behaviour of the adhesive should be studied under aging test conditions. Lapique and Redford (Lapique and

Redford, 2002) have recently studied such an aging test (40°C in water vapour) on the Araldite 2014 epoxy adhesive samples and the adhesive properties recorded over a period of 36 days. Araldite 2014 is an adhesive paste that can be cured at room temperature. This can be important in commercial applications where the substrates to be joint do not tolerate high temperature. As seen in Fig. 2.2, the measurement of the weight of the samples shows a weight increase due to an increasing water content in the epoxy with the exposure time. The weight increases with the square root of time in agreement with the standard Fickian diffusion. According to Figure 2.2 the water diffusion continues even after 36 days and no equilibrium state is reached during that period of time. Water works usually as plasticizer leading to a softening of the material. This is also the case for the epoxy adhesive Araldite 2014. Figure 2.3 shows how the mechanical properties (stress at break, E-modulus) and deformation at break) are affected by the exposure time and thus by water content. As Lapique and Redford (Lapique and Redford, 2002) concluded, the E-modulus and the stress at break are lowered while the deformation at break and the plastic contribution to the total deformation are increased with increasing aging time. Some form of substrate pre-treatment is always necessary to achieve a satisfactory level of bond strength. In order to obtain a strong and stable bond between a substrate (such as a metal) and the adhesive, the naturally formed surface oxide on metal has to be removed and replaced with a new, continuous, solid and corrosion resistant oxide layer during such a surface pre-treatment process. Almost all treatment methods do bring some degree of change in surface roughness but grit-blasting is usually considered as one of the most effective methods to control the desired level of surface roughness and joint strength (Shahid and Hashim, 2002). Grit-blasting does not only remove weak boundary layers but can also alter the chemical characteristics of the adherents (Harris and Beevers, 1998).

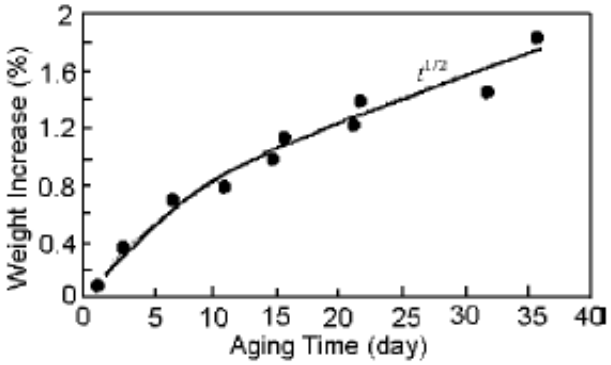

Figure 2. 2 *Weight increase versus aging time during aging test for samples with a thickness of 1.5 mm. The weight increase follows a* $t^{1/2}$ *law (Lapique and Redford, 2002).*

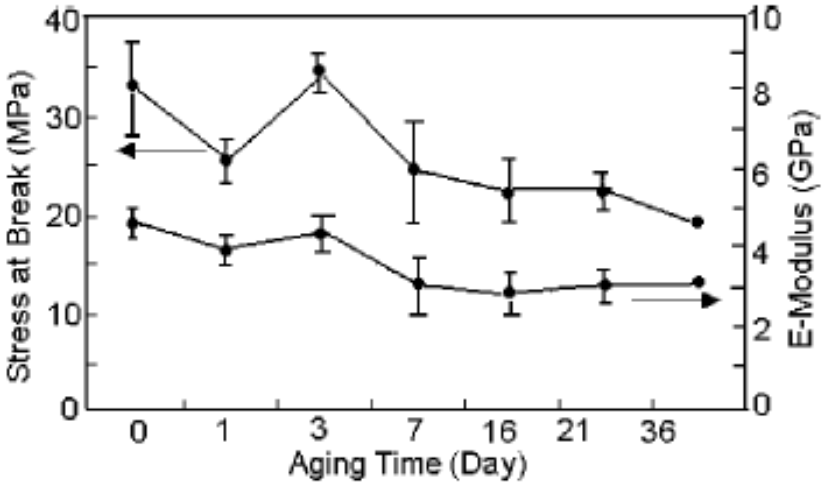

Figure 2. 3 *Mechanical properties (i.e., stress at break, E-modulus) during aging test measured in tension. Each point is the average of measurements performed on five samples (Lapique and Redford, 2002).*

Surface contamination is a widespread problem in the adhesive bonding of some parts such as micro-assemblies, and therefore calls for a convenient method to assess the cleanliness of the adherents before introducing the adhesive to the microsystem. As pointed out by Woerdeman *et al.* (Woerdeman et al., 2002), surface cleaning or preparation by means of solvents is the most common process step in many electronic manufacturing operations. Understanding the link between surface preparation and adhesion can lead to a reduction in the time required for development and testing of cleaning procedures. It can also lead to improved bond lines and enhanced manufacturability, enabling product realization for encapsulated components (Woerdeman et al., 2002). Molecular modelling has been employed to elucidate the behaviour of a low molecular weight contaminant near an interface between a polymer adhesive and a substrate (see for example references (Shanahan, 2000, Emerson et al., 2000, Fink and McCullough, 1999, CURRO, 1997, Curro and Schweizer, 1987, Schweizer and Curro, 1987). Depending on the substrate polymer and polymer-polymer interactions, as well as the molecular architecture of the contaminant and polymer, the contaminant can preferentially diffuse toward the interface (Fink and McCullough, 1999). When this happens, the contaminant molecules will displace the polymer from the interface, as illustrated in Figure 2.4, resulting in a degradation of the adhesive bond strength (Emerson et al., 2000). Another molecular modelling has also been undertaken by Shanahan (Shanahan, 2000) to examine the role of diffusion in the wetting of a contaminated surface.

Results of modeling indicate that a thin layer of a second liquid present on the substrate (the contaminant) can penetrate the sessile drop of liquid deposited on the solid surface and gradually change the effective interfacial free energy between the substrate and the drop (Shanahan, 2000).

Figure 2. 4 *Schematic of a polymer adhesive/substrate interface in the absence (left) and presence (right) of surface contamination. In the latter case, the contaminant molecules can displace the polymer from the interface resulting in a degradation of the adhesive bond strength (Woerdeman et al., 2002).*

In previous works (Baldan, 2004) the surface assessment in bonded, co-bonded, and co-cured composite structures was investigated. As underlined in previous sections, the contamination prior to bonding is not merely an issue of cleanliness, but one of the reactivity and surface energy, which relates to the wettability. Mahoney (Mahoney, 1988) has studied this problem. Surface contamination may cause insufficient wetting by the adhesive in the liquid state for the creating of a durable bond (Baldan, 2004). However, these contaminants are not the only cause of such a condition. For example, composite laminates cured against an inert (inactive) surface are far harder for adhesives to wet than are the underlying surfaces exposed by abrasion. The nature of the adhesive also has an effect on the bond strength. It was observed that a composite peel-ply surface, to which one epoxy film adhesive does appear to bond securely if cured at 177◦C, is not even wet by a room-temperature curing paste adhesive (Baldan, 2004). One reason for this is that the hot-bond adhesive becomes fluid during cure, while the paste adhesive maintains a high viscosity. The paste adhesive, when it is separated prematurely under a shear load, was embossed by a perfect replicate of every filament in the peel ply surface to which it had refused to bond. The hot bonded structures, on the other hand, had been used without failure for years. Studying the wettability problem, it is necessary that the surface tension of the liquid adhesive should be lower than the critical surface tension of the adherent (Baldan, 2004). A four fold reduction in the adhesive energy (work of adhesion) of carbon-epoxy laminates due to the presence of water, has been

found, explaining thereby why it is then so much more difficult for adhesives to bond than when everything is dry. The reliable surface pre-treatment is abrasion of the CFRP composite surface by some means of sanding or (fine grit) blasting (Baldan, 2004); this was recognized as long ago as 1976 (Crane et al., 1976).

2.7 Adhesive bonding of aircraft structure

Short details (Higgins, 2000) of the historical use of adhesive bonding on commercial aircraft and how the adhesive materials developed are given. Adhesive bonding of aircraft primary structures has been in use for over 50 years and is still in use on current aircraft projects as a direct alternative to riveting. Bonding of stringers to skins for both fuselage and wing construction and of metallic honeycomb to skins for elevators, ailerons, tabs and spoilers are the main uses for adhesives. The adhesive materials used for these purposes fall into three distinct groups. These are:

(a) Metal/metal - Hot cure
(b) Metal/metal honeycomb - Hot cure
(c) Metal to metal - cold cure

2.7.1 Metal/metal - hot cure

The hot cure adhesive materials used by the aircraft industry are mainly based on either phenolic or epoxy resin systems. Phenolic-based hot-bonded systems cure by condensation reactions, which means that water vapour is generated during the cure. To prevent the bond line being pushed apart by the vapour release, high pressures need to be applied across the joint during the reaction period. This in turn effectively limits the bond widths to approximately 300 mm if optimum glue line thickness is to be achieved.

2.7.2 Metal/metal honeycomb bonds - hot cure

Only epoxy systems are used for these applications. Epoxy adhesives form very mobile liquids as they reach the cure temperature and would run out of joints in metal to metal bonding situations if they do not contain flow modifying additives or scrim. If run out occurs, voids will be present in the glue line. This mobility is an asset in metal-to-metal honeycomb bonding since the flow and reticulation characteristics cause the adhesive to pull back from the honeycomb cell centres and form a massive fillet at the cell wall to skin interface giving a stronger bond. Since epoxy resin is required anyway for the metal to metal bonding of flange edges on these constructions, the

convenience of having to use only one type of adhesive for bonding the entire structure makes it the popular choice for such parts.

2.7.3 Structural metal to metal - cold cure

There are numerous two-part curing epoxy systems available. The Araldite series being particularly well known. They are cured by catalytic reaction when the base resin and the catalyst are mixed together. At room temperature, these adhesives require over seven days to reach full cure but both reach 90% of full cure strength within 48 h. Full cure can also be achieved by heating the bonded structure at 60-70°C for 4 h. The most important category of structural adhesives is that of the metal to metal hot cure types and a comparison of their room temperature mechanical properties are shown in Table 2.4.

Table 2. 4 *Comparison of room temperature mechanical properties. Metal-to metal bonding of the main hot cure adhesives (National specifications covering these adhesives are: DTD 5577 (UK), MMM-A-132A & MIL-A-25463 (USA). Typical room temperature values for cold cure epoxy adhesives are: Lap shear 27-35 MPa and Peel 130N/25.4 mm.)*

Adhesive	Lap shear strength (MPa)	Peel strength (N/25.4 mm)
Redux 775	27–35	180–270
Redux 308A/NA	40–45	200–310
FM73	35–40	245–350
AF163-2	35–40	245–330
EA 9330.1	27–35	120–155
SW 9323B/A150	27–35	120–155

Table 2. 5 *Comparison of strength at service temperatures*

Adhesive	Lap shear	(MPa min) at
	(− 55°C)	(+ 80°C)
Redux Film 775	20	10
FM47	20	9
AF31	16	14
Redux308A/NA	30	25
FM73	30	25
AF163-2	30	25
EA9330.1	12	6
SW9323B/A-150	12	16

Subsonic aircraft are designed to perform within a temperature range of 80 - 55°C and the properties of the adhesives at these temperatures have to be considered by designers. Typically, the lap shear strength of the adhesives at these extremes of operating temperature are shown in Table 2.5. Faced with these figures it is tempting to conclude that the epoxy systems are superior to the phenolic systems. However, structural engineers considering adhesive bonding for primary structures need also to concern themselves with the durability of the bonded joints in service, the effects of fluids contacted in service (i.e. water, fuel, oil, Skydrol, de-icing fluids, etc.) as well as the effects of high humidity. Both epoxy and phenolic adhesive bonded joints have good resistance to fluid immersion tests but the phenolics perform better in high temperature/high humidity or warm (353°C) wet ageing testing and this is borne out by performance in service. Adhesive systems used on aircraft British Aerospace aircraft and their predecessor aircraft manufacturers as well as Fokker aircraft have used Redux 775 in liquid and powder and film form for making primary aircraft structure. Other manufacturers have used epoxy adhesives. The historical record is as follows (Table 2.6):

Table 2. 6 *The historical record of used epoxy adhesives on aircraft British Aerospace*

Other aircraft bonded with Redux 775

Aircraft	First flown
Liquid & powder system	
Fokker F27 Friendship	1955
Fokker F28 Friendship	1967
Fokker 50 Turbo-Prop	1985
Fokker 100 Regional Jet	1988
Film system	
Fokker 50 Turbo-Prop	1995
Fokker 100 Regional Jet	1995

Aircraft bonded with hot cure epoxy

Aircraft	First flown		Adhesive used
Boeing 727	1963		Cytec FM1000
Boeing 737	1967		Cytec FM1000
Handley Page (joined to BAe in 1980)			
Jetstream 31	1967		Cytec FM1000
Jetstream 31	1982	>	Hexcel Redux 308A
Jetstream 31	1991	>	3M AF163-2 (a)
Jetstream 41	1991		3M AF163-2 (a)
SAAB 340	1983		Cytec FM73 (a)
Airbus A300	1972		Cytec FM123-2
Airbus A300		>	Cytec FM123-5
Airbus A300		>	3M AF126
Airbus A300	1982	>	Cytec FM73 (a)
Airbus A300	1991	>	3M AF163-2 (a)
Airbus A310	1982		Cytec FM73 (a)
Airbus A310	1991	>	3M AF 163-2 (a)

2.8 Nanoreinforced adhesive

Polymer nanocomposites manufactured from an effective dispersion of nanofillers (nanoparticles, nanofibres, nanotubes, etc.) into a polymeric matrix (thermoplastic or thermosetting) have been proposed as a powerful tool for generating new multifunctional materials with improved mechanical, physical and chemical properties. Due to their small size and large surface area, nano-reinforcements would be able to provide unique combination of properties, which are not possible to be reached for conventional fillers with sizes in the micrometer range. Of particular importance, it is the requirement of achieving a good distribution of the nanofiller in the polymer, in order to obtain the pursued increases in properties, without loss of other characteristics of the nanocomposite (i.e. processability) because of the high tendency to particle aggregation. The development and commercialization of nanoparticles such as nanoclays, carbon nanotubes (CNT) or nanofibers (CNF), inorganic nanoparticles and other, offer new possibilities to tailor adhesives in the

nanoscale range. Due to the large surface area of the nanosized particles only small amounts are needed to cause significant changes in the resulting properties of the nanocomposite adhesives. It could provide a new generation of structural adhesives with combination of thermal, electrical or thermomechanical properties which also provide higher environmental durability because of their lower water absorption and enhanced ageing properties. The potential of nanofillers for adhesive formulations is promising, and their effects, most of them based on the chemical and physical interactions developed between the nanoparticle surface and the resin at the reinforcement-matrix interfaces, can be classified on the following groups:

1) Mechanical properties
2) Electrical properties
3) Thermal Properties and Thermal Stability
4) Gas and Liquid Barrier Properties
5) Adhesives reinforced with inorganic nanoparticles

2.8.1 Mechanical properties

Many of the new applications of structural adhesives (i.e. transportation application such as aircraft industry) require stable materials under service conditions, which imply high temperature environments, beside to be resistant to failure resulting from vibration and fatigue loading. The addition of nanofillers to base adhesive formulations generally increases their modulus and mechanical strength. However, the main objective in these cases is to increase fracture toughness without loss of adhesive characteristics. Research in improving the fracture toughness of brittle polymers (i.e. thermosets) using nanoreinforcements holds great promise. Although the toughness of these brittle resins is usually increased by means of the addition of rubber fillers, other mechanical properties are usually degraded. For example, the improvement of the toughness of epoxy resins by incorporating nanofillers (i.e CNTs) in the resin system has been reported by numerous researchers. The participation of new mechanisms of fracture energy consumption generated by the interaction between cracks and nanofillers (crack deflection, crack bridging, fiber pull-out, etc) is considered responsible of the toughening effect associated to the nanoreinforcement addition. Gojny et al. (2005) (Gojny et al., 2005b) have published an overview in *Composites Science and Technology* over the influence of nanofiller on the fracture toughness of brittle epoxy resins and the related micromechanical mechanisms. These authors consider toughening mechanisms participate at two different dimensional levels: 1) micro-mechanical mechanisms, such as crack deflection at agglomerates, crack pinning, crack blunting and the extension of the plastic

deformation zone and 2) nano-mechanical mechanisms, such as interfacial debonding, pullout and crack bridging with participation of the nano-sized structure of CNTs. Improvements in toughness with addition of low contents of nanofiller have been reported for numerous authors, not only in the case of nanoreinforced polymers but also in situations in which the nanoreinforced matrix is included in a more complex system such as continuous fiber reinforced composites. The manufacture of multiscale composites by incorporation of nanofiller inside the matrix composite is also considerate as a potential method to improve those properties which are highly depended on the matrix (among them, thoughness). Manufacture of these composites requires that nanoreinforced resins keep their rheological and wetting characteristics to make possible the infiltration of fibre performs. Both types of properties are also required by nanoreinforced adhesives. In this research line, R. Sadeghian et al. (2006) (Sadeghian et al., 2006) have manufactured by Vaccum Resin Transfer Moulding (VARTM) hybrid composites constituted by CNF nanoreinforced polyester/glass fiber, improving the mode-I delamination resistance GIC about 100 %when CNF concentration up to 1 wt% is incorporated in the polyester matrix. These authors characterized also the viscosity dependence on the CNF concentration noticing a notable increase in resin viscosity when we CNF concentration raised from 1 to 1.5 wt%. This problem, which limits the processability of multiscale composites by infiltration methods, must be considered also in the case of nanoreinforced adhesives.

2.8.2 Electrical properties

In relation with the electrical properties, one of the most interesting fields of application is the incorporation of carbon nanotubes or carbon nanofiber as fillers in electrical conductive adhesives. The aim is to improve the performance of conductive adhesives in comparison to common products. An increase of electrical conductivity is observed in these kinds of nanocomposites with increasing CNT or CNF contents, showing clear percolation behaviour. The conductivities of the many of the developed composites show magnitudes below materials like copper. The percolation threshold values depend on the type of nanoreinforcement, being lower in the case of CNT than for CNF. The method of dispersion also has a dramatic influence on the conductivities of the nanocomposites, both for the effectiveness of the dispersion and for the effect of the applied dispersion method (mechanic stirring, ultrasonication, calendering, etc) on the nanorinforcement integrity. High energetic dispersion processes may damage the nanofillers decreasing their aspect ratio, which affect to the percolation behaviour. The electrical conductivity is usually detrimentally influenced by

the application of functionalization treatments to the carbon nanoreinforcement. Although these kinds of treatments (oxidation, amination, fluoridation, etc.) usually improve the nanofiller dispersion and favour the formation of covalent bond with the polymer matrix, they are always connected to structural changes (i.e rupture of the CNTs, resulting in a reduced aspect ratio) and, therefore, to a reduction of the electrical conductivity.

2.8.3 Thermal Properties and Thermal Stability

Thermal stability is one of the most important properties of polymer nanocomposites for potential applications as functional or structural components at elevated temperatures. Thermal stability and degradation behaviour of nanocomposites have been studied by several researchers. For example, Sarathi et al. (2007) (Sarathi et al., 2007) showed that the addition of nanoclays (i.e organo-montmorillonites) in epoxy increases the heat deflection temperature up to a critical percentage of nanoclay in epoxy, about 5 wt % above which it reaches a steady state. Addition of nanoclays also improves the thermal stability reducing, in relation with unreinforced epoxy, the loss of weight measured during a thermogravimetric analysis. Decomposition temperatures of nanocomposites generally increased with increasing nanofiller contents, indicating that the thermal decomposition of the matrix is retarded by the presence of the nanoreinforcement. These results may be attributed to the physical barrier effect, having experimental proofs that not only nanoclays but also CNTs impede the propagation of decomposition reactions in the nanocomposites (Kim and Kim, 2006). Other thermal property that can be controlled by the addition of low amount of nanoparticles is the coefficient of thermal expansion (CTE). In the specific case of thermosetting resins, the CTE values can be differenced below and above the glass transition temperature (T_g). Considering the application of these resins as adhesive, the most useful CTE concerns the temperature below T_g, since adhesive would lose most of its mechanical properties at temperatures higher than T_g. Since CNT shows negative CTEs values (longitudinal CTE of SWNTs has been estimated to be $-12 \times 10^{-6}\ K^{-1}$ while a transverse CTE was predicted to be $-1.5 \times 10^{-6}\ K^{-1}$) (Jiang et al., 2004, Kwon et al., 2004), the additions of SWCNTs could lead to a lower CTE in SWNT nanocomposites. This effect will be so much remarkable when dispersion of nanoreinforcement is more effective. For example, S. Wang et al. (Wang et al., 2007) have shown that the CTE of the functionalized SWCNTs–epoxy composites below T_g could be diminished by 52 and 42% by the incorporation of 1% by weight of nanotubes which were subjected to simple functionalization treatments (mechanical chopping and oxidization) to improve their dispersion. The addition of some kind of nanofillers (i.e. CNT) can also increase the thermal conductivity of nanocomposites. Heimann et al.

(2008) (Heimann et al., 2008), have shown that the thermal conductivity rises almost linearly with rising content of CNT in the polymer matrix (epoxy matrix). The composite with the highest portion of CNT tested (10 wt %) points out an enhancement nearly 4.4 times compared to the matrix without CNT; no influence of the method of dispersion could be observed.

2.8.4 Gas and Liquid Barrier Properties

The barrier properties of the nanocomposites are considerably improved as compared to that of pure or macroscopically filled polymers. The reason for the dramatic drop in permeability has been attributed to the existence of well dispersed nanoreinforcements with a large aspect ratio (nanoclays, CNT, CNF). Most studies on polymer nanocomposite barrier properties are based on the tortuous pathway concept (Nielsen, 1967), where the nanofiller phase is assumed to be impermeable for gas and liquid molecules, which forces the gas molecules to follow a tortuous path thereby increasing the effective path length for diffusion. One of the potential advantages of nanoreinforced adhesives related with these barrier properties is use as a moisture barrier. Reductions in moisture permeability in the range of 57- 86% for epoxy resins nanoreinforced with nanoclays have been determined, deducing that the very large aspect ratio of the clay platelets is the main factor to reach an effectively increased the moisture penetration path, which is responsible for the reduced permeability (Kim et al., 2005a). Although nanoplatelets have been shown as very effective gas and liquid barriers in polymeric matrices, recent studies on the transport properties, sorption and diffusion of water vapour carried out on epoxy resin filled with multi-walled carbon nanotubes, have also showed the improved effect of the barrier properties with increasing MWCNT concentration (Guadagno et al., 2009). Water absorption is a property of polymer which can be improved by the dispersion of nanofillers. This improvement can be significant for resins which are under prolonged water exposure, such as epoxy. The substantial decrease of permeability brought about by nanocomposite structures is a major advantage of polymer– clay nanocomposites, due to the tortuous path presented by high aspect ratio clay. The Toyota researchers determined that the rate of water absorption in their polyamide 6-clay nanocomposite was reduced by 40% compared with the pristine polymer. However, these results are more contradictory in the case epoxy matrix nanocomposites where only the rate of absorption is reduced, while the equilibrium water uptake is relatively unaffected. In spite of those potential advantages of the nanoreinforced adhesives, the incorporation of nanofillers into the adhesive may originate problems associated to the increase in viscosity and the modification of the wetting behaviour with regard to the neat adhesive. It is enough shown that the addition of nanoparticles into liquid resins increases their viscosity; and for the particular case of CNTs, it has been

found that increase in the viscosity of the nanocomposites filled with CNTs was much higher than increase in the viscosity of polymer composites filled with carbon fibers (CF) or carbon black (CB). Beside, nanocomposites filled with functionalized CNTs, that have better dispersion of the CNT, show a complex viscosity at low frequency.

2.8.5 Adhesives reinforced with inorganic nanoparticles

Due to the novelty of the nanocomposites, there are not much scientific researches, which analyse the viability for the use of nanoreinforced polymers as adhesives. Further, the most of the found publications about nanoreinforced adhesives are centred in the reinforcement of epoxy adhesives with different kinds of carbon nanotubes. This is probably associated to the fact that the epoxy resins reinforced with carbon nanotubes are being currently the most studied nanocomposites by the scientific community. Even so, several researches have been found about the reinforcement of adhesives with inorganic nanoparticles. The nature of the added nanofiller is varied, being nano-sized particles of silica and alumina some of the most used. Also, the published results are varied. Among other reasons, the study of the adhesive ability of a resin, modified or not, depends on several factors, such as the nature of the adherents and the applied surface treatments on them, the geometry of the joints (single lap, butt, T-joing, etc) and the type of test carried out to determine the strength of the joints (lap shear, peel, pull off, wedge, etc). Besides all these variables, new ones are added, which are associated with the own manufacture of nanocomposites, like the dispersion techniques and methods applied, the previous chemical treatments carried out over nanofiller surfaces and the geometry, structure and other characteristics own of nanoreinforcements, among others. The most of bibliography found about the addition of nanofiller into the adhesives is mainly based on epoxy adhesives. Compared with other adhesives, epoxy ones produce joints with high shear strength and excellent creep properties. The delamination resistance and impact of the epoxy joints are, however, relatively low. Due to their good properties, these adhesives are frequently used in high responsibility applications where their relative high cost is not as relevant. It is expected that the advantages obtained by the addition of the relative expensive nano-scale filler compensate the increase of price of the adhesive. In fact, the addition of nanofiller into epoxy adhesives could enhance the main debilities of the epoxy joints, such as their strength and toughness. Moreover, it should increase the electrical conductivity of these resins, becoming from isolator to conductive materials. This is especially interesting because of the epoxy adhesives are frequently used for joining metals and carbon fiber reinforced composites. Both are electrical conductors and it will be very profitable that their joint remains this electrical behaviour, using an electrical

conductive adhesive. Lanlan Zhai and collaborators have published several researches on the effect of the addition of alumina nano-particles in epoxy adhesives (Zhai et al., 2008, Zhai et al., 2006), analysing their pull-off strength over steel. It is probed that the addition of alumina nanoparticles causes a drastic increase of the adhesive strength, which reaches the maximum value when the nanofiller content is 2 wt %. The pull-off strength of this nano-reinforced adhesive is almost five times higher than that of pure epoxy adhesive. This increase is intimately associated with a change in failure mode, which becomes from interfacial failure for non-modified adhesive to a mixed cohesive-interfacial failure mode for the joints bonded with nanoreinforced adhesives. At high nano-alumina contents, the adhesive strength falls because the surface wetting ability of the adhesive is reduced by the increase of its viscosity. The modification of adhesives by the addition of alumina nanoparticles has been also studied in epoxy-based film adhesives, which are incrementing their use for joining aluminium and polymer composite parts in the aircraft industry. These applications typically require the modification of epoxy formulations to increase the adhesion, toughness and peel strength of the joints, because they are usually subjected to vibration and fatigue loads besides high service temperature environments. Gilbert et al. (2003) (Gilbert et al., 2003) confirmed that the addition of 5 wt % nano-alumina into an epoxy formulation that was filmed on polyester random mat scrim achieved increases in the peel strength of almost 50% and in shear strength of 15% for joints of aluminium substrates. Lanlan Zhai et al. (2006) (Zhai et al., 2006) published a comparative study about the effectiveness of different kind of inorganic nanoparticles on the stickiness of epoxy adhesives. In particular, they used nanoparticles of Al_2O_3 (whose average diameter was 80 nm), nano-$CaCO_3$ (with 40 - 80 nm of diameter) and nano-SiO_2 (whose size was 10 – 20 nm in diameter). These nanofillers were added in 2 wt % regard to the epoxy adhesive mass. Low carbon steel sheets were used as adherents, which were abraded with different silicon carbide paper, polished to an optical flatness and finally degreased and dried. The adhesion strength, measured through pull-off adhesion test, of the epoxy adhesives incorporating three kinds of nanoparticles was greatly improved compared with pure epoxy adhesive. The highest increase is obtained by the adhesive reinforced with nanoparticles of alumina, from 3.4 to 18.4 MPa, while the strength of the nano-$CaCO_3$ modified epoxy adhesive was as much as that of nano-SiO_2 modified system, no more than 12 MPa. The increase of adhesive strength by the addition of nanofillers into the adhesives implies a stronger anchoring associated to changes on the physical and chemical properties of the modified adhesives. The different enhancements found as function of nanoparticle nature may be attributed to the chemical properties of nanoparticles, which may have influence in the chemical interaction of the surfaces of steel and epoxy adhesives, producing some chemical bonds on the interface and therefore

enhancing the adhesion strength. The formation of bridges between the adhesive and the adherents was confirmed by the analysis of the interface morphology through scanning electron microscopy. Polyhedral-oligomeric-silsesquioxanes (POSS) are other kind of inorganic silica particles which are actually commercialized, being nano-charges of 1.5 nm in size with organic substituents. The substituents can be inactive, physically compatibles with the matrix, or reactive, which promote curing or grafting reactions with the polymer. The effect of the addition of low amounts of POSS into epoxy adhesives is strongly dependent on the nanostructure of the epoxy/POSS network, which in turn depends on the functional groups (reactive or nonreactive) of the POSS (Dodiuk et al., 2005). The highest values of shear and peel strength are obtained when the crosslinking degree of nanoreinforced adhesive is high. Due to the large surface area of POSS, only relatively small amounts (< 4 wt %) are needed to cause significant changes on the properties of the epoxy resin. In fact, excess of POSS amount implies the plasticization of the matrix, decreasing the joint strength. Finally, Patel et al. (2006) (Patel et al., 2006) analysed the effect of the addition of an organically modified montmorillonite nanoclay, commonly named Cloisite 10A, on the joint strength bonded with a very soft acrylic adhesive. With a high surface energy adherent, like aluminium, clay nanoreinforced adhesives displayed gradual increment in peel strength with the increase of filler content, measuring enhancements of up 45% regard to neat adhesive. However, the observed improvement with low surface energy substrate, polypropylene, was lower. This indicates a favourable interaction between the silicates and aluminium substrate. The lap shear strength spectacularly increases with the nanoclay addition, up to 146, 130 and 142% in joints of aluminium-aluminium, wood-wood and polypropylene-polypropylene, respectively. Besides the adhesive properties, the addition of nanoclay into the adhesives enhances their barrier performance. This is especially interesting in the use of polyurethane adhesives (Osman et al., 2003). They are commonly used in producing laminates for food packing due to their flexibility and wide application temperature range. However, their use is limited due to their low barrier performance, as oxygen and humidity barriers. The inclusion of small volume fractions of montmorillonite in polyurethane adhesives decreases their gas transmission rate due to the impermeability of the inorganic nanoparticles. The following tables collect a summary of the most relevant results published about the mechanical properties of the joints bonded with neat and nanoreinforced epoxy adhesives, which were determined by lap shear (Table 2.7), peel (Table 2.8) test.

Table 2. 7 *Lap shear strength of different adhesive joints: comparison between neat and nanoreinforced epoxy adhesive*

Filler	Adherent	Neat adhesive	Nanoreinforced adhesive	Variation (%)	Ref.
Al_2O_3 nanoparticles	Al	237 Mpa	273 Mpa	+15	(Gilbert et al., 2003)
SiO_2 nanoparticles	Al	25.5 Mpa	25.8 Mpa	+12	(Klug and Seferis, 1999)
	Al	20.8 Mpa	23 Mpa	+11	(Kinloch et al., 2003)
	Ti	25 Mpa	40 Mpa	+60	(Bhowmik et al., 2009)
POSS	Al	21 Mpa	24 Mpa	+14	(Dodiuk et al., 2005)
MWCNT	CF/epoxy	-	-	+46	(Hsiao et al., 2003)
Al_2O_3 nanofibers	Al	237 Mpa	265 Mpa	+12	(Gilbert et al., 2003)
	Al-CF/epoxy	-	-	+30	(Meguid and Sun, 2004a)
CNF	PMMA	28 Mpa	32.5 Mpa	+16	(Xu et al., 2007)
	CF/epoxy	11.9 Mpa	12.8 Mpa	+8	(Prolongo et al., 2009a)

Table 2. 8 *Peel strength of different adhesive joints: comparison between neat and nanoreinforced epoxy adhesive*

Filler	Adherent	Neat adhesive	Nanoreinforced adhesive	Variation (%)	Ref.
Al_2O_3 nanoparticles	Al	87 N	130 N	+49	(Gilbert et al., 2003)
SiO_2 nanoparticles	Al	3.1 N/mm	5.5 N/mm	+77	(Kinloch et al., 2003)
POSS	Al	0.19 N/mm	0.49 N/mm	+158	(Dodiuk et al., 2005)
Al_2O_3 nanofibers	Al	87 N	119 N	+37	(Gilbert et al., 2003)

This page intentionally left blank

Chapter Three

3. Influence of carbon nanofillers on the curing kinetics of epoxy resin adhesive

In this chapter, the curing kinetic reaction of a carbon/epoxy nanocomposites based systems was investigated by Differential Scanning Calorimeter. This study aims to know the curing parameters of the epoxy conductive mixture used as adhesive

3.1 Generalities and remarks

Epoxy resin is widely used for carbon fiber-reinforced composites (CFRCs), due to its excellent processability and properties (Mäder, 1997, Kim and Mai, 1998, Jang, 1994) . In the manufacturing of CFRCs based epoxy resins, the curing reactions are partially responsible of the adhesion between the matrix and fibers, and play a crucial role in determining the mechanical properties of the finished composite products. In order to meet high structural performance requirements for new CFRC applications, the performance of epoxy resin needs to be enhanced. For many applications, such as aerospace and aeronautics, the rapid development of nanoscience and technology offers the possibility to produce materials with properties that would be unattainable by traditional thermosetting resins. The use of carbon nanotubes (CNTs), graphitic carbon nanofibers (CNFs) and graphene-based nanoparticles as polymer reinforcements is a particularly attractive option to enhance the current polymer matrix properties. These nanofillers are used to enhance or provide physical properties, such as high storage moduli, suitable thermal expansion, thermal and electrical conductivity, and magnetic recording properties (Kawaguchi and Pearson, 2003, Mijović and Wang, 1989, Jia et al., 2002). The addition of nanofillers can influence the interaction of the polymer matrix with fiber reinforcements and the resin curing process. The processing behaviour of neat polymer and their nanocomposites are significantly different. An understanding of the curing process of the nano-modified epoxy matrix can help to design and manufacture composite parts characterized by enhanced electrical and mechanical properties. Generally epoxy resins, obtained by solidifying the only epoxy precursor with hardeners for structural materials, are brittle and have poor resistance to crack propagation (Vakil and Martin, 1992, Iijima et al., 1993). To overcome this drawback, the epoxy resins are mixed with modifying agents, such as low molecular weight polymers, reactive oligomeric compounds, plasticizers, reactive diluents, etc. which modify the viscosity of the resin so that the processability of the system is not impaired (Jagadeesh et al., 2000, Mustaţă and Cascaval, 1997, Thakkar et al., 1990, Won et al., 1990, Frigione et al., 1995). On the other hand, these components can strongly modify the curing kinetic. Kinetic analyses of pure epoxy resin carried out by differential scanning calorimetry (DSC) data have shown a wide range of activation energy values (28–158 kJ/mol) (Roşu et al., 2002, Sbirrazzuoli et al., 2003). Although a variation in the activation energy for pure epoxy resin has been reported by many authors (Roşu et al., 2002, Sbirrazzuoli et al., 2003), this aspect of the curing kinetics is still a matter of debate, in fact several manuscripts have reported constant values in the activation energy during the curing reaction (Liang et al., 2006, Catalani and Bonicelli, 2005). On the other hand, with the massive and rapid development of nanocomposites, different studies have also been aimed to understand the

effects of carbon nanofillers on the curing kinetics of epoxy resins (Opalički et al., 1996, Su and Woo, 1997, Chiao, 1990, Mijović et al., 1984, Gupta et al., 1983, Jana and Zhong, 2009, Seyhan et al., 2009, Bae et al., 2002, Xie et al., 2005, Xie et al., 2004, Puglia et al., 2003). Very few efforts have been aimed to study the effect of (carbon nanostructured forms (CNTs, CNFs, graphene-based nanoparticles etc.)) on the curing reactions of the tetrafunctional epoxy resins. This type of epoxy precursor is of great scientific and industrial interest, especially in light of the very performing results already published on mixtures based on this precursor loaded with unidimensional and bidimensional carbon nanofillers. In particular, interesting values in the dc volume conductivity of the resin filled with CNTs and CNFs were found (Guadagno et al., 2014b). The electrical percolation threshold (EPT) for the composite filled with CNTs and CNFs, falls in the range [0.1, 0.32] wt% and, beyond the EPT, the electrical conductivity can reach values higher than 1-2 S/m. Furthermore, low cost fillers, such as highly exfoliated graphite, might be more relevant and competitive to simultaneously impart electrical conductivity and strong mechanical reinforcement to the resin (Guadagno et al., 2015a). Graphene based nanoparticles, embedded in this tetrafunctional epoxy precursor, are also able to enhance adhesive properties (Vietri et al., 2014). Generally, after the selection of promising industrial formulations, the knowledge of aspects related to their curing kinetic is a fundamental requirement to optimize the manufacturing processes and therefore the properties of the final materials. This work is aimed to study the curing kinetics of very promising nanofilled epoxy systems recently developed. In particular, three types of nanofillers have been selected: a) CNTs, b) CNFs and c) carboxylated exfoliated graphite CpEG. These nanofillers have been chosen because are among the best performing filler to enhance the electrical properties of epoxy resins and CFRCs (high electrical conductivity and low EPT) (Guadagno et al., 2015e, Guadagno et al., 2015b, Guadagno et al., 2013, Guadagno et al., 2015a, Guadagno et al., 2014b). Furthermore, the chosen nanofillers have proven to simultaneously enhance mechanical performance (Guadagno et al., 2015e, Guadagno et al., 2013, Guadagno et al., 2015a). A concentration by weight of 0.5 % of nanofiller was used because this amount is beyond the EPT and it is able to enhance all the analyzed properties (Guadagno et al., 2013, Vietri et al., 2014, Guadagno et al., 2015a, Guadagno et al., 2014b).

The choice of the epoxy mixture determines the final properties of the cured resin especially in terms of mechanical and thermal properties. Generally, a tetrafunctional precursor assures good properties of the cured resin due to the high level of crosslinking density. The advantages of the use of DDS hardener is the high glass transition, the better chemical resistance and the thermal properties of the resulting network compared with aliphatic and cycloaliphatic amine-cured network. An epoxy precursor such as the TGMDA hardened with

DDS is characterized by very good thermal and mechanical properties, but it is brittle and characterized by poor resistance to crack propagation. To overcome this drawback, this epoxy precursor was mixed with modifying agents, such as low molecular weight polymer reactive oligomeric compounds, plasticizers, fillers, reactive diluents, etc. which modify the viscosity of the resin so that the processability of the system is not impaired (Guadagno et al., 2014a, Nobile et al., 2015, Roşu et al., 2002). Diluents are used in the formulation to reduce the viscosity or/and to eliminate the need of solvents. They are grouped into two types: reactive diluents and non-reactive diluents. Reactive diluents are mono-epoxide compounds, which participate in the curing reaction and reduce the crosslinking density. However, the addition of diluent is generally associated with a reduction in mechanical strength, modulus and glass transition temperature (T_g). Therefore, the amount of diluent must be optimised by critically analyzing the thermo-mechanical properties while keeping the technical specification for a particular application in mind. In this paper the diglycidylether of 1,4 butanediol reactive diluent was select.

3.2 Materials and sample preparation

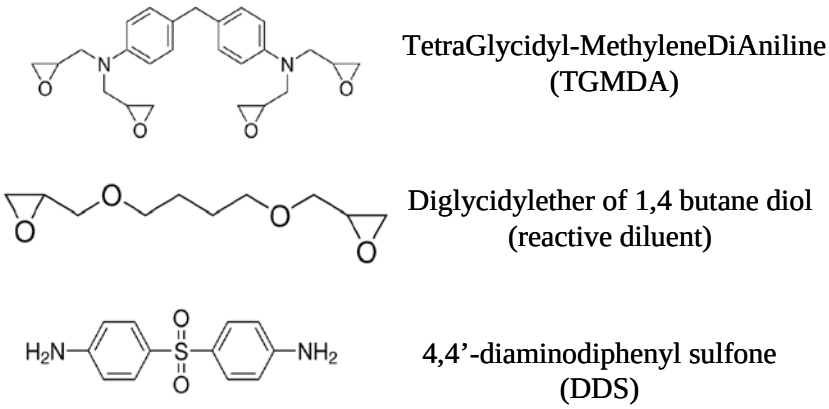

Figure 3. 1 *Molecular structure of the chemical compounds.*

Figure 3.1 shows the chemical structures of the compounds used in this work. We have considered three types of fillers: carbon nanotubes and carbon nanofibers that have one-dimensional (1D) predominant shape and highly exfoliated graphite that has a two dimensional (2D) predominant shape. The CNTs (3100 grade) were obtained from Nanocyl S.A. The specific surface area of multi-wall carbon nanotubes determined by using the BET method is around 250–300 m^2g^{-1}, the carbon purity is > 95 % with a metal oxide impurity < 5 % as it results by thermogravimetric analysis (TGA). A detailed analysis

of the morphological parameters of the CNTs has been carried out by high resolution transmission electron microscopy (HR-TEM). Most of CNTs are characterized by an outer diameter ranging from 10 to 30 nm, but an outer diameter lower than 10 nm or larger than 80 nm has been also observed. Lengths of CNTs range from hundreds of nanometers to tens of micrometers. Number of walls varies from 4 to 20 in most nanotubes (Guadagno et al., 2011, Guadagno et al., 2009). CNFs in the form of powders used in this study were produced at Applied Sciences Inc. and were from the Pyrograf III family. The CNFs were obtained by heat treatment at T=2500 °C starting from sample PR25XTPS1100 in order to provide the best combination of mechanical and electrical properties (Guadagno et al., 2013). The heat treatment was performed in an atmosphere controlled batch furnace. Approximately 300 g of nanofibers were placed in a ceramic crucible for the heat treatment. The furnace was purged with nitrogen gas for 1 h prior to heating. The heating rate was 100 °C/h and the furnace was held at a temperature of 2500 °C for 1 h prior to cooling (Guadagno et al., 2013). Previous papers highlighted that the heat treatment strongly influences the degree of structural ordering and therefore the bonding states of carbon atoms in the nanofiber structure (Guadagno et al., 2013). It causes a significant transformation in the hybridization state of the bonded carbon atoms. The enhancement in the fiber structural perfection very positively affects the electrical conductivity of the nanofiber-reinforced resins leading to an increase in the conductivity at very low filler concentration (Guadagno et al., 2013). The sample CpEG was prepared as follows: a mixture containing nitric and sulphuric acid and natural graphite was used (Vietri et al., 2014). After 24 h of reaction, intercalation within graphene sheets took place to form intercalated graphite compound. Then the mixture was filtered, washed with water, and dried in an oven at low temperatures. The intercalated graphite compound was subjected to sudden heat treatment temperature of 900 °C and rapid expansion then occurred. The expansion ratio was as high as 300 times. The considered filler has a two dimensional (2D) predominant shape and it is obtained with an exfoliation procedure from natural graphite, that leads to obtain 2D conductive particles with an average diameter of 500 μm. The average value of Brunauer-Emmett-Teller specific surface area (S_{BET}) has been found to be 16.3 m^2g^{-1}.

Five systems were prepared. In the first system, the epoxy precursor TGMDA was mixed with a stoichiometric amount of DDS, in an oil bath at 120 °C, (sample acronym TGMDA_DDS). The mixture was mechanically stirred until a homogeneous mixture was observed. In the second system, the epoxy matrix was obtained by mixing TGMDA with reactive diluent (diglycidylether of 1,4 butane diol) at a concentration of 80 %:20 % (by wt) epoxide to diluent. The advantage of the used reactive diluent has been evidenced in previous work focused on the viscoelastic properties of CNF/epoxy resins. The inclusion of the reactive diluent diglycidylether of 1,4 butane diol in the epoxy resin based

on the TGMDA precursor significantly reduces the viscosity values of the TGMDA, thus favouring the manufacturing process of the nanofilled resin (Guadagno et al., 2014a, Nobile et al., 2015). Furthermore, the presence of oxirane rings in the reactive diluent allows efficient crosslinking reactions with the chains of the diluent included in the epoxy network. DDS was added at a stoichiometric concentration with respect to all epoxy rings (sample acronym TGMDA_DDS_DILUENT). In the nanofilled resins corresponding to the last three systems, CNTs, CNFs and CpEG were embedded at loading rate of 0.5% by weight in the epoxy mixture TGMDA-DDS-DILUENT by using ultrasonication for 20 minutes (Hielscher model UP200S- 24 kHz high power ultrasonic probe). These nanocomposites (based on TGMDA_DDS_DILUENT epoxy mixture) are named respectively as follows: CNTs system, CNFs system, CpEG system.

3.2.1 Methods: Differential Scanning Calorimeter (DSC) and Scanning Electron Microscopy (SEM)

The DSC instrument measures heat flow into or from a sample under heating, cooling or isothermal conditions. DSC measures the quantitative heat flow as a direct function of time or of the sample temperature. This heat flow temperature data provides extremely valuable information on key physical and chemical properties associated with thermosetting materials, including: glass transition temperature (T_g), onset and end of cure, heat of curing, maximum rate of curing, percentage of curing, heat capacities. These properties can then be used to address some of the everyday problems, which confront the manufacturer, or user of thermosetting resins. Differences between isothermal and dynamic curing kinetics have been an ongoing debate in the literature from the early days of kinetic modeling and commercial DSC's (1960's-70's), to recent literature reviews (Calado and Advani, 2000). For purely kinetic studies, dynamic tests are still considered more reliable since their baselines, start and end points can be defined more easily. However, isothermal tests (or their residuals) are necessary for diffusion modeling. In general, cure models are not compared to both isothermal and dynamic data, although those pursuing advanced modeling programs assert that the two test modes should be used as complimentary data sources to cover the widest range of temperatures, degrees of cure, and material behaviour as possible (Skordos and Partridge, 2001, Flammersheim and Opfermann, 2002).
A differential scanning calorimeter (Mettler DSC 822) was used for the dynamic and isothermal cure experiments and for data analysis under a nitrogen flow of 20 ml/min. To select suitable temperatures for the required isothermal experiments, a dynamic DSC scan at a heating rate of 10 °C/min was first obtained (see Figure 3.2). Values of temperature above but near the

onset of reaction were chosen. This method could avoid the improper choice of temperature, which may be too high or too low. Isothermal experiments were carried out at 180 °C, 190 °C, 200 °C, 210 °C, and 220 °C. The reaction was considered complete when the signal leveled off to baseline. The total area under the isotherm curve, based on the extrapolated baseline at the end of the reaction, was used to calculate the isothermal heat of reaction, $\Delta H_i(t)$ (i= 180 °C, 190 °C, 220 °C), at a given temperature (see Figure 3. 2). After each isothermal scan, the sample was rapidly cooled in the DSC cell to 30 °C and then reheated at 10 °C/min to 300 °C to determine the residual heat of reaction, $\Delta H_{residue}$ (see the inset of Figure 3.3) .

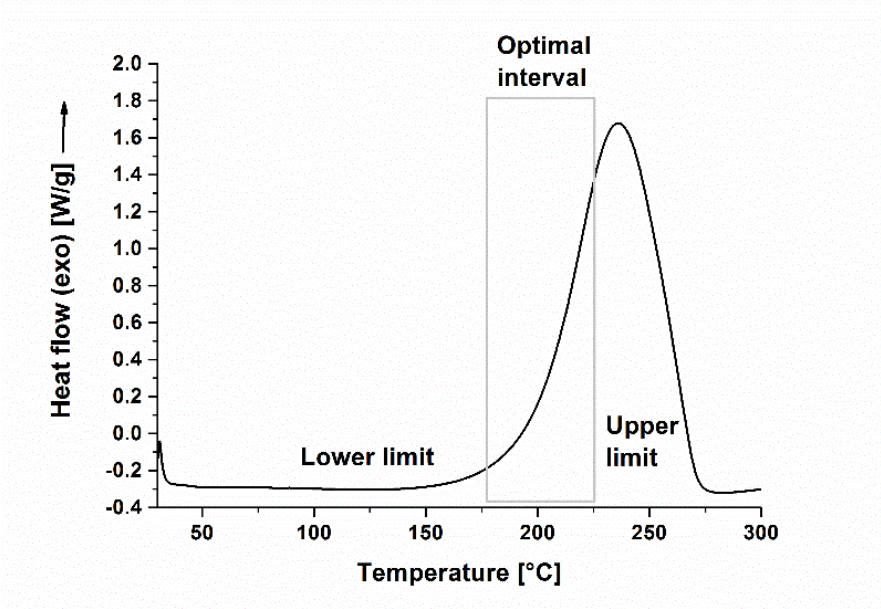

Figure 3. 2 *Selection of isothermal curing temperature.*

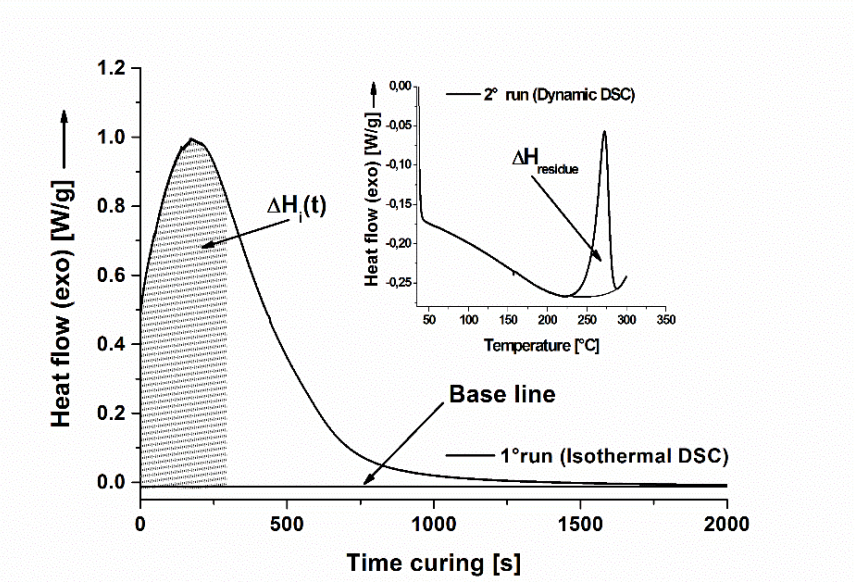

Figure 3. 3 A typical isothermal DSC curing curve.

The total heat evolved during the curing reaction is $\Delta H_{tot}=\Delta H_i+\Delta H_{residue}$ where ΔH_i is the total heat released during the cycle isothermal. The degree of cure, α, is related to the enthalpy released during the exothermic reaction of the resin components. The relation is given in Equation (1), where $\Delta H_i(t)$ is the partial heat of reaction at a certain time and ΔH_{tot} is the total heat of reaction.

$$\alpha(T,t)=\frac{1}{\Delta H_{tot}}\int_0^t\left(\frac{dH}{dt}\right)dt=\frac{\Delta H_i(t)}{\Delta H_{tot}} \tag{1}$$

The rate of reaction as a function of time has been calculated from the rate of heat flow measured in isothermal DSC experiments:

$$\frac{d\alpha}{dt}=\frac{dH/dt}{\Delta H_{tot}} \tag{2}$$

The dynamic cure experiments were performed at 2.5, 5, 10 and 20 °C/min from 30 to 300 °C. Micrographs of the carbon nanofillers CNTs, CNFs and CpEG and their corresponding nanocomposites were obtained using a Scanning electron microscopy (SEM, mod. LEO 1525, Carl Zeiss SMT AG, Oberkochen, Germany). All the samples were placed on a carbon tab previously stuck to an aluminum stub (Agar Scientific, Stansted, UK) and

were covered with a 250-A° -thick gold film using a sputter coater (Agar mod. 108 A). Nanofilled sample sections were cut from solid samples by a sledge microtome. These slices were etched before the observation by SEM. The etching reagent was prepared by stirring 1.0 g potassium permanganate in a solution mixture of 95 mL sulfuric acid (95 % - 97 %) and 48 mL orthophosphoric acid (85 %). The filled resins were immersed into the fresh etching reagent at room temperature and held under agitation for 36 h. Subsequent washings were done using a cold mixture of two parts by volume of concentrated sulfuric acid and seven parts of water. Afterward the samples were washed again with 30 % aqueous hydrogen peroxide to remove any manganese dioxide. The samples were finally washed with distilled water and kept under vacuum for 5 days before being subjected to morphological analysis.

3.5 Results and discussion

3.3.1 Morphological investigation

The inclusion in the resin of one-dimensional fillers does not lead to big differences in the curing kinetics behaviour with respect to the raw epoxy. An increase in the activation energy is found in the case of highly exfoliated graphite. It is likely due to a reduction of free molecular segments of the epoxy network. In order to fully understand the influence of carbon nanofillers (CNTs, CNFs, CpEG) on the curing kinetics of Epoxy-Amine Resin, the morphologies of both carbon nanoparticles and nanofilled systems were characterized. SEM investigation on the carbonaceous nanofillers was performed to analyze their morphological features before their incorporation into the epoxy precursors (see Figure 3.4). The morphological features of CNTs are very different from the other unidimensional filler CNF. They tend to assemble due to the more intense van der Waals interactions between monofilaments characterized by lower value in the diameters with respect to the CNFs. In Figure 3.4 we can observe that the CNFs are characterized by straighter walls where the nested configuration, typical of the as made CNFs, is not clearly visible, according to the previous results (Nobile et al., 2015, Guadagno et al., 2013). The heat treatment seems able to statistically reduce this effect. In fact after heat-treating the as made nanofibers to a temperature of 2500°C, the graphene layers became straight, and the minimum interlayer spacing was reached for the nanofibers. Lengths of CNFs range from about 50 to 100 μm and the diameter of CNFs range from 125 to 150 nm. SEM image of the CpEG sample shows a fluffy morphology, characteristic of graphite subjected to heat treatment, where we can see few layers of large surface area highly wrinkled and folded.

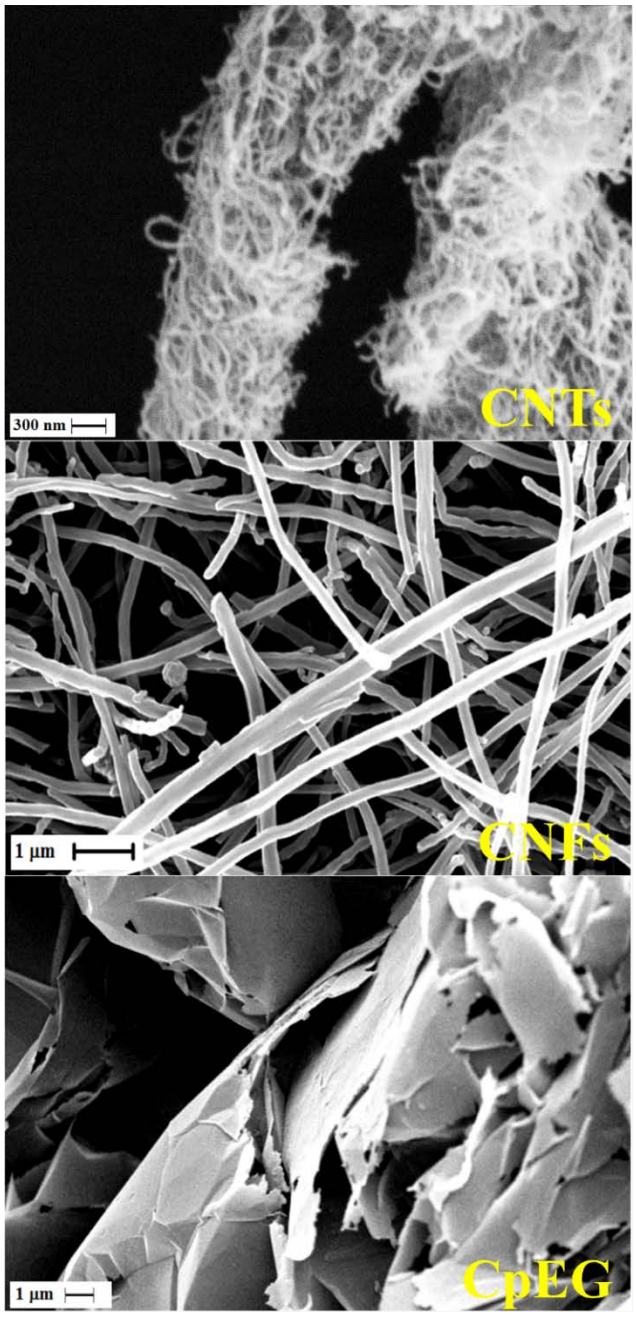

Figure 3. 4 *SEM images of the three different carbonaceous nanofillers*

The morphological feature of the nanofillers has proven to play a relevant role in determining the electrical and mechanical properties of the analyzed nano-filled resins (Vietri et al., 2014, Guadagno et al., 2015a). The results on the electrical properties obtained for the composite with MWCNT and CNFs, above the percolation threshold, are among the highest values of electrical conductivity obtained for epoxy systems (Guadagno et al., 2015a). At low filler contents, the composite exhibits an electrical conductivity comparable to that of the pure polymer. Instead, near the percolation threshold which is different for the diverse systems, the composite exhibits a transition from an insulating to a conducting behaviour. For both composites, the percolation threshold is lower than 0.3% by weight. At higher filler concentrations the electrical conductivity reaches a plateau at a value several orders of magnitude above that of the neat resin.

Concerning the filler CpEG, a careful morphological investigation of the sample loaded with CpEG was already performed in literature (Guadagno et al., 2015a). The results for the composite with CpEG highlight the relevant influence of the exfoliation degree and the role of edge-carboxylated graphite layers to originate self-assembly structures embedded in the polymeric matrix (Guadagno et al., 2015a). Detailed analysis at nanoscale, carried out by means of Transmission Electron Microscopy (TEM) and Atomic Force Microscopy (AFM), highlighted that Graphene layers inside the epoxy matrix may serve as building blocks of complex systems that could outperform the host matrix (Guadagno et al., 2015a). Groups on EG responsible of the self-assembled structures were highlighted by elementary analysis (presence of functional groups containing C and O), FT/IR analysis and thermogravimetric investigation (Guadagno et al., 2015a). In particular, the CpEG sample highlighted self-assembly structures created by edge-carboxylated graphene layers or graphitic blocks which can provide superb polymer–CpEG interactions through intermolecular hydrogen bonding also with the polar groups of the resin network (Guadagno et al., 2015a). This strategy favors the interfacial interaction between polymer and carbon layer enhancing the electrical percolation paths and mechanical performance. An increase in the mechanical performance in terms of tensile strength and Young's modulus of thermoplastic nanocomposites, due to the effect of nanofiller (CNT) functionalization and hence the enhancement of the interfacial interaction, was already reported by other authors (Kim et al., 2007, Yu et al., 2014)

In order to analyze the homogeneity of the nanofiller dispersion in the polymeric matrix, morphological analysis by SEM was carried out on etched samples to remove the resin surrounding the nanofillers, leaving them bare. Fig. 3.5 shows SEM images of the fracture surface of the three epoxy-based composites filled with 0.5 wt% loading of nanofillers (CNTs system, CNFs system and CpEG system respectively). The used etching procedure, reported in the experimental, mainly consumes the surface layers of the polymeric

matrix. We observe that the same etching procedure seems to be more efficient for composites filled with CNTs and CNFs. In fact, in this case we observe whole lengths of the CNTs and CNFs segments released from the residual resin fraction, highlighting a homogeneous structure for both the samples, in which the nanofillers are uniformly distributed in the epoxy matrix. The observation of the image in Figure 3.5 shows that only a few layers of graphene appear bare and clearly visible in the surface, emerging from the resin. This can be explained assuming that strong interconnections between CpEG particles and residual polymeric matrix remain after the etching attack. Edge-carboxylated graphene nanosheets by increasing the CpEG/epoxy matrix interaction favor a more efficient load transfer and consequently determine a strong mechanical reinforcement in the elastic modulus (Guadagno et al., 2015a).

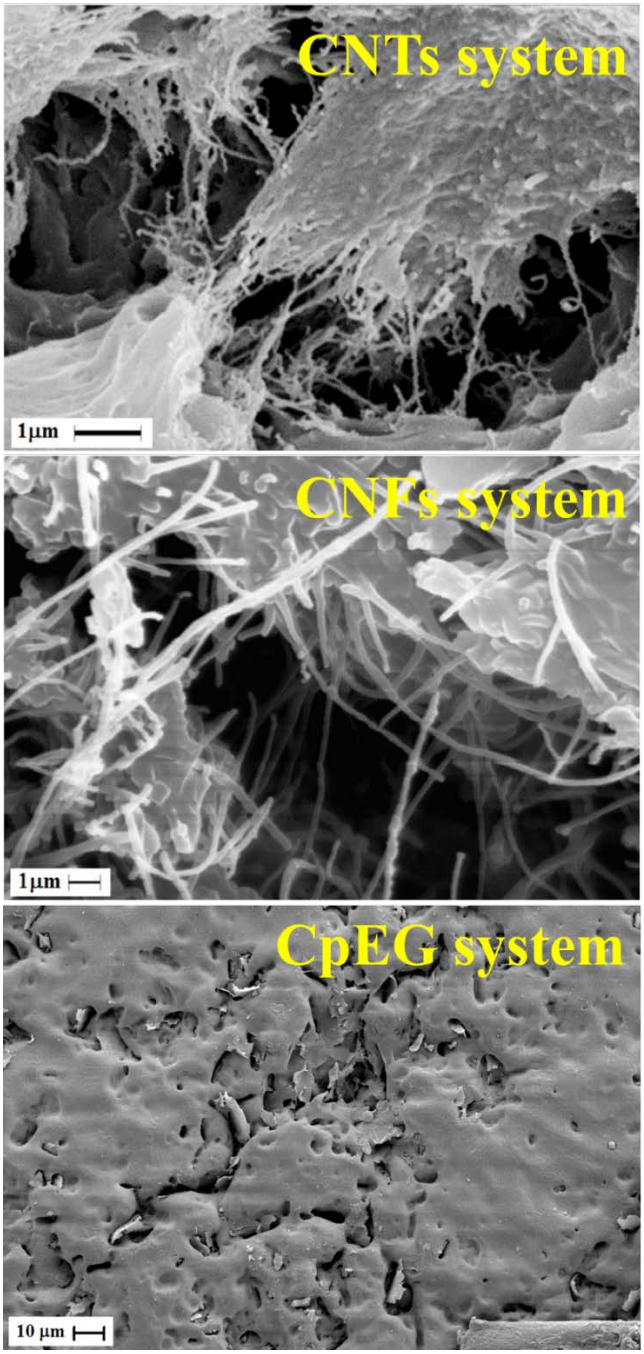

Figure 3. 5 *SEM images of the fracture surface of the three different epoxy systems with 0.5 wt% loading of nanofillers*

3.3.2 Curing behaviours (Isothermal DSC analysis)

A series of isothermal reaction rate curves for sample TGMDA_DDS (obtained from DSC measurements), as a function of time, is shown in Figure 3.6.

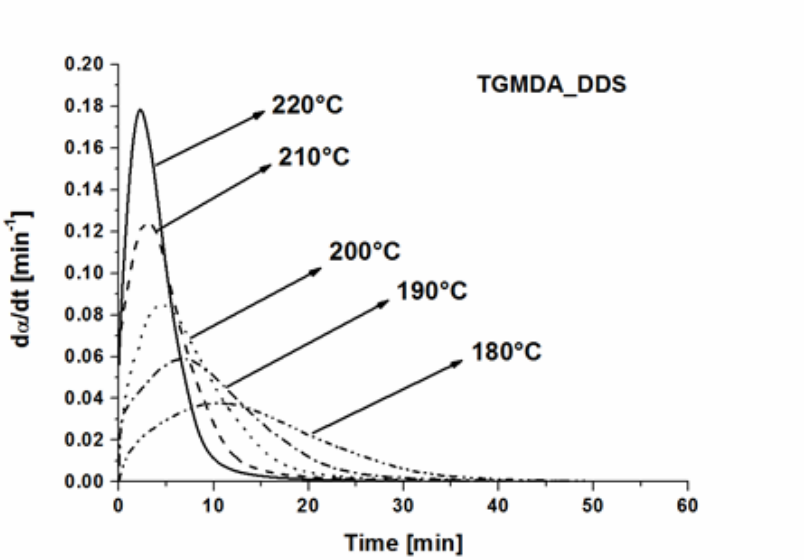

Figure 3. 6 *Isothermal reaction rate as a function of time at different curing temperature for TGMDA_DDS.*

The curve profiles highlight that the reaction rate increases rapidly because of the auto-acceleration and reaches a maximum. After this point it starts to decrease and gradually dies out. The increase in temperature of the curing reaction influences the value of the reaction rate at the maximum. The peak of the reaction rate becomes higher and shifts to a shorter time along with the increasing the curing temperature. The plot shows the maximum in the $d\alpha/dt$ versus time-curve at $t \neq 0$; which is characteristic for autocatalytic reactions (Keenan, 1987, Chiao, 1990). By partial integration of areas under the experimental curves in Figure 3.3, the fractional conversion as a function of time has been obtained.

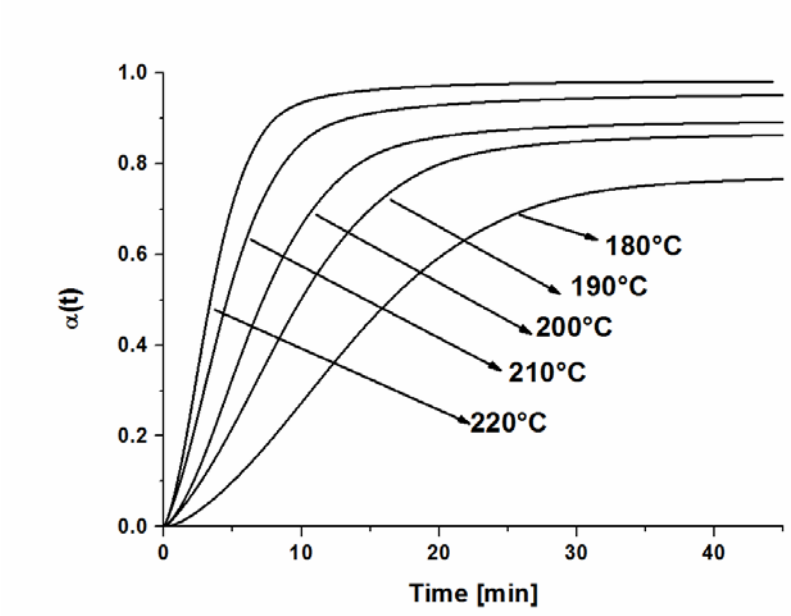

Figure 3. 7 *Isothermal fractional conversion as a function of time at different curing temperature for TGMDA_DDS.*

Figure 3.7 presents the plot of curing reaction conversion (calculated from the experimental data) versus time at different isothermal temperatures. Initially, the conversion level increases with time and finally approaches a limiting conversion. The higher the curing temperatures the higher the limiting fractional conversion is reached. This is to be expected since in step of polymerisation the original monomer disappears early in the reaction and after the gel point most of reactive functional groups are attached to the cross-linked network. Different models have been proposed to describe the curing behaviour of thermoset resins. For amine-cured epoxy resins, it is generally accepted that two main addition reactions, described as primary and secondary-amine ring-opening, are occurring 47.(Su and Woo, 1995) In this work Kamal's model (describing the chemically controlled cure), arising from the autocatalytic reaction mechanism is applied to our isothermal data. Kamal proposed the following expression (Jungang et al., 2002):

$$\frac{d\alpha}{dt} = \left(k_1 + k_2\alpha^m\right)(1-\alpha)^n \qquad (3)$$

where m and n are the reaction orders, and k_1, k_2 are the rate parameters which are functions of temperature. Non-linear regression analysis is used for the computation of the parameters: m, n and k_2; while the reaction rate constant k_1 was determined as the initial reaction rate at t = 0, given by the intercept of curves of the reaction rate versus time. In order to incorporate the effects of diffusion on curing kinetics, several ways have been proposed. One way is to invoke the Rabinowitch concept (Rabinowitch, 1937), which defines the overall rate constants k_1 and k_2 in Eq. (3) as a function of the chemically controlled rate constant (k_c) and the diffusion term (k_d)

$$\frac{1}{k_i} = \frac{1}{k_c} + \frac{1}{k_d} \tag{4}$$

where i = 1 and 2. The diffusion term can assume either the modified WLF form (Wisanrakkit and Gillham, 1990) or modified Doolittle free volume form (Simon and Gillham, 1993). Another way of incorporating the effects of diffusion is to define a diffusion factor (f_d) (Fournier et al., 1996) which equals to the ratio of the measured rate of reaction to the chemically controlled rate of reaction (i.e., in the absence of diffusion). Thus, the overall kinetic expression in form of Eq. (3) can be expressed as

$$\frac{d\alpha}{dt} = \left(k_1 + k_2\alpha^m\right)(1-\alpha)^n \, f_d(\alpha) \tag{5}$$

A commonly used expression for f_d, which was originally proposed by Chern and Poehlein (Chern and Poehlein, 1987), has the final form (Ratna, 2009) of

$$f_d(\alpha) = \frac{1}{1+\exp\left[C\left(\alpha-\alpha_c\right)\right]} \tag{6}$$

where C and α_c are temperature-dependent fitting parameters. When α is much lower than the critical conversion α_c, $f_d(\alpha)$ approaches unity and the effects of diffusion are negligible. However, when α approaches α_c, $f_d(\alpha)$ decreases and eventually vanishes with further increase in conversion.

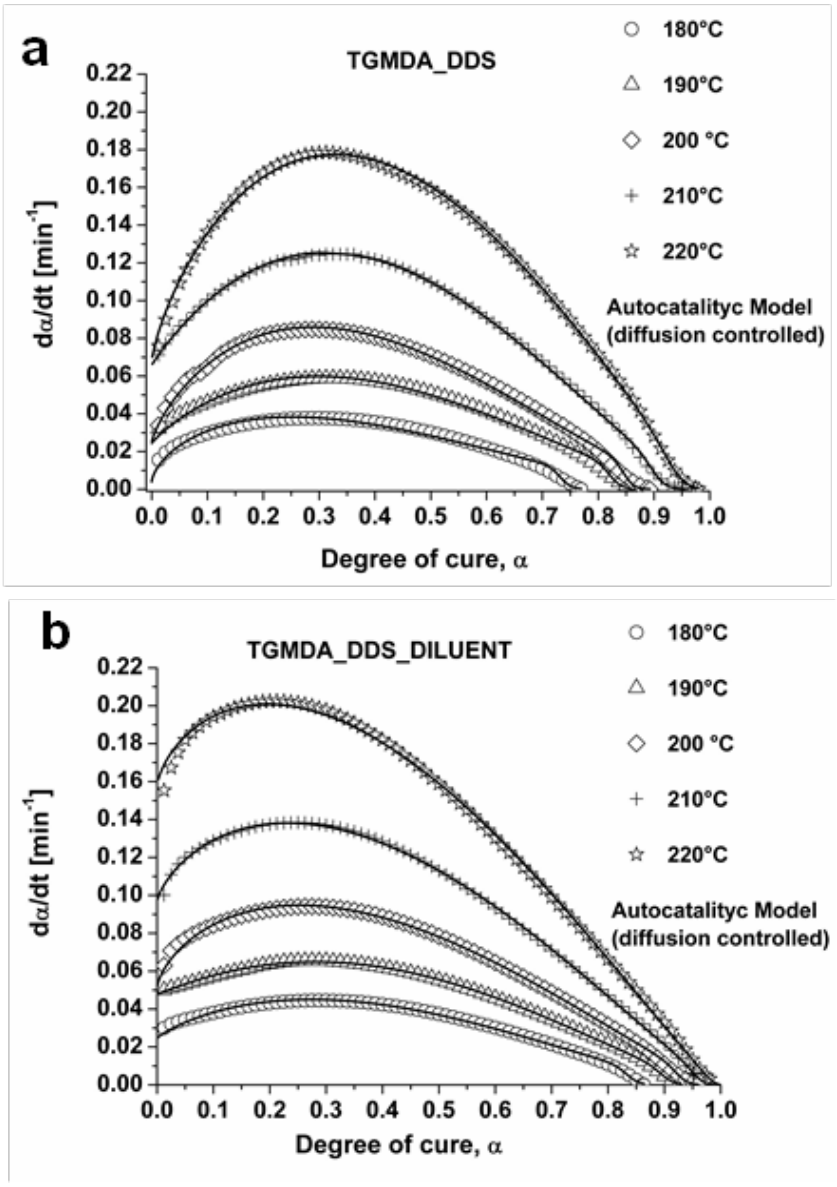

Figure 3. 8 *Comparison of calculated data included the diffusion effect (solid line) with experimental data (symbols) for the system TGMDA_DDS a) and TGMDA_DDS_DILUENT b) respectively.*

Table 3. 1 *Values of the kinetic parameters each sample obtained*

T (°C)	k_1 [min^{-1}]	k_2 [min^{-1}]	n	m	m+n	α_c	α_{max}	E_1 [KJ/mol]	E_2 [KJ/mol]	ln A_1	ln A_2
	TGMDA_DDS										
180	**0.0039**	**0.1456**	**1.78**	**0.64**	**2.42**	**0.734**	**0.770**				
190	**0.0244**	**0.2531**	**1.67**	**0.92**	**2.58**	**0.824**	**0.865**				
200	**0.0250**	**0.3361**	**1.63**	**0.80**	**2.43**	**0.848**	**0.893**	**125.73**	**60.35**	**28.32**	**14.20**
210	**0.0658**	**0.4707**	**1.48**	**0.97**	**2.45**	**0.903**	**0.952**				
220	**0.0680**	**0.5375**	**1.24**	**0.79**	**2.03**	**0.940**	**0.981**				
	TGMDA_DDS_DILUENT										
180	**0.0246**	**0.1543**	**1.56**	**0.88**	**2.43**	**0.837**	**0.864**				
190	**0.0480**	**0.2106**	**1.44**	**1.04**	**2.48**	**0.900**	**0.929**				
200	**0.0510**	**0.2223**	**1.28**	**0.69**	**1.96**	**0.927**	**0.960**	**81.84**	**34.21**	**18.04**	**7.24**
210	**0.0964**	**0.2794**	**1.22**	**0.74**	**1.96**	**0.960**	**0.987**				
220	**0.1578**	**0.3360**	**1.18**	**0.73**	**1.91**	**0.991**	**1.000**				
	CpEG system										
180	**0.0213**	**0.1292**	**1.42**	**0.76**	**2.17**	**0.861**	**0.888**				
190	**0.0434**	**0.1790**	**1.31**	**0.67**	**1.98**	**0.888**	**0.922**				
200	**0.0682**	**0.2060**	**1.34**	**0.76**	**2.10**	**0.902**	**0.942**	**79.46**	**49.33**	**17.40**	**11.04**
210	**0.1044**	**0.2726**	**1.21**	**0.79**	**2.00**	**0.963**	**0.988**				
220	**0.1152**	**0.3961**	**1.19**	**0.69**	**1.88**	**0.994**	**1.000**				
	CNTs system										
180	**0.0239**	**0.1529**	**1.55**	**0.81**	**2.36**	**0.855**	**0.882**				
190	**0.0445**	**0.1611**	**1.45**	**0.80**	**2.25**	**0.892**	**0.921**				
200	**0.0702**	**0.2063**	**1.30**	**0.80**	**2.11**	**0.924**	**0.958**	**85.89**	**39.99**	**19.13**	**8.65**
210	**0.1004**	**0.2867**	**1.24**	**0.79**	**2.03**	**0.970**	**0.989**				
220	**0.1602**	**0.3376**	**1.23**	**0.78**	**2.01**	**1.003**	**1.000**				
	CNFs system										
180	**0.0262**	**0.1558**	**1.56**	**0.94**	**2.50**	**0.865**	**0.890**				
190	**0.0346**	**0.1950**	**1.45**	**0.84**	**2.29**	**0.891**	**0.921**				
200	**0.0714**	**0.2132**	**1.29**	**0.86**	**2.14**	**0.940**	**0.970**	**84.30**	**41.82**	**18.66**	**9.21**
210	**0.0882**	**0.3202**	**1.27**	**0.86**	**2.13**	**0.973**	**0.991**				
220	**0.1588**	**0.3757**	**1.24**	**0.90**	**2.14**	**0.989**	**1.000**				

The comparison, for the samples TGMDA_DDS and TGMDA_DDS_DILUENT, of the best fitted, to Eq. (5), curves with the corresponding experimental data is shown in Figure 3.8.
Figure 3.8 clearly shows that Eq. (5) leads to a very good description of the experimental data in the whole range of α. The kinetic parameters determined for the amine-cured TGMDA resin system are listed in Table 1 along with the correlation coefficient values for the curve fit. The maximum degree of cure

α_{max} increased with higher temperatures. The critical degree of cure α_c increases with temperature. The reason for the decreasing effect of diffusion with higher temperature is that the thermal energy is high enough to maintain high molecular mobility to continue the cure (Du et al., 2004). The values of the reaction rate constants is between 0.039 min^{-1} and 0.680 min^{-1} for the primary and between 0.1456 min^{-1} and 0.5375 $min^{-1}$for the secondary reaction. The reaction rate constants k_1 and k_2 increase with the temperature. The temperature dependence of the rate constants is given by the Arrhenius expressions in Equation (7), where i indicates the primary or secondary amine-epoxy reaction, A_i is the pre-exponential factor, E_i the activation energy, R is the universal gas constant and T the reaction temperature.

$$k_i = A_i \exp^{\frac{-E_i}{RT}} \quad i=1,2 \tag{7}$$

Once the rate constants were identified, the activation energy E_i for both parts of the reaction and correlating pre-exponential factor A_i were derived from the slope and intercept of the plot $\ln(k_i)$ as a function of 1/T (1/K).(see Figure 3.9)

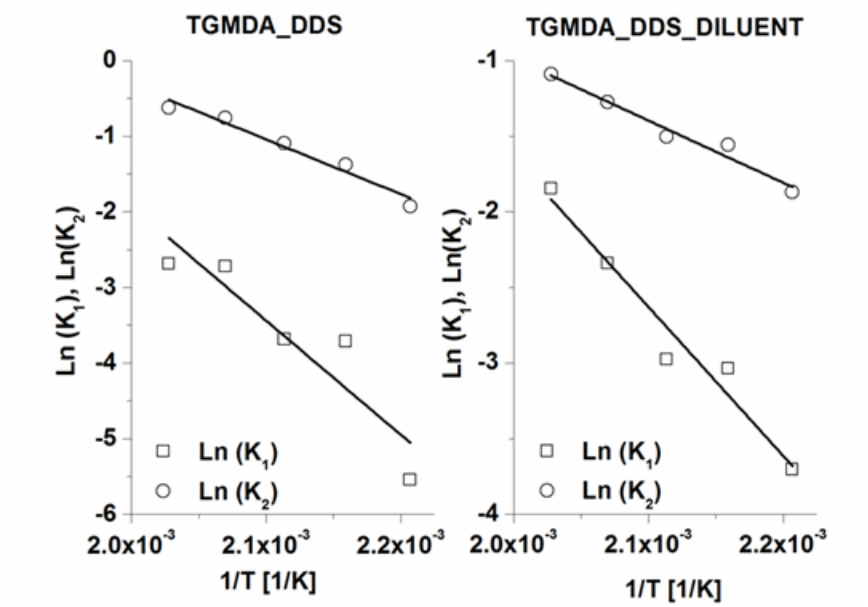

Figure 3. 9 *Curve of ln (k_1) and ln (k_2) against 1/T for the samples TGMDA_DDS and TGMDA_DDS_DILUENT.*

Table 3.1 shows the kinetic parameters obtained for the epoxy resin system with the reactive diluent by the isothermal DSC analysis. The activation

energy E_1 and E_2 decreased significantly compared to the system without the reactive diluent. This means that the new epoxy system needs a lower amount of heat to curing. In particular, E_2 decreases by about approximately 50 %, compared to the value obtained with the system TGMDA-DDS. The effect of the reactive diluent is remarkable for secondary amine-epoxy reaction. This result leads to consider the possibility of being able to cure the resin at lower temperatures. This consideration is evident in the Figure 3.10 in which the profiles of isothermal heating at 220 °C for the two systems considered and the subsequent heating in dynamic mode are shown.

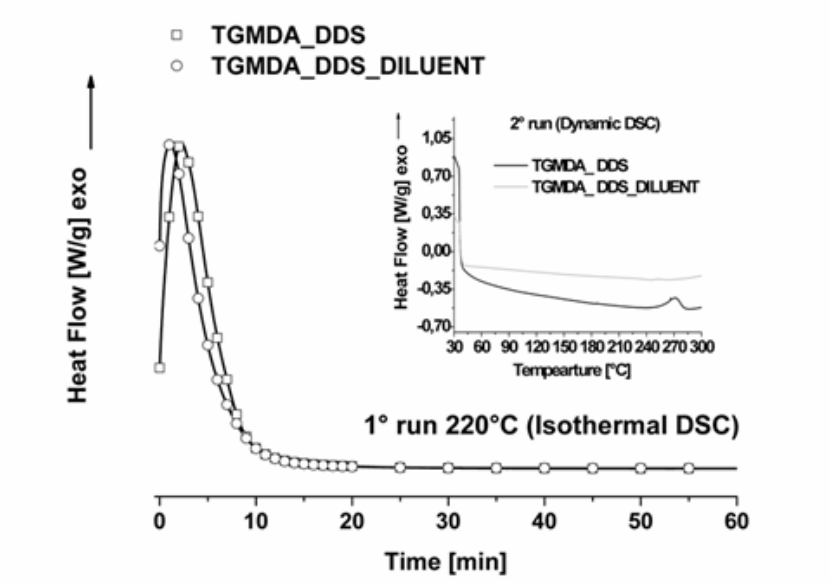

Figure 3. 10 *Isothermal DSC curing curve for the system TGMDA_DDS and TGMDA_DDS_DILUENT.*

The peak temperature decreases from a value of 134 seconds for the system TGMDA_DDS to 66 seconds for the system TGMDA_DDS_DILUENT, while the residual heat of reaction is absent for the epoxy system with the reactive diluent (see inset Figure 3.10). This effect is more pronounced if the temperature of cure is lower, in fact the difference in maximum conversion (Table 3.1) obtained for both systems increases with the decrease of the temperature of cure as is evident in Figure 3.11. This very interesting result highlights that a lower temperature of the curing process can be used in the formulation with the reactive diluent.

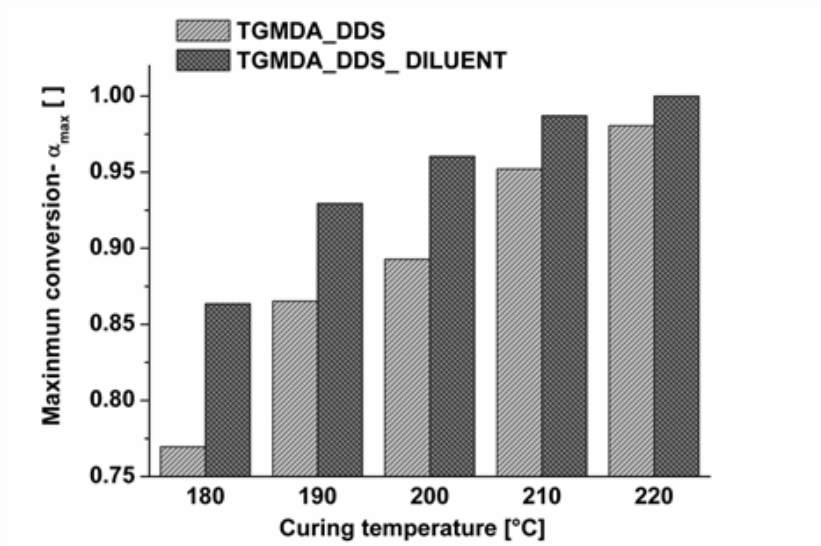

Figure 3. 11 *The maximum degree of cure α_{max} vs curing temperature for the system TGMDA_DDS and TGMDA_DDS_DILUENT.*

For systems loaded with different fillers, Table 3.1 shows that the value of E_1 and E_2 are similar to the values of the system with the diluent reactive except for the value E_2 obtained for the exfoliated graphite composite. It changes from 34 KJ/mol of the raw resin to 49 KJ/mol of the composite. E_2 is the activation energy for secondary amine-epoxy reaction when the viscosity is increased with the increase of the curing degree, thus more energy was required to overcome the motion among molecule chains. The obstacle opposed by exfoliated graphite decreases the free movement of molecules of the epoxy resin which translates to an increase of E_2

3.3.3 Dynamic DSC analysis (Iso-conversional methods and model-free kinetics)

If changes in the mechanism are associated with changes in the activation energy, they can be detected by using the model-free iso-conversional methods (Sbirrazzuoli et al., 1997, Vyazovkin and Sbirrazzuoli, 1999a, Vyazovkin and Sbirrazzuoli, 1996, Vyazovkin and Sbirrazzuoli, 1999b, Turi, 2012, Zvetkov, 2001). These methods are based on the iso-conversional principle that states that the reaction rate at constant extent of conversion is only a function of the temperature.

$$\left[\frac{d\ln(d\alpha/dt)}{dt}\right]_{\alpha} = -\frac{E_{\alpha}}{R} \tag{8}$$

Henceforth the subscript α indicates the values related to a given extent of conversion). E_{α} is computed for various α values ranging between 0 and 1. For single step reactions, E_{α} is constant over the whole temperature (or conversion) interval. For multi-step kinetics, E_{α} will vary with α and this reflects the variation in relative contributions of single steps to the overall reaction rate. The goal of the model-free kinetics (MFK) and of the isoconversional analysis is to use this variation, as additional information on the reaction mechanism (Sbirrazzuoli et al., 2003, Sbirrazzuoli et al., 1997, Vyazovkin and Sbirrazzuoli, 1999a, Vyazovkin and Sbirrazzuoli, 1996, Vyazovkin and Sbirrazzuoli, 1999b, Du et al., 2004, Turi, 2012, Zvetkov, 2001). Common integral methods make use of various approximations to evaluate the so-called "temperature integral" (Sbirrazzuoli et al., 1997, Vyazovkin and Sbirrazzuoli, 1999a, Vyazovkin and Sbirrazzuoli, 1996, Vyazovkin and Sbirrazzuoli, 1999b, Turi, 2012). The use of differential methods, i.e. Friedman method in the case of iso-conversional methods, avoids this limitation inherent of integral methods, but differential methods are known to be noise sensitive if no modification is used (Sbirrazzuoli et al., 1997, Vyazovkin and Sbirrazzuoli, 1996). For these reasons, Sbirrazzuoli et al. (Sbirrazzuoli et al., 1997) and Vyazovkin (Vyazovkin, 2001, Vyazovkin, 1997) have developed integral methods based on numerical integration. The method proposed by Sbirrazzuoli et al. (Sbirrazzuoli et al., 1997) was called "Ozawa corrected method" while that of Vyazovkin (Vyazovkin, 2001, Vyazovkin, 1997) is the "advanced isoconversional method". An additional advantage of the advanced iso-conversional method is that it is not limited to linear temperature programs, and it takes into account possible variations in the activation energy. To estimate the E_{α} -dependencies for epoxy cures, we used the advanced iso-conversional method developed by Vyazovkin (Vyazovkin, 2001, Vyazovkin, 1997). According to this method, for a set of n experiments carried out at different arbitrary heating programs $T_i(t)$, the activation energy is determined at any particular value of α by finding the value of E_{α} that minimizes the function

$$\sum_{i=1}^{n}\sum_{j\neq i}^{n}\frac{J\left[E_{\alpha},T_i(t_{\alpha})\right]}{J\left[E_{\alpha},T_j(t_{\alpha})\right]} \tag{9}$$

In Eq. 9 the integral

$$J\left[E_\alpha, T_i\left(t_\alpha\right)\right] \equiv \int_{t_{\alpha-\Delta\alpha}}^{t_\varepsilon} \exp\left[\frac{-E_\beta}{RT_i\left(t\right)}\right] dt \tag{10}$$

is evaluated numerically for a set of experimental heating programs. Integration is performed over small time segments (Eq.(10)) that allows for eliminating a systematic error occurring in the usual integral methods when E_α varies significantly with α. In Eq. (10), α is varied from Δα to 1− Δα with a step $\Delta\alpha = m^{-1}$, where m is the number of intervals chosen for analysis.
The eq. (9) can be further rearranged as follows:

$$\sum_{i=1}^{n} \sum_{j \neq i}^{n} \frac{I\left[E_\alpha, T_{\alpha,i}\right]\beta_j}{I\left[E_\alpha, T_{\alpha,j}\right]\beta_i} \tag{11}$$

where β is the heating rate and $I[E_\alpha, T_{\alpha,i}]$ is determined by with the help of a Doyle's approximation (Doyle, 1962)

$$I\left(E_\alpha, T_{\alpha,i}\right) \cong \frac{E_\alpha}{R} \exp\left(-5.331 - 1.052\frac{E_\alpha}{RT_{\alpha,i}}\right) \tag{12}$$

The minimization procedure is repeated for each value of α to determine the E_α dependence. Iso-conversional methods determine the E_α values independent of the pre-exponential factors, which are not directly produced by these methods. This allows the elimination of the bias from the value of the activation energy which could be caused by its strong correlation with the pre-exponential factor that is generally found when both parameters are fitted simultaneously (Sbirrazzuoli et al., 2000). By contrast with usual iso-conversional methods, sample (non-linear) temperature variations and non-linear interpolation algorithm were used to compute the E_α -dependence, for both isothermal and non-isothermal data. The curing reaction of epoxy resin was investigated by DSC at four different heating rates (β= 2.5, 5, 10, 20 °C/min) from 30 to 300 °C; Figure 3.12a shows a typical example of DSC thermograms for epoxy resin while Figure 3.12b shows the variation of the fractional conversion (α) as a function of temperature for the epoxy, where

$$\alpha\left(T, \beta\right) = \frac{\Delta H_\beta\left(T\right)}{\Delta H_{tot}} \tag{13}$$

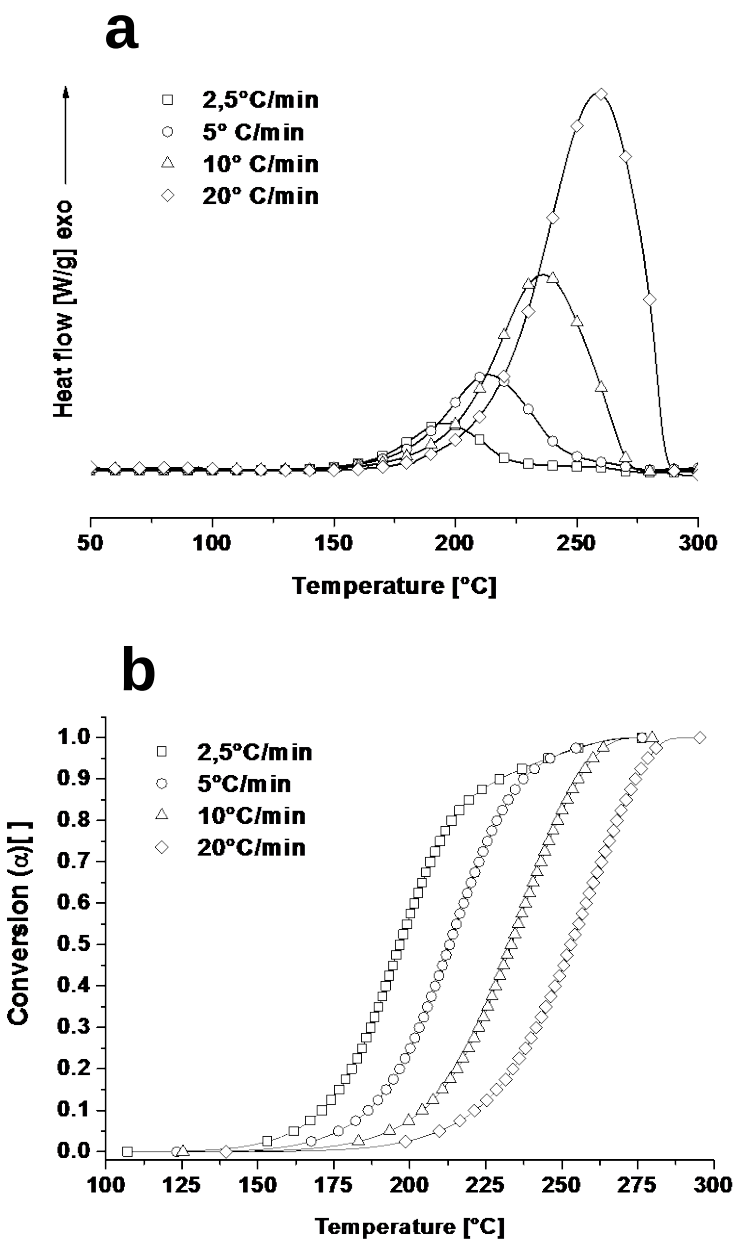

Figure 3. 12 *A typical dynamic DSC curing curve.*

The application of Eq. (11) to non-isothermal data, give rise to the dependencies of E_α on α as is shown in figure 3.12. The activation energy of

TGMDA-DDS system increases with the increasing of the curing degree in epoxy system, and the value of activation energy ranged from 70 kJ/mol to 170 kJ/mol. The viscosity increased with the increase of the curing degree, thus more energy was required to overcome the motion among molecule chains. With the curing reaction proceeding, the curing degree increased, and the free volume only allowed local motions of the chain segments. Therefore, a great degree of cooperatives among the chain segments were required to initiate translational motion of the segments. This would results in a large energy barrier of the segment motion, which was reflected through activation energy at later curing stages.

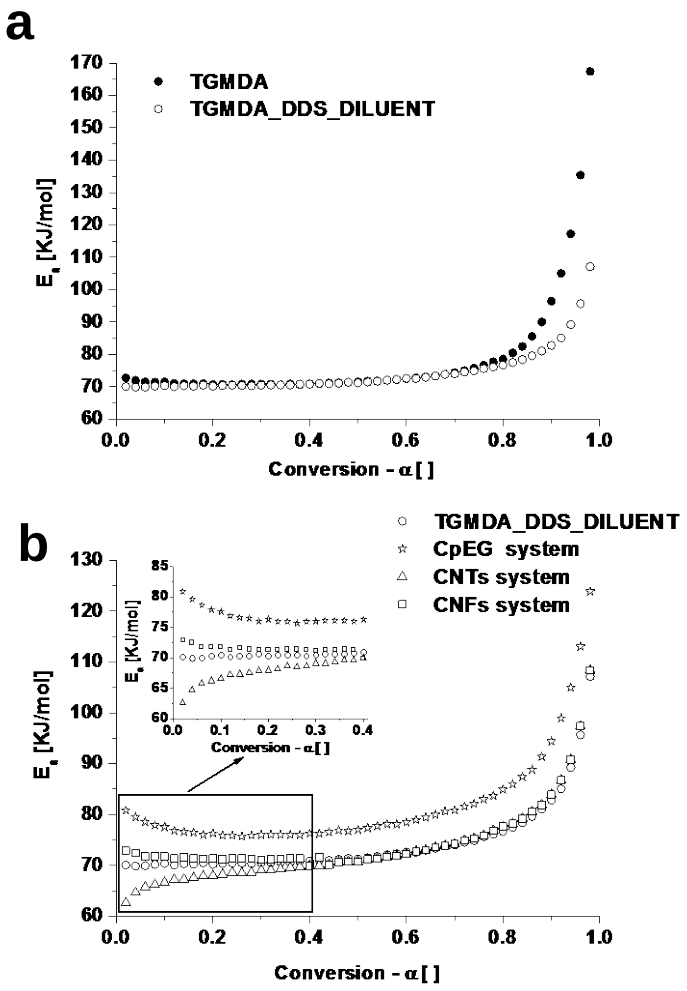

Figure 3. 13 *Variation of the activation energy with conversion obtained for all sample.*

Figure 3.13a shows that the activation energy remains substantially the same for conversions under α= 0.7 for both systems, TGMDA_DDS and TGMDA_DDS_DILUENT. For $\alpha > 0.7$ E_a is lower for the system containing the diluent. In previous studies (Roşu et al., 2002), Rosu et al. have found that the presence of the reactive diluent leads to an increase of the cure range and decrease of E_a. This behaviour can be related to more comprehensive cure to the decrease of the viscosity. The decrease of the viscosity, obtained by the introduction of reactive diluent, allows the upper local motions of the chain segments. This would results in a smaller energy barrier of the segment motion, which is reflected on activation energy at later curing stages, in fact the isothermal analysis shows that the introduction of the diluent decreases particularly the activation energy of secondary amine-epoxy reaction. An additional confirmation of this effect was obtained by the dynamic DSC analysis that shows a decrease of the activation energy due to the introduction of reactive diluent, for $\alpha > 0.7$. This value is in the range of conversions (0.6-0.8) (Li et al., 2012) in which it is considered that the reaction of secondary amine is active. The dynamic DSC analysis (see Figure 3.13b) shows that the behavior of one-dimensional fillers is similar to the raw resin for $\alpha > 0.4$. The effects of viscosity due to the increase of the curing degree seem to remain unaffected by the presence of the filler . The reason for this is probably due to the low concentration by weight of the filler. For $\alpha < 0.4$, in the early curing stage, the activation energy for CNT-composite slightly decreases, while for CNF-composite, the behavior is similar to the raw resin. In the literature, different works were dedicated to the determination of the effect of CNT on the curing kinetics of an epoxy resin. Xie et al. (Xie et al., 2004) also reported an acceleration effect in the case of multi-wall carbon nanotubes (MWCNT) for the TGDDM/DDS epoxy system using isothermal DSC. The higher initial reaction rate of the composites compared to the unfilled resin, the decrease of the time at maximum reaction rate and of the activation energy with increasing MWCNT content were the indication of the acceleration effect. Evidence of the presence of hydroxyl groups (–OH) on the surface of the MWCNT by FTIR spectroscopy which have a catalytic effect on epoxy ring opening was in that case the source of the modified cure. The last stage of the cure remained unaffected by MWCNT. The same group studied the effect of carbon nanofibers (CNF) on the cure behaviour of the same epoxy system (Xie et al., 2005). They found a very small acceleration effect of CNF in the early stage of the reaction suggested by the decrease of the activation energy with an increase of the CNF content. On the other hand, the CNF hinders the reaction after that step. The origin of the acceleration effect cannot be clearly determined in their work due to the absence of surface characterization of the CNT material. The high percentage of catalyst particles in the CNT raw material may be a plausible source of the early cure initiation. In these

investigations (Xie et al., 2005, Xie et al., 2004, Puglia et al., 2003), it is believed that the modification of the cure behaviour in its early stage can be attributed to surface functional groups on CNT or catalyst particles. Wu et al. (Wu and Chung, 2004) studied the effect of three different carbon fillers (carbon fiber, carbon nanofiber and carbon black) on the cure reaction of the DGEBF/TETA epoxy system. They reported an increase of the total heat of reaction and a decrease of the temperature at the heat flow peak for all fillers. By comparing the effect of different pre-treatments of the carbon fibers, they explained the increase in the total heat of reaction as a result of the presence of surface functional groups on the fillers. The authors found that the acceleration effect, that is the decrease of the peak temperature, was closely related to the specific surface area (SSA) of the filler, in view of the proportionality between the SSA and the peak temperature drop (the higher the SSA, the higher the temperature drop). In the case of this last paper, the fillers were manually dispersed in the resin and the filler content was high (around 20 wt%). The authors did not give indication on the dispersion state of the fillers; it is likely that, for this concentration of nanofillers, strong heterogeneity due to nanofiller aggregates were formed. In our case CNT and CNF do not have any functional group, but both have small residual metal oxides. This probably explains the effect of the small decrease of the activation energy obtained in the initial stage in the CNT-composite. However the CNFs do not have effect on E_a, most likely, because the metal oxides are distributed around over a smaller surface area (Average specific surface area = 65-75 m^2g^{-1}) (De Vivo et al., 2015) with respect to CNTs (250-300 m^2g^{-1}) (Guadagno et al., 2011). In fact the CNF is an unidimensional filler as CNT, but it is characterized by a different aspect ratio length/ diameter. In fact, the length of CNT is into a range from 0.1 to 10 μm with an average diameter of 10 nm; the length of CNF is into a range from 50 to 100 μm and a diameter into a range from 125 to 150 nm. The catalytic effect is greater if the specific surface area is higher (Wu and Chung, 2004). Jana and Zhong (Jana and Zhong, 2009) found that expanded graphite (EG) did not significantly impede the cure reaction of epoxy. Guo et al. (Guo et al., 2009) reported that at lower concentrations (1 phr) of EG, compared with the curing activation energy (E_a) of the neat epoxy resin, the composite with EG had a lower E_a before the gelation and a higher E_a after the gelation. At higher concentrations of EG (5 phr), however, in the whole conversion range, the composite with EG showed a higher E_a compared with the neat epoxy resin. In particular Jana and Zhong (Jana and Zhong, 2009), observe that the graphite particles were comparatively heavier than epoxy resin molecules, therefore these particles could be seen as obstacles to free movement of molecules. In addition, with more conversion of the pure epoxy the viscosity of the GP/epoxy system increased and movement of epoxy molecules decreased. To initiate a translational motion of epoxy molecules, a great degree of cooperation

between molecules was needed. This cooperation between epoxy molecules generated an additional amount of energy barrier to the motion of molecules and a higher amount of activation energy was needed for the conversion. Data here shown on dynamic analysis (see Figure 3.13) evidence that the exfoliated graphite is characterized by an activation energy higher than the raw resin in the entire conversion range; and isothermal analysis (see Table 3.1) highlights that the value of E_1 and E_2 are similar for all the analyzed nanofillers, except for the value E_2 obtained for the exfoliated graphite composite. For this last filler, an increase of ~ 44 % in E_2 was detected with respect to the reference sample (TGMDA_DDS_DILUENT). Furthermore, an increase with respect to the other nanofiller (MWCNTs and CNFs) is also observed. The behaviour of the sample filled with graphite-based nanoparticles is in agreement with the general trend observed by other authors for a higher concentration of the filler and different approaches based on constant and variable activation energy to analyse the DSC curves (Jana and Zhong, 2009). It is worth noting that an effective comparison is not possible due to the different approaches used in the experimental tests and the different procedure of graphite preparation. However, a such increase in the E_2 for a low amount of CpEG seems effectively relevant. This unexpected relevant increase is very likely due to self-assembly structure generated by edge-carboxylated layers inside the epoxy matrix. This architecture, on the one hand is able to enhance the electrical percolation paths and mechanical performance; on the other hand constitutes a sort of rigid nano-cages where the curing reactions must be active under condition of reduced mobility for the segmental parts of the resins. This hypothesis is confirmed by the following observation: only the E_2 value is higher than the values of E_2 related to other mono-dimensional nanofiller. Furthermore, a slight decrease is observed in E_1 value with respect to the samples loaded with MWCNTs and CNFs. This is exactly the expected result, if we consider that the functional groups on the graphene edges contributes to facilitate the curing reactions. In fact, the expected result for E_1 value is a general increase due to the physical impediment caused by the nanofillers to the network formation in the domains of the resin. This is in agreement with the observed values for CNTs and CNFs, while a value similar to the reference sample (TGMDA_DDS_DILUENT) is observed for CpEG sample. In literature, graphene and exfoliated graphite used to impart functional properties or simply as reinforcement for the polymer, were produced using different procedure and then different structure, functionalizations and morphological features. For this reason, it is really necessary an accurate characterization of the nanofiller to understand the correlations between structural and morphological organization of graphene-based materials and curing kinetics of the nanofilled formulations. The measurements carried out in this paper employed a nanofiller exhaustively characterized in a previous manuscript (Guadagno et al., 2015a). In particular, in this paper a sample of

exfoliated graphite able to enhance electrical and mechanical properties of the resin was used (see section 3.4.1). It is very likely that the increase of the activation energy, in the exfoliated graphite composite, is determined by the same mechanisms responsible of the beneficial effects on other properties such as electrical and mechanical properties (Guadagno et al., 2015a).

3.4 Conclusion

In this work, the curing kinetic reaction of a carbon/epoxy nanocomposites based systems was investigated by DSC. The dynamic experiments show that the presence of the reactive diluent leads to a decrease of the activation energy for $\alpha > 0.7$ for which it is considered that the reaction of secondary amine is active. Under the isothermal condition, the Kamal's diffusion controlled model confirm this effect, in fact the activation energies E_1 and E_2 decreased significantly, compared to the system without the reactive diluent, in particular E_2 decreases by about approximately 50%, compared to the value obtained with the system TGMDA-DDS. The effect of the nanofillers in the TGMDA_DDS_Diluent system was analysed. The inclusion in the resin of one-dimensional fillers does not lead to big differences in the curing kinetics behaviour with respect to the unfilled epoxy mixture (TGMDA_DDS_DILUENT). Conversely, an increase in the activation energy E_2 related to secondary amine-epoxy reaction is found in the case of highly exfoliated graphite even for a very low percentage of filler (0.5 % by wt). This increase is very likely due to self-assembly structure generated by the edge-carboxylated layers of graphite nanoparticles inside the epoxy matrix. This architecture constitutes a sort of rigid nano-cages where the final curing reactions must be active under condition of more reduced mobility with respect to the conditions experimented by other mono-dimensional nanofillers. This hypothesis seems to be confirmed by the higher value of E_2 and the slight decrease in E_1 value observed for the nanocomposites loaded with graphite-based nanoparticles with respect to other mono-dimensional nanofillers.

This page intentionally left blank

Chapter Four

4. Interaction between Carbon Nanoparticles and Epoxy Resin by the study of the effect the Mechanical, Electrical and Transport Properties

The focus of this chapter is the design of the epoxy formulations conductive adhesive, by tuning the amount of hardener, in order to reduce the moisture content and provide additional functional performance, such as mechanical and electrical properties

4.1 Generalities and remarks

Several key factors must be taken into account in the choice of nanocomposites for structural applications. A proper selection of matrix and nanofiller, together with the fascinating possibility to transfer the very interesting nanostructure properties to the final material, can allow to meet specific and heavy requirements able to breach the wall of the current limitations in specific fields. The recent ability of material scientists in the control of matter behavior at nanoscale level can be exploited to design a new generation of emerging materials able to simultaneously satisfy several structural and functional requirements. For instance, in the field of primary aeronautical structures, through a tailored transfer of nanoparticle properties to the structural resins, new potential perspectives are foreseen. Low-weight green aircrafts at low fuel consumption make feasible substantial decreases in the cost and environmental impact simultaneously enhancing material performance. The benefits of resistant low-weight composites, compared to the usual metal-alloys, have led to the recent trend of increased use of the former with respect to the more traditional metallic components. The advent of carbon-fiber composites has been primarily driven by the need to reduce structural weight and hence cost and environmental impact (a reduction of 1 kg of saved fuel equates to a reduction of 3.15 kg of CO_2 emissions) (Scelsi et al., 2011). Furthermore, the high specific strength and stiffness, and corrosion and fatigue resistance of carbon-fiber composite materials make them highly suitable for lightweight aerostructures. At the same time, several drawbacks of these materials prohibit their use to the extent where instead their full potential could be exploited. In this regard, strong limitations are due to the impossibility of current aeronautical materials to satisfy special needs able to meet the high standards and fulfil the requirements in this field (Larsson, 2002). In service condition, in fact, aircraft materials can be subjected to atmospheric hazards (lightning, icing, heavy precipitation, hail, etc.) and/or adverse environmental conditions (strong humidity, wide temperature variations, etc.) (Petrov et al., 2008). Functional nanocomposites can be designed to possess attributes beyond the basic strength and stiffness that typically drive the science and engineering of the material for structural systems. For instance, currently rotor blades for wind energy turbines and aeronautical components (fuselage, wings, etc.) are usually made of glass-fiber or carbon-fiber reinforced resins which are insulating materials. To head off the remarkable risk of a puncture of structural parts, during a lightening event, or in general to optimize optical, electromagnetic and mechanical properties of the formulation, higher electrical and thermal conductivities are required. These properties must be imparted without additional weight and preserving the corrosion resistance typical of composite material (e.g without high concentration of metallic particles or metallic skins on the panels etc.).

Very low amounts of electrical conductive nanoparticles embedded in epoxy resin, or introduced between-lamina interfaces, can help for example to address limitations related to the electrical and thermal insulating properties which negatively impact on the design of anti-lightning properties, anti-icing systems and thermal dissipation phenomena (Kotsilkova et al., 2015, Yasmin and Daniel, 2004, Zhou et al., 2008, Guadagno et al., 2014b, Guadagno et al., 2011). Furthermore, water transport properties, such as diffusion and sorption of water in aeronautical resins must be driven towards the smallest possible values. It is well known, in fact, that water vapor absorption decreases the performance of aircraft materials for the adverse effects on the physico-mechanical properties, corrosion and weight. Data concerning the effect of water absorption on the mechanical properties of epoxy resins show a dramatic lowering of the glass transition temperature (T_g) and the consequent degradation of high-temperature properties. Petherick et al. proposed that this depression of T_g is caused by disruption of the strong hydrogen bonds in the cured network, and their replacement with weaker water-related hydrogen bonds (Sarti and Apicella, 1980). In the field of structural materials for aircraft/aerospace applications more work has been done on the moisture content of the resin TetraGlycidyl-MethyleneDiAniline (TGMDA), cured with 4,4'-diaminodiphenyl sulfone (DDS) for its properties which allow higher operating temperatures maintaining the mechanical performance. Despite these excellent properties, in many cases the more common bifunctional epoxy precursor DGEBA is used because the water content absorbed by epoxy resins based on TGMDA is reported to be higher than DGEBA and other common epoxy resins applied as structural resins. In fact, TGMDA/DDS systems are reported to absorb as much as 6.5 wt% water; Liu et al. reported for this system a value of 7.76% (at 23°C) (Liu et al., 2005) and Li et al. the value of 6.48% (at 35°C) (Li et al., 2009). A higher water content results in a dramatic drop in T_g (Thomas and Windle, 1980, Sarti, 1979). In this paper, a nanofilled epoxy resin, able to overcome criticalities related to insulating properties and based on TGMDA/DDS system characterized by a low moisture content, is described. The use of a reactive diluent diluent, 1,4-butandiol diglycidyl ether (BDE), inside the unfilled and nanofilled epoxy precursor based on TGMDA has proven to be of benefit for decreasing the viscosity of the epoxy matrix (Nobile et al., 2015, Guadagno et al., 2015c). This decrease is particularly advantageous for thermosetting resins filled with nanoparticles which tend to dramatically increase the viscosity of the resin (Guadagno et al., 2015b, Guadagno et al., 2014b). Furthermore, the appropriate choice of the amount of hardening agent can reduce the moisture absorbed in the epoxy matrix giving low values in the equilibrium concentration of water (C_{eq}) also after conditioning the samples at 120°C under vacuum for 24 hours. This last experimental procedure has proven to be

very effective to remove also the bonded water in the molecular structure. Experimental results highlight that the chemical structure of the formulated epoxy mixture (using a non-stoichiometric amount of hardener) manifests peculiar properties with respect to the water sorption due to a strong reduction in the number of polar groups and sites able to bond water molecules in the case of nanofilled formulations. MWCNTs, CNFs and graphene-based nanoparticles (CpEG) have been embedded into the epoxy formulation and the effect of nanofillers on the water transport properties and mechanical performance has been investigated.
Combined advantages originated by suitable carbon based nanoparticles and phase composition of the resin can open potential perspectives of the formulated nanocomposites in the field of specific structural applications. In this paper, the interrelated nature of aspects concerning the moisture transport in unfilled and nanofilled amine-cured epoxy resin is studied and discussed.

4.2 Materials and Sample preparation

The epoxy matrix was prepared by mixing the epoxy precursor, tetraglycidylmethylenedianiline (TGMDA) (epoxy equivalent weight 117–133 g/eq), with an epoxy reactive monomer 1-4 butanedioldiglycidyl ether (BDE) that acts as a reactive diluent. The curing agent used for this study is 4,4-diaminodiphenyl sulfone (DDS). The epoxy mixture was obtained by mixing TGMDA with BDE monomer at a concentration of 80%:20% (by wt) epoxide to diluent. The curing agent was added at stoichiometric and non-stoichiometric amount with respect to the epoxy rings (TGMDA and BDE). The sample hardened with a stoichiometric amount of DDS without reactive diluent is named TGMDA+DDS, whereas the sample with reactive diluent is named TGMDA/BDE+DDS. For the samples where hardener agent was added at non-stoichiometric ratios of amine/epoxy, DDS at 44.4 phr was used. This resin was named TGMDA/BDE+DDS(NS).
The reactive diluent has proven to be beneficial for improving the curing degree of nanofilled epoxy mixtures. It increases the mobility of reactive groups resulting in a higher cure degree than the epoxy precursor alone (Guadagno et al., 2014b) This effect is particularly advantageous for resins filled with nanoparticles where higher temperature treatments are needed, compared to the unfilled resin, to reach the same cure degree.
In this study, as nanofiller, different carbon nanostructured particles, MWCNTs, CNFs, CpEG were embedded in the epoxy matrix with the aim of improving other physical properties of the resin. It is well known from the literature that different nanostructured forms of carbon can be employed to impart functional properties to the hosting polymeric matrix or can be dispersed in the polymer as mechanical reinforcements. Currently, carbon

nanofillers are obtained using several methods resulting in different morphological features, structures and functionalization nature. A thorough knowledge of the correlations between structural/morphological characterization and nanofiller/hosting matrix properties necessarily requires a laborious and accurate analysis. Data here shown are discussed also in light of previous publications (Guadagno et al., 2015a, Guadagno et al., 2013, Guadagno et al., 2011) in which a deep analysis of the nanofiller properties and the role of the structural parameters and functionalization nature on the properties of the resulting nanocomposites have been investigated; so the reader is referred to the previous articles for the detailed characterization. The MWCNTs (3100 Grade) were purchased from Nanocyl S.A. Transmission electron microscopy (TEM) investigation has shown for MWCNTs an outer diameter ranging from 10 to 30 nm. The length of MWCNTs is from hundreds of nanometers to some micrometer. The number of walls varies from 4 to 20 in most nanotubes. The specific surface area of MWCNTs determined with the Brunauer–Emmett–Teller (BET) method is around 250-300 m^2/g; the carbon purity is > 95% with a metal oxide impurity <5% as it results by thermogravimetric analysis. CNFs in the form of powders used in this study were produced at Applied Sciences Inc. and were from the Pyrograf III family. The as-received CNFs used in this study are labelled as PR25XTPS1100 where XT indicates the debulked form of the PR25 family, PS indicates the grade produced by pyrolytically stripping the as-produced fiber to remove polyaromatic hydrocarbons from the fiber surface and 1100 is the temperature in the process production. The PR25XTPS1100 carbon nanofibers were heat-treated to 2500°C to provide the best combination of mechanical and electrical properties (Guadagno et al., 2013). The CNFs obtained by heat treatment at T=2500°C are here named CNFs. The heat treatment was performed in an atmosphere controlled batch furnace. Approximately 300 g of nanofibers were placed in a ceramic crucible for the heat treatment. The furnace was purged with nitrogen gas for 1 h prior to heating. The sample of graphene-based nanoparticles consists of carboxylated partially exfoliated graphite (CpEG). It has been prepared with the aim to achieve consistent comprehension about the water transport properties of resins filled with graphene-based nanoparticles. This sample was prepared as follows: a mixture containing nitric and sulphuric acid and natural graphite was used. After 24 h of reaction, intercalation within graphene sheets took place to form intercalated graphite compound. Then the mixture was filtered, washed with water, and dried in an oven at low temperatures. The intercalated graphite compound was subjected to sudden heat treatment temperature of 900°C and rapid expansion then occurred. The expansion ratio was as high as 300 times. Changes in the degree of exfoliation were obtained by varying the resident time in the fluidized bed as the time increases, the trapped intercalate and/or gases would have a second the chance

to escape causing further expansion and exfoliation. In this paper, a sample characterized by a degree of exfoliated phase of 60% was used.
The considered filler has a two dimensional (2D) predominant shape and it is obtained with an exfoliation procedure from natural graphite, that leads to obtain 2D conductive particles with an average diameter of 500 μm (Guadagno et al., 2015a). Epoxy blend and DDS were mixed at 120°C and the nanofillers were added and incorporated into the matrix via ultrasonication for 20 min. An ultrasonic device, Hielscher model UP200S (200 W, 24 kHz) was used. The epoxy mixture TGMDA/BDE+DDS was filled with nanofillers at two different concentrations (0.5% and 1% by wt). These nanofiller concentrations were chosen because the curves of dc volume conductivity vs. nanofiller concentration highlighted that the nanofilled samples were beyond the electrical percolation threshold (EPT) (Guadagno et al., 2015a, Guadagno et al., 2013, Sarti, 1979). All the unfilled and filled epoxy mixtures were cured at 125°C for 1 h and 200°C for 3 h. In this paper, composites with MWCNTs, CNFs and CpEG are named X (type of nanofiller) (NS), where X represents the nanofiller percentage. As example 0.5%CpEG (NS) is the epoxy mixture TGMDA /BDE+DDS(NS) filled with CpEG nanofiller at 0.5% concentration w/w%. Similary 0.5% CpEG is the epoxy mixture TGMDA /BDE+DDS filled with CpEG nanofiller at 0.5% concentration w/w%.

4.3 Characterization

4.3.1 Transport Properties

The fully cured epoxy resin samples have been cut into samples with dimensions of 40×20×0.50 mm^3 immediately after the curing cycle. The thickness of the water absorption test samples was made small, deliberately, compared to its width and length, such as edge effects could be ignored and simple one-dimensional diffusion model analysis can be applied without incurring significant error. After conditioning samples at 120°C under vacuum for 24 hours to ensure complete dryness, the specimens were placed into distilled water chambers maintained at constant temperatures of 25°C. This methodology has been selected after different mechanical tests, which have proven that the drastic treatment at 120°C under vacuum for 24 hours is able to remove all the water in the resin (including bound water). This also causes the disappearance of the peak related to the presence of bound water in the dynamic mechanical spectrum.
The specimens were weighed periodically using a digital balance with 0.01 mg resolution to determine the percent weight change, and, thus, water uptake. The water gain percentage, C_t %, was determined from the equation 1:

$$C_t = \frac{W_t - W_d}{W_t} * 100 \quad (1)$$

In eq.1, W_t is the weight of the water-sorbed epoxy specimen at t time and W_d is the initial weight of the dry specimen. The equilibrium concentration of water C_{eq} was calculated considering the maximum amount of absorbed water (plateau condition in Figure 4.1).
The specimens were periodically removed, dried and immediately weighed, and then returned to the water bath. The step of drying is performed to ensure the removal of excessive surface (superficial) water, specimens were gently wiped dry using clean, lint-free tissue paper. The described absorption procedure yielded a series of water gain versus time curves (see Figures. 4.1-4.2).

4.3.2 SEM Analysis

Micrographs of the epoxy nanocomposites based on the carbon nanofillers CNTs, CNFs and CpEG were obtained using SEM (mod. LEO 1525, Carl Zeiss SMT AG, Oberkochen, Germany). All the samples were placed on a carbon tab previously stuck to an aluminium stub (Agar Scientific, Stansted, UK) and were covered with a 250 Å-thick gold film using a sputter coater (Agar mod. 108 A). Nanofilled sample sections were cut from solid samples by a sledge microtome. These slices were etched before the observation by SEM. The etching reagent was prepared by stirring 1.0 g potassium permanganate in a solution mixture of 95 mL sulfuric acid (95–97%) and 48 mL orthophosphoric acid (85%). The filled resins were immersed into the fresh etching reagent at room temperature and held under agitation for 36 h. Subsequent washings were done using a cold mixture of two partsby volume of concentrated sulfuric acid and seven parts of water. Afterward the samples were washed again with 30% aqueous hydrogen peroxide to remove any manganese dioxide. The samples were finally washed with distilled water and kept under vacuum for 5 days before being subjected to morphological analysis.

4.3.3 Dynamic mechanical analysis

Dynamic mechanical properties of the samples were performed with a dynamic mechanical thermo-analyzer (Tritec 2000 DMA -Triton Technology). Solid samples with dimensions 2x10x 35 mm^3 were tested by applying a variable flexural deformation in three points bending mode. The displacement amplitude was set to 0.03 mm, whereas the measurements were

performed at the frequency of 1 Hz. The range of temperature was from -90°C to 315°C at the scanning rate of 3°C/min.

4.3.4 FT/IR analysis

FTIR spectra were obtained at a resolution of 2.0 cm^{-1} with a FTIR (BRUKER Vertex70) spectrometer equipped with deuterated triglycine sulfate (DTGS) detector and a KBr beam splitter, using KBr pellets. The frequency scale was internally calibrated to 0.01 cm^{-1} using a He−Ne laser. 32 scans were signal averaged to reduce the noise.

4.3.5 Electrical Properties

The electrical characterization of the nanocomposites focused on the DC volume conductivity was performed on disk shaped specimens of about 2 mm of thickness and 50 mm of diameter. In order to reduce possible effects due to surface roughness and to ensure an ohmic contact with the measuring electrodes, the samples were coated by using a silver paint with a thickness of about 50 μm and characterized by a surface resistivity of 0.001 Ω·cm. The measurement system, remotely controlled by the software LABVIEW®, is composed by a suitable shielded cell with temperature control, a multimeter Keithley 6517A with function of voltage generator (max ±1000V) and voltmeter (max ± 200 V) and an ammeter HP34401A (min current 0.1μA) for samples above the Electrical Percolation Threshold (EPT), whereas for those below EPT a multimeter Keithley 6517A with function of voltage generator (max ±1000V) and pico-ammeter (min current 0.1fA) is used.

4.4 Results and discussion

4.4.1 Characterization of the unfilled epoxy matrix: water transport properties

Figure 4.1 illustrates the curves reporting the data of water concentration vs. time for the unfilled epoxy mixtures for a water activity (a=1) at the temperature of 25°C. As described in the experimental section, the samples have been conditioned at 120°C under vacuum for 24 hours to ensure complete dryness and then the specimens were placed into distilled water chambers maintained at constant temperatures of 25°C. Formulations hardened using non-stoichiometric and stoichiometric amount of hardener agent (DDS) have been analysed. As described in the experimental section, in part of the formulations, DDS was added at a non-stoichiometric amount (80% by weight with respect to the stoichiometric amount) (acronym sample:

TGMDA/BDE+DDS(NS)). The sorption at equilibrium of liquid water (C_{eq}) decreases from 6.81 (TGMDA+DDS) to 5.76 for the sample TGMDA/BDE+DDS solidified in stoichiometric concentration of hardener and to 4.83 for the sample TGMDA/BDE+DDS(NS) solidified in non-stoichiometric condition. The resin reduces the value in Ceq from a minimum of 15% at a maximum of 30%.

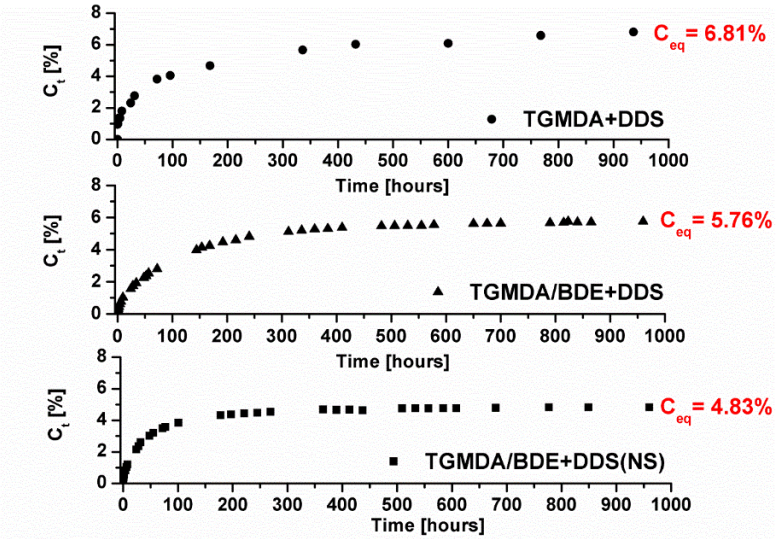

Figure 4. 1 *The concentration at time (C_t) as a function of the time (hours) of the epoxy resin (without BDE), and the epoxy mixture containing the diluent at stoichiometric and non-stoichiometric ratios of amine/epoxy.*

This percentage is very relevant for application of epoxy resins in aeronautics or other structural applications, because absorbed moisture reduces the matrix-dominated mechanical properties. Absorbed moisture also causes the matrix to swell. This swelling relieves locked-in thermal strains from elevated temperature curing. These strains can be large and large panels, fixed at their edges, can buckle due to the swelling strains. Furthermore, during freeze-thaw cycles, the absorbed moisture expands during freezing and can crack the matrix and, during thermal spikes, absorbed moisture can turn to steam. When the internal steam pressure exceeds the flatwise tensile strength of the composite, the laminate will delaminate. The epoxy mixture TGMDA/BDE+DDS(NS) hardened with a non-stoichiometric ratio of hardener, for which the most significant reduction in C_{eq} was observed, has been selected to prepare the nanocomposites filled with the chosen nanoparticles. Figure 4.2 illustrates the curves reporting the data of water concentration vs. time for the epoxy mixtures filled with MWCNTs, CNF

2500 and CpEG at two different concentrations. The experimental conditions are the same used to collect the data of Figure 4.1.

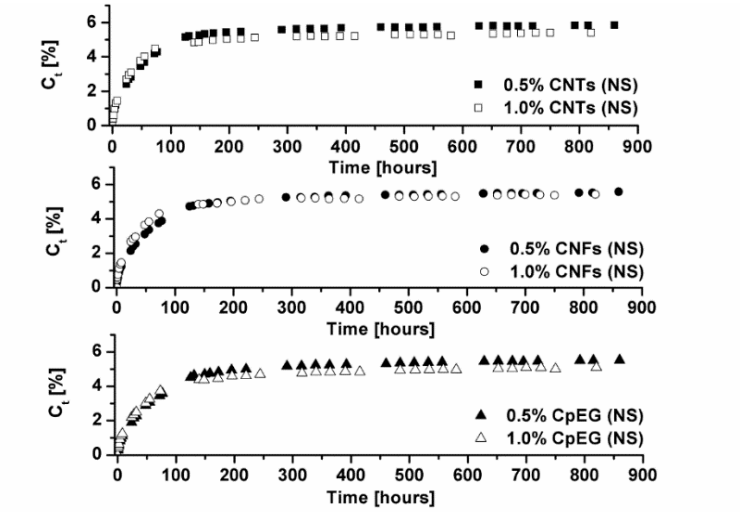

Figure 4. 2 *The concentration at time (C_t) as a function of the time (hours) of epoxy mixtures filled with MWCNTs, CNF 2500 and EC at 0.5 wt% and 1.0 wt%.*

Figure 4.3 shows the sorption values at equilibrium (C_{eq}) of liquid water of the different tested nanofilled resins.

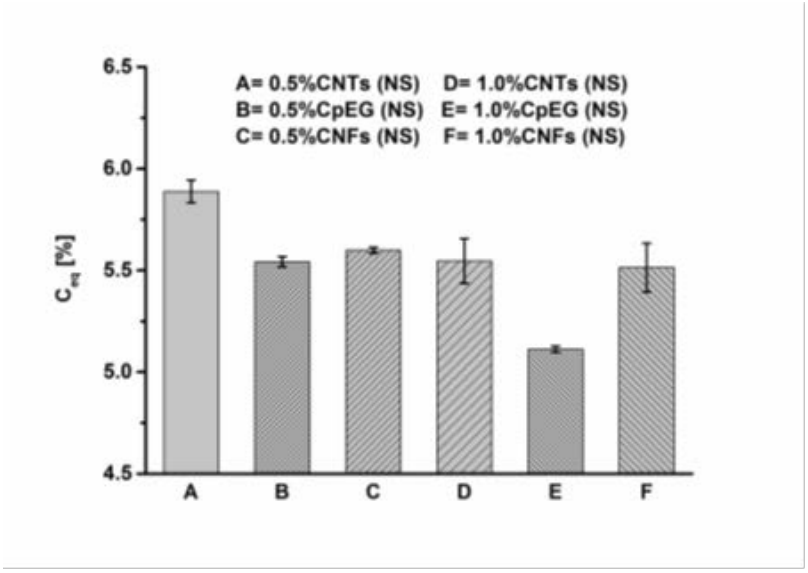

Figure 4. 3 *The sorption values at equilibrium (C_{eq}) of liquid water of the various tested nanofilled resins.*

The data highlight that, also at high water activity (a=1), the nanofilled samples having the same thickness are characterized by values of C_{eq} only slightly higher than the unfilled matrix. Hence, these data prove that advantages in the water transport properties can be combined with the better mechanical and electrical performance of the nanofilled formulations. It is also evident that for the same nanofiller, an increase in the nanofiller concentrations causes a decrease in sorption values. The best results are obtained using CpEG as nanofiller. It is worth noting that the structural and morphological analysis highlighted that this sample is composed by graphene layers and very thin graphitic blocks; it represent the best combination to optimize mechanical and electrical properties of nanofilled samples also with respect to graphene single layers (Guadagno et al., 2015a). This result evidences that the presence of graphene sheets and thin graphite blocks together with the nature of the epoxy matrix certainly create a synergistic effect that makes this sample especially suitable in the field of structural resins such as aeronautical, nautical and wind turbine materials. This beneficial effect can be exploited in addition to other very promising properties of graphene based materials (Guadagno et al., 2015d, Scherillo et al., 2014, Yan et al., 2014, Bunch et al., 2008, Dikin et al., 2007, Vietri et al., 2014, Blake et al., 2008, Kim et al., 2009, Eda et al., 2008, Geim and Novoselov, 2007, Guadagno et al., 2015a). In Figure 4.4, we observe a Fickian behavior, that is a linear dependence of the reduced sorption on square root of time, a curvature for $C_t/C_{eq} > 0.7$ and a constant value at equilibrium.

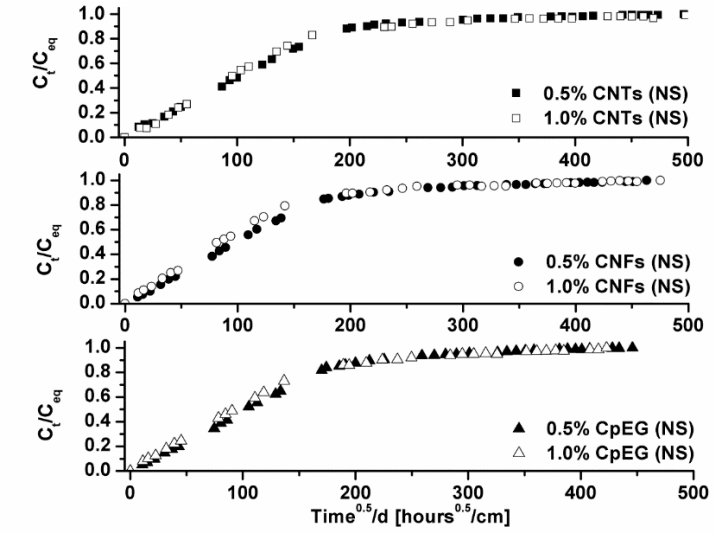

Figure 4. 4 *C_t/C_{eq} against the square root of time of the resin with 0.5% and 1.0% of MWCNTs, CNFs and CpEG.*

This Fickian behavior gives the possibility to derive the diffusion parameter, D, by the first linear part of the curve, by the eq. (2)

$$\frac{C_t}{C_{eq}} = \frac{4}{d}\left(\frac{Dt}{\pi}\right)^{\frac{1}{2}} \quad (2)$$

where C_{eq} is the equilibrium concentration of water, C_t the concentration at time t, d (cm) is the thickness of the sample, and D (cm^2/s) the mean diffusion coefficient. The diffusion parameter, D (cm^2s^{-1}), of the analysed samples, is shown in Table 4.1. The value of D is between $1.11x10^{-9}$ and $1.35x10^{-9}$ cm^2/s. It is evident that the diffusion of water molecules into the samples with different nanofillers follows the same curve. These results highlight that the small percentage of nanofiller (max 1%) has no effect on the Diffusion coefficient. If we compare the results related to the sample TGMDA/BDE+DDS with data reported for the TGMDA+DDS system (without BDE), we can note that a lower value of absorbed water is obtained for the epoxy mixture TGMDA/BDE+DDS(NS) and also for the nanofilled epoxy resins. This value is almost comparable with the value obtained for DGEBA cured with DDS in stoichiometric amount 4.03% or cured with a tertiary amine which leads to polyetherification by nucleophilic ring opening of oxirane ring originating a network with significant differences (Guadagno et al., 2009) compared with those obtained with primary amines as in the case of the present paper.

Table 4. 1 *The diffusion parameter, D (cm^2s^{-1}), of the analysed samples*

Samples	D (cm^2/s)
TGMDA/BDE+DDS (NS)	**1.39E-09 ± 4.94E-10**
0.5%CNTs (NS)	**1.25E-09 ±3.40E-11**
0.5%CpEG (NS)	**1.52E-09 ±2.60E-10**
0.5%CNFs (NS)	**1.31E-09 ±1.08E-10**
1.0%CNTs (NS)	**1.44E-09 ±5.45E-11**
1.0%CpEG (NS)	**1.36E-09 ±1.71E-10**
1.0%CNFs (NS	**1.83E-09 ±1.51E-10**

4.4.2 Morphological investigation of the carbon based epoxy nanocomposites

In order to analyze the homogeneity of the nanofiller dispersion in the polymeric matrix, morphological analysis by SEM was carried out on etched samples to remove the resin surrounding the nanofillers, leaving them bare. Figure 4.5 shows SEM images of the fracture surface of the three epoxy-based composites filled with 0.5 wt% loading of nanofillers (CNTs, CNFs and CpEG, respectively). The used etching procedure, reported in the experimental, mainly consumes the surface layers of the polymeric matrix. We observe that the same etching procedure seems to be more efficient for composites filled with CNTs and CNFs. In fact, in this case we observe whole lengths of the CNTs and CNFs segments released from the residual resin fraction, highlighting a homogeneous structure for both the samples, in which the nanofillers seems uniformly distributed in the epoxy matrix. The observation of the image in Figure 5 also highlights that only a few layers of graphene appear bare and clearly visible in the surface, emerging from the resin. This can be explained assuming that strong interconnections between CpEG particles and the residual polymeric matrix remain after the etching attack. Edge carboxylated graphene nanosheets by increasing the CpEG/ epoxy matrix interaction favor a more efficient load transfer and consequently determine a strong mechanical reinforcement in the elastic modulus as described in the following section related to the dynamic mechanical properties of the nanocomposites.

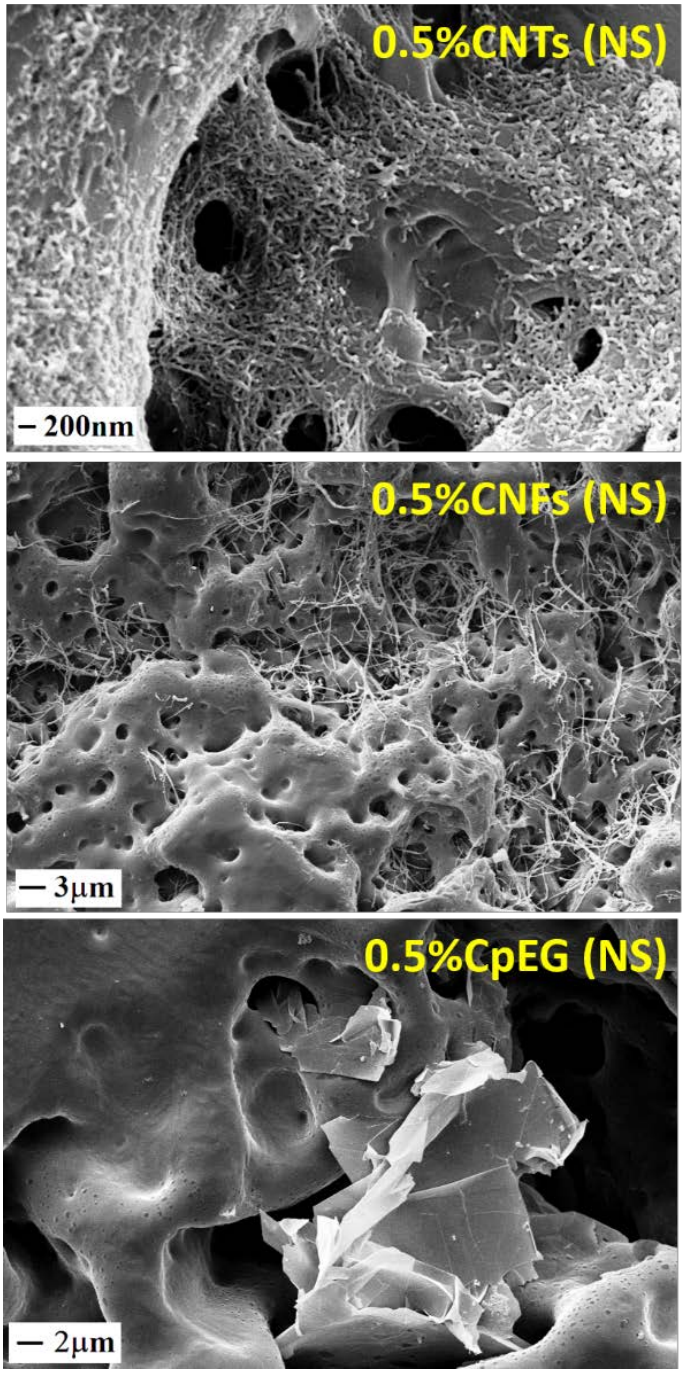

Figure 4. 5 *SEM images of the fracture surface of the three different epoxy nanocomposites with 0.5 wt% loading of nanofillers.*

4.4.3 Dynamic Mechanical Analysis (DMA)

In order to fully understand the influence of carbon nanofillers (CNTs, CNFs, CpEG) on the unfilled and nanofilled epoxy-amine resins hardened in stoichiometric and non-stoichiometric condition, dynamic mechanical analysis was performed. The storage modulus, E' (MPa), and the loss factor, tanδ, of the unfilled epoxy formulation, and the composites with a concentration of 0.5% by weight of nanoparticles are shown in Figures 4.6-4.7. All the samples show very high values of the storage modulus in the normal operational temperature range of structural materials; E' is higher than 2000 MPa in the very wide temperature range of -100 ÷ 100 °C. The profile of the curves in Figure 4.6 shows a slow and progressive decrease of E' up to 50°C, followed by an almost constant value in the range between 50 ÷ 200 °C before the principal drop, due to the glass transition temperature T_g which is evident between 200 ÷ 300 °C. The presence of the T_g in this range is also confirmed by the mechanical spectrum of the samples shown in Figure 4.7.

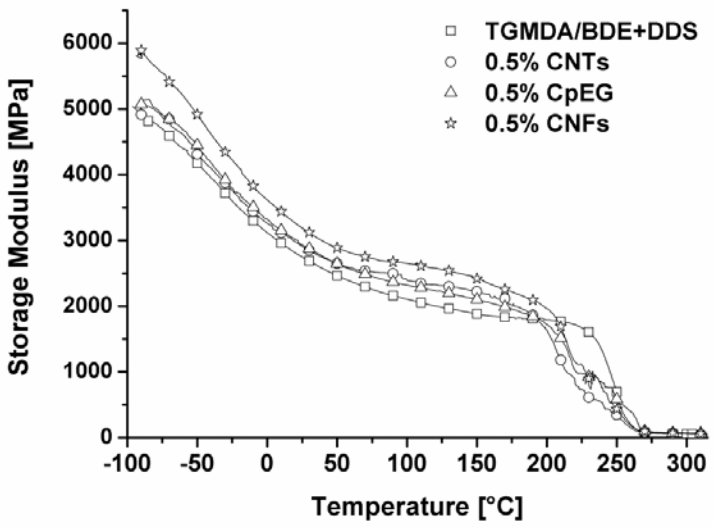

Figure 4. 6 *Storage modulus of the unfilled epoxy formulation (TGMDA/BDE+DDS) and epoxy formulations at loading rate of 0.5% by weight of a) MWCNTs (CNTs system), b) CpEG (CpEG system) and c) CNFs (CNFs system).*

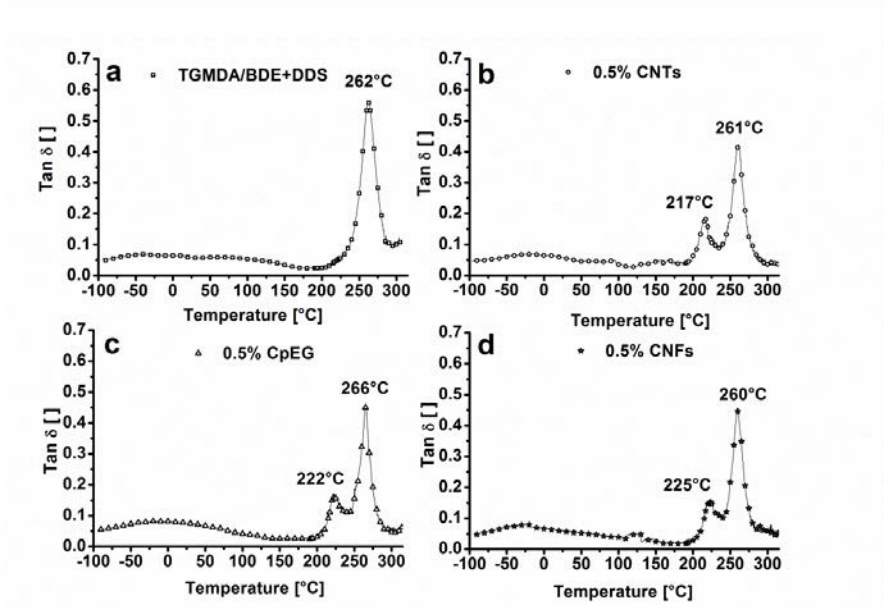

Figure 4. 7 *Loss factor (tan δ) of the unfilled epoxy formulation a) TGMDA/BDE+DDS and epoxy formulations at loading rate of 0.5% by weight of b) MWCNTs, c) CpEG and d) CNFs.*

In particular, the highest peak, which is associated with the sample's glass transition, or α transition, in the mechanical spectra is centred at 262°C for the unfilled sample, 261°C for the sample filled with CNTs, 260°C for the sample with CNFs and 266°C for the sample with CpEG. It is worth noting that for this type of nanofilled sample an increase in the activation energy E2 related to secondary amine-epoxy reaction was also found. This increase was ascribed to self-assembly structure generated by the edge-carboxylated layers of graphite nanoparticles inside the epoxy matrix in such a way to form architectures constituted of rigid nano-cages where the final curing reactions must be active under condition of more reduced mobility with respect to the conditions experimented by other mono-dimensional nanofillers (Vertuccio et al., 2015). To better understand the influence of the nanofiller on the α transition, and also to avoid confusing effects with the effect of hardener amount, a non-stoichiometric amount of hardener has been also employed to solidify the unfilled epoxy formulation before to draw conclusions on the nanocharged samples. Figure 4.8a shows the loss factor (tanδ) of the unfilled epoxy formulations TGMDA/BDE+DDS(NS) hardened with the chosen non-stoichiometric amount of DDS. The loss factor of the sample solidified in stoichiometric ratio of hardener is also shown for comparison. The intensity of the main transition, α transition, is affect by the stoichiometry and therefore

by the curing degree of the resin, furthermore samples hardened with non-stoichiometric amount exhibit two distinct peaks most likely due to fractions with different crosslinking density characterized by two different values of T_g (see Figure 4.8b). The more the peak at a lower T_g raises, the more the peak at a higher T_g decreases, suggesting that the two phases can coexist in the resin with different percentages depending on the stoichiometric amount of hardener. Furthermore, in the unfilled sample hardened in stoichiometric condition, the epoxide oxygen seems to be involved in a much more amount of crosslinking bonds, also limiting crankshaft rotation of the glycidyl crosslinking segments, on the contrary of what occurs in the sample cured in non-stoichiometric amount of DDS. In fact, is evident in Figure 8a that the other two weak transitions, the β transition (between -100 and 30 °C) and the γ transition (between 30 and 120 ÷140 °C) are much more pronounced. It has been suggested that the β transition can be due to crankshaft rotations of the glycidyl crosslinking segments (Pogany, 1970, May and Weir, 1962), it also represents stress relaxation which contributes the toughness of diamine-cured epoxy formulation. Whereas, unreacted molecular segments and/or material inhomogeneities from region of different crosslink density could be responsible for the γ transition. It is worth noting that the entity of the observed transitions is also dependent on the moisture content (see Figure 4.9) where the Loss factor (tanδ) and the storage modulus of the wet sample (immersed in water for 1000 hours before the DMA analysis) solidified in stoichiometric condition are shown together with the curves of the dray sample of Figure 4.8a. The moisture content shifts the main peak to lower temperatures (252°C) and causes the appearance of other two transition centred at 220°C and 180°C respectively. These transitions are strictly related to plasticization effects caused by absorbed water. For this reason, as described in the experimental part, all the samples under investigations have been conditioned at 120°C under vacuum for 24 hours before the DMA analysis. This condition has proven to be very effective to eliminate also bonded water molecules. The described treatment allows to simplify the understanding on the influence of the hardener ratio on the mechanical spectrum. This consideration has been also applied to the formulated nanocomposites.

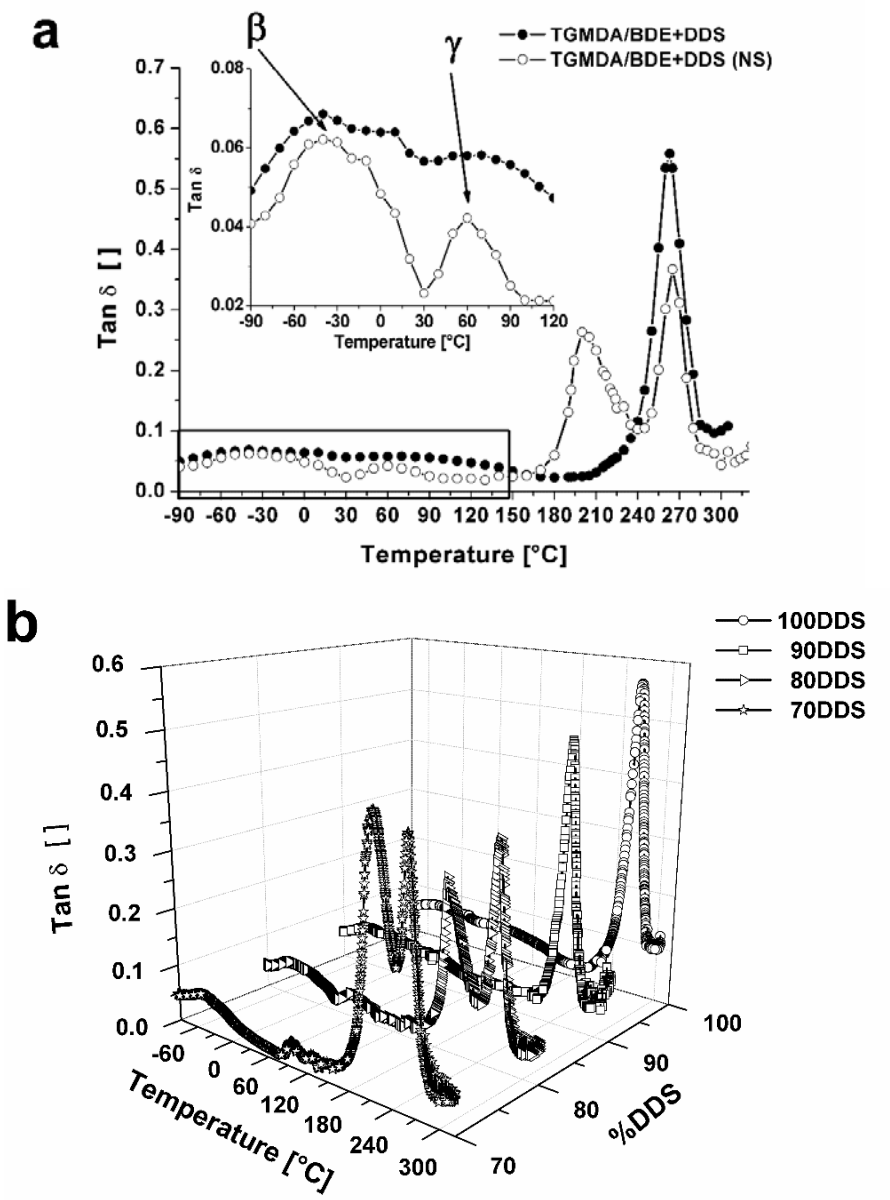

Figure 4. 8 *Loss factor (tanδ) of the unfilled epoxy formulation: a) stoichiometric system (TGMDA/BDE+DDS) and non-stoichiometric system (TGMDA/BDE+DDS(NS)); b) Loss factor (tanδ) of the unfilled epoxy formulations hardened with stoichiometric and different non-stoichiometric amounts of DDS.*

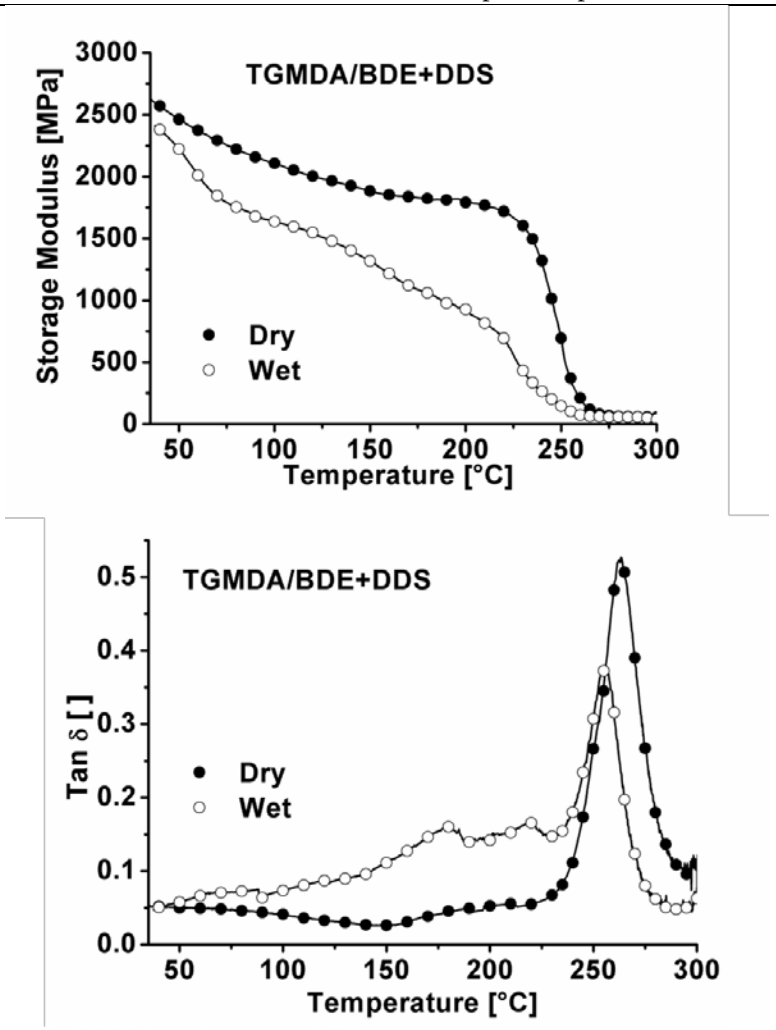

Figure 4. 9 *Loss factor (tanδ) and Storage Modulus of the Dry and Wet epoxy formulation hardened with a stoichiometric ratio of DDS (TGMDA/BDE+DDS).*

It is worth noting that for many papers reported in literature, a such drastic treatment has not been performed; hence the understanding of the effect the nanofiller on the mechanical spectrum is complicated by overlapping effects. To study the effect of nanofiller on the dynamic mechanical properties of the epoxy formulations; all the nanocomposites were analysed in completely dry conditions. Considering that all the nanocharged samples solidified in stoichiometric conditions have been cured using the same curing cycle, it is evident that the nanofiller exerts on the resin the same influence of a non-

stoichiometric amount of DDS. This behaviour is also confirmed by the data of Figure 4.10 which shows the reaction enthalpy and the curing degree for the unfilled and filled systems cured in stoichiometric conditions. The inclusion of the filler causes a decrease of the reaction enthalpy and the curing degree.

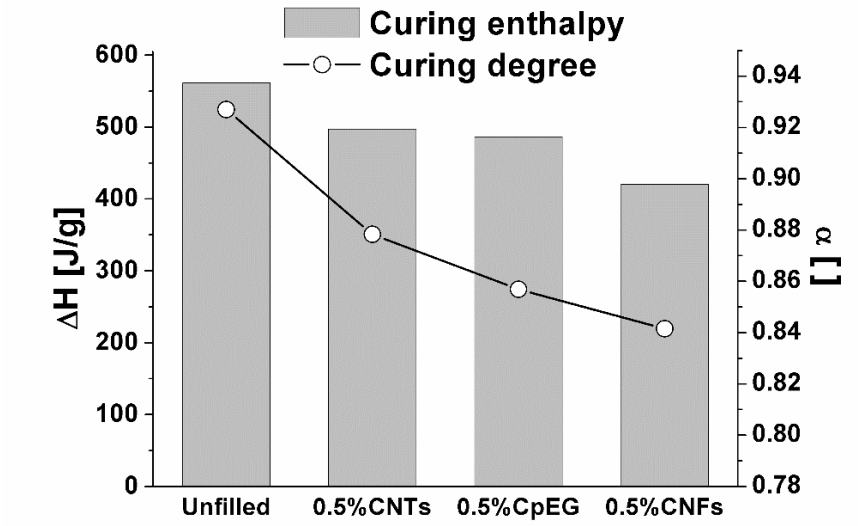

Figure 4. 10 *Reaction enthalpy and the curing degree of unfilled samples and filled samples (0.5% by weight of nanofiller).*

These results are most likely due to an interruption of the cross-linking reactions during the curing cycle. It is well known that this interruption leads to a change in the glass transition temperature (Zhou et al., 2009). In our case, the introduction of the filler into a tetra-functional epoxy precursor, does not determine a significant change in the main glass transition temperature (see Figure 4.7), but the formation of a fraction of the resin with a lower T_g. In fact, the transitions in the mechanical spectra at 217°C (CNTs), 222°C (CpEG) and 225°C (CNFs) represent a phase with greater mobility of chain segments, most probably closely linked to the filler. The increased mobility allows a better transfer of load on the filler, as shown by the value of storage modulus (see Figure 4.6) which is comparable or higher than the unfilled resin. All the analysed nanofillers are responsible for forming in the resin this second phase characterized by different crosslinking density with different values of T_g depending on the nanofiller nature. In this regard, it can be noticed that the value of the T_g at higher temperature is 260/261, almost the same, for the samples filled with CNT and CNFs, whereas for the sample with CpEG this value is 266°C. This increase could be due to the nature of the functionalized

graphene-based nanoparticles. For this type of nanoparticles, it has been proved that, due to the high exfoliation degree and the role of edge-carboxylated graphite layers, the nanoparticles are able to give self-assembled structures embedded in the polymeric matrix (Guadagno et al., 2015a). In this last paper, it has been proven that graphene layers inside the matrix may serve as building blocks which may hinder the chain mobility resulting in a higher T_g (main transition). It is worth noting that this increase in T_g cannot be caused by a higher curing degree because as described before, the inclusion of all filler causes a lack of homogeneity in the cross-linking density with a lower curing degree (see Figure 4.10). The effect of the filler on many mechanical parameters of the nanocharged polymers is hard to understand in light of different data in literature. Carbon nanoparticles are widely used as a reinforcing agent in epoxy resins for improving their mechanical, thermal and electrical properties. It is well known that the addition of carbon nanoparticles into the resin matrix can dramatically change its hardness, tensile strength, elastic modulus and electrical conductivity (Allaoui et al., 2002). Specifically, the effects of the nanofillers in polymer composites on the glass transition (T_g) and on the relaxation behaviour of the polymer matrix have been studied for different filled resin composites. However, the remarks on T_g variation are controversial as in some cases an increase in T_g with filler content is reported in the literature (Allaoui and El Bounia, 2009), yet the opposite result is possible as well. Furthermore, the variation of T_g as a function of filler content in epoxy nanocomposites shows an initial decrease up to a certain content value followed by an increase at higher filler loading. A coherent picture among all data described in literature is almost impossible due to significant changes in the amount of components, in the nature of hardener, epoxy precursor and nanofiller, and most of all in the curing cycles and dispersion methods adopted by different authors. Furthermore, the entity of the nanofiller reinforcing effect was also found to be strongly dependent on the nature of the epoxy formulation (Guadagno et al., 2009, Guadagno et al., 2011). Therefore, the actual effect of the filler on the T_g necessitates further clarification. In general, the amount, the dispersion and the surface characteristics of the nanoparticles were found to play an important role in the variation of T_g and the mechanical properties of the nanocomposites. In epoxy nanocomposites and generally in thermoset nanocomposites there is an additional difficulty with respect to the thermoplastic nanocomposites. In particular, the curing conditions of the nanocomposites and related results are different from those of the pure epoxy probably due to the effect of the nanoparticles on the crosslinking mechanisms. In the present work, the effect of the nanofiller on T_g and storage modulus has been analyzed by choosing the appropriate conditions/parameters to keep constant: matrix nature, ratio of epoxy precursor/ hardener, curing cycles and studied/controlled treatments to avoid

the presence of free and bound water molecules in the matrix, which can also be responsible of changes in the mechanical parameters. The DMA curves of Figures 4.6-4.7 show that the introduction of the filler (in completely dry samples) increases the storage modulus of few hundred MPa, in the range from room temperature to 200°C, for the CpEG and the CNTs system, around a thousand of MPa, in the range of temperature from -90 to 200°C for the CNFs system for the same amount of nanoparticles. For all the filled systems a new glass transition is obtained at lower temperatures. The height and width of the peaks in tan delta spectra provide additional information about the relaxation behaviour of these samples. The height of the main peak at 262°C for the neat resin has a value 0.60, while for the nanocomposites, it varies between 0.4 and 0.45. This implies that the nanocomposites exhibit more elastic behaviour than the neat resin. The change in the width of the peak at higher temperature suggests a narrow distribution of relaxation times for the resin filled with nanoparticles, presumably due to a phase segregation of the more cured resin at high crosslinking density from the domains where nanoparticle/polymer interactions are relevant, and hence different and lower mobility is expected for this second phase at lower T_g. This indicates, at a first glance, the existence of at least two underlying mechanisms of alfa-relaxation. The first mechanism (higher T_g) is caused by the reaction of the crosslinking agent with the epoxy groups giving rise to the dominant alfa-relaxation, while the second one appears as a result of the filler's effect on the curing reaction. The formation of a few nm thick intermediate layer on the resin-filler interface, probably occurs before the full cure of the composite, thereby inducing the growth of the secondary peak at lower T_g. On the other hand, due to the impossibility to extend the tri-dimensional network in the space filled by the nanoparticles, a more mobile phase also composed of network segments polymerized by chain extension is expected in the zones around the nanofiller surfaces.

Concerning the effect of the nanofiller on the resin hardened in non-stoichiometric conditions, a synergism between nanofiller effect and low DDS level is observed. Figure 4.11 shows the storage modulus (a, c and e) and the loss factor (tanδ) (b, d, f) of the unfilled epoxy formulation TGMDA/BDE+DDS(NS) and epoxy formulations at loading rate of 0.5% and 1% by weight of: MWCNTs (CNTs system), CpEG (CpEG system) and CNFs (CNFs system).

In Figure 4.11, the non-stoichiometric systems are considered for two different percentages of nanoparticles to understand the effect of the filler concentration.

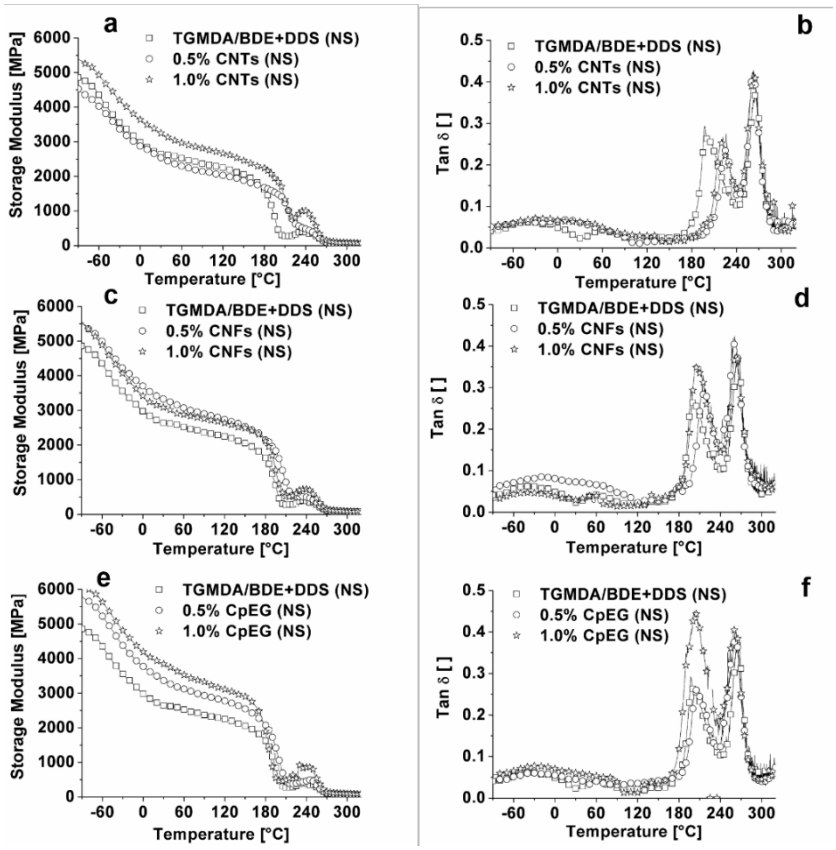

Figure 4. 11 *Storage modulus (a, c and e) and the loss factor (tanδ) (b, d, f) of the unfilled epoxy formulation TGMDA/BDE+DDS(NS) and epoxy formulations at loading rate of 0.5% and 1% by weight of: MWCNTs (CNTs system), CpEG (CpEG system) and CNFs (CNFs system) hardened in no-stoichiometric condition.*

It can be observed that, compared with the sample in Figure 4.7, the height of the peak corresponding to the lower T_g is relevant, because the inclusion of nanofiller and the non-stoichiometric amount of hardener cause the same effects. Furthermore, wide and temperature of this peak is strongly dependent on the amount and nature of the filler. In the sample filled with 1% by weight of CpEG, the entity of this peak is more relevant with respect to the peak at higher T_g (see Figure 4.11f), and correspondingly a strong reinforcement effect is observed in the storage modulus (see Figure 4.11e). The higher amount of nanofiller (1%) with respect to the amount of 0.5% also causes a noticeable broadening of the peak highlighting that many of the mechanical properties of the material (damping effect, toughness, flexibility etc.) are

completely different from the unfilled sample. A reinforcing effect is observed for all the nanofillers (except for MWCNTs at lower concentration of filler), and the more reinforcing effect is observed for CpEG. It is worth noting that, in the resin filled with CpEG, the carboxylated groups on the edges of graphene/graphitic blocks strongly interact with the layer at lower T_g, also forming resin cured with different mechanisms due to the effect of carboxylated groups on the curing mechanisms of the resin. Nanofiller functionalization can provide superb polymer–particle interactions which are very effective for improving the mechanical characteristics, but at same time may worsen electrical conductivity of the nanofilled polymer as it occurs for functionalized CNFs (without graphitization treatment at 2500°C) (Guadagno et al., 2013). In the nanocomposites filled with CpEG nanoparticles, we get a significant advancement on these two fronts simultaneously and on the transport properties of the nanocomposite. These simultaneous enhancements in the different properties are most likely due to the same effect already described in a previous paper (Guadagno et al., 2015a). In particular, self-assembly mechanisms determined by attractive interactions based on hydrogen bonding between edge-carboxylated graphitic blocks, were found. The presence of very thin graphitic block self-assembled along the samples is able to increase mechanical and electrical properties, but also able to further reduce the moisture content. Another important consideration concerns the interaction of CNTs with the epoxy matrix; even if the sample of CNT ((3100 Grade) was known (from Nanocyl S.A.) as non-functionalized filler; the Raman and FT/IR spectra (Guadagno et al., 2011) do not correspond to carbon nanotube surfaces completely devoid of functional groups on the walls. This causes a non-negligible reinforcing effect (see storage modulus of the unfilled and filled samples in Figure 4.11a) most of all at concentration of filler higher than 0.5 by weight.

Fortunately, many data already described in literature can be used to understand the observed behaviors. In fact, although epoxy resins can be cured with different families of hardeners, most studies so far performed have been devoted to different aspects related to epoxy resins cured with amine curing agents. In cured epoxies, the three dimensional molecular structure determines the glass transition temperature and, as consequence, many physical properties of the material. In turn, the molecular network structure depends on the chosen pre-polymers, the curing agents nature, the stoichiometric ratio, the cure cycle and the advance of cross-linking reaction as well. Changes in network structure invariably cause modifications in chemical, physical and mechanical properties of the material. Therefore, while it is of the utmost importance to establish a set of correlations between the chemistry, the processing and the physical properties, this task results of a formidable difficulty and many parameters have to be fixed to investigate just one aspect of the problem. In particular, from the chemical point of view, it is well known that the cure

reactions of epoxy resins are very complex because many reactive processes simultaneously occur; furthermore other events, such as gelation and vitrification phenomena, the autocatalytic effect in the early stages of curing, and the change from chemical control to diffusion control in the later stages of curing, can complicate the analysis. The cross-linking reactions between epoxy pre-polymers and amine hardeners generally involve the opening of the epoxy ring by reaction with amine hydrogen or with the formed hydroxyl (etherification reaction), as shown in Figure 4.12.

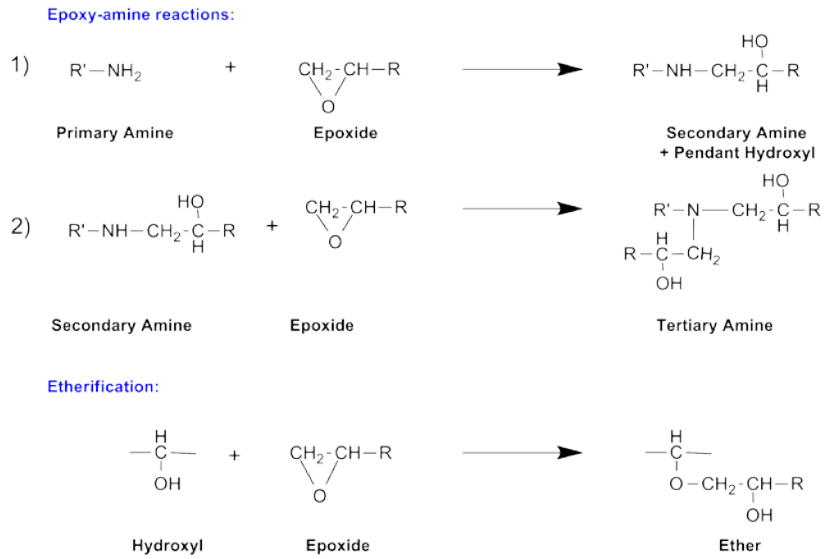

Figure 4. 12 *Scheme of cross-linking reactions between epoxy pre-polymers and amine hardeners*

This scheme consists in: 1) primary amine addition; 2) secondary amine addition; 3) etherification. The intensive cross-linking occurring in the region between the above transitions reduces molecular mobility, and the cure changes from a kinetic to a diffusion regime. The etherification reaction can occur between a hydroxyl group formed in the first stage, and an epoxy to form an ether link. This etherification reaction can also occur with the catalytic effect of a tertiary amine or other additives in the cure mixture, and in this case, it is called homo-polymerization, not giving a network but a linear polymer. In this paper, to simplify the complexity of the different systems and better understand the effect of the different fillers, the competition between the possible paths of the cure reaction has been firstly studied by varying the stoichiometric ratio between epoxy and amine hardeners using the same epoxy formulation and curing cycle. Indeed, it has been recognized that a variation of the stoichiometric ratio of epoxy to curing agent can have a significant

effect on the final mechanical properties of the cured resin, and therefore this is one of the most important aspect to be taken into account before considering the effect of the nanofillers. In conclusion, a very important result of this investigation is that the filler tends to create a phase with increased mobility of the chains, segmental parts of the epoxy network around the filler which causes an increase in the more mobile phase (which is also caused by defect of hardener). In fact, the transition at lower temperature can represent chain segments partially cured or chain segments obtained by etherification reactions between functional groups of the filler and epoxy precursors. These kinds of reactions are also expected in unfilled samples cured with non-stoichiometric amount of hardener. In this case, the etherification reaction is expect to be more relevant with respect to the samples cured using a stoichiometric amount of hardener. Considering the effect of high epoxy/amine ratios compared to the stoichiometric system, both phenomena occur in the nanofilled formulations containing embedded CNTs and most of all CpEG. The etherification reactions between functional groups on the nanofiller surface and the epoxy resin determine a reinforcing effect of the nanofiller because the load is better transferred to the high strength nanofiller. This is reflected in the increase of the storage modulus, whereas the etherification reactions inside the epoxy resin, non-involving the nanofiller, determine a decrease in the storage modulus. Of course, these effects are balanced in nanofilled epoxy mixture cured in no-stoichiometric conditions.

4.4.4 FTIR Analysis

Figure 4.13 shows the FT/IR spectra of the unfilled epoxy formulations hardened with non-stoichiometric amount of DDS in two different spectral ranges: a) range 3700-2700 cm^{-1}, b) range 1700-400 cm^{-1}. The reactions 1) and 2) of the scheme in Figure 4.12, namely primary amine addition and secondary amine addition are completed for all the samples, also for the sample hardened with a stoichiometric amount of DDS (TGMDA/BDE+DDS). In fact, no N-H signals are observed in all spectra shown in Figure 4.13a. In particular, primary amines for which two weak absorption bands (N-H stretching vibrations), one at 3471 cm^{-1} and the other near 3373 cm^{-1} are expected, are completely absent. The absence of these bands indicates that no “free” asymmetrical and symmetrical N-H stretching modes are active in the samples. Also the band at 3240 cm^{-1} which is the Fermi resonance band with overtone of the band at 1617 cm^{-1} related to the N-H bend (scissoring) is absent. Secondary amines show a single weak band in the 3350-3310 cm^{-1} region. The absence of this last signal also proves the completion of the secondary amine addition. In the region between 3000 and 3750 cm^{-1},

the spectra only show the O-H stretching vibration with a typical profile of stretching modes involved in intermolecular hydrogen bonding.

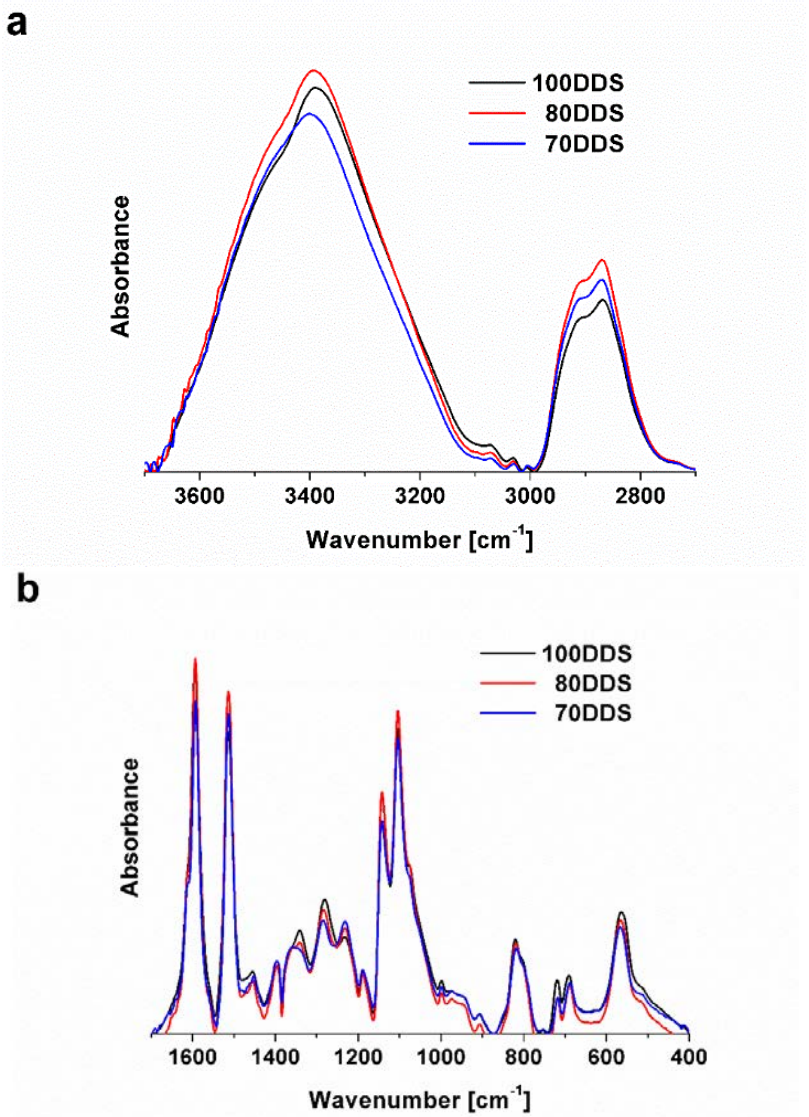

Figure 4. 13 *FT/IR spectra of the unfilled epoxy formulations hardened with non-stoichiometric amount of DDS in two different spectral ranges: a) range 3700-2700 cm^{-1}, b) range 1700-400 cm^{-1}.*

Figure 4.14 shows an enlargment of the spectra in the region between 1150-1400 cm^{-1} where the most significant changes of the spectra can be observed.

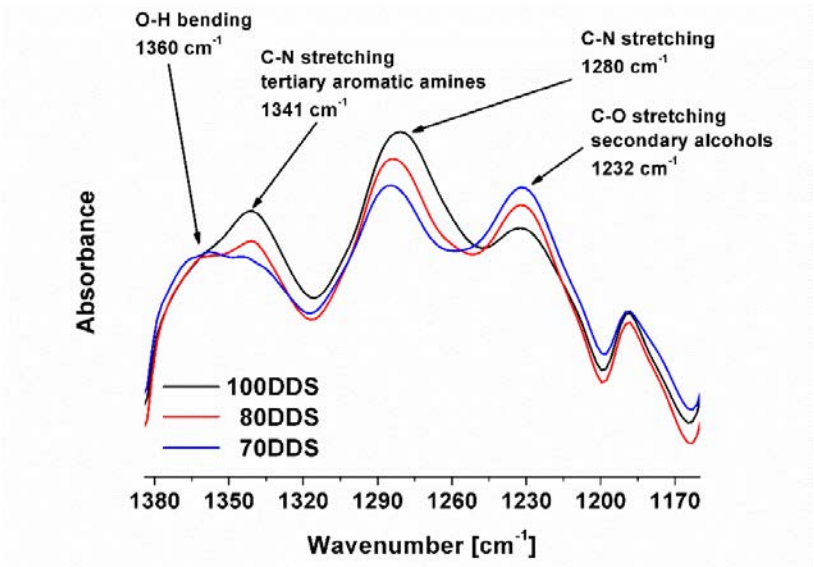

Figure 4. 14 *FT/IR spectra in the range 1150-1450 cm^{-1} of the unfilled epoxy formulations hardened with stoichiometric and non-stoichiometric amount of DDS.*

In the range 1310-1360 cm^{-1}, the C-N stretch at 1341 cm^{-1} of tertiary aromatic amines are visible for all the samples. This signal is higher and well-defined in the sample solidified in stoichiometry condition. It overlaps with the asymmetric SO_2 stretching (DDS) between 1300-1350 cm^{-1}. This last signal is expected to be less intense for the sample 70DDS and 80DDS with respect to the sample solidified in stoichiometric condition of hardener (100 DDS). The signal of the O-H bending vibration centered at 1360 cm^{-1} seems to be more relevant for the samples solidified in non-stoichiometric condition due to the decrease C-N stretch signal at 1341 cm^{-1}. A similar effect is observed for the peaks at 1232 cm^{-1} due to C-O stretching vibration of secondary alcohols. They seem more intense for the samples 80DDS and 70DDS with respect to the sample TGMDA/BDE+DDS because the band at 1280 cm^{-1} is less intense in the samples 80DDS and 70DDS.
In light of these spectroscopic results and studies already available from the literature, we can explain the low moisture content of samples hardened in non-stoichiometric conditions. A careful study of the molecular mechanisms of moisture transport in epoxy resins was performed by Christopher L. Soles et al. which developed a plausible molecular picture of the diffusion process (Soles and Yee, 2000). In their analysis, the topology, polarity, and molecular motions combine to control transport. In particular, the polarity of the resin is of relevant importance in determining the equilibrium concentration of water. They observed that less polar resins (non-amine series), absorb a little amount

of water compared to the resins hardened with amines. It is worth noting that the intrinsic hole volume elements, active in the water transport, are localized at the crosslink junctions, which are also the locations of the polar hydroxyls and amines. The polar hydroxyls determine intersegmental and intrasegmental N---HO hydrogen bonds allowing water molecules to interact with the amine and hydroxyl groups. This type of interaction blocks the involved nanopores (hole volume elements) and impedes the water transport. In our case, even if the epoxy systems are solidified with the same hardener, a smaller number of nitrogen atoms, responsible of polar sites, are present in the resin solidified in non-stoichiometric conditions as highlighted by FT/IR analysis. Figure 4.15 shows the FTIR spectra of the samples solidified in non-stoichiometric condition containing embedded three types of nanofillers, in two different spectral ranges: a) 4000-500 cm^{-1} and b) 1380-1170 cm^{-1}. The presence of nanofiller, at the investigated concentrations, seems to have small effect on the FT/IR spectra. In particular, for the sample filled with CpEG no differences with respect to other nanofillers are observed in the profile of the spectrum. This result highlights that the lower moisture content is due to factors independent of the chemical nature of the resin network. As no large differences in the diffusion parameter are observed for the sample filled with CpEG with respect to other nanofilles, it is very likely that the lower moisture content is due to self-assembled effects which form structures entrapping part of the resin fraction and do not allow the interaction of water molecules with all the polar sites of the resin. This mechanism could also be active in parts of resin comprised between graphene sheets which partly enclose a fraction of the resin. On the other hand, data in the previous section have shown that an impediment to the full cross-linking reactions caused by the nanofillers is observed. This impediment or interruption is localized in the zones surrounding the nanofillers. This effect is more marked for the sample loaded with CpEG highlighting that more extended zones in contact with the nanofiller hinder the crosslinking reactions (see dynamic mechanical results of Figure 4.11 and the data on the Reaction enthalpies of Figure 4.10). A very similar mechanism may be responsible for hindering the interaction of the polar sites of the resin with the water molecules.

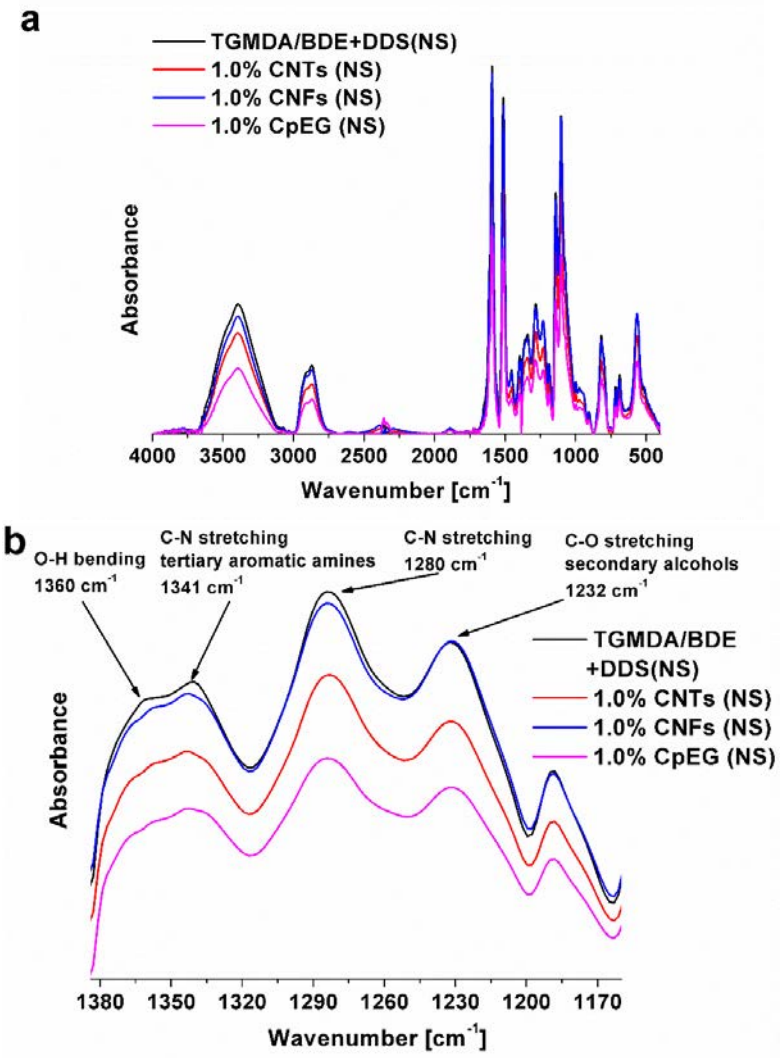

Figure 4. 15 *FTIR spectra of the samples solidified in non-stoichiometric condition containing embedded three types of nanofillers, in two different spectral ranges: a) 4000-500 cm^{-1} and b) 1380-1170 cm^{-1}.*

4.4.5 Electrical Properties

The electrical conductivity of nanocomposites exhibits a remarkable increase from that typical of the pure resin (few pS/m) to that of a conductor once the filler concentration increases over an electrical percolation threshold (EPT) due to the formation of conductive paths in the structure. Figure 4.16 shows the DC volume conductivity measured at room temperature as a function of

the filler concentration (wt%) for the three types of carbon-based particles considered in the present study. Regardless of the filler and according to the percolation theory, as the filler amounts (i.e. ϕ) increases beyond the threshold value (ϕ_c), the electrical conductivity follows the classical power law (eq. 3):

$$\sigma=\sigma_0(\phi-\phi_c)^t \quad (3)$$

where σ_0 is the intrinsic conductivity of the filler and *t* is a critical exponent depending on the dimensionality of the percolating structure.

By increasing the filler percentage, higher values of electrical conductivity are achievied for all types of the resulting composites. More in detail, at the highest investigated concentration, i.e. 1 wt%, 2 wt% and 1,8 wt% for nanocomposites filled with CNTs, CNFs and CpEg, the corresponding conductivities reach the values of 0.29 S/m, 2 S/m and 0.096 S/m, respectively. Although the best performance in terms of electrical conductivity, for comparable reinforcement amounts are achieved by using filler of one-dimensional type (CNTs and CNFs), the potentially high aspect ratio of graphene sheets (i.e CpEG), defined for such type of filler as the ratio between its maximum lateral dimension and the thickness, combined with their phisical and chemical properties, may have favorable impact on improving the percolating network at low filler loadings. In fact, the experimental characterization reveals an interesting difference as it concerns the electrical percolation threshold achieved with the three fillers. In particular, for both one-dimensional fillers (CNTs and CNFs), the EPT values fall in a comparable range, i.e. [0.1-0.32] and [0.05-0.32]%wt, respectively. Instead, the electrical percolation threshold is in a narrower interval [0.025-0.1]%wt for the composites reinforced with bi-dimensional CpEG filler. This means that CpEG reinforcements are able to create percolation conductive pathways more easily and with lower filler amounts through the insulating resin compared to the one-dimensional fillers. This result may be attributed to two mechanisms: the concentration of carboxylated groups localized at the edge of graphene sheets and the filler aspect ratio. The higher concentration of carboxylated groups responsible of attractive intermulecolar bonding affects the filler/resin compatibility between the dispersed particles thus favoring the creation of the electrical networks with an “optimized” sort of self-assembled structures (Guadagno et al., 2015a) (i.e. with shorter average distances betwen conductive fillers).

Moreover, as it regards the filler aspect ratio (AR), different literature studies on carbon-based reinforced composites have identified this parameter as a critical factor (De Vivo et al., 2015, Shehzad et al., 2013). In particular, the relationship EPT $\propto$ 1/AR can be adopted indicating that an higheraspect ratio

leads to an improved electrical connectedness of the carbon-based network at lower filler amounts.

Morphological analyses carried out on the fillers reveals an indicative AR of [1, 1.6, 100]x10^3 for CNT, CNF and CpEG respectively, thus confirming that an increase of the AR plays a key role in lowering the EPT in nanocomposites, in agreement with literature data (Bellucci et al., 2015).

From the insets of each percolation curve of Figure 4.16 reporting the log-log plots of the experimental conductivity vs. filler concentration, the characteristic parameters of the percolation law can be estimated. In particular, the value for the critical exponent *t* can be obtained as the slope of the linear fit. The estimated values, i.e. 2.2 for both CNTs and CNFs reinforced composites, are found to agree with universal values, reflecting an effective 3D organization of the percolating structure consistent with 1-D type of filler (Nan et al., 2010). For composites filled with CpEG, it is interesting to note that the value of the exponent *t* decreases significantly showing a value equal to 1.1, since the nanoparticles exhibit two-dimensional shape.

The presence of insulating resin around the carbon-based nanomaterials prevents direct electrical connection. This has been observed for example in amine-grafted MWCNT/epoxy composites in which a thick polymer layer forms an extra phase on the carbon nanotube walls thus affecting the electrical properties of the resulting composite (Kotsilkova et al., 2015, Guadagno et al., 2011).

In the limit of a certain cut-off distance, the tunneling effect provides that electrons can flow through a barrier between adjacent electrically particles forming quantum tunneling junctions.

The conduction mechanism in such a system can be modeled with a resistance R_{tunnel} according to the following expression:

$$R_{tunnel} = \frac{h^2 d}{A e^2 \sqrt{2m\lambda}} exp^{\left(\frac{4\pi d}{h}\sqrt{2m\lambda}\right)} \quad (4)$$

In the above equation *h* is Planck's constant, *A* and *d* are the cross-sectional area and the distance between the filler (coincident with the thickness of the insulating resin wrapped around the particles) respectively, *e* is the electron charge, *m* is the mass of an electron and λ represents the height of the barrier which typically takes values of a few eV. It is evident as the tunneling effect depends strongly on the thickness of the insulating resin (i.e. *d*) around the filler that must be sufficiently thin to allow the tunneling conduction between neighbor conductive particles. Thicknesses larger than about 1.8 nm lead to composite conductivity values typical of an insulator material. A classic approach adopted in order to check if the electron tunneling is the main electrical transport mechanism in such nanofilled resins is to observe the

occurence of the following relationship (Kilbride et al., 2002, Mdarhri et al., 2008, Connor et al., 1998, Guadagno et al., 2014b)

$$\ln(\sigma) \propto \emptyset^{-1/3} \quad (5)$$

i.e. a linear relation between the electrical conductivity (in logarithmic scale) and $\phi^{-1/3}$, valid for concentrations (ϕ) above the electrical percolation threshold. For our systems this is shown in Figure 4.16d. The dashed lines are fit curves of the experimental data (markers): the value of R^2 very close to 1 confirms the effectiveness of the tunneling modulated charge transport conjecture. As a consequence, the current and therefore the electrical conductivity of the resulting nanocomposites strongly depends on the interaction between the host matrix and the adopted filler and not only on the intrinsic conductivity of the latter (Guadagno et al., 2015e, De Vivo et al., 2014, Plyushch et al., 2016). In particular, the electrical properties are related to the morphology of conductive network which in turn is affected by the dispersion technique and manufacturing process (i.e. cure temperature, chemical interactions between the filler and surrounding resin, etc.). Such results are also supported by the experimental characterization (see red markers in each percolation curve of Figure 4.16) carried out on nanocomposites prepared by stoichiometric and non-stoichiometric concentrations of hardener. For two selected filler concentrations of each carbon-based particle (i.e 0.5 wt% and 1 wt%), the electrical conductivity of the formulations with non-stoichiometric ratio of hardener are greater than the conductivity achieved in the stoichiometric case. This phenomenon is more evident for the 0.5 wt% concentration of filler since the conductivity increases of about one order of magnitude. In fact, in this case, the measured electrical conductivity varies from to 0.01 S/m up to 0.29 S/m and from 0.04 S/m up to 0.31 S/m for composites reinforced with CNTs and CpeG, respectively. The observed improvement in the electrical conductivity associated to the use of hardener in non-stoichiometric ratio could be ascribed to a reduction of the viscosity of the resin; in fact the decrease in viscosity promotes better dispersion of the particles within the hosting polymer thus favoring the creation of conductive electrical networks. Further study on this aspect entangling also the behavior of the dielectric properties of the nanocomposites is now underway and will be presented in a forthcoming paper.

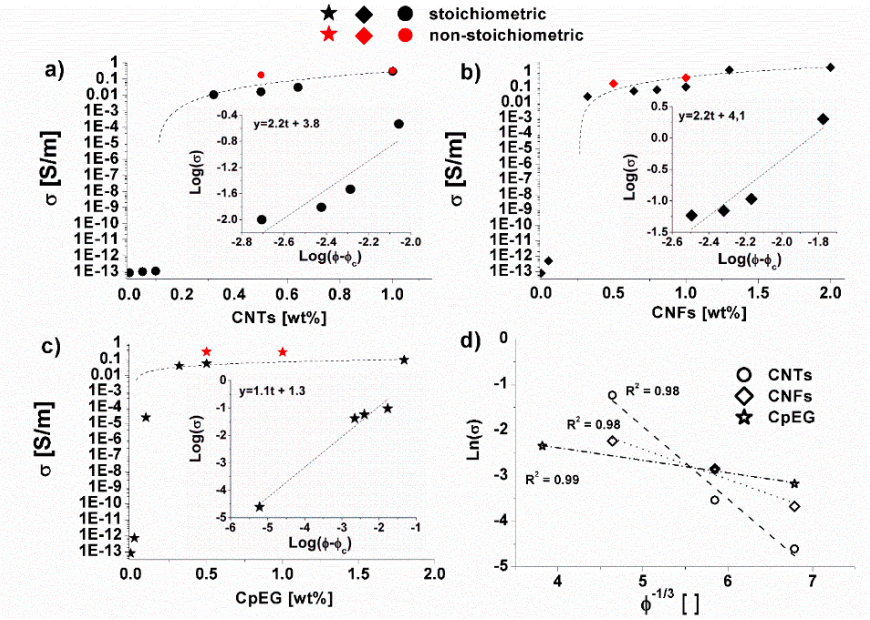

Figure 4. 16 *DC volume conductivity of the nanocomposites versus filler weight percentage. The inset shows the log-log plot of the electrical conductivity as a function of (ϕ-ϕ_c) with a linear fit for composites reinforced with a) CNTs; b) CNFs; c) CpEG. d) Plot of the natural logarithm of DC conductivity for sample above the EPT against $\phi^{-1/3}$. The dashed line is a fit of the DC data (marker) to eq. 4.*

4.5 Conclusions

We have formulated, prepared and characterized an epoxy resin mixture based on a tetrafunctional epoxy precursors, the TetraGlycidyl-MethyleneDiAniline (TGMDA) able to decrease the moisture content of the unfilled and nanofilled samples. The sorption at equilibrium of liquid water (C_{eq}) decreases from 6.81 to 5.76 for the sample TGMDA/BDE+DDS solidified in stoichiometric concentration of hardener and to 4.83 for the sample TGMDA/BDE+80DDS(NS) solidified in non-stoichiometric condition. The resin reduces the value in C_{eq} from a minimum of 15% at a maximum of 30%. This percentage is very relevant for many industrial applications. The nanofilled samples are characterized by values of C_{eq} only slightly higher than the unfilled matrix. The composites obtained with CpEG are characterized by the lowest value, among all considered systems, of the moisture content. To understand this behavior and the effect of nanofiller, many systems have been analyzed. It has been found that the nanocomposite filled with CpEG is also

characterized by low electrical percolation threshold (EPT) that falls in the narrow interval [0.025-0.1]%wt and improved mechanical properties. Among the graphene-based nanoparticles CpEG sample was chosen after a detailed study aimed at finding effective strategies to transfer some of excellent physical properties of graphene layers to epoxy matrices. The evaluation of edge structures of very similar graphene-based materials, differing only for the concentration of carboxylated group on the edges, highlighted that the effect on the electrical and mechanical properties is impressive. The chemistry of graphene edges strongly affects the physical properties of the resin where these nanoparticles are embedded. In particular, it was found that with samples constituted by roughly 50% of graphite with a correlation length perpendicular to the structural layers ranging between 12 nm e 9.8 nm and 50% of exfoliated graphene, for standard epoxy composites, electrical percolation threshold can be achieved with nanofiller concentration less than 0.5% by weight. This value of nanofiller concentration allows to reach DC electrical conductivity raging between 1-2 S/m. The good electrical and mechanical performance was ascribed to self-assembly mechanisms determined by attractive interactions between edge-carboxylated graphene particles. The self-assembly of layers due to the attractive interactions between edge-carboxylated graphene particles was found to favor the electrical percolative paths. Edge-carboxylation also increases the nanofiller/epoxy matrix interaction determining a relevant reinforcement in the elastic modulus. This controllable feature of the nanoparticles can be an alternative parameter to design epoxy resins where high electrical conductivity is required at very low filler concentration. Data here shown highlight that nanocomposites obtained using the epoxy matrix hardened in non-stoichiometric condition are also able to further enhance the electrical conductivity; at 0.5% of filler, an increase in the electrical conductivity of 1 order of magnitude is observed. In fact, the measured electrical conductivity varies from to 0.01 S/m up to 0.29 S/m and from 0.04 S/m up to 0.31 S/m for composites reinforced with CNTs and CpeG, respectively.

Hence, CpEG nanoparticles at 0.5% by weight, are particularly able to increase electrical conductivity and reduce the moisture content making them particularly advantageous for applications in the field of the wind energy, aviation and shipbuilding. It is worth noting that the composition of the graphene-based nanoparticles (CpEG) gives particular advantages to combine the described properties. In fact, it was highlighted that, for balk samples, perfect graphene layers (without defects) originated from full exfoliated graphite tend to reassemble during the manufacturing of the nanocomposites. Indeed, strong functionalization procedures are needed to obtain graphene in the form of single layer embedded in the polymeric matrix. In this last case, the functional groups attached to the graphene layers prevent the re-

assembling of layers due to steric and energy factors. Unfortunately, due to the transition from sp^2 to sp^3-hybridization of carbon atoms, functionalized single layers (SL) of graphene tend to lose a large amount of delocalized electrons and, therefore, the very interesting electronic properties of graphene, hence reducing the electrical conductivity of graphene-based nanocomposites. This effect is further worsened by the difficulty of single layers to form conductive paths inside the bulk polymeric matrix due to characteristic morphological features of functionalized SL graphene layers. In fact, the functional groups act as defects imparting to the layers strong tendencies to screw up which lead to severe inhomogeneities in the nanofiller dispersion also preventing the formation of conductive pathways. On the other hand, significant benefits in terms of physical properties can be achieved for ultrathin graphitic stacks which preserve a large part of sp^2-hydridized carbon atoms, and hence their graphene-like electronic properties. A deep balance and control of the inherent complexity of these systems at nanoscale level may drive the changes in the nanocomposite properties towards the set goals. In light of these considerations, samples of partially exfoliated graphite have been considered both to avoid the negative effect of single graphene layers and to maximize the beneficial effects of graphene-based materials for bulk samples. Self-assembling effects can be also responsible for the lower moisture content. Self-assembled structures can entrap part of the resin fraction hindering the interaction of water molecules with all the polar sites of the resin. This mechanism could also be active in parts of resin comprised between graphene sheets which partly enclose a fraction of the resin. Dynamic mechanical results have shown that the filler tends to create a phase with increased mobility of the chains, segmental parts of the epoxy network around the filler which causes an increase in the more mobile phase (which is also caused by defect of hardener). This effect is more marked for the sample loaded with CpEG highlighting that more extended zones are in contact with the nanofiller. A very similar mechanism may be responsible to hinder the interaction of the polar sites of the resin with the water molecules. Furthermore, in this manuscript, many aspects related to the variation of the T_g due to the inclusion of the nanofiller in the resin have been analyzed. Concerning this aspect, is worth noting that, so far the influence of carbon nanotubes on both the cure kinetics and the physical properties of the resins has been reported, in particular considering the variation of the glass transition temperature for pristine resin and in presence of CNT. However, conflicting results have been reported and the effect of CNT on the T_g needed to be clarified. In this paper, we have analyzed the unfilled resin hardened in stoichiometric and non-stoichiometric condition to better understand the effect of different nanofiller on the T_g of the nanocomposites. Results here discussed highlight that the impossibility to extend the tri-dimensional network in the space filled by the nanoparticles is responsible of a more

mobile phase determining an additional T_g at lower temperature with respect to the main glass transition temperature. Concerning the effect of nanofiller on the resin hardened in non-stoichiometric conditions, a synergism between nanofiller effect and low DDS level is observed. The fraction of the more mobile phase is strictly related to the amount and nature of the nanofiller, as well as the temperature range where the movements of the molecular segments are activated.

This page intentionally left blank

Chapter Five

5. Development of structural epoxy adhesives nano-charged with carbon nanofiller

The focus of this chapter is the development of new adhesive formulations, based on epoxy/nanostructured carbon forms. The reinforced adhesives are used for bonding carbon nanofilled/epoxy composite adherents. Mechanical strength and adhesion properties for the different joint configurations are carried out.

5.1 Generalities and remarks

Adhesively bonded joints are increasing alternatives to mechanical joints in engineering applications and provide many advantages over conventional mechanical seal. To join such composite parts, polymer adhesives such as epoxies are commonly used. Using adhesive bonding for joining composite parts provides many advantages such as low cost, high strength to weight ratio, low stress concentration, fewer processing requirements and superior fatigue resistance and environmental resistance (Hsiao et al., 2003). Adhesion between the polymer (composite) surface of adherents and polymeric adhesive substrate is suitably controlled by the chemical groups at or near the interface which lead to a better performance of bonded joint in their application (Awaja et al., 2009). Several papers have been published on the inclusion of nanostructured carbon forms inside epoxy adhesives in order to enhance the mechanical strength and toughness of the bonded joints (Burkholder et al., 2011, Meguid and Sun, 2004a, Yu et al., 2009, Hsiao et al., 2003). Yu et al. (2009) studied the mechanical behavior and durability in humid environments of the aluminum joints bonded with an epoxy adhesive reinforced with multi-walled carbon nanotubes (MWCNTs)(Yu et al., 2009). Likewise, Hsiao et al. (2003) studied the mechanical strength of epoxy/MWCNT reinforced adhesive to join carbon graphite fiber/epoxy composite adherents (Hsiao et al., 2003), while other researcher studied the adhesive properties of nanoreinforced epoxy adhesive using dissimilar joints composed of carbon fiber/epoxy laminate and aluminum alloy (Meguid and Sun, 2004a). In any case, the presence of uniformly dispersed CNTs inside the adhesive paste was found to be able to increase bonding strength, Young's modulus as well as ultimate tensile strength of the adhesive. An improvement of CNT's reinforcement on fracture strength for adhesive joints was also observed between steel–composite interfaces and composite– composite interfaces (Burkholder et al., 2011). MWCNTs embedded in the adhesive at a percentage of 1 wt% enhanced fracture toughness for both steel–composite and composite–composite adhesive joints. Adhesive performance of epoxy-based materials was investigated also considering the effects of inorganic nanoparticle inclusions on the adhesive strength of a hybrid sol–gel epoxy system used to joint, either aluminium substrate, and mild steel substrate (May et al., 2010). The mechanical performance of different formulations was characterized by shear and tensile tests to define the influence of nanofillers on adhesive strength performance of the modified epoxy/ hybrid sol–gel. The incorporation of a selected ratio of inorganic nanoparticles in the epoxy/sol–gel adhesive improves the adhesion performance between substrate surfaces. At the same time, it is well known in literature that one of the main predicted advantages related to the inclusion of conductive nanoparticles into epoxy resin is the improvement of its electrical behavior (De Vivo et al., 2012a,

Guadagno et al., 2011, Nan et al., 2010, Wang et al., 2006, Gojny et al., 2005a). In fact, different types of carbon nanofillers are electrical conductor materials, which well dispersed in the matrix, can drastically increase electrical properties of epoxy based adhesives also using a very low percentage of nanofiller. This property is of special relevance in the joint of electrical conductive substrates and makes adhesive epoxy/nanostructured carbon forms to become a promising new frontier in nanoreinforced adhesive for structural applications. The development of conductive epoxy adhesive to be used in the aeronautic field to join parts of primary structure is a current need with a view to optimizing efficiency of joints while preserving the conductivity of lightweight materials able to provide also in the joints good lightening protection (Guadagno et al., 2012b, De Vivo et al., 2012b, Guadagno et al., 2011). The enhancement in different properties of epoxy-based materials and or/adhesives depend on numerous parameters, such as the chemical nature of nanofiller, adhesive and adherents, the applied surface treatment or the tested properties (Gude et al., 2011, Prolongo et al., 2010b). In the present study, we used as fillers heat-treated carbon nanofibers (CNFs), exfoliated graphite and carbon nanotubes

5.2 Materials and Sample preparation

Vapor-grown carbon nanofibers (CNFs) used in this study were produced at Applied Sciences Inc. and were from the Pyrograf III family. The CNFs used in this study are respectively labeled as PR25XTPS2500 and PR24XTHHT where XT indicates the debulked form of the both PR25 and PR24 family, PS indicates the grade produced by pyrolytically stripping the as-produced fiber to remove polyaromatic hydrocarbons from the fiber surface, 2500 is the temperature of the heat-treatment and HHT indicates the grade produced by heat-treating the as-produced carbon nanofiber to 3000 °C. Exfoliated graphite (EG) is obtained by rapid heating of a graphite intercalation compound (GIC). Exfoliated graphite nanoparticles are composed of stacks of nanosheets that may vary from 4 to 40 nm as resulted from X-ray and SEM investigations.

The MWCNTs (3100 Grade) were purchased from Nanocyl S.A. Transmission electron microscopy (TEM) investigation has shown for MWCNTs an outer diameter ranging from 10 to 30 nm. The length of MWCNTs is from hundreds of nanometers to some micrometer. The number of walls varies from 4 to 20 in most nanotubes. The specific surface area of MWCNTs determined with the Brunauer–Emmett–Teller (BET) method is around 250-300 m^2/g; the carbon purity is > 95% with a metal oxide impurity <5% as it results by thermogravimetric analysis. Tests were carried out on eight series of samples, each one characterized by different combination

between adherents and adhesive formulations. The combinations are shown in Table 5.1 and table 5.2. Different nanofiller percentages were used in preparing the nanofilled formulations. These percentages were chosen to significantly improve mechanical behaviour, and at same time, electrical conductivity. All the nanofilled adhesives, reached or were just beyond the EPT (Guadagno et al., 2012b, Nan et al., 2010).
Epoxy mixture with fillers were obtained in a similar manner to those described in chapter 4.
Materials (unfilled and nanofilled epoxy mixture) were cured in two different mold geometry configurations made of Teflon (PTFE). The molds were designed by referring to existing international standard practice in the design of the specimens, in particular ASTM D 2094 and ASTM D 1002 were considered (Figure 5.1a and b). In this way, a suitable configuration of specimens for tensile butt joint (referred to ASTM D 2095), and single lap joint (referred to ASTM D 3163) were respectively obtained to measure mechanical strength and adhesion properties in the different joint configurations.

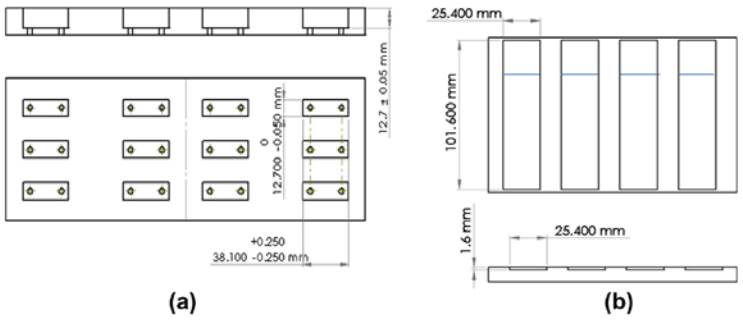

Figure 5. 1 *(a) Schematic cavity geometry for tensile butt joint and (b) schematic cavity geometry for lap joint shear adherent*

The epoxy matrix was prepared by mixing the epoxy precursor, tetraglycidylmethylenedianiline (TGMDA) (epoxy equivalent weight 117–133 g/eq), with an epoxy reactive monomer 1-4 butanedioldiglycidyl ether (BDE) that acts as a reactive diluent. The curing agent used for this study is 4,4-diaminodiphenyl sulfone (DDS). The epoxy mixture was obtained by mixing TGMDA with BDE monomer at a concentration of 80%:20% (by wt) epoxide to diluent. The curing agent was added at stoichiometric and non-stoichiometric amount with respect to the epoxy rings (TGMDA and BDE). Stoichiometric composites with the filler, are named Epoxy X (type of nanofiller), where X represents the nanofiller percentage. As example, Epoxy 1.3% HHT24 is the epoxy mixture TGMDA /BDE+DDS at 1.3% concentration by weight of carbon nanofiber HHT24. Similarly, non-

stoichiometric composites with filler are named Epoxy (NS) X (type of nanofiller). As example Epoxy (NS) 0.5 % MWCNT is the epoxy mixture TGMDA /BDE+DDS (NS) at 0.5% concentration by weight of carbon nanotubes.

Table 5. 1 *Summary of prepared samples (stoichiometric systems)*

Sample label	Adherent composition (ASTM D 2095/ASTM D 3163)	Adhesive composition
A	**Epoxy 1.3%HHT24**	**Epoxy 1.3%HHT24**
B	**Epoxy 1.3%HHT25**	**Epoxy**
C	**Epoxy**	**Epoxy 1.3%HHT24**
D	**Epoxy**	**Epoxy**
E	**Epoxy**	**Epoxy 3.7% EG**
F	**Epoxy**	**Epoxy 5.0%PRXTPS2500**
G	**Epoxy**	**Epoxy 1.3%PRXTPS2501**
H	**Epoxy 1.3%PRXTPS2501**	**Epoxy 1.3%PRXTPS2501**

Table 5. 2 *Summary of prepared samples (non-stoichiometric systems)*

Sample label	Adherent composition (ASTM D 3163)	Adhesive composition
A'	**Epoxy**	**Epoxy**
B'	**Epoxy**	**Epoxy (NS)**
C'	**Epoxy**	**Epoxy (NS) 0.5%MWCNT**
D'	**Epoxy 0.5%MWCNT**	**Epoxy (NS) 0.5%MWCNT**

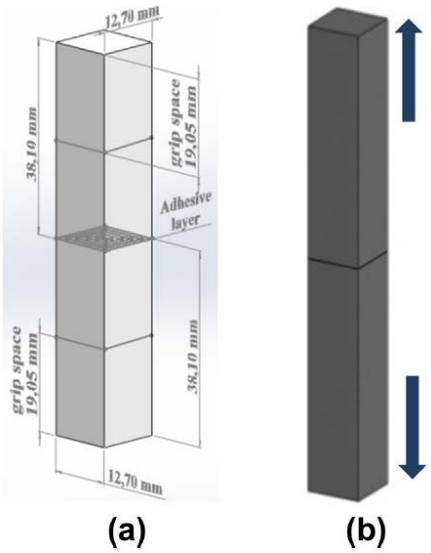

Figure 5. 2 *(a) Schematic of the tensile butt joint strength test specimens (referred to ASTM D2095) and (b) schematic of the butt joint (load direction)*

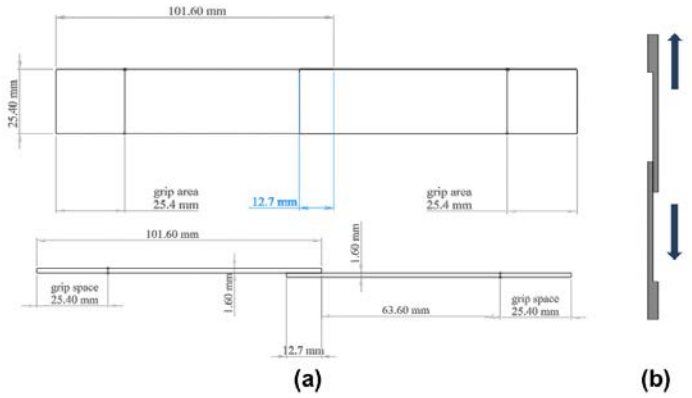

Figure 5. 3 *(a) Schematic of the single lap-joint shear strength test specimens (referred to ASTM D3163) and (b) schematic of the single lap-joint shear (load direction)*

Figures. 5.2a and b and 5.3a and b show schematics of the tests set up used for the tensile and shear testing of the sample interfaces. These configurations were suitable selected as they are simple to make and assemble and involve different stress conditions mode to test the bonded joint between the adherent in axially and shear direction (Messler, 1993, Tsai and Morton, 1994). To

assemble the adherents a very thin layer of adhesive was used (see Table 1). The thickness of the samples was measured using a digital caliper (average thickness 0.2 mm). For each type of combinations (adherents/adhesive), three different samples were tested and average measurement scatter turned out to be close to instrument accuracy. Before adhesive bonding, mechanical surface treatment (grit blasting) was performed for improving the adhesion between the parts.

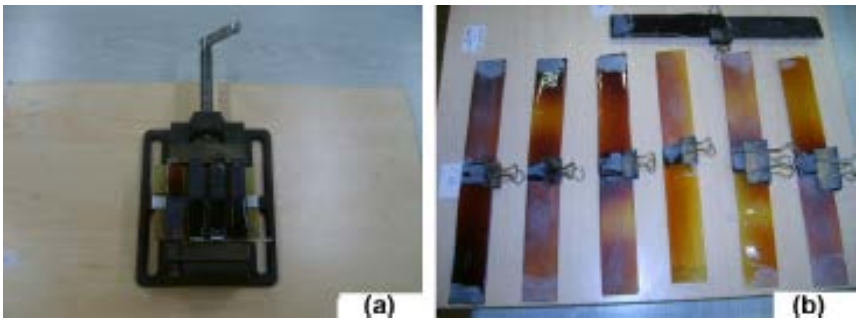

Figure 5. 4 *(a) Assembly of the tensile butt joint specimens under uniform compression (before curing) and (b) assembly of the single lap joint shear specimens under uniform compression (before curing).*

Once the adhesive was placed between the overlap area, either the butt joint, than the single lap-joint samples were uniformly compressed in the overlapped adhesion area using two suitable devices based on clamping system (see Figure 5.4a and b). They just ap-ply weak pressure to allow the alignment of the adherents and no effects on the thickness of the adhesive layers are observed by measuring thickness of the adhesion layer after the curing process. The samples were then placed inside a convection oven followed by a curing cycle.

5.3 Results and discussion

5.3.1 Stoichiometric systems characterization

Adhesive tests were carried out using an electro-hydraulic servo-controlled testing machine (Instron mod. 4301). Ultimate tensile and shear strength of the nano-reinforced interface were measured. The loading was applied perpendicularly to the bonding plane, and the test procedures were carried out as ASTM D 2095 and ASTM D 3163 standard requirements. Tensile butt joint Ultimate strengths to-failure of the analyzed formulations are listed in Table 5.3.

Table 5. 3 *Summary of tensile butt and shear joint strength data*

Sample label	ASTM D2095 Tensile strength at break (MPa)	ASTM D3163 Shear strength at break (MPa)
A	**9.360±0.073**	**6.430±0.070**
B	**4.079±1.200**	**3.843±0.344**
C	**8.339±0.800**	**4.693±0.213**
D	**9.090±1.650**	**3.864±0.123**
E	**7.310±0.235**	**1.160±0.047**
F	**2.702±0.257**	**2.276±0.086**
G	**16.100±0.620**	**5.422±0.921**
H	**20.465±1.135**	**5.612±0.501**

It is worth noting that data in Table 5.3 for samples D (adherent–epoxy mixture, adhesive–epoxy mixture) and E (adherent–epoxy mixture, adhesive–epoxy mixture filled with 3.7 wt/wt% exfoliated graphite), in lap joint shear configurations, (bold values), refer to samples failed in the bonded joint. A general view of these data highlights a strengthening of joint resistance as a result of embedded nanofiller; even if the amount of nanofiller plays a very relevant role in determining this behaviour. Samples A and H, which are made of nanofilled adhesive and nanofilled adherent with a percentage of 1.3 wt/wt% of CNFs, exhibit a very good adhesion behaviour. In particular, sample H shows the best performance in the tensile strength parameter in butt joints configuration, whereas sample A exhibits the highest value of the same parameter in the lap-shear joints configuration. However, sample H, also in the case of lap-shear joints configuration, shows a significant strength, exceeded only sample A. Further, sample G, where only the adhesive past is loaded with 1.3% of CNFs (PR-XT PS 2500) shows a behaviour in the adhesive performance better than samples B, D, E and F where the adhesive paste are unfilled (samples B and D) or filled with high percentage of nanofillers (samples E and F). Considering all the results, we can certainly draw two important conclusions:

(a) the best adhesive behaviour is obtained for samples filled with a low percentage CNFs (samples A and H) and with strong similarity in the chemical composition between adherents and adhesive (see samples A and H);

(b) in the performed tests (involving unfilled adherents and nanofilled adhesive) the best performance is obtained for low concentration of nanofiller

(see samples F and G); in addition, CNFs heat-treated at 2500 °C show a better behaviour than CNFs heat-treated at 3000 °C (see samples C and G).
The performed tests evidence the great potential of adhesive formulations as samples A and H in the field of structural adhesive materials. In fact, if the need arises, the structural adhesive can be tailored to replace the common adhesive with conductive adhesive to bond new nanofilled materials currently under investigation in the field of aeronautic and aerospace materials. Furthermore, market research indicates a more attractive price for the nanoparticles and many progress have been made in reducing difficulties related to the step of nanofiller dispersion. As already observed for different types of nanofillers in previous papers (Saeed and Zhan, 2007, Meguid and Sun, 2004a), also for carbon nanofibers, there is an optimum amount of nanofiller, which leads to significant improvement in mechanical behavior of the bonded joint. In fact, we can observed that, at higher nanofiller contents (i.e. 3.7 wt/wt% and 5 wt/wt%), the properties degrade to below the ones of the neat epoxy adhesive. Similar results were obtained in single lap joint shear tests.

Figure 5. 5 *Detail of failure of bonded joints occurred in butt joint tests.*

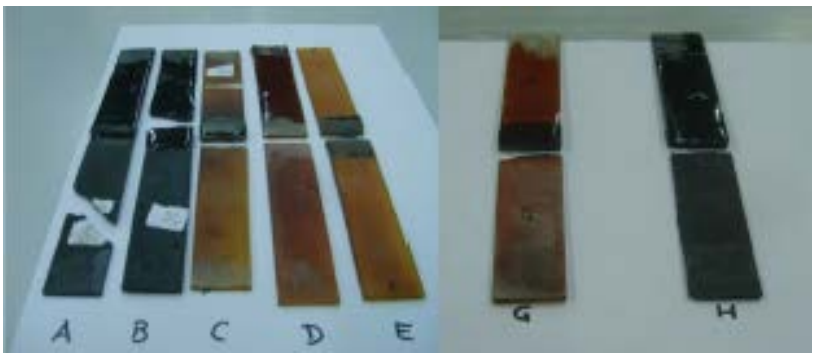

Figure 5. 6 *Detail of failure of bonded joints occurred in lap joint shear tests.*

It is well known that it is the combination of adhesion and cohesive strength which determine bonding effectiveness. Cohesion is defined as the internal strength of an adhesive as a result of a variety of interactions within the adhesive. Adhesion is the bonding of one material to another, namely an adhesive to a substrate, due to a variety of possible interactions. Generally, there are two possible mechanisms of failure, namely adhesive failure and cohesive failure. Adhesive failure is the inter-facial failure between the adhesive and one of the adherents, which is indicative of a weak-boundary layer adhesion. On the other hand, cohesive failure occurs when the fracture results in a layer of adhesive remaining on both adherent surfaces, or, when the adherent fails before the adhesive with fracture almost contained in the adherent (Suo, 2001, Tsai and Morton, 1994). In our samples, failure in the bonded zone occurred for all the butt bonded joint samples tested by tensile mode (see Figure 5.5). Different behavior was highlighted in single lap joint tests. In fact, sample D and E (Figure 5.6), the adhesive breaks apart, and the failure occurred in the overlapped zone, although sample D exhibited high mechanical strength response (see Table 5.3). In other cases, inclusion of nanofiller in the adhesive paste, leads to no failure in the overlapped zone, because, the nano-reinforcement effectively transferred the load into the adherents, whether they were filled or unfilled. This last observation also highlights that a very important role in the joint behavior is also the nature of the interface adhesive/adherent, in fact also sample B shows a good behavior because the nanofillers interact in the interface zone.

5.3.2 Morphological investigation of fracture surface of the bonding areas of stoichiometric systems

Scanning Electron Microscopy (SEM) was carried out using FESEM (FE-SEM, mod. LEO 1525, Carl Zeiss SMT AG, Oberkochen, Germany) with the aim of studying the morphology of the detached zones. The fracture surfaces of the bonding areas were preliminary coated with a thin gold layer of 250 Å.

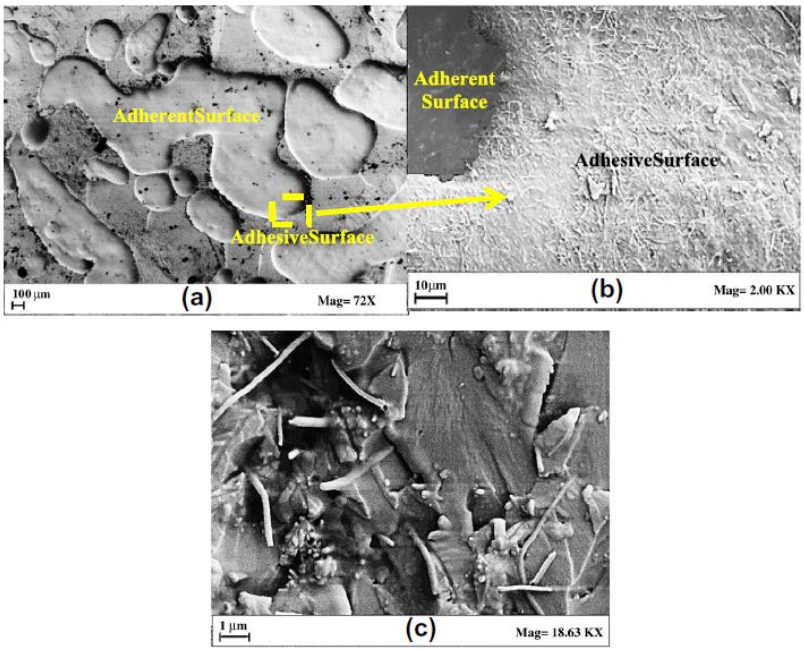

Figure 5. 7 *(a and b) FE-SEM micrograph of fracture surface of the bonding areas-sample A failure in tensile test and (c) detail of magnifications of neighbor region.*

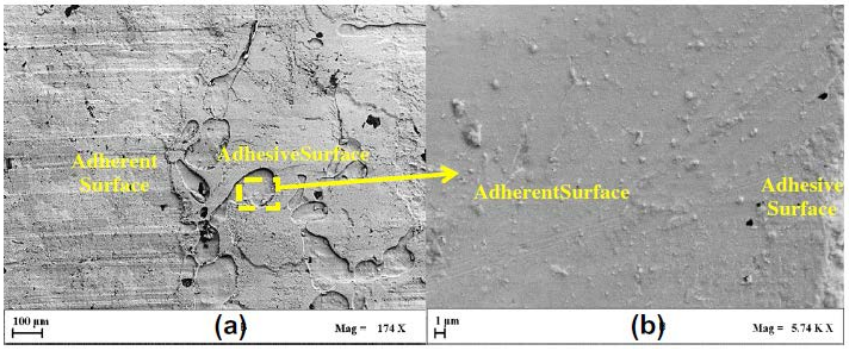

Figure 5. 8 *(a) FE-SEM micrograph of fracture surfaces of the bonding areas-sample B failure in tensile test and (b) detail of magnifications of neighbor region.*

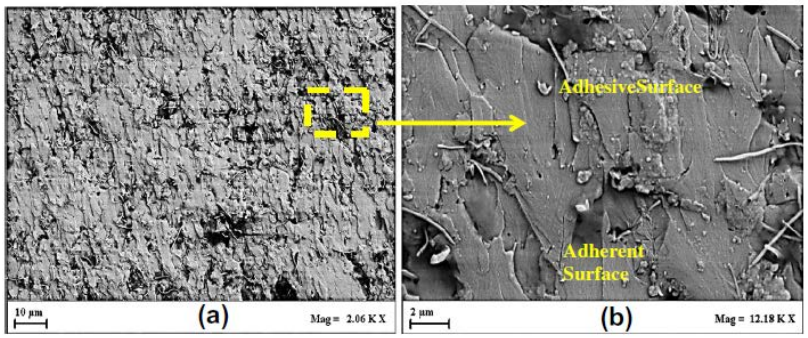

Figure 5. 9 *(a) FE-SEM micrograph of fracture surfaces of the bonding areas-sample C failure in tensile test and (b) detail of magnifications of neighbor region.*

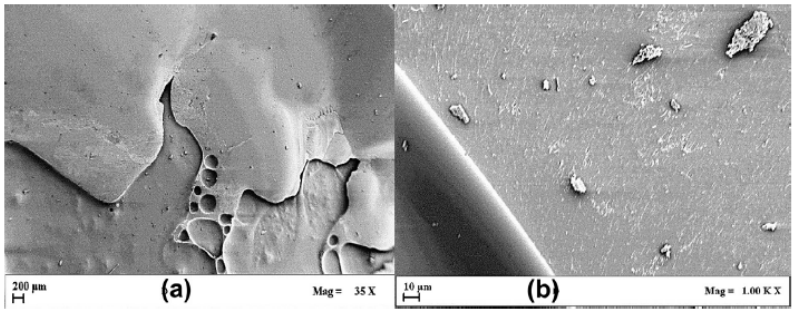

Figure 5. 10 *(a) FE-SEM micrograph of fracture surfaces of the bonding areas-sample D failure in tensile test and (b) detail of magnifications of neighbor region.*

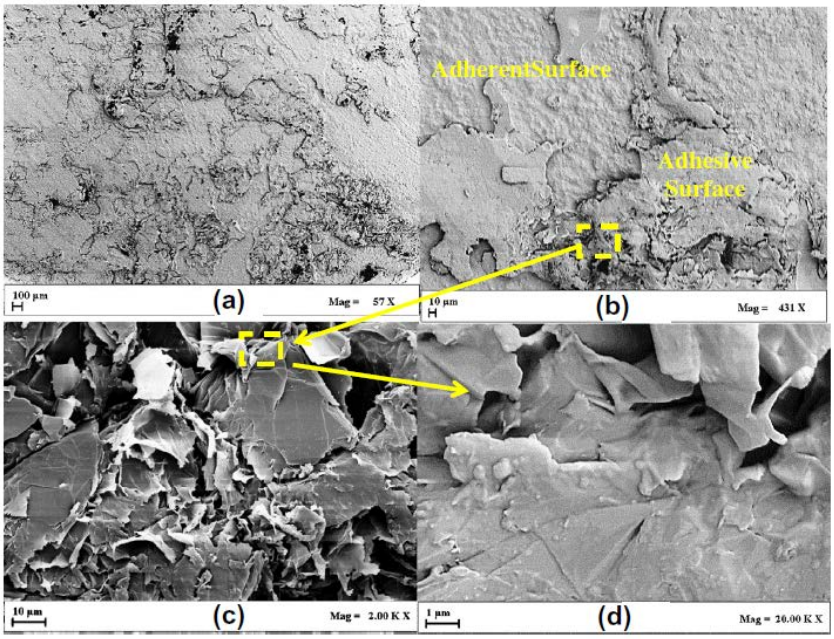

Figure 5. 11 *(a and b) FE-SEM micrograph of fracture surfaces of the bonding areas-sample E failure in tensile test and (c and d) detail of magnifications of neighbor region.*

Figures 5.7–5.11 show SEM micrographs of fracture surface of butt joint tested in tensile mode. The inclusion of nano-reinforcement into the epoxy adhesive improves mechanical strength of the adhesive layer; it effectively transfer the external load to the adhesive layer containing nanofibers, and failure occurred also in the nanofibers (see Figures 5.7b and 5.9b), which

behave as the strongest part of the composite adhesive. In the same zones, few CNFs are even pulled out of the resin leaving micro and nanometric voids (see Figures 5.7c–5.9b). In this regard, it is worth noting that no etching procedure was performed on the fracture surface before the morphological investigation. It is well known in the literature that the morphological investigation, by means of SEM investigations of nanofillers inside polymeric matrix, require pre-treatment of sample surfaces with etching procedure [27–30](Guadagno et al., 2010a, De Vivo et al., 2013, Guadagno et al., 2012a, Guadagno et al., 2009). The simple fact of observing some nanofibers so clearly (see Figs. 7c and 9b) evidences that they have endured a load which has caused their detachment from the matrix. In the case of sample B, prepared by joining the nanofilled adherents with unfilled epoxy adhesive (see Figure 5.8), no exposed CNF's are observable. In this case, the failure of joint occurred at the epoxy along the bonding interface. This behavior might explain the lower values in the tensile strength of sample B with respect to the previous sample or samples such as H, G and C samples. FE-SEM micrographs of bonding surface for unfilled joint (Figure 5.10) show remnants of adhesive paste on unfilled surface which appear as a failure in the adhesive. Images on the fracture surfaces of sample E (see Figure 5.11) show that the external load to which the joint is subjected, was supported by adhesive layer; in fact, the exfoliated graphene platelets are pulled out of the plan of interface. This occurrence confirms the same behavior observed for the fiber-reinforced adhesive with a substantial difference: the high amount of exfoliated graphite platelets weakens the interaction between filler and matrix.

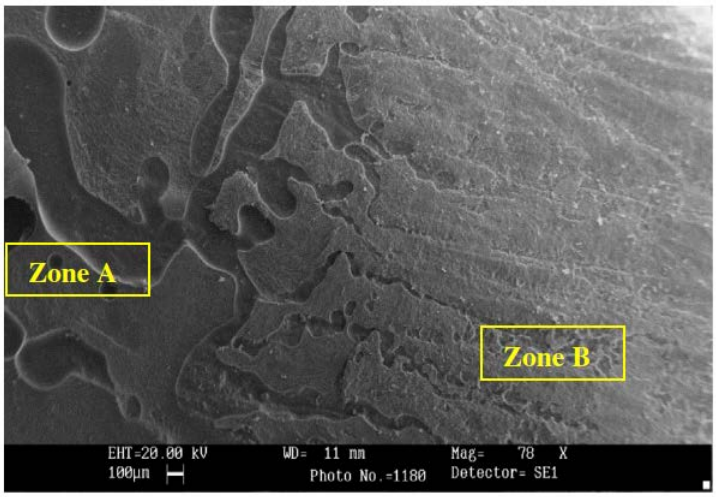

Figure 5. 12 *FE-SEM micrograph of fracture surfaces of the bonding areas-sample G failure in butt joint test.*

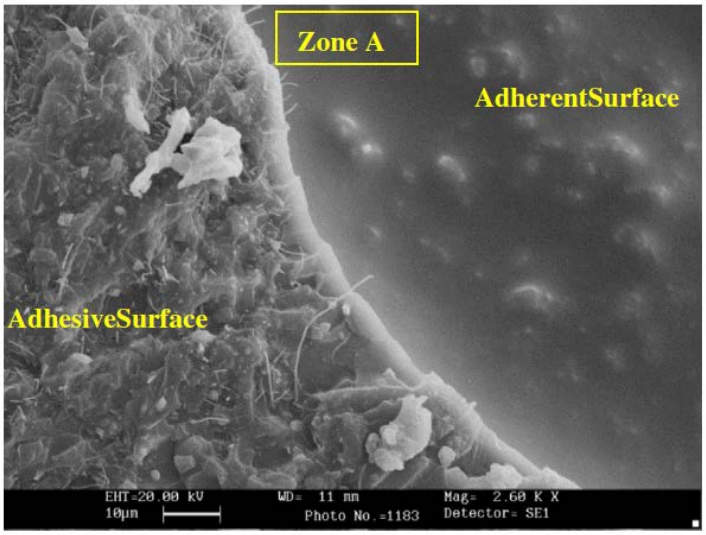

Figure 5. 13 *FE-SEM magnification micrograph of the neighbor regions of fracture surfaces of the bonding areas-sample G failure in butt joint test (zone A).*

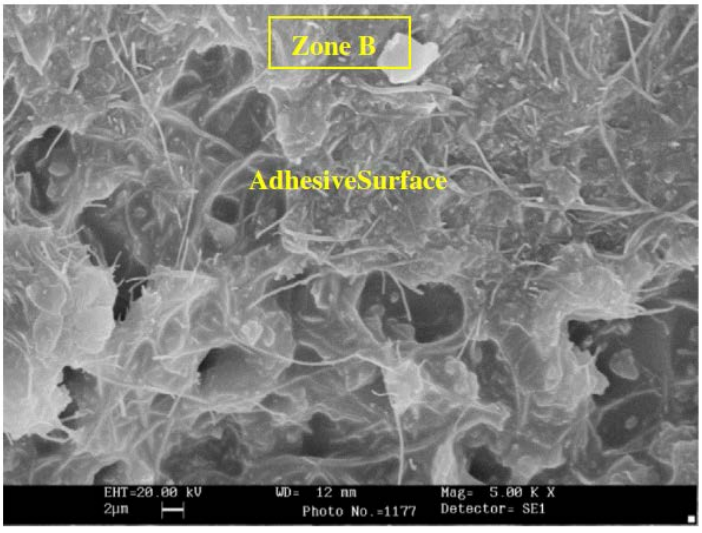

Figure 5. 14 *FE-SEM magnification micrograph of the neighbor regions of fracture surfaces of the bonding areas-sample G failure in butt joint test (zone B)*

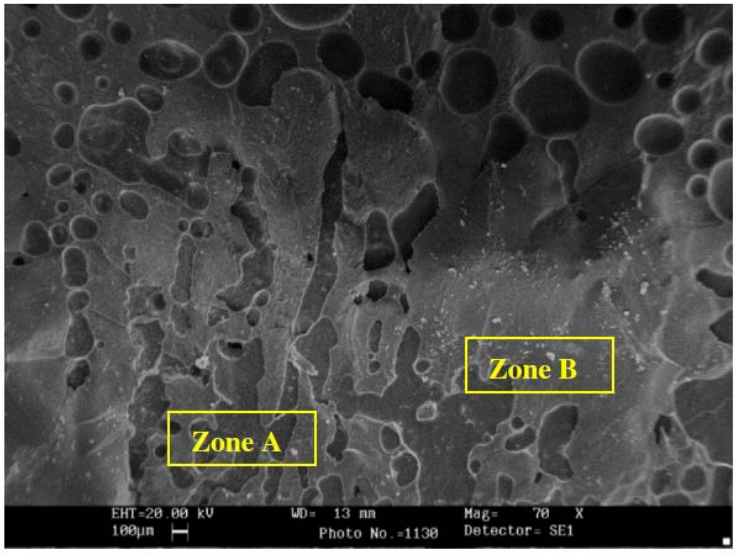

Figure 5. 15 *FE-SEM micrograph of fracture surfaces of the bonding areas-sample H failure in butt joint test.*

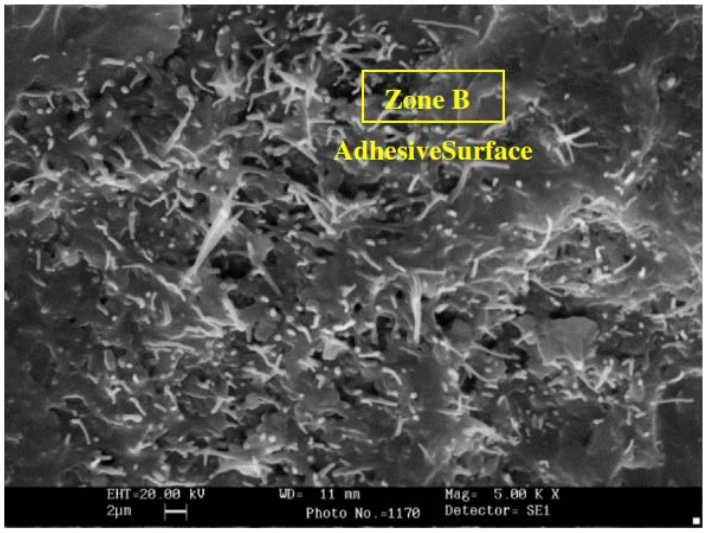

Figure 5. 16 *FE-SEM micrograph of fracture surfaces of the bonding areas-sample H failure in butt joint test.*

Figure 5.15 shows the fracture surface of sample G: in this case, two regions are clearly observed. In particular, dark zones (see zone A) corresponding to the failure between adhesive paste and adherent surface are distinguishable

from the clear ones (see zone B) containing remnants of nanofilled adhesive. A magnification of the neighbor regions highlights the difference in phase compositions of the two different areas (see Figure 5.16). The dark ones differ from the others for the absence of CNFs; in fact, in the clear zones we can also see the distribution of the nanofibers and the effect of the tensile load on their interaction with the epoxy matrix. The influence of the tensile strength experimented during the test causes a weakening of the interaction between CNF walls and epoxy matrix as evidenced from many nanofibers pulled out at the interface. In Figure 5.17 of the same sample, we can see the morphology of a large zone. The different colours of the same morphological feature indicates a cohesive failure inside of the nanofilled adhesive paste. In this morphological analysis, a particular attention is focused on sample H which has shown the best adhesive behavior. Figure 5.18 shows the fracture surface of sample H at low magnification. The shades of grey seem to indicate that the majority of the surface is involved in a cohesive failure (zone B). This hypothesis is confirmed by other images at higher magnifications in the regions with clear tonality (see Figure 5.19) where we can see an effect very similar to that of sample G (Figure 5.17) in the regions where cohesive failures were observed.

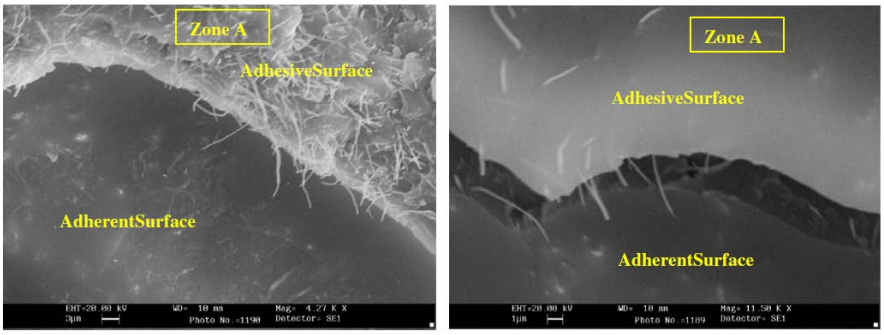

Figure 5. 17 *FE-SEM magnification micrograph of fracture surfaces of the bonding areas-sample H failure in butt joint test (zone A)*

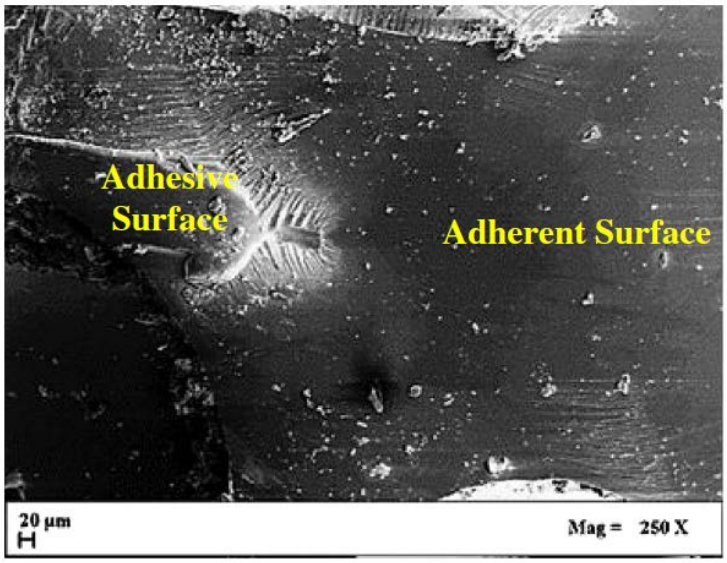

Figure 5. 18 *FE-SEM micrograph of fracture surfaces of the bonding areas-sample D failure in lap joint shear test.*

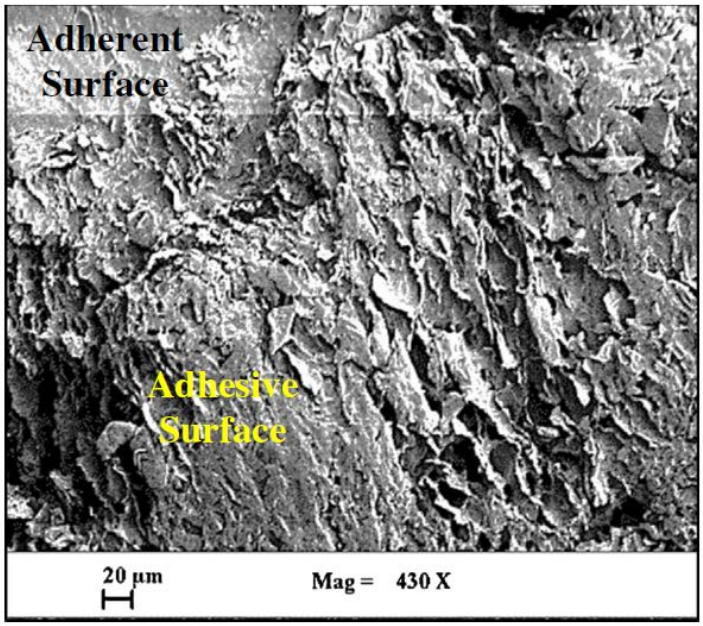

Figure 5. 19 *FE-SEM micrograph of fracture surfaces of the bonding areas-sample E failure in lap joint shear test.*

In Figure 5.17 we show the fracture surface of neighbor regions (see zone A) in sample H. We can see that in some regions (at lower area percentage than the clear ones), the adhesive failure is observed; but in this case many CNFs are observable between the adherent surface and the adhesive paste. The CNFs seem detached from the resin showing a position of nanofibers subjected a strong tensile stress between the two faces. This last observation seems suggest that a stronger bond exists at the interface of sample H as a result of the strengthening effect resulting from the dispersed nanofillers and the strong compatibility between adherents and adhesive due to a very similar chemical composition. Figures. 5.18 and 5.19 show the micrograph of the fracture surface of single lap joint tested in tensile mode refer to un-reinforced epoxy bonded joint (sample D), and for sample E. Either way, it was possible to observe a cohesive failure mechanism in bonded joint, and in particular, Figure 5.19 shows the presence of typical graphene platelets in adhesive paste which remained on the fracture surface. From an overall view on the results, the reinforcement effect due to nanometric filler has proven to be very effective in improving the attractive interaction between adhesive formulations and adherent surfaces. If we observe the morphology of sample A and H, at higher magnification (Figures 5.7b–5.17b), we can hypothesize that the network of nanomesh strongly increases the cumulative effect of Van der Waals interactions; their intensity is also amplified by the presence of the same nanofiller in the interface of adherent and epoxy adhesive. In the case of nanofiller or filler constitute of exfoliated graphite a negative effect is detected for the analyzed junctions. It is worth noting that in this last case the activities are in progress because in this paper, we have only used high nanofiller/filler concentration because our aim was to formulate a conductive epoxy adhesive and in the case of exfoliated graphite, the electrical percolation threshold was found for a higher percentage of filler [31](Lamberti et al., 2013).

5.3.3 Non-stoichiometric systems characterization

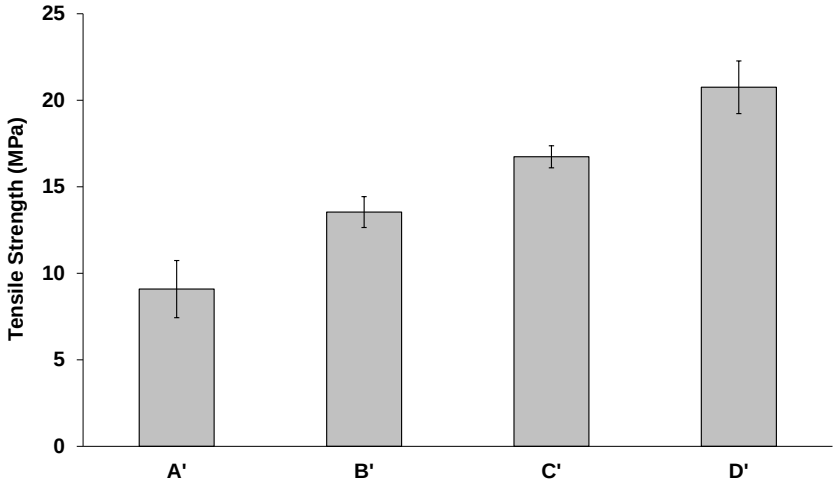

Figure 5. 20 *Histogram of tensile butt joint strength values non-stoichiometric systems*

Figure 5.20 shows that for the non-stoichiometric system, the tensile strength increases of 49% compared to the stoichiometric system. The inclusion of CNT's in the adhesive significantly improves mechanical behaviour of the bonded joint. In fact, by comparison of samples C' and D' with sample B', increases in tensile strength values of 25% and 54% respectively were achieved. In particular, for sample C', the inclusion of nano-reinforcement into the epoxy adhesive improves mechanical strength of the adhesive layer; it effectively transfer the external load to the adhesive layer containing MWCNTs, and failure occurred also in MWCNTs which behave as the strongest part of the composite adhesive. Figure 5.21 (SEM micrograph) shows several CNTs pulled out of the resin at interfaces between adhesive past and adherents.

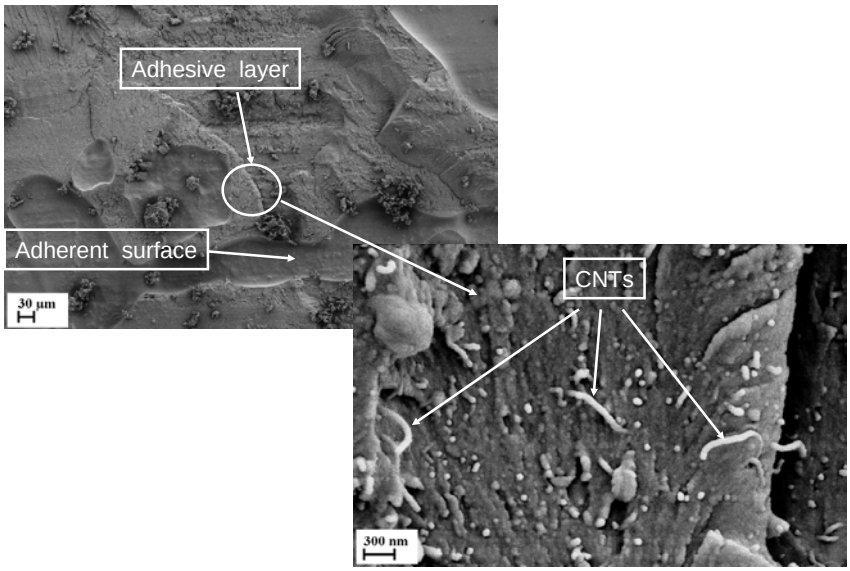

Figure 5. 21 *FE-SEM detail of the failure mode of sample D'*

Figure 5. 22 *Detail of the mechanism failure in the adherents of sample D'*

A different failure mechanism is involved in the case of sample D', which exhibits the best performance in tensile test. For this sample, replicated tests indicate that the failure mode of the joint occurs in the adherents, as shown in Figure 5.22. These results suggest that when CNT were incorporated also in the adherents, the failure between adhesive and adherents was more hindered than the joints with unfilled adherents (sample C'- case), indicating that at the

interfaces between adhesive past and adherents are active very strong attractive interactions forces. Therefore, the strategy to use CNTs in both adherents and adhesive paste allows to obtain a good compromise between the need to obtain a toughened bonded joint, with relatively high mechanical strength, and at same time, a joint composed of adhesive paste at low moisture content and high electrical conductivity(Guadagno et al., 2015c). The behaviour of sample D' demonstrated that the incorporation of CNTs only in the adherents was not sufficient to strengthen the bonded joint. In a previous paper (Guadagno et al., 2015d), the reinforcement effect due to graphene platelets has proven to be very effective in improving the attractive interaction between adhesive and adherent surface. In fact, the addition of an appropriate amount of graphene platelets into an epoxy adhesive formulation designed for structural application caused a significant improvement in the mechanical performance of the joints. This beneficial effect could be due to the cumulative joined effects of intermolecular interactions, such as intermolecular hydrogen bonding between the hydroxyl or carboxylic groups of graphene platelets and OH groups of cross-linked epoxy resins (Guadagno et al., 2015d).
In our case the tensile strength obtained is more high (20.75MPa), with a filler 1D. This value was also obtained for the modification of the structure of the matrix, as shown previously, thanks to the presence of a double phase transition (see chapter 4). In conclusion, adhesive properties can also be changed through appropriate modulation of matrix components.

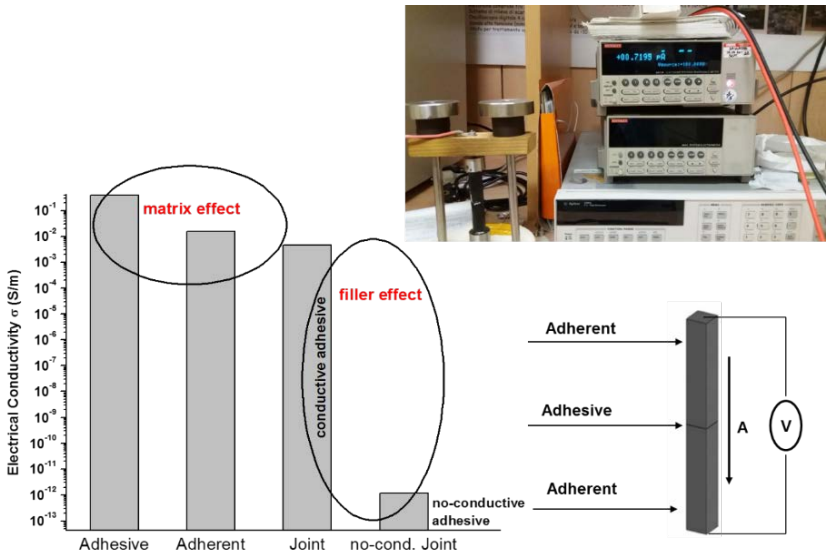

Figure 5. 23 *DC volume conductivity of the nanofilled composites and the on bonded joints*

In order to evaluate the electrical conductivity of the joint, electrical measurements were carried out on bonded joints, in which the adherent is constituted by Epoxy 0.5%MWCNT, the adhesive from Epoxy (NS) 0.5%MWCNT in the case of conductive material, Epoxy (NS) in the case of non-conductive material. The transversal surfaces of the joint were coated with silver paint in order to operate voltage/current measurements. Figure 5.23 shows the values of electrical conductivity of the adherent, of the adhesive and of the bonded joint. The electrical conduction of the joint depends on the conductivity of the individual elements of the joint (adherent/adhesive) and of the electrical conductivity at the interface adherent/adhesive. This occurs if the adhesive is conductive. If the adhesive is insulating as in the case of the unfilled resin, the electrical conductivity of the adhesive prevails over all others factors, infact the value of electrical conductivity of joint, with the no conductive adhesive is 10^{-12} S/m.

5.4 Conclusions

The addition of carbon nanofillers into an epoxy adhesive formulation caused a significant improvement in the bond strength of the joints, changing the failure mode of joints in single lap joint shear tests. The fracture of joints bonded with unfilled epoxy adhesive occurred at the epoxy along the bonding interface, and no significant damages were observed on the composite adherents. In contrast, the failure observed in nanoreinforced joints was cohesive in the adherents. The nanore-inforcing effectively transfer the load to in the adherents and the failure was in the composite. At higher nanofiller contents, (3.7 and 5 wt/wt%), adverse effects in bonded joints performance were observed. This occurrence might have resulted from aggregation and poor dispersion of the nanofiller into epoxy matrix, or also due to different nature between adherent surfaces and adhesive. Finally, adhesive properties can also be changed through appropriate modulation of matrix components that leads with at a better transfer of the load on the filler, as carbon nanotubes.

This page intentionally left blank

Chapter Six

6. Development of conductive adhesive, for Aircraft Primary Structures, by using carbon nanotubes and liquid rubber.

The aim of this chapter is to obtain a conductive adhesive, modifying the developed system in previous chapters by using a liquid rubber, in order to obtain high performance in the lap shear strength (LSS) with adherents in carbon fiber reinforced plastics. The study highlights the relations between the performance in the LSS and the structure of the polymer matrix by mechanical and microscopy analysis

6.1 Generalities and remarks

The adhesively bonded joints, in which an adhesive is placed between the surfaces of adherents and chemically cured, are increasingly being pursued as alternatives to mechanical joints in aerospace and other engineering applications. They provide many advantages over conventional mechanical fasteners such as lower weight, cheaper manufacturing cost, and improved damage tolerance (J.Bishopp, 2011). While electrically conductive adhesives (ECAs) also exist and are used in the electronic industry, conventional ECAs require 25–30% by volume (80% by weight) of conductive filler (J.Bishopp, 2011). Due to this high loading of filler, most commonly silver particles, only a small portion of the shear strength is retained and existing ECAs are not suitable for aerospace structural applications. Hence, although structural adhesives are already common on aircraft, riveting is still the only current solution for electrical bonding (Jakubinek et al., 2015b). A significant progress in the field of structural joints is the replacement of traditional rivets with structural epoxy conductive adhesives. The possibility to use adhesives for high structural materials (aeronautical, naval or infrastructural etc.) can simplify the design process of composite structures by reducing the thickness of structural components with consequent reduction of weight and materials. Furthermore, together with a cheaper joining process, the use of adhesive bonded joints entails other advantages among which a) the corrosion prevention: adhesive joints are not as sensible to crevice or deposition corrosion as solder and mechanical joints; b) fatigue resistance: a properly designed adhesively bonded joint eliminates or reduces the stress concentration at fasteners and increases the fatigue life of a given joint; c) preservation of the structural integrity of structural components such as carbon fibers reinforced composites (CFRCs), and d) reduction of additional holes in the resins impregnating carbon fabric/epoxy laminates and rivet weight.

The development of electrical conductive adhesives with good structural bonding capability is required in order to address the mentioned challenges and also to impart functional properties. The development of conductive epoxy adhesive to be used in the aeronautic field to join parts of primary structure is a current need with a view to optimizing efficiency of joints while preserving the conductivity of lightweight materials able to provide also in the joints good lightening protection. The enhancement in different properties of epoxy-based materials and or/adhesives depend on numerous parameters, such as the chemical nature of nanofiller, adhesive and adherents, the applied surface treatment or the tested properties (Prolongo et al., 2009b, Lafdi et al., 2008, Gude et al., 2011). Many researchers focused their research toward the development of new multifunctional adhesives for structural applications,

based on appropriate epoxy resin nano-modified with carbon nanostructured forms, able to hinder the insulator properties of resin if employed beyond their Electrical Percolation Threshold (EPT) (Jakubinek et al., 2015b, Guadagno et al., 2015d, Prolongo et al., 2010c, Vietri et al., 2014, Gkikas et al., 2012c, Meguid and Sun, 2004b, Billias and Borders, 1984). CNTs are known as materials with very remarkable electronic, thermal, optical, mechanical, spectroscopic and chemical properties, which have been attributed to the bonding structure of the CNTs (Hollertz et al., 2011, Reich et al., 2008, Qian et al., 2002, Yakobson and Avouris, 2001). The epoxy resins are reactive monomers, which are commonly cured with amine to form thermosetting polymers. If the epoxy is cured with an aromatic amine of sufficient functionality, the result is a highly cross-linked network with relatively high stiffness, glass transition temperature (T_g) and chemical resistance. Unfortunately, Epoxy resins are brittle materials that have fracture energies some two orders of magnitude lower than modern thermoplastics and other high performance materials (Rezaifard et al., 1993). In order to remain competitive as the materials of choice for many applications such as adhesives and composite matrices, the epoxies are modified to improve their fracture toughness. The techniques that allow the tailoring of the resin properties are in the forefront of scientific research. These techniques have the target in maximizing the dissipated energy through either the plastic deformation of the matrix, e.g. the inclusion of elastomers which increase the resin toughness (Pearson and Yee, 1989), or the modification of the crack initiation and propagation process e.g. ceramic modified polymers that inhibit interlaminar crack propagation. The most common methods of rubber toughening are by the use of liquid rubbers or preformed rubber particles. In the former method, the rubber is initially dissolved into the epoxy resin (Sultan and McGarry, 1973, Sultan et al., 1971), but during cure the rubber phase separates as a discrete particulate phase. Extensive studies (Moschiar et al., 1991, Verchere et al., 1991a, Verchere et al., 1990b, Williams et al., 1983) have shown that the phase separation process is a result of the decrease in configurational entropy due to the increase in molecular weight as the epoxy cures. This changes the free energy of mixing leading to a decrease in the solubility of the rubber that provides the driving force for phase separation. Thus the functionality of the matrix monomers, which control the development of the network and the cross-link density of the epoxy matrix, has an effect on the phase precipitation process. The particle size and concentration of the precipitated rubber also depends on the curing process and the interaction between the rubber and the epoxy resin. With butadiene-based rubbers, the solubility may be increased by forming a copolymer with the more polar acrylonitrile monomer. Another way that the liquid rubber may be modified to alter their interaction with the matrix is by functionalising the chain ends

with carboxyl, amine or epoxide groups that may couple with the reacting matrix (Chen et al., 1993, Verchere et al., 1990b, Riew and Kinloch, 1993).

6.2 Materials and Sample preparation

The composite mixture consists of a precursor tetraglycidylmethylenedianiline (TGMDA) an epoxy reactive monomer 1-4 butanedioldiglycidyl ether (BDE) that acts as a reactive diluent and the 4,4-diaminodiphenyl sulfone (DDS) as curing agent. These components were supplied by Sigma Aldrich. The elastomer employed is a carboxyl-terminated butadiene acrylonitrile copolymer (CTBN) from Hycar-Reactive Liquid Polymers, with Mn = 3600 containing terminal carboxy groups (COOH content of $0.67x10^{-3}$ equiv/g of CTBN and 18 w/w% of CN). The triphenylphosphine is employed as catalyst for the reaction between the epoxy and the carboxy groups. In order to obtain miscibility between epoxy precursor and CTNB, two precursor-elastomer (TGMDA-CTNB) masterbatch are prepared. The first is prepared by addition of 12.5 phr of CTBN and 10 phr of triphenylphophine in the precursor resin. This mixture is heated at 170 °C, using an oil bath and mechanical agitation promoted by an electric stirrer, for 24 h. The second system is prepared by addition of 25 phr of CTBN and 40 phr of triphenylphophine in the precursor resin. This mixture is heated at 200 °C, using an oil bath and mechanical agitation promoted by an electric stirrer, for 14 h. The epoxy mixture is obtained by mixing the TGMDA-CTNB system with BDE monomer at a concentration TGMDA/BDE of 80%:20% by wt. This particular epoxy formulation has proven to be very effective for improving nanofiller dispersion due to a decrease in the viscosity (Guadagno et al., 2014b, Nobile et al., 2015). The curing agent (DDS) is added. The concentration of DDS used is such as to reduce the moisture content, which is a very critical characteristic for aeronautic materials (Guadagno et al., 2015c). Epoxy blend and DDS are mixed at 120 °C and the MWCNTs (3100 Grade purchased from Nanocyl S.A) were added and incorporated into the matrix by using an ultrasonication for 20 min (Hielscher model UP200S-24 kHz high power ultrasonic probe) in order to obtain a homogeneous dispersion. All the mixtures are cured by a two-stage curing cycles: a first isothermal stage was carried out at the lower temperature of 125 °C for 1 hour and the second isothermal stage at higher temperatures of 200 °C for 3 hours.
Table 6.1 summarises the experimental mixtures used to fabricate these epoxy systems, where TC_x is the TGMDA/CTNB system, EPC_x is the epoxy resin cured with the hardener and x are the phr of CTNB.

Table 6. 1 *Composition in parts per hundred parts of precursor (phr) for each component in the final materials*

Sample cod	TGMDA-CTNB (phr)	TGMDA-CTNB-BDE (phr)
TC_0	**100/0**	
$TC_{12.5}$	**100/12.5**	
TC_{25}	**100/25**	
EPC0		**100/0/25**
EPC12.5		**100/12.5/25**
EPC25		**100/25/25**

6.3 Characterization Methods

6.3.1 Mechanical test

Adhesive tests were carried out using Dual Column testing system (Instron mod. 5967). The specimens were placed in the testing machine and the loading by setting a crosshead speed of 12.7 mm min^{-1} (0.5 inch min^{-1}) as standard requirements. Five specimens were tested for each adhesive composition. Tensile properties are evaluated with the crosshead speed of 1 mm/min. The obtained values were taken from an average of five specimens each with a dimension 80 x10 x 3 mm^3

6.3.2 FT/IR analysis

FTIR spectra were obtained at a resolution of 2.0 cm^{-1} with a FTIR (BRUKER Vertex70) spectrometer equipped with deuterated triglycine sulfate (DTGS) detector and a KBr beam splitter, using KBr pellets. The frequency scale was internally calibrated to 0.01 cm^{-1} using a He−Ne laser. 32 scans were signal averaged to reduce the noise.

6.3.3 Dynamic mechanical analysis

Dynamic mechanical properties of the samples were performed with a dynamic mechanical thermo-analyzer (Tritec 2000 DMA -Triton Technology). Solid samples with dimensions 2x10x 35 mm^3 were tested by applying a variable flexural deformation in three points bending mode . The displacement amplitude was set to 0.03 mm, whereas the measurements were performed at the frequency of 1 Hz. The range of temperature was from -90°C to 315°C at the scanning rate of 3°C/min.

6.3.4 SEM Analysis

Micrographs of the formulated nanocomposites were obtained using SEM (mod. LEO 1525, Carl Zeiss SMT AG, Oberkochen, Germany). All the samples were placed on a carbon tab previously stuck to an aluminium stub (Agar Scientific, Stansted, UK) and were covered with a 250 Å-thick gold film using a sputter coater (Agar mod. 108 A). Nanofilled sample sections were cut from solid samples by a sledge microtome. These slices were etched before the observation by SEM. The etching reagent was prepared by stirring 1.0 g potassium permanganate in a solution mixture of 95 mL sulfuric acid (95–97%) and 48 mL orthophosphoric acid (85%). The filled resins were immersed into the fresh etching reagent at room temperature and held under agitation for 36 h. Subsequent washings were done using a cold mixture of two parts by volume of concentrated sulfuric acid and seven parts of water. Afterward the samples were washed again with 30% aqueous hydrogen peroxide to remove any manganese dioxide. The samples were finally washed with distilled water and kept under vacuum for 5 days before being subjected to morphological analysis.

6.3.5 Electrical Properties

The electrical characterization of the nanocomposites focused on the DC volume conductivity was performed on disk shaped specimens of about 2 mm of thickness and 50 mm of diameter. In order to reduce possible effects due to surface roughness and to ensure an ohmic contact with the measuring electrodes, the samples were coated by using a silver paint with a thickness of about 50 μm and characterized by a surface resistivity of 0.001 Ω·cm. The measurement system, remotely controlled by the software LABVIEW®, is composed by a suitable shielded cell with temperature control, a multimeter Keithley 6517A with function of voltage generator (max ±1000V) and voltmeter (max ± 200 V) and an ammeter HP34401A (min current 0.1μA) for samples above the Electrical Percolation Threshold (EPT), whereas for those

below EPT a multimeter Keithley 6517A with function of voltage generator (max ±1000V) and pico-ammeter (min current 0.1fA) is used.

6.4 Joint preparation and testing

The adherents are obtained from laminate of fibre renforced composites supplied by Leonardo-Finemeccanica. The rectangular adherent, referring to existing international standard ASTM D 5868 standard requirements (101.6 mm by 25.4 mm by 1.0 mm) were obtained for the purpose (see figure 6.1a). The adhesive strength is determined by single lap shear test in accordance with the description given in ASTM D5868. The overlap length of the bonding region is 25 mm. The bonding area has a constant width of 25 mm. The carbon fiber/epoxy laminates, used as adherents, were treated by etching mixture (Vertuccio et al., 2015) for five hours. Following surface preparation of the composite adherents, joint panels were assembled. The adhesive was degassed in vacuum, before application. After applying the adhesive, the joint was assembled and cured. The joint assembled has been wrapped in an adhesive film in order to avoid the leakage of the resin during the cure. A simple clamping arrangement has allowed to apply a uniform pressure over the entire surface of overlap of the joint during cure (see figure 6.1 b). The maximum shear stress (LSS) acting on the joints is computed as:

$$LLS = \frac{F_{\max}}{bl} \tag{1}$$

where F_{max} is the maximum load registered during the tensile tests, b and l are respectively the width and the length of the overlapping area of the joint.

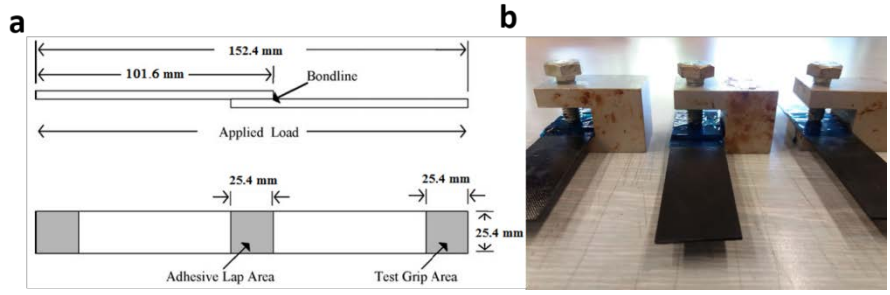

Figure 6. 1 *a) Single-lap shear joint configuration, b) clamping arrangement over surface of overlap of the joint*

The surface treatment of the adherents increases the adhesion in the joint. Figure 6.2 shows the values of the lap shear test for EPC0 adhesive. The LSS

value increased by about 34%. Probably, the etching mixtures allows oxidizing the surface of the adherent and at the same time, it allows increasing the surface roughness. The images in figure 6.2 show as the surface of adherent treated, presents an amount of adhesive higher compared to that obtained with the absence of surface treatment

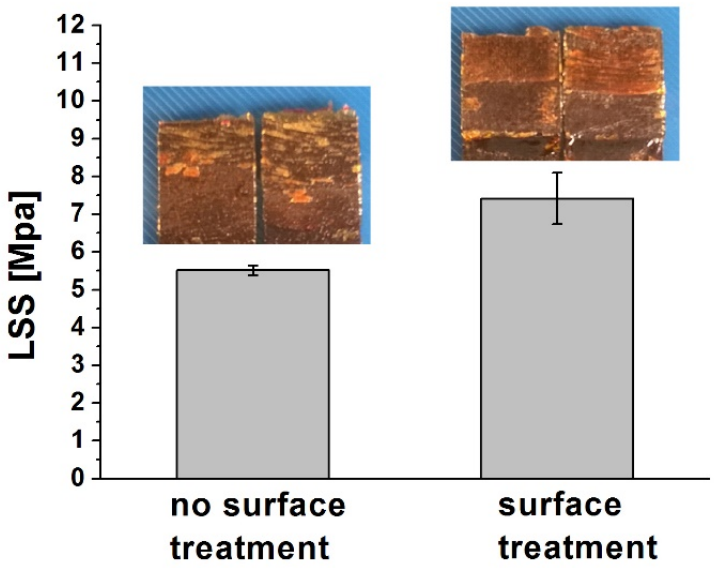

Figure 6. 2 *Lap shear strength for both treated and untreated adherents*

6.5 Results and discussion

6.5.1 IR characterization

The triphenylphosphine (PPh_3) is used as a pre-reaction catalyst to promote the reaction between the epoxy groups and the carboxylic acid groups of carboxyl-terminated butadiene acrylonitrile copolymer. The nucleophilic attack by triphenylphosphine opens the epoxy ring, producing a phosphonium salt. The carboxylic anion reacts with the electrophilic carbon attached to the positive phosphorus, regenerating the catalyst.

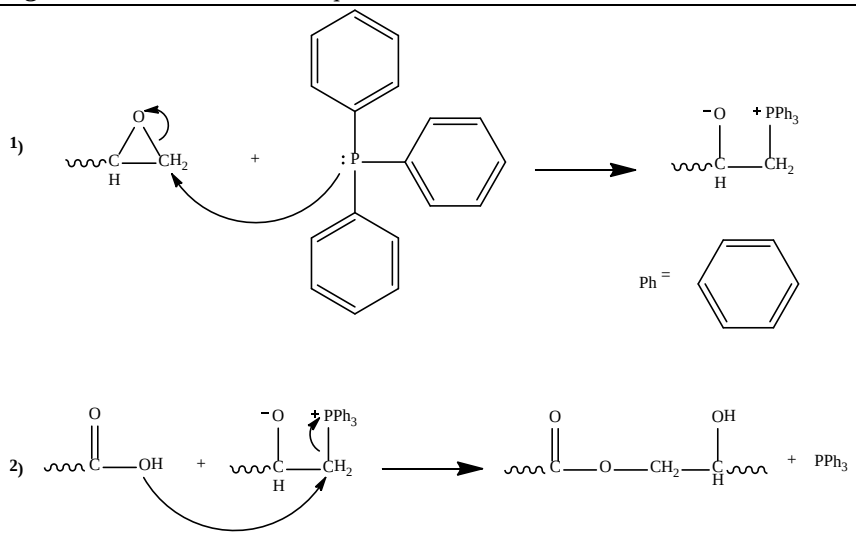

Figure 6. 3 *Reaction scheme showing the formation of functional group ester in the reaction between epoxy group of TGMDA and COOH group of CTNB*

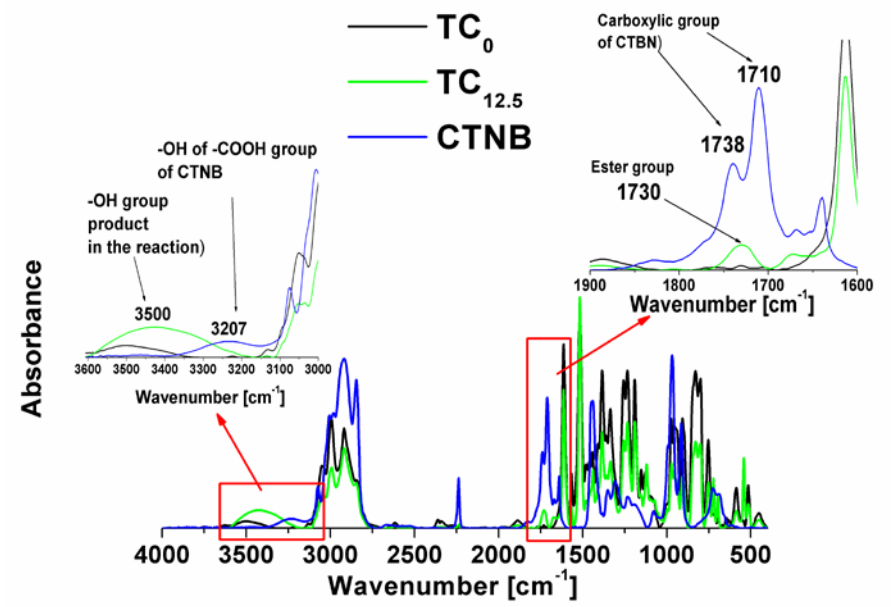

Figure 6. 4 *FTIR spectra of TC_0 system , $TC_{12.5}$ system and CTNB rubber*

Below is shown the FTIR characterization for the system containing 12.5 phr of CTNB. In an attempt to elucidate the reaction of the formation of TGMDA-CTBN pre-polymer, the samples are analyzed by FTIR. The absorption bands

at 1738 cm^{-1} and at 1710 cm^{-1}, which can be ascribed to the carboxylic group of CTBN, are not observed in the FTIR spectrum of TGMDA_CTNB system (see figure 6.4). On the other hand, an absorption band at 1730 cm^{-1} was observed that may indicate the formation of the functional group ester (see figure 6.4) (Ramos et al., 2005). The absence of the absorption band at 3207 cm^{-1}, which can be ascribed to the –OH of –COOH group of CTBN and the presence of an absorption band at 3500 cm^{-1}, that can be ascribed to the –OH group product in the reaction (see figure 6.3),(Akbari et al., 2013, Ramos et al., 2005). Therefore, FTIR results indicate the formation of the proposed links as shown in reaction scheme, which are necessary for an efficient stress transfer between the rubber particles and the epoxy matrix (Bucknall, 1977).

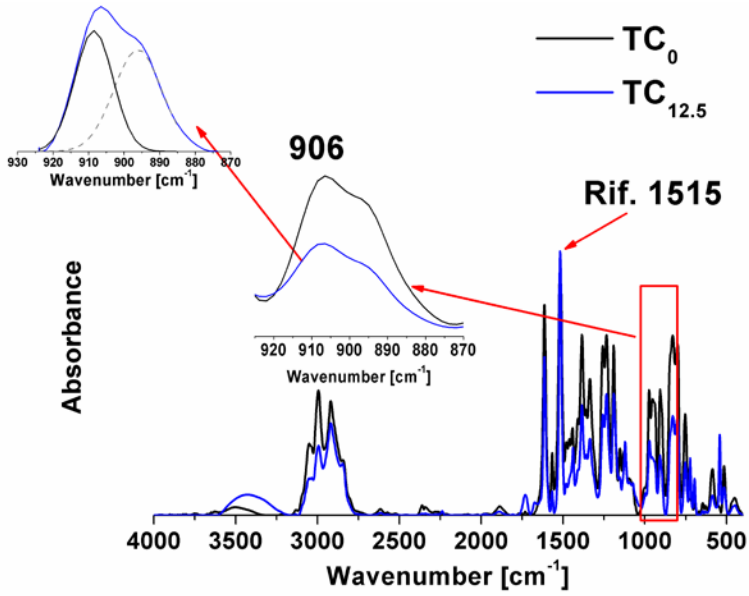

Figure 6. 5 *FTIR spectra of TC_0 system and $TC_{12.5}$ system.*

Figure 6.5 shows the peak at 906 cm^{-1}, which can be ascribed to the oxirane group of precursor (Morgan and Mones, 1987). When CTBN is added to precursor, generally it is expected that the oxirane ring is opened by the carboxyl functional group of the CTBN as it is shown in figure 3. As can be seen in Figure 6.5 between TGMDA and TGMDA_CTNB system, significant differences could be observed. In order to evaluate the effective reduction of the peak relative to the oxirane group, the intensity of the latter it has been normalized to the peak at 1515 cm^{-1} associated with the phenyl group, which is assumed chemically unmodified during the reaction. (Morgan and Mones, 1987) The ratio ($R= A_{peak\ 906}/A_{peak\ 1515}$) of the subtended areas is evaluated for TGMDA systems and TGMDA_CTNB respectively (The peak function was

a mixed Gauss–Lorentz line shape; This is calculated, by a non-linear curve fitting of data, the height, the full width al half height (FWHH) and the position of the individual components) (Maddams, 1980). Figure 6.5 shows in detail the peaks taken into account and the resulting relationships. The ratio R varies by about 30% from a value of 0.15 for the TGMDA system to a value of 0.10 for the TGMDA_CTNB. In a similar way was made a FTIR analysis, not shown here, for the system with 25 phr of CTNB, in order to verify the successful reaction between the oxirane ring of the epoxy precursor and the carboxylic group of the CTNB

6.5.2 Mechanical properties (CTNB effect)

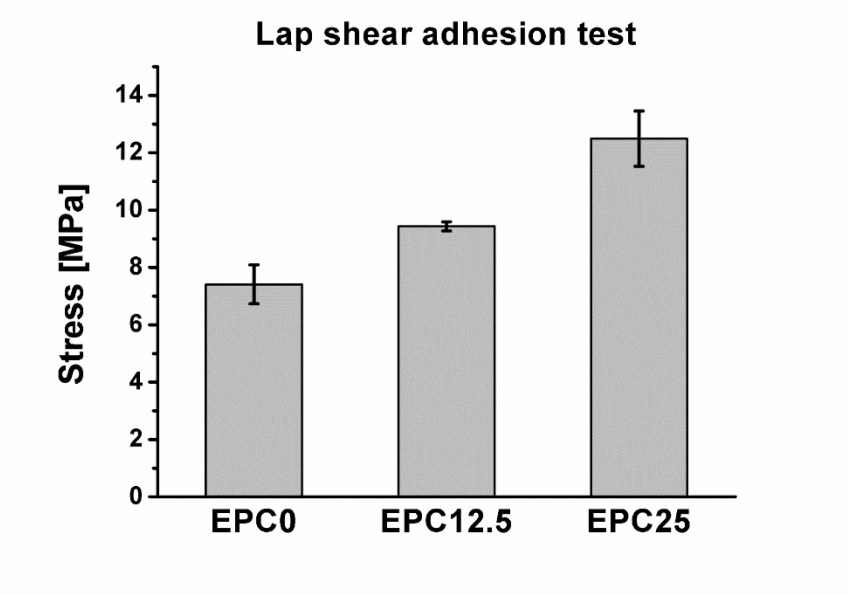

Figure 6. 6 *Lap shear strength of epoxy resin with the CTNB*

The adhesive properties of the resin were evaluated by varying the amount of elastomer. Figure 6.6 shows that the modified resin adhesive properties increase with the increasing of amount of CTNB. In particular, there is an increase of 27 % for the EPC12.5 sample and an increase of 69 % for the EPC25 sample. The cured rubber-modified epoxy exhibit a two-phase microstructure consisting of relatively small rubbery particles dispersed and bonded in an epoxy matrix. This microstructure results in a material that has a considerable higher toughness compared to the unmodified system (Ramos

et al., 2005). The change of structure, obtained by introducing of CTNB, is analyzed by an evaluation of the mechanical properties.

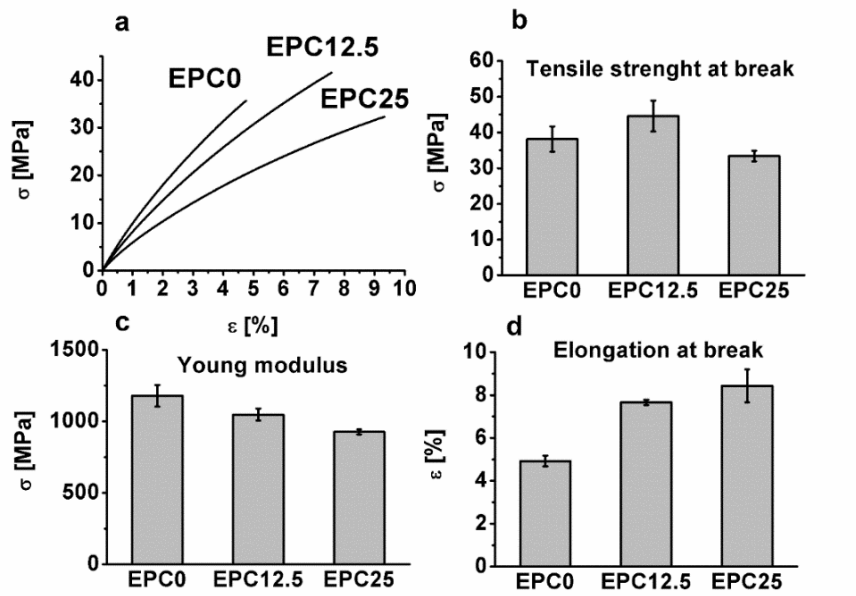

Figure 6. 7 *Mechanical properties of CTNB_modified epoxy resins*

Figure 6.7a shows the stress–strain curves of one sample as representative of each CTBN-modified epoxy resins as well as neat epoxy sample. The brittle fracture, the absence of yielding and non-linear viscoelastic behaviour, are confirmations for the neat epoxy resin; whereas, the CTBN-modified epoxy resins exhibit large deformation and higher strain-at-break. From Figure 6.7, it is observed that the CTBN improves the toughness of epoxy resin. The tensile strength, the modulus and the elongation-at-break are plotted (see figures 6.7b, 6.7c, 6.7d) with the variation of CTBN content in the blend of epoxy/rubber samples. Fig. 5b shows that the tensile strength initially increases from 38.1 MPa to 44.6 MPa by about 17.1 %, compared with neat epoxy as 12.5 phr CTBN is added in the blend of epoxy. An increase in tensile strength might have demonstrated some types of interaction between the rubber particles (CTBN) with epoxy resin, which might have been mechanically stronger than the unmodified blend system (Shukla and Srivastava, 2006). Beyond 12.5 phr, the reduction in the value of tensile strength of modified blend, may be ascribed to the lowering in cross-linking density of the epoxy network as the modifier occupies the reaction centres during modification. For the decrease in the tensile strength, different discussions were given by Huang and Kinloch (Huang and Kinloch, 1992) and

Shukla and Srivastava (Shukla and Srivastava, 2006). Kinloch et al. conclude that the value of tensile strength decreases with the presence of micro voids, but Srivastava et al. conclude that the lowered tensile strength could be interpreted with the stress concentration effect of the rubber particles. A continuous decrease in the modulus is observed with the concentration of the CTBN (Figure 6.7c). The modulus decreases from to about 1.17 GPa, by about 25 %, compared with the neat epoxy resin. The decrease in modulus can be due to lower modulus of elastomer phase than the modulus of the epoxy phase. Generally, when a rubber modifier is added to the epoxy resin, its elastomeric character enforces a decrease in modulus (Saadati et al., 2005, Tripathi and Srivastava, 2007).The elongation-at-break of the modified epoxies increases continuously with the increasing rubber phase content in the blend samples (Figure 6.7d). The elongation-at-break increases from about 4.9 to 8.4 % with the increase of CTBN amount from zero phr to 25 phr. This increase could be a reason for a good adhesion via a chemical reaction between the rubber and epoxy phase(Bucknall, 1977).

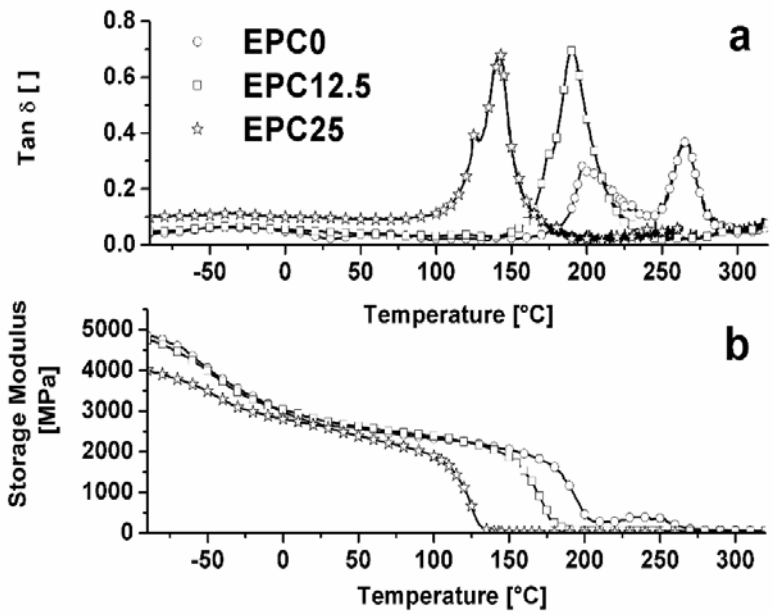

Figure 6. 8 *Tan δ a) and storage modulus b) of CTNB_modified epoxy resins*

Figure 6.8a shows the loss factor (tan δ) of the epoxy formulation EPC0. The intensity of the main transition, α transition, is affect by the stoichiometry and therefore by the curing degree of the resin, in fact the samples EPC0 exhibit two distinct peaks most likely due to fractions with different crosslinking

density characterized by two different values of T_g (Guadagno et al., 2015c). The first peak at the highest temperature is about 267 ° C while the peak at the lower temperature to about 200 ° C. This suggest that two phases can coexist in the resin with different percentages depending on the stoichiometric amount of hardener. The introduction of CTNB determines a reduction of the glass transition temperature. The reduction consists of a peak value of 190 ° C for the sample with 12.5 phr of elastomer and of 143 ° C for the EPT25 sample. Furthermore, the glass transition temperature itself is presented as a single phase, demonstrating the homogeneity of the distribution of the rubber in the thermosetting matrix. In a previous work (Stewart et al., 2007) the authors affirm that the plasticiser works to promote the onset of the transition and a higher volume of non-agglomerated plasticiser causes a lower T_g and an increased adhesive performance. A lower glass transition temperature, results in lower modulus values in particular for the mixture of rubber with 25phr. These results confirm that the introduction of CTNB, has an action plasticizer in the matrix. This action leads to get better adhesive properties. Many discussions have been made about why this behaviour. The crack front pinning results when a crack front meets a number of toughened particles. The crack is forced to propagate around these particles, as they resist its progress. This creates a deformation in the crack and an increased level of energy is required by the crack to maintain progress. This mechanism can also cause particles de-bonding in severe cases, which helps to blunt the crack tip, increasing the fracture toughness of the material. An increase in the energy required to maintain the propagation of the crack is seen here too which helps to improve the adhesion of the material (Baldan, 2004). Initiation of crack tip deformation processes is found to occur through the translational motion of the entire crack front (Baldan, 2004). The propagation of crack through the rubber particles causes small voids to cavitate (Dean et al., 2004). The cavitation is a major mechanism of the increase the fracture energy of the adhesives. The stress is further dissipated through the growth of such voids until ultimately the coalescence occurs (Argon and Cohen, 2003, Shieu, 1997, Chikhi et al., 2002, Kinloch, 2012). The crack bridging can occur as the particles are stretched from their initial sites and the progress of the crack is inhibited. In this research, it is found that the majority of mechanical properties deteriorate as the proportion of CTBN is increased. The elastic modulus, the tensile strength and the glass transition temperature are all reported to decrease, but the shear strength are improved. For a brittle adhesive, which has high crosslink density and high cohesive strength, but low chain flexibility, the increase of the chain flexibility can reduce the concentration of external stress and enhance the ability of the adhesive to inhibit the crack propagation. Therefore, the lap shear strength is increased (Bever, 1985).

6.5.3 Electrical properties

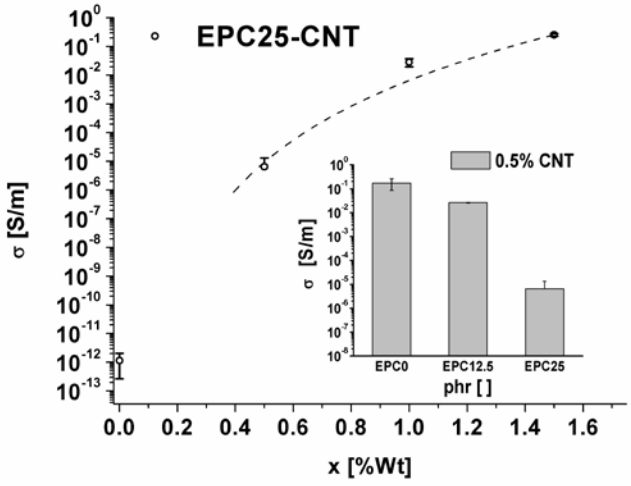

Figure 6. 9 *Electrical conductivity of CNT/system with 25 phr of elastomer; Inset: Electrical conductivity of the samples at 0.5% CNT vs amount CTNB*

The electrical conductivity of mixtures of CNTs and polymers is a widely investigated subject (Sandler et al., 1999, Song and Youn, 2005, Martin et al., 2005, Sandler et al., 2003, Moisala et al., 2006, Du et al., 2005, Kim et al., 2005b, Kovacs et al., 2007, Špitalský et al., 2009, Guadagno et al., 2010b). The conduction in CNTs composites has been explained by considering that, conductive paths are formed in the composite when the CNT concentration x increases over a threshold value x_c, causing in the material a conversion from an insulator to a conductor. The percolation theory describes the dependence of the conductivity σ on the filler concentration by a scaling law of the form $\sigma = \sigma_0(x-x_c)^t$ where x_c is the percolation threshold and t an exponent depending on the system dimensionality(Du et al., 2005, Kim et al., 2005b, Kovacs et al., 2007, Moisala et al., 2006, Sandler et al., 2003, Martin et al., 2005, Špitalský et al., 2009, Guadagno et al., 2010b, De Vivo et al., 2009, Gorrasi et al., 2007, Kymakis and Amaratunga, 2006, Bauhofer and Kovacs, 2009). In particular, in Ref. (Bauhofer and Kovacs, 2009), some general results concerning a systematic correlation between material characteristics (polymeric matrices, CNT type, synthesis method, treatment, etc.) and parameters describing the percolation law are presented. The behaviour of the static volume conductivity of MWCNTs vs. the filler concentration at room temperature for the composites with 25 phr of elastomer is summarized in Figure 6.9. Some remarkable differences can be evidenced from such plots. As shown in Figure 6.9, the epoxy composite exhibits the typical abrupt

increase of the conductivity from the value of the pure epoxy resin ($1.16 \cdot 10^{-12}$ S/m) to a very high one ($2.8 \cdot 10^{-2}$ S/m) predicted by the percolation theory with a $x_c \leq 1.0\%$. By increasing the MWCNT percentage up to 1.5%, a high value of conductivity ($2.6 \cdot 10^{-1}$ S/m) is achieved. The conductivity does not reach the values obtained for dense films at the explored concentrations levels of CNTs ($\approx 10^3$ S/m)(Guadagno et al., 2011) owing to the effect of nanotube/nanotube contact resistance described in (Li et al., 2007). In their studies on the role of tunnelling resistance in the electrical conductivity of carbon nanotube-based composites, Li et al. (Li et al., 2007) using Monte Carlo simulations found that the tunnelling resistance plays a dominant role in the electrical conductivity of composites.In particular, according to the model proposed in Ref. (Li et al., 2007), a variable tunneling (contact) resistance between nanotubes due to insulating wrappings (sheaths) of different thickness may be considered to explain the observed differences. This theory may explain the behavior of the electrical conductivity variation shown in the inset of Figure 6.9. The inset of Figure 6.9 shows the variation of the electrical conductivity vs. the amount of CTNB, for sample filled with 0.5% by weight of carbon nanotubes. A reduction of 5 orders of magnitude is obtained, for the composite with 25 phr of CTNB, compared to EPC0 sample. This change between the two composites can be attributed to an increase of the tunneling resistance due to the combined presence of a brittle phase and a toughened phase and, probably, to a different distribution of the carbon nanotubes in the matrix. In any case high values of electrical conductivity, comparable to those obtained in our previous papers (Guadagno et al., 2011), were obtained by increasing the concentration for carbon nanotubes of only one percentage point.

6.5.4 Mechanical properties (carbon nanotubes effect)

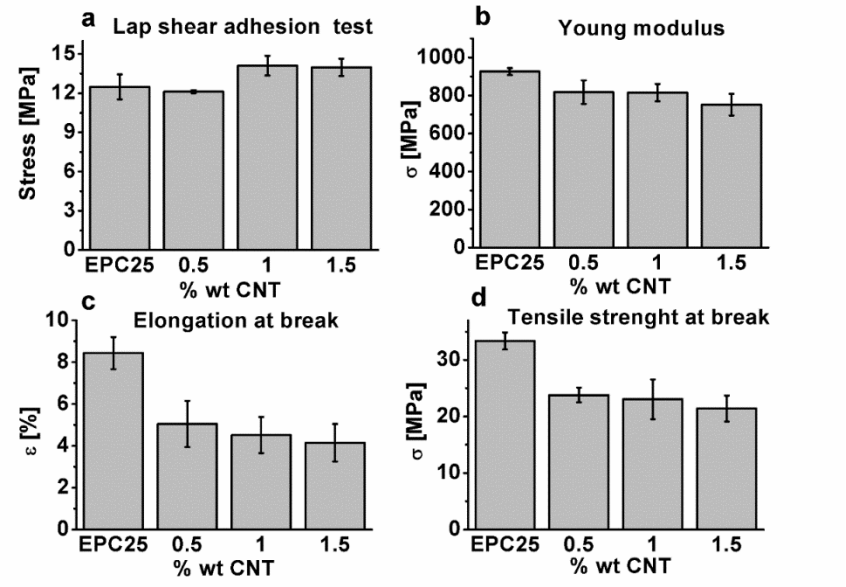

Figure 6. 10 *Mechanical properties CNT/system with 25 phr of elastomer: a) LSS, b)Young modulus, c) Elongation at break, d) Tensile strength at break*

The adhesive properties of the resin, with 25 phr elastomer, were evaluated by varying the amount of carbon nanotubes. The figure 10a shows that the modified resin adhesive properties increase with increasing of amount of carbon nanotubes. The adhesive properties of the resin increase by about 13% for the sample containing 1% by weight of the CNT, while the lap shear strength remains on the maximum average value of 14 MPa with a maximum value of about 15 MPa for the sample loaded with 1% of carbon nanotubes. The values obtained in this study are higher than those obtained in previous papers, with conductive adhesives, in which the fiber reinforced laminates adherents are used, and in which the ASTM 5868 standard was used. While there are many reports on the electrical conductivity and mechanical properties of bulk CNT-polymer composites, there are relatively few reports of performance tests based on end-use applications (e.g., adhesive joints). Such studies are important as the application performance can differ from that expected from the bulk properties (Rosca and Hoa, 2011, Ashrafi et al., 2012), and joint-strength is not necessarily well predicted by bulk mechanical properties. Nearly all studies have employed MWCNTs and single lap shear tests. Improvements in lap-shear strength of ≈10–40% have been achieved in

several instances (Zhang et al., 2012, Liu and Bae, 2011, Srivastava, 2011, Meguid and Sun, 2004a). Improved fracture toughness in wedge tests for aluminium–aluminium joints with SWCNT–adhesive composites also has been demonstrated (Ashrafi et al., 2012). Even fewer studies have considered the joint electrical performance. Good electrical conductivities (e.g., $s \approx 0.1$ S m^{-1} for 1 wt%, 1 S m^{-1} for 2 wt%, and 100 S m^{-1} for 12 wt%) were reported with relatively large amounts of MWCNTs in epoxy, but with decreased lap shear strength compared to the unfilled epoxy (Meguid and Sun, 2004a). The just mentioned improvements in lap shear test do not exceed the absolute values of LSS of 10-12 MPa. In addition, the test mode and the standards used are not unique. This creates high difficulty of evaluation of performance obtained, especially if we want to consider the combined effect of adhesive properties, electrical properties, mechanical properties, glass transition temperature, etc. In Figure 6.10b,c,d, the change in the mechanical properties are shown. In particular, we found a decrease in mechanical properties (Young modulus, tensile strength at break, elongation at break) to grow the carbon nanotubes amount. A similar behavior was obtained from Meguid et al. (Meguid and Sun, 2004a) but only to high concentrations of nanoparticles. While, it is known that the introduction of small percentages of carbon nanotubes leads to an improvement of the mechanical properties (Schadler et al., 1998, Gojny et al., 2004). Song et al. (Song and Youn, 2005) affirm that a good dispersion of the filler allows to improve the mechanical properties with the introduction of carbon nanotubes. In our case, in previous papers (Guadagno et al., 2014b) the introduction of carbon nanotubes in a mixture similar to the one obtained in this work and in the absence of elastomer, has allowed to obtain, in the dynamic mechanical analysis, a higher modulus compared to the unfilled resin. Probably, the presence of the elastomer, in the conductive resin, interrupts the nanotubes network, determining a reduction of the electrical conductivity in the composite, as we show in the inset of the figure 6.9. This not good global distribution affects on the mechanical properties of the resin but not in the adhesive properties. An explanation of the phenomenon is clear in dynamic mechanical analysis.

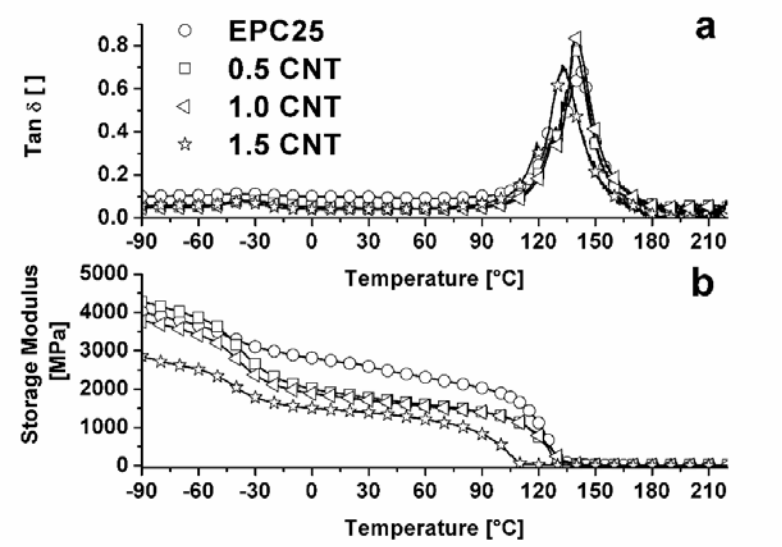

Figure 6. 11 *Tan δ a) and storage modulus b) of CNT/system with 25 phr of elastomer*

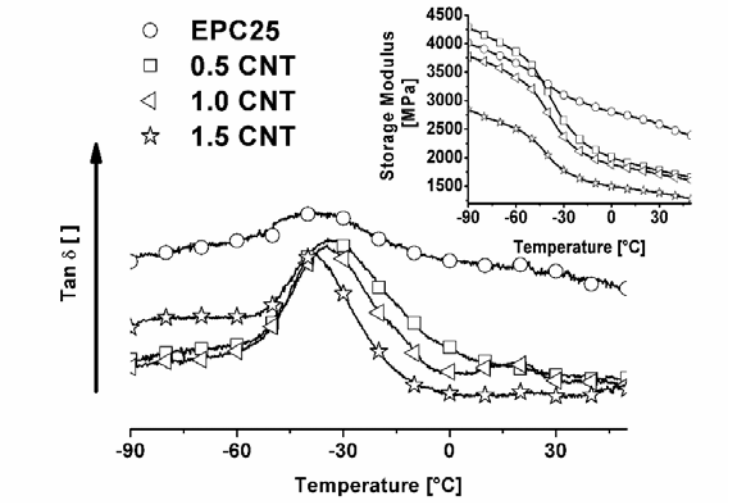

Figure 6. 12 *Magnification Tan δ and storage modulus (inset) of CNT/system with 25 phr of elastomer in the range temperature from -90°C to 50°C*

Figure 6.11 shows the behaviour of tan δ (Figure 6.11a) and of the storage modulus (Figure 6.11b) vs. the temperature. The introduction of carbon nanotubes does not cause essential differences in the glass transition

temperature which remains substantially at the value of 140 ° C, except for the system containing 1.5% by weight of CNT which has a T_g = 132 ° C. The modulus decreases with the increase of carbon nanotubes concentration. Specifically, the decrease is around 0.9 GPa in the temperature range between 0 ° C and 90 ° C, for systems that contain up to 1% of CNT. For higher values of concentration of CNT, the decrease in the modulus is highest in the entire temperature range.

A poor dispersion degree of the carbon nanotubes has determined this behaviour. The presence of the elastomer and of the filler increases the viscosity (Prolongo et al., 2010a, Ratna, 2001) of the mixture making it less effective the effect of sonication. The abrupt decrease of the module is achieved at low temperatures (see Figure 6.12), in the temperature range from -90 ° C to 0 ° C, in which there is a different transition attributed to the presence of CTBN. The introduction of carbon nanotubes leads to a greater presence of this phase, which shifts to lower temperature. The presence of this phase has already been discussed in previous papers. Barcia et al. (Barcia et al., 2003) assert that the peak at low temperature appears in the same glass transition region relative to the polybutadiene phase. They assume that, in all the modified networks there is a phase separation due to the presence of rubber particles in the modified epoxy resin are not fully dissolved into the epoxy matrix. Wise et al. (Wise et al., 2000). found that the magnitude of the peak at low temperature increases when the rubber level is raised. An explanation can be that the lowering of the CTBN rubber T_g may be due to compositional heterogeneity of acrylonitrile in the copolymer chains, which causes compositional fractionation of the acrylonitrile–butadiene copolymer during the phase precipitation process. This could cause the nonpolar, butadiene-rich component of the CTBN copolymer to be preferentially expelled from the more polar matrix thus leading to a reduction in the T_g of the dispersed phase because the butadiene-rich CTBN has a lower T_g. In our case, the evident presence of the low-temperature phase is determined by the introduction of carbon nanotubes. The reason for this, is due, probably, to the fact that the carbon nanotubes hinder the crosslinking reaction between the chain segments composed by the precursor linked to the elastomer, creating a separate phase formed by chain segments of precursor/elastomer. Finally, although the carbon nanotubes cause a reduction in the mechanical properties, reducing the cohesive forces of the adhesive, they increase the adhesion in the joint. The adhesion enhancement may be attributed to the CNTs/epoxy interface which activated mechanisms at the nanoscale such as crack bifurcation and arrest, delaying thus the global shear failure (Gkikas et al., 2012b). Interestingly enough, the enhancement was only observed for 1% CNT, indicating that adhesion improvement was becoming statistically significant after a critical loading.

5.5.5 Morphological Investigation

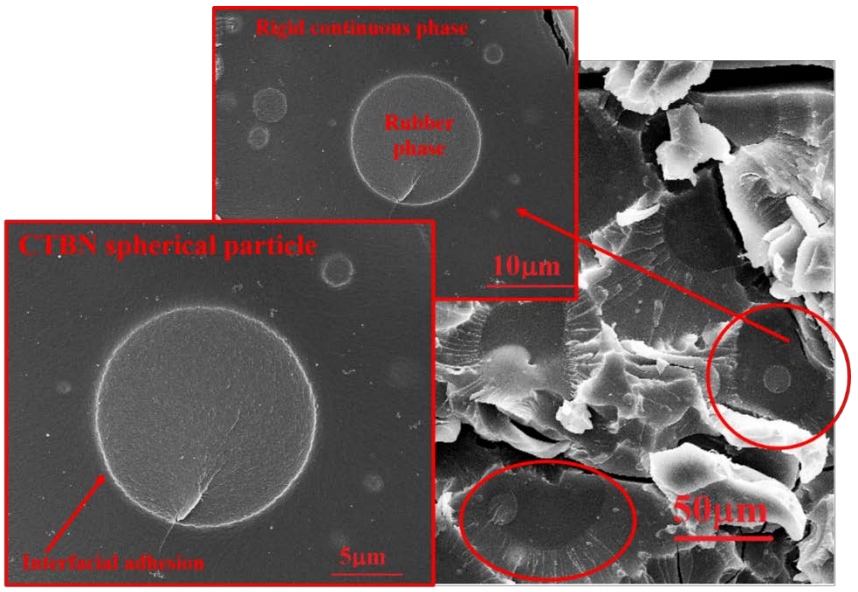

Figure 6. 13 *SEM images of the fracture surface of system with the elastomer at 25 phr (EPC25)*

In order to analyze the homogeneity of the nanofiller dispersion in the polymeric matrix, morphological analysis by SEM was carried out on etched samples to remove the resin surrounding the nanofiller, leaving them bare. Figure 6.13 shows SEM images of the fracture surface of system with the elastomer at 25 phr (EPC25).The fractured surfaces of the CTBN-modified epoxy matrix shows two-phase morphology with a scattered rubber phase (CTBN spherical particles) and a rigid continuous phase (epoxy matrix). The size of rubber particles in blend sample containing 25 phr of CTBN, is in the range of few micron, except in the case of a few elements that are around to a size of 15 microns. The increase in the rubber particles, in the epoxy matrix, leads to an effect of plasticization which causes the deterioration of important properties as compared to the unmodified resin (Verchere et al., 1990a, Hwang et al., 1989, Verchere et al., 1991b), confirming the results obtained in figure 6.7. Barcia el al. (Barcia et al., 2003) , in previous work, observed a heterogeneous morphology resulted in opaque samples. The holes observed in the micrograph are related to the rubber particles that were withdrawn from the surface after the treatment with solvent, indicating no chemical bond between the blend components. In our case, one can observe the presence of several rubber particles that were not extracted with the etching treatment,

indicating strong interfacial adhesion between the epoxy precursor and the elastomer.

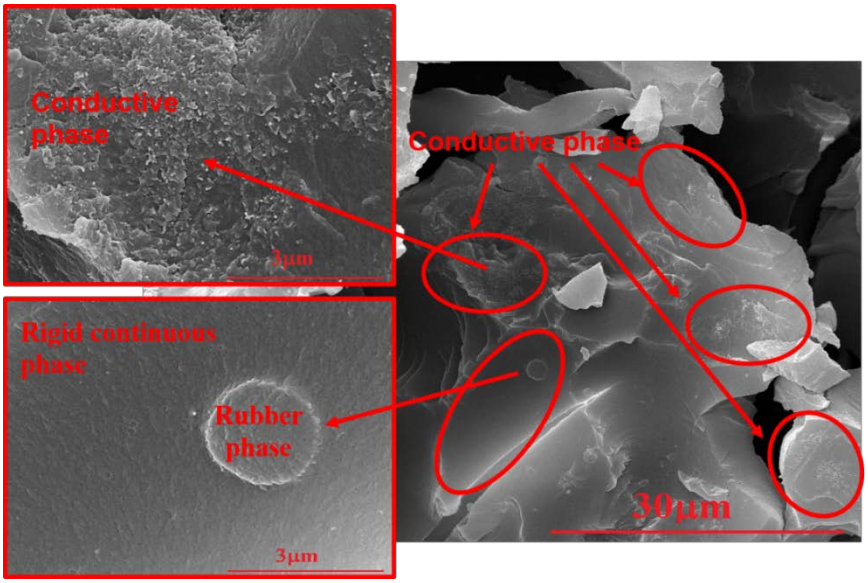

Figure 6. 14 *SEM images of the fracture surface of system 25 phr CTBN / epoxy with a 1.0% carbon nanotubes.*

Figure 6.14 shows the system 25 phr CTBN / epoxy with a 1.0% by weight of the amount of carbon nanotubes. The image reveals two separate areas, one with the presence of only the carbon nanotubes, the other with the presence of the only elastomer. Probably this configuration, composed of two macro phases, a conductive and the other insulating, determines the presence of T_g at low temperatures found in figure 6.12. In addition, this phase not only leads to a decrease of the mechanical properties but also leads to a not good distribution of the carbon nanotubes, interrupting the percolation network (see inset of fig. 6.9). An increase of the amount of the carbon nanotubes, on the one hand allows to make the conductive system (see fig 6.9) from the other reduces the mechanical properties (see fig. 6.10).

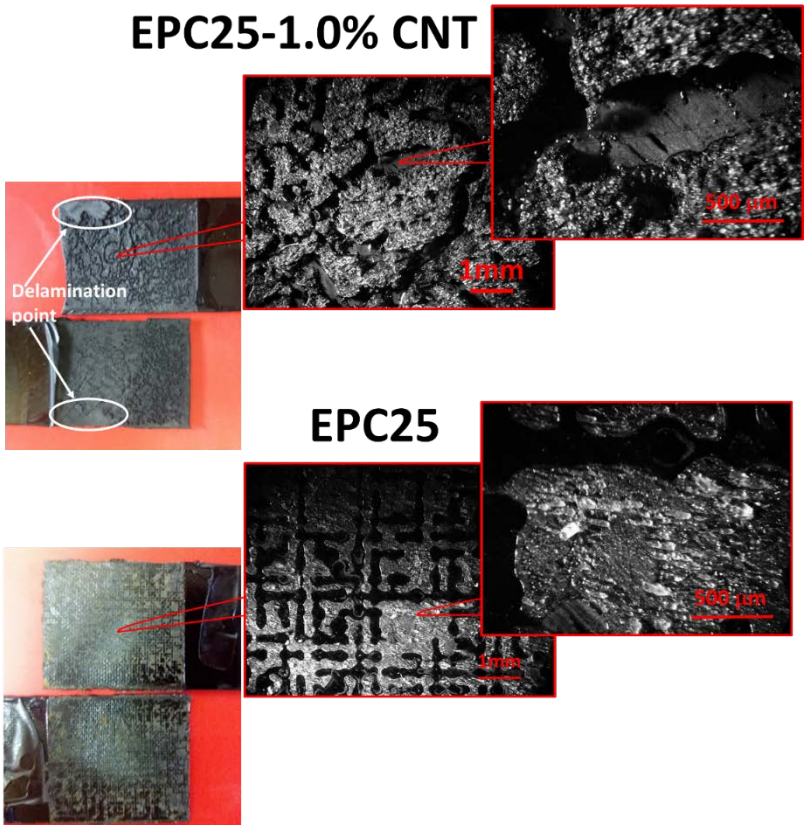

Figure 6. 15 *Optical images of fracture surfaces of the tested adhesive joints*

The fracture surfaces of the tested adhesive joints are examined using optical microscopy and scanning electron microscopy.
Figure 6.15 shows the joint surface tested with the EPC25 adhesive with 1% by weight of the CNT. The adhesive uniformly covers the surface of the joint, except for a zone, circled in white, which has a cohesive failure. In this case, the cohesive failure in the laminate indicates a crack propagation between the surface resin layer and the first layer of carbon fiber. From a careful observation with an optical microscope, the surface of the joint presents the channel in which the fiber is stripped. Even in such areas, phenomena of delamination of the upper layers of carbon fiber, are obtained. The failure mode is mixed adhesive/delamination in the joints bonded with nano-reinforced epoxy adhesive. On the contrary, the neat epoxy adhesive (see figure 6.15) it is distributed on the surface of the joint, on a regular basis, following the adherent's surface but in lower amount. The delamination phenomena do not occur and the failure mode is adhesive. The comparison

between the two surfaces analyzed explains the effect of carbon nanotubes on the adhesion performance in the joint. If on the one hand, the nano-reinforced system, allows having a larger contact surface with the surface of adherent, on the other, it causes phenomena of delamination on the surface of the adherent. The two effects are balanced partially, resulting in a moderate increase in adhesive performance with the introduction of carbon nanotube

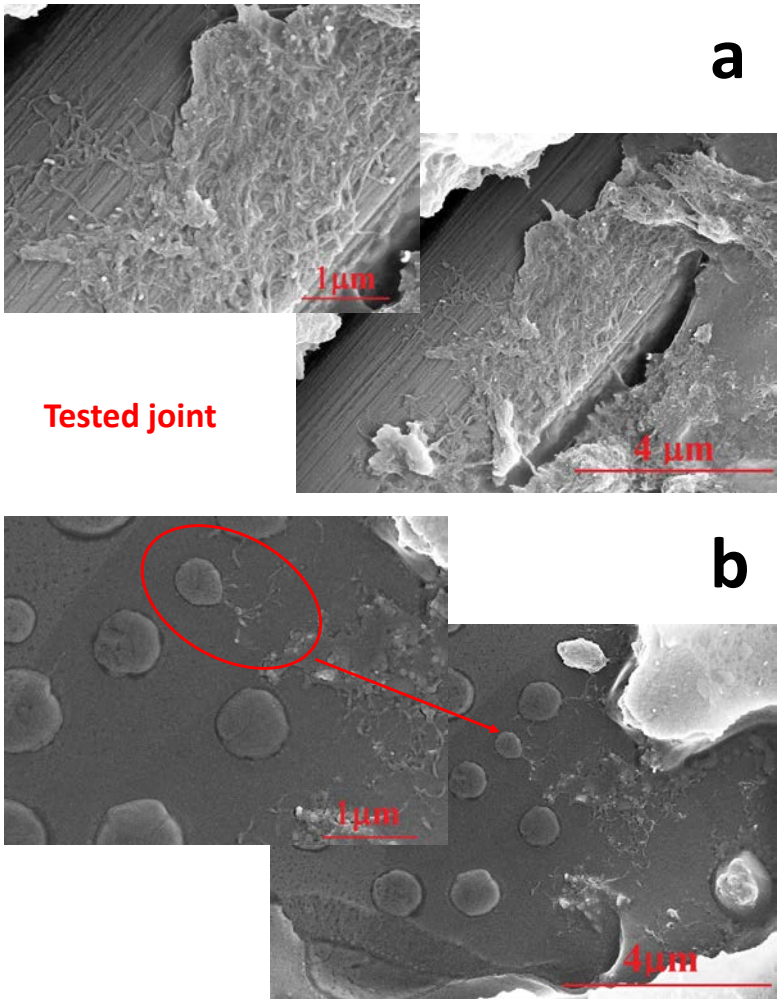

Figure 6. 16 *SEM images of the joint surface tested with the EPC25 adhesive with 1% by weight of the CNT*

A careful observation of the SEM images of the joint surface tested with the EPC25 adhesive with 1% by weight of the CNT, clarifies the various aspects

discussed so far. Figure 6.16 in up, shows a zone in which the surface area of the resin on the fibers is removed during the adhesion test. On the surface of the naked fiber, remains a thin resin film impregnated with carbon nanotubes that, as mentioned before, enable the best points of contact with the adherent. Figure 6.16 in down shows a different zone of the joint surface tested in which the elastomer and the carbon nanotubes are present. The carbon nanotubes are dispersed among the particles of elastomer, but not within them. This testifies to the fact that in addition at the macro phases, which are mentioned before, also are present phases in which the percolation network of carbon nanotubes, is interrupted by the presence of the elastomer particles, with the consequent reduction of the electrical conductivity.

6.6 Conclusions

The mechanical properties have shown that a) the presence of the elastomer allows obtaining a matrix with greater flexibility, improving, in this way, the adhesive properties of the material. In contrast, the elastomer does not allow the formation of an electrical percolation network if not for a higher amount of conductive filler; b) the conductive filler, on the one hand, determines the formation of the conductive paths and a decrease of the mechanical properties, on the other hand, it allows better adhesion between CFRP adherents. For this reason, only a correct combination of elastomer and carbon nanotubes, allows obtaining a conductive adhesive with high performance.

Final conclusion

Nano-modified epoxy adhesive able to decrease the moisture content and increase electrical and mechanical properties have been designed and obtained.

Kinetic analysis has shown which,

a) the introduction of the diluent in epoxy resin, decreases the activation energy of amine-epoxy reaction;
b) the inclusion in the resin of one-dimensional fillers does not lead to big differences in the curing kinetics behaviour with respect to the raw epoxy. A reduction of free molecular segments of the epoxy network entrapped inside self-assembly structures of highly exfoliated graphite has determined an increase in the activation energy of amine-epoxy reaction.

Dynamic mechanical analysis has shown that the nanoparticles are responsible of a more mobile phase, in the structure of the resin, determining an additional glass transition at lower temperature with respect to the main glass transition temperature.

The mobile phase increases with a reduction of amount of hardener, allowing a reduction of the equilibrium concentration of water, up to a maximum 30%. This more mobile phase also is related to the amount and the nature of the nanofiller, in fact, the presence of the filler, causes an increase of this phase, with an improvement of the electrical properties, storage modulus, and tensile butt joint strength.

The inclusion of an elastomer in the matrix has been necessary in order to inhibit interlaminar crack propagation, in the configuration lap shear strength (LSS), with adherents in carbon fiber reinforced plastics (CFRP). A correct combination of elastomer and carbon nanotubes, has allowed obtaining a conductive adhesive with high performance.

In the future work, edge-carboxylated nanosheets will be used in order to obtain, on the one hand, a relevant reinforcement in the elastic modulus (an increase cohesive forces), and on the other, an improvement of the interaction between nano-reinforced adhesive and the surface of the adherents in CFRP (an increase adhesive forces).

This choice will allow obtaining a better performance of the adhesive, keeping high the electrical conductivity of system

References

AKBARI, R., BEHESHTY, M. H. & SHERVIN, M. 2013. Toughening of dicyandiamide-cured DGEBA-based epoxy resins by CTBN liquid rubber. *Iranian Polymer Journal,* 22**,** 313-324.

ALLAOUI, A., BAI, S., CHENG, H.-M. & BAI, J. 2002. Mechanical and electrical properties of a MWNT/epoxy composite. *Composites Science and Technology,* 62**,** 1993-1998.

ALLAOUI, A. & EL BOUNIA, N.-E. 2009. How carbon nanotubes affect the cure kinetics and glass transition temperature of their epoxy composites?-a review. *Express Polymer Letters,* 3**,** 588-594.

ARGON, A. & COHEN, R. 2003. Toughenability of polymers. *Polymer,* 44**,** 6013-6032.

ARNOLD, J., SANDERS, C., BELLEVOU, D., MARTINELLI, A. & GASKIN, G. Surface treatment of titanium for adhesive bonding. Proc. 29th International SAMPE Technical Conference, 1997. 345.

ASHRAFI, B., JOHNSTON, A., JAKUBINEK, M., MARTINEZ-RUBI, Y., SIMARD, B. & HUBERT, P. Effect of single-walled carbon nanotubes on processing and property enhancement of epoxy adhesives and laminates. International SAMPE Technical Conference, 2012.

AWAJA, F., GILBERT, M., KELLY, G., FOX, B. & PIGRAM, P. J. 2009. Adhesion of polymers. *Progress in polymer science,* 34**,** 948-968.

BAE, J., JANG, J. & YOON, S.-H. 2002. Cure Behavior of the Liquid-Crystalline Epoxy/Carbon Nanotube System and the Effect of Surface Treatment of Carbon Fillers on Cure Reaction. *Macromolecular Chemistry and Physics,* 203**,** 2196-2204.

BALDAN, A. 2004. Adhesively-bonded joints and repairs in metallic alloys, polymers and composite materials: adhesives, adhesion theories and surface pretreatment. *Journal of materials science,* 39**,** 1-49.

BARCIA, F. L., AMARAL, T. P. & SOARES, B. G. 2003. Synthesis and properties of epoxy resin modified with epoxy-terminated liquid polybutadiene. *Polymer,* 44**,** 5811-5819.

BAUHOFER, W. & KOVACS, J. Z. 2009. A review and analysis of electrical percolation in carbon nanotube polymer composites. *Composites Science and Technology,* 69**,** 1486-1498.

BELLUCCI, S., BISTARELLI, S., CATALDO, A., MICCIULLA, F., KRANAUSKAITE, I., MACUTKEVIC, J., BANYS, J., VOLYNETS, N., PADDUBSKAYA, A. & BYCHANOK, D. 2015. Broadband Dielectric Spectroscopy of Composites Filled With Various Carbon Materials. *IEEE Transactions on Microwave Theory and Techniques,* 63**,** 2024-2031.

BEVER, M. B. 1985. Encyclopedia of materials science and engineering.

BHOWMIK, S., BENEDICTUS, R., POULIS, J., BONIN, H. & BUI, V. 2009. High-performance nanoadhesive bonding of titanium for aerospace and space applications. *International Journal of Adhesion and Adhesives,* 29**,** 259-267.

BILLIAS, M. G. & BORDERS, M. E. 1984. Electrically conductive structural adhesive. Google Patents.

BLAKE, P., BRIMICOMBE, P. D., NAIR, R. R., BOOTH, T. J., JIANG, D., SCHEDIN, F., PONOMARENKO, L. A., MOROZOV, S. V., GLEESON, H. F. & HILL, E. W. 2008. Graphene-based liquid crystal device. *Nano letters,* 8**,** 1704-1708.

BRAZEL, C. S. & ROSEN, S. L. 2012. *Fundamental principles of polymeric materials*, John Wiley & Sons.

BREWIS, D. 1992. Treatise on adhesion and adhesives, volume 7: Edited by JD Minford Marcel Dekker Inc, New York and Basel, 1991,£ 100.64. Elsevier.

BROAD, R., FRENCH, J. & SAUER, J. 1999. CLP new, effective, ecological surface pretreatment for highly durable adhesively bonded metal joints. *International journal of adhesion and adhesives,* 19**,** 193-198.

BROCKMANN, W., HENNEMANN, O.-D., KOLLEK, H. & MATZ, C. 1986. Adhesion in bonded aluminium joints for aircraft construction. *International journal of adhesion and adhesives,* 6**,** 115-IN1.

BUCKNALL, C. B. 1977. *Toughened plastics*, Springer.

BUNCH, J. S., VERBRIDGE, S. S., ALDEN, J. S., VAN DER ZANDE, A. M., PARPIA, J. M., CRAIGHEAD, H. G. & MCEUEN, P. L. 2008. Impermeable atomic membranes from graphene sheets. *Nano letters,* 8**,** 2458-2462.

BURKHOLDER, G. L., KWON, Y. W. & POLLAK, R. D. 2011. Effect of carbon nanotube reinforcement on fracture strength of composite adhesive joints. *Journal of materials science,* 46**,** 3370-3377.

CALADO, V. M. & ADVANI, S. G. 2000. Thermoset resin cure kinetics and rheology. *Transport processes in composites. A. Loos, R. Dave (Eds.), A Review of Cure Kinetics and Chemorheology for Thermosett Resins in Transport Processes in Composites***,** 32-107.

CATALANI, A. & BONICELLI, M. G. 2005. Kinetics of the curing reaction of a diglycidyl ether of bisphenol A with a modified polyamine. *Thermochimica acta,* 438**,** 126-129.

CHEN, D., PASCAULT, J. P. & SAUTEREAU, H. 1993. Rubber-modified epoxies. I. Influence of presence of a low level of rubber on the polymerization. *Polymer international,* 32**,** 361-367.

CHERN, C.-S. & POEHLEIN, G. 1987. A kinetic model for curing reactions of epoxides with amines. *Polymer Engineering & Science,* 27**,** 788-795.

CHIAO, L. 1990. Mechanistic reaction kinetics of 4, 4'-diaminodiphenyl, sulfone cured tetraglycidyl-4, 4'-diaminodiphenylmethane epoxy resins. *Macromolecules,* 23**,** 1286-1290.

CHIKHI, N., FELLAHI, S. & BAKAR, M. 2002. Modification of epoxy resin using reactive liquid (ATBN) rubber. *European Polymer Journal,* 38**,** 251-264.

CONNOR, M. T., ROY, S., EZQUERRA, T. A. & CALLEJA, F. J. B. 1998. Broadband ac conductivity of conductor-polymer composites. *Physical Review B,* 57**,** 2286.

CRANE, L., HAMERMESH, C. & MAUS, L. 1976. Surface treatment of cured epoxy graphite composites to improve adhesive bonding. *SAMPE Journal,* 12**,** 6-9.

CRITCHLOW, G. & BREWIS, D. 1995. Influence of surface macroroughness on the durability of epoxide-aluminium joints. *International journal of adhesion and adhesives,* 15**,** 173-176.

CURRO, J. G. 1997. Integral equation theories of the structure, thermodynamics, and phase transitions of polymer fluids. *Advances in***,** 1.

CURRO, J. G. & SCHWEIZER, K. S. 1987. Equilibrium theory of polymer liquids: linear chains. *The Journal of chemical physics,* 87**,** 1842-1846.

DAVIES, G., GROFF, G. & ZATORSKI, R. 1997. Plasma Sprayed Coatings as Treatments for Aluminum, Titanium and Steel Adherends. *Surface and interface analysis,* 25**,** 366-373.

DE GENNES, P.-G. 1985. Wetting: statics and dynamics. *Reviews of modern physics,* 57**,** 827.

DE VIVO, B., GUADAGNO, L., LAMBERTI, P., RAIMO, R., SARTO, M. S., TAMBURRANO, A., TUCCI, V. & VERTUCCIO, L. Electromagnetic properties of carbon nano tube/epoxy nanocomposites. 2009 International Symposium on Electromagnetic Compatibility-EMC Europe, 2009.

DE VIVO, B., GUADAGNO, L., LAMBERTI, P., RAIMONDO, M., SPINELLI, G., TUCCI, V., VERTUCCIO, L. & VITTORIA, V. Electrical properties of multi-walled carbon nanotube/tetrafunctional

epoxy-amine composites. 6TH INTERNATIONAL CONFERENCE ON TIMES OF POLYMERS (TOP) AND COMPOSITES, 2012a. AIP Publishing, 199-201.

DE VIVO, B., LAMBERTI, P., SPINELLI, G. & TUCCI, V. 2014. A morphological and structural approach to evaluate the electromagnetic performances of composites based on random networks of carbon nanotubes. *Journal of Applied Physics,* 115**,** 154311.

DE VIVO, B., LAMBERTI, P., SPINELLI, G., TUCCI, V., GUADAGNO, L. & RAIMONDO, M. 2015. The effect of filler aspect ratio on the electromagnetic properties of carbon-nanofibers reinforced composites. *Journal of Applied Physics,* 118**,** 064302.

DE VIVO, B., LAMBERTI, P., SPINELLI, G., TUCCI, V., GUADAGNO, L., RAIMONDO, M., VERTUCCIO, L. & VITTORIA, V. 2013. Improvement of the electrical conductivity in multiphase epoxy-based MWCNT nanocomposites by means of an optimized clay content. *Composites Science and Technology,* 89**,** 69-76.

DE VIVO, B., LAMBERTI, P., TUCCI, V., GUADAGNO, L., VERTUCCIO, L., VITTORIA, V. & SORRENTINO, A. 2012b. Comparison of the physical properties of epoxy-based composites filled with different types of carbon nanotubes for aeronautic applications. *Advances in Polymer Technology,* 31**,** 205-218.

DEAN, G., CROCKER, L., READ, B. & WRIGHT, L. 2004. Prediction of deformation and failure of rubber-toughened adhesive joints. *International journal of adhesion and adhesives,* 24**,** 295-306.

DEGARMO, E. P., BLACK, J. T., KOHSER, R. A. & KLAMECKI, B. E. 1997. *Materials and process in manufacturing,* Prentice Hall.

DIKIN, D. A., STANKOVICH, S., ZIMNEY, E. J., PINER, R. D., DOMMETT, G. H., EVMENENKO, G., NGUYEN, S. T. & RUOFF, R. S. 2007. Preparation and characterization of graphene oxide paper. *Nature,* 448**,** 457-460.

DODIUK, H., BLINSKY, I., DOTAN, A. & BUCHMAN, A. 2005. Nanotailoring of epoxy adhesives by polyhedral-oligomeric-sil-sesquioxanes (POSS). *International journal of adhesion and adhesives,* 25**,** 211-218.

DOYLE, C. 1962. Estimating isothermal life from thermogravimetric data. *Journal of Applied Polymer Science,* 6**,** 639-642.

DU, F., FISCHER, J. E. & WINEY, K. I. 2005. Effect of nanotube alignment on percolation conductivity in carbon nanotube/polymer composites. *Physical Review B,* 72**,** 121404.

DU, S., GUO, Z. S., ZHANG, B. & WU, Z. 2004. Cure kinetics of epoxy resin used for advanced composites. *Polymer international,* 53**,** 1343-1347.

EDA, G., FANCHINI, G. & CHHOWALLA, M. 2008. Large-area ultrathin films of reduced graphene oxide as a transparent and flexible electronic material. *Nature nanotechnology,* 3**,** 270-274.

EMERSON, J. A., GUESS, T. R., ADKINS, C. L. J., CURRO, J. G., REEDY JR, E. D., LOPEZ, E. P. & LEMKE, P. A. 2000. Investigation of the impact of cleaning on the adhesive bond and the process implications. Sandia National Labs., Albuquerque, NM (US).

FINK, B. & MCCULLOUGH, R. 1999. Interphase research issues. *Composites Part A: Applied science and manufacturing,* 30**,** 1-2.

FLAMMERSHEIM, H.-J. R. & OPFERMANN, J. R. 2002. Kinetic evaluation of DSC curves for reacting systems with variable stoichiometric compositions. *Thermochimica acta,* 388**,** 389-400.

FLINN, R. A., FLINN, R. A. & PAUL, K. 1989. *Engineering materials and their applications,* McGraw-Hill.

FOURNIER, J., WILLIAMS, G., DUCH, C. & ALDRIDGE, G. A. 1996. Changes in molecular dynamics during bulk polymerization of an epoxide-amine system as studied by dielectric relaxation spectroscopy. *Macromolecules,* 29**,** 7097-7107.

FRIGIONE, M., MASCIA, L. & ACIERNO, D. 1995. Oligomeric and polymeric modifiers for toughening of epoxy resins. *European Polymer Journal,* 31**,** 1021-1029.

GARTON, A. & DALY, J. H. 1985. Characterization of the aramid: epoxy and carbon: epoxy interphases. *Polymer composites,* 6**,** 195-200.

GEIM, A. K. & NOVOSELOV, K. S. 2007. The rise of graphene. *Nature materials,* 6**,** 183-191.

GILBERT, E. N., HAYES, B. S. & SEFERIS, J. C. 2003. Nano-alumina modified epoxy based film adhesives. *Polymer Engineering & Science,* 43**,** 1096-1104.

GKIKAS, G., BARKOULA, N. M. & PAIPETIS, A. S. 2012a. Effect of dispersion conditions on the thermo-mechanical and toughness properties of multi walled carbon nanotubes-reinforced epoxy. *Composites Part B: Engineering,* 43**,** 2697-2705.

GKIKAS, G., SIOULAS, D., LEKATOU, A., BARKOULA, N. & PAIPETIS, A. 2012b. Enhanced bonded aircraft repair using nano-modified adhesives. *Materials & Design,* 41**,** 394-402.

GKIKAS, G., SIOULAS, D., LEKATOU, A., BARKOULA, N. M. & PAIPETIS, A. S. 2012c. Enhanced bonded aircraft repair using nano-modified adhesives. *Materials & Design,* 41**,** 394-402.

GOJNY, F., WICHMANN, M., K[illegible]PKE, U., FIEDLER, B. & SCHULTE, K. 2004. Carbon nanotube-reinforced epoxy-composites: enhanced stiffness and fracture toughness at low nanotube content. *Composites Science and Technology,* 64**,** 2363-2371.

GOJNY, F. H., WICHMANN, M. H., FIEDLER, B., BAUHOFER, W. & SCHULTE, K. 2005a. Influence of nano-modification on the mechanical and electrical properties of conventional fibre-reinforced composites. *Composites Part A: Applied Science and Manufacturing,* 36**,** 1525-1535.

GOJNY, F. H., WICHMANN, M. H., FIEDLER, B. & SCHULTE, K. 2005b. Influence of different carbon nanotubes on the mechanical properties of epoxy matrix composites-a comparative study. *Composites Science and Technology,* 65**,** 2300-2313.

GORRASI, G., SARNO, M., DI BARTOLOMEO, A., SANNINO, D., CIAMBELLI, P. & VITTORIA, V. 2007. Incorporation of carbon nanotubes into polyethylene by high energy ball milling: morphology and physical properties. *Journal of Polymer Science Part B: Polymer Physics,* 45**,** 597-606.

GUADAGNO, L., DE VIVO, B., DI BARTOLOMEO, A., LAMBERTI, P., SORRENTINO, A., TUCCI, V., VERTUCCIO, L. & VITTORIA, V. 2011. Effect of functionalization on the thermo-mechanical and electrical behavior of multi-wall carbon nanotube/epoxy composites. *Carbon,* 49**,** 1919-1930.

GUADAGNO, L., NADDEO, C., RAIMONDO, M., GORRASI, G. & VITTORIA, V. 2010a. Effect of carbon nanotubes on the photo-oxidative durability of syndiotactic polypropylene. *Polymer Degradation and Stability,* 95**,** 1614-1626.

GUADAGNO, L., NADDEO, C., VITTORIA, V., SORRENTINO, A., VERTUCCIO, L., RAIMONDO, M., TUCCI, V., DE VIVO, B., LAMBERTI, P. & IANNUZZO, G. 2010b. Cure behavior and physical properties of epoxy resin-filled with multiwalled carbon nanotubes. *Journal of nanoscience and nanotechnology,* 10**,** 2686-2693.

GUADAGNO, L., RAIMONDO, M., LAFDI, K., FIERRO, A., ROSOLIA, S. & NOBILE, M. R. Influence of nanofiller morphology on the viscoelastic properties of CNF/epoxy resins. AIP Conference Proceedings, 2014a.

GUADAGNO, L., RAIMONDO, M., NADDEO, C., DI BARTOLOMEO, A. & LAFDI, K. 2012a. Influence of multiwall carbon nanotubes on morphological and structural changes during UV irradiation of syndiotactic polypropylene films. *Journal of Polymer Science Part B: Polymer Physics,* 50**,** 963-975.

GUADAGNO, L., RAIMONDO, M., VERTUCCIO, L., MAURO, M., GUERRA, G., LAFDI, K., DE VIVO, B., LAMBERTI, P., SPINELLI, G. & TUCCI, V. 2015a. Optimization of graphene-based materials outperforming host epoxy matrices. *RSC Advances,* 5**,** 36969-36978.

GUADAGNO, L., RAIMONDO, M., VIETRI, U., VERTUCCIO, L., BARRA, G., DE VIVO, B., LAMBERTI, P., SPINELLI, G., TUCCI, V. & VOLPONI, R. 2015b. Effective formulation and processing of nanofilled carbon fiber reinforced composites. *RSC Advances,* 5**,** 6033-6042.

GUADAGNO, L., RAIMONDO, M., VITTORIA, V., LAFDI, K., DE VIVO, B., LAMBERTI, P., SPINELLI, G. & TUCCI, V. Role of The Carbon Nanofiber Defects On The Electrical Properties of CNF-Based Composites. ACMA Int Symp on Aircraft Materials (Fez, Maroc 09 May 2012), 2012b. 55-6.

GUADAGNO, L., RAIMONDO, M., VITTORIA, V., VERTUCCIO, L., LAFDI, K., DE VIVO, B., LAMBERTI, P., SPINELLI, G. & TUCCI, V. 2013. The role of carbon nanofiber defects on the electrical and mechanical properties of CNF-based resins. *Nanotechnology,* 24**,** 305704.

GUADAGNO, L., RAIMONDO, M., VITTORIA, V., VERTUCCIO, L., NADDEO, C., LAMBERTI, P., TUCCI, V. & RUSSO, S. 2015c. Epoxy resin with low humidity content. Google Patents.

GUADAGNO, L., RAIMONDO, M., VITTORIA, V., VERTUCCIO, L., NADDEO, C., RUSSO, S., DE VIVO, B., LAMBERTI, P., SPINELLI, G. & TUCCI, V. 2014b. Development of epoxy mixtures for application in aeronautics and aerospace. *RSC Advances,* 4**,** 15474-15488.

GUADAGNO, L., SARNO, M., VIETRI, U., RAIMONDO, M., CIRILLO, C. & CIAMBELLI, P. 2015d. Graphene-based structural adhesive to enhance adhesion performance. *RSC Advances,* 5**,** 27874-27886.

GUADAGNO, L., VERTUCCIO, L., SORRENTINO, A., RAIMONDO, M., NADDEO, C., VITTORIA, V., IANNUZZO, G., CALVI, E. & RUSSO, S. 2009. Mechanical and barrier properties of epoxy resin filled with multi-walled carbon nanotubes. *Carbon,* 47**,** 2419-2430.

GUADAGNO, L., VIETRI, U., RAIMONDO, M., VERTUCCIO, L., BARRA, G., DE VIVO, B., LAMBERTI, P., SPINELLI, G., TUCCI, V. & DE NICOLA, F. 2015e. Correlation between electrical conductivity and manufacturing processes of nanofilled carbon fiber reinforced composites. *Composites Part B: Engineering,* 80**,** 7-14.

GUDE, M., PROLONGO, S., G╡╠MEZ-DEL R╡╦O, T. & URENA, A. 2011. Mode-I adhesive fracture energy of carbon fibre composite joints with nanoreinforced epoxy adhesives. *International Journal of Adhesion and Adhesives,* 31**,** 695-703.

GUO, B., WAN, J., LEI, Y. & JIA, D. 2009. Curing behaviour of epoxy resin/graphite composites containing ionic liquid. *Journal of Physics D: Applied Physics,* 42**,** 145307.

GUPTA, A., CIZMECIOGLU, M., COULTER, D., LIANG, R., YAVROUIAN, A., TSAY, F. & MOACANIN, J. 1983. The mechanism of cure of tetraglycidyl diaminodiphenyl methane with diaminodiphenyl sulfone. *Journal of Applied Polymer Science,* 28**,** 1011-1024.

GUTOWSKI, T. G., CAI, Z., SOLL, W. & BONHOMME, L. The mechanics of composites deformation during manufacturing processes. American Society for Composites, First Technical Conference, 1986. 154-163.

HARPER-TERVET, J. & NEFF, D. 1983. Evaluation of the Alkaline Peroxide Pre-Bond surface Treatment for Titanium. DTIC Document.

HARRIS, A. & BEEVERS, A. Grit blasting of surfaces for adhesive bonding. Conf Proc Structural Adhesives in Engineering V. Bristol: Institute of Materials, 1998.

HARRIS, A. & BEEVERS, A. 1999. The effects of grit-blasting on surface properties for adhesion. *International Journal of Adhesion and Adhesives,* 19**,** 445-452.

HEIMANN, M., WIRTS-RUETTERS, M., BOEHME, B. & WOLTER, K.-J. Investigations of carbon nanotubes epoxy composites for electronics packaging. 2008 58th Electronic Components and Technology Conference, 2008. IEEE, 1731-1736.

HIGGINS, A. 2000. Adhesive bonding of aircraft structures. *International Journal of Adhesion and Adhesives,* 20**,** 367-376.

HOLLERTZ, R., CHATTERJEE, S., GUTMANN, H., GEIGER, T., N Ì ESCH, F. & CHU, B. 2011. Improvement of toughness and electrical properties of epoxy composites with carbon nanotubes prepared by industrially relevant processes. *Nanotechnology,* 22**,** 125702.

HSIAO, K.-T., ALMS, J. & ADVANI, S. G. 2003. Use of epoxy/multiwalled carbon nanotubes as adhesives to join graphite fibre reinforced polymer composites. *Nanotechnology,* 14**,** 791.

HUANG, Y. & KINLOCH, A. 1992. The toughness of epoxy polymers containing microvoids. *Polymer,* 33**,** 1330-1332.

HWANG, J.-F., MANSON, J., HERTZBERG, R., MILLER, G. & SPERLING, L. 1989. Structure-property relationships in rubber-toughened epoxies. *Polymer Engineering & Science,* 29**,** 1466-1476.

IIJIMA, T., MIURA, S., FUKUDA, W. & TOMOI, M. 1993. Effect of cross-link density on modification of epoxy resins by N-phenylmaleimide-styrene copolymers. *European polymer journal,* 29**,** 1103-1113.

ISHIDA, H. 1988. Interfaces in polymer, ceramic, and metal matrix composites; Proceedings of the Second International Conference on Composite Interfaces (ICCI-II), Cleveland, OH, June 13-17, 1988. Elsevier, New York, NY.

J.BISHOPP 2011. Adhesives for aerospace structures. *In:* S, E. (ed.) *Handbook of adhesives and surface preparation.* William Andrew.

JAGADEESH, K., GURURAJA RAO, J., SHASHIKIRAN, K., SUVARNA, S., AMBEKAR, S. Y., SALETORE, M., BISWAS, C. & RAJANNA, A. 2000. Cure kinetics of multifunctional epoxies with 2, 2'-dichloro-4, 4'-diaminodiphenylmethane as hardener. *Journal of applied polymer science,* 77**,** 2097-2103.

JAKUBINEK, M. B., ASHRAFI, B., ZHANG, Y., MARTINEZ-RUBI, Y., KINGSTON, C. T., JOHNSTON, A. & SIMARD, B. 2015a. Single-walled carbon nanotub-epoxy composites for structural and conductive aerospace adhesives. *Composites Part B: Engineering,* 69**,** 87-93.

JAKUBINEK, M. B., ASHRAFI, B., ZHANG, Y., MARTINEZ-RUBI, Y., KINGSTON, C. T., JOHNSTON, A. & SIMARD, B. 2015b. Single-walled carbon nanotube-epoxy composites for structural and conductive aerospace adhesives. *Composites Part B: Engineering,* 69**,** 87-93.

JANA, S. & ZHONG, W.-H. K. 2009. Curing characteristics of an epoxy resin in the presence of ball-milled graphite particles. *Journal of materials science,* 44**,** 1987-1997.

JANG, B. Z. 1994. Advanced polymer composites: principles and applications. *ASM International, Materials Park, OH 44073-0002, USA, 1994. 305*.

JIA, W., TCHOUDAKOV, R., JOSEPH, R., NARKIS, M. & SIEGMANN, A. 2002. The conductivity behavior of multi-component epoxy, metal particle, carbon black, carbon fibril composites. *Journal of applied polymer science,* 85**,** 1706-1713.

JIANG, H., LIU, B., HUANG, Y. & HWANG, K. 2004. Thermal expansion of single wall carbon nanotubes. *Journal of engineering materials and technology,* 126**,** 265-270.

JUNGANG, G., DELING, L., SHIGANG, S. & GUODONG, L. 2002. Curing kinetics and thermal property characterization of a bisphenol-F epoxy resin and DDO system. *Journal of applied polymer science,* 83**,** 1586-1595.

KAWAGUCHI, T. & PEARSON, R. A. 2003. The effect of particle-matrix adhesion on the mechanical behavior of glass filled epoxies: Part 1. A study on yield behavior and cohesive strength. *Polymer,* 44**,** 4229-4238.

KEENAN, M. 1987. Autocatalytic cure kinetics from DSC measurements: zero initial cure rate. *Journal of applied polymer science,* 33**,** 1725-1734.

KILBRIDE, B. E., COLEMAN, J., FRAYSSE, J., FOURNET, P., CADEK, M., DRURY, A., HUTZLER, S., ROTH, S. & BLAU, W. 2002. Experimental observation of scaling laws for alternating current and direct current conductivity in polymer-carbon nanotube composite thin films. *Journal of Applied Physics,* 92**,** 4024-4030.

KIM, H.-S., PARK, B. H., YOON, J.-S. & JIN, H.-J. 2007. Thermal and electrical properties of poly (L-lactide)-graft-multiwalled carbon nanotube composites. *European polymer journal,* 43**,** 1729-1735.

KIM, J.-K., HU, C., WOO, R. S. & SHAM, M.-L. 2005a. Moisture barrier characteristics of organoclay-epoxy nanocomposites. *Composites Science and Technology,* 65**,** 805-813.

KIM, J.-K. & MAI, Y.-W. 1998. *Engineered interfaces in fiber reinforced composites,* Elsevier.

KIM, J. Y. & KIM, S. H. 2006. Influence of multiwall carbon nanotube on physical properties of poly (ethylene 2, 6-naphthalate) nanocomposites. *Journal of Polymer Science Part B: Polymer Physics,* 44**,** 1062-1071.

KIM, K. S., ZHAO, Y., JANG, H., LEE, S. Y., KIM, J. M., KIM, K. S., AHN, J.-H., KIM, P., CHOI, J.-Y. & HONG, B. H. 2009. Large-scale pattern growth of graphene films for stretchable transparent electrodes. *Nature,* 457**,** 706-710.

KIM, Y. J., SHIN, T. S., DO CHOI, H., KWON, J. H., CHUNG, Y.-C. & YOON, H. G. 2005b. Electrical conductivity of chemically modified multiwalled carbon nanotube/epoxy composites. *Carbon,* 43**,** 23-30.

KINLOCH, A. 2012. *Adhesion and adhesives: science and technology,* Springer Science & Business Media.

KINLOCH, A., LEE, J., TAYLOR, A., SPRENGER, S., EGER, C. & EGAN, D. 2003. Toughening structural adhesives via nano-and micro-phase inclusions. *The Journal of Adhesion,* 79**,** 867-873.

KLUG, J. H. & SEFERIS, J. C. 1999. Phase separation influence on the performance of CTBN-toughened epoxy adhesives. *Polymer Engineering & Science,* 39**,** 1837-1848.

KOTSILKOVA, R., IVANOV, E., BYCHANOK, D., PADDUBSKAYA, A., DEMIDENKO, M., MACUTKEVIC, J., MAKSIMENKO, S. & KUZHIR, P. 2015. Effects of sonochemical modification of carbon nanotubes on electrical and electromagnetic shielding properties of epoxy composites. *Composites Science and Technology,* 106**,** 85-92.

KOVACS, J. Z., VELAGALA, B. S., SCHULTE, K. & BAUHOFER, W. 2007. Two percolation thresholds in carbon nanotube epoxy composites. *Composites Science and Technology,* 67**,** 922-928.

KWON, Y.-K., BERBER, S. & TOMÁNEK, D. 2004. Thermal contraction of carbon fullerenes and nanotubes. *Physical review letters,* 92**,** 015901.

KYMAKIS, E. & AMARATUNGA, G. A. 2006. Electrical properties of single-wall carbon nanotube-polymer composite films. *Journal of applied physics,* 99**,** 084302.

LAFDI, K., FOX, W., MATZEK, M. & YILDIZ, E. 2008. Effect of carbon nanofiber-matrix adhesion on polymeric nanocomposite properties: part II. *Journal of nanomaterials,* 2008**,** 5.

LAMBERTI, P., SPINELLI, G. & TUCCI, V. Effect of conductive nanofiller structures on electrical properties of epoxy composite for aeronautic applications. ICEAF III 3rd International Conference of Engineering Against Failure, 2013. 26-28.

LANDROCK, A. H. & EBNESAJJAD, S. 2008. *Adhesives technology handbook*, William Andrew.

LAPIQUE, F. & REDFORD, K. 2002. Curing effects on viscosity and mechanical properties of a commercial epoxy resin adhesive. *International journal of adhesion and adhesives,* 22**,** 337-346.

LARSSON, A. 2002. The interaction between a lightning flash and an aircraft in flight. *Comptes Rendus Physique,* 3**,** 1423-1444.

LENNON, P., ESPUCHE, E., SAUTEREAU, H. & SAGE, D. 1999. Influence of microwave plasma treatment on the wettability and the adhesive properties of polyamides films with an epoxy resin. *International journal of adhesion and adhesives,* 19**,** 273-279.

LI, C., THOSTENSON, E. T. & CHOU, T.-W. 2007. Dominant role of tunneling resistance in the electrical conductivity of carbon nanotube-based composites. *Applied Physics Letters,* 91**,** 223114.

LI, L., YU, Y., WU, Q., ZHAN, G. & LI, S. 2009. Effect of chemical structure on the water sorption of amine-cured epoxy resins. *Corrosion Science,* 51**,** 3000-3006.

LI, Q., LI, X. & MENG, Y. 2012. Curing of DGEBA epoxy using a phenol-terminated hyperbranched curing agent: Cure kinetics, gelation, and the TTT cure diagram. *Thermochimica acta,* 549**,** 69-80.

LIANG, Y., JING, D., QU, B.-J. & SHI, W.-F. 2006. Cure kinetics of DGEBA with hyperbranched poly (3-hydroxyphenyl) phosphate as curing agent studied by non-isothermal DSC. *Chemical Research in Chinese Universities,* 22**,** 118-122.

LIU, W., HOA, S. V. & PUGH, M. 2005. Fracture toughness and water uptake of high-performance epoxy/nanoclay nanocomposites. *Composites Science and Technology,* 65**,** 2364-2373.

LIU, Z. & BAE, D. H. 2011. A study on joining technology of aluminum alloy sheet using nano-adhesives. *International Journal of Modern Physics B,* 25**,** 4265-4268.

MADDAMS, W. 1980. The scope and limitations of curve fitting. *Applied Spectroscopy,* 34**,** 245-267.

MÄDER, E. 1997. Study of fibre surface treatments for control of interphase properties in composites. *Composites science and technology,* 57**,** 1077-1088.
MAHONEY, C. 1988. Fundamental factors influencing the performance of structural adhesives. Internal Report, Dexter Adhesives and Structural Materials Division, The Dexter Corporation.
MARTIN, C., SANDLER, J., WINDLE, A., SCHWARZ, M.-K., BAUHOFER, W., SCHULTE, K. & SHAFFER, M. 2005. Electric field-induced aligned multi-wall carbon nanotube networks in epoxy composites. *Polymer,* 46**,** 877-886.
MAY, C. & WEIR, F. 1962. Dynamic mechanical properties of epoxy resins. *Polymer Engineering & Science,* 2**,** 207-212.
MAY, M., WANG, H. & AKID, R. 2010. Effects of the addition of inorganic nanoparticles on the adhesive strength of a hybrid sol-gel epoxy system. *International Journal of Adhesion and Adhesives,* 30**,** 505-512.
MDARHRI, A., CARMONA, F., BROSSEAU, C. & DELHAES, P. 2008. Direct current electrical and microwave properties of polymer-multiwalled carbon nanotubes composites. *Journal of applied physics,* 103**,** 054303.
MEGUID, S. & SUN, Y. 2004a. On the tensile and shear strength of nano-reinforced composite interfaces. *Materials & design,* 25**,** 289-296.
MEGUID, S. A. & SUN, Y. 2004b. On the tensile and shear strength of nano-reinforced composite interfaces. *Materials & Design,* 25**,** 289-296.
MESSLER, R. W. 1993. *Joining of advanced materials*, Butterworths.
MIJOVIĆ, J., KIM, J. & SLABY, J. 1984. Cure kinetics of epoxy formulations of the type used in advanced composites. *Journal of applied polymer science,* 29**,** 1449-1462.
MIJOVIĆ, J. & WANG, H. 1989. Cure kinetics of neat and graphite-fiber-reinforced epoxy formulations. *Journal of applied polymer science,* 37**,** 2661-2673.
MOISALA, A., LI, Q., KINLOCH, I. & WINDLE, A. 2006. Thermal and electrical conductivity of single-and multi-walled carbon nanotube-epoxy composites. *Composites science and technology,* 66**,** 1285-1288.
MOLITOR, P., BARRON, V. & YOUNG, T. 2001. Surface treatment of titanium for adhesive bonding to polymer composites: a review. *International Journal of Adhesion and Adhesives,* 21**,** 129-136.
MOLITOR, P. & YOUNG, T. 2002. Adhesives bonding of a titanium alloy to a glass fibre reinforced composite material. *International journal of adhesion and adhesives,* 22**,** 101-107.
MORGAN, R. J. & MONES, E. T. 1987. The cure reactions, network structure, and mechanical response of diaminodiphenyl sulfone-cured

tetraglycidyl 4, 4' diaminodiphenyl methane epoxies. *Journal of applied polymer science,* 33**,** 999-1020.

MOSCHIAR, S., RICCARDI, C., WILLIAMS, R., VERCHERE, D., SAUTEREAU, H. & PASCAULT, J. 1991. Rubber-modified epoxies. III. Analysis of experimental trends through a phase separation model. *Journal of applied polymer science,* 42**,** 717-735.

MUSTAŢĂ, F. & CASCAVAL, C. N. 1997. Rheological and thermal behaviour of an epoxy resin modified with reactive diluents. *Journal of polymer engineering,* 17**,** 491-506.

NAN, C.-W., SHEN, Y. & MA, J. 2010. Physical properties of composites near percolation. *Annual Review of Materials Research,* 40**,** 131-151.

NIEBEL, B. W., DRAPER, A. B. & WYSK, R. A. 1989. *Modern manufacturing process engineering,* McGraw-Hill College.

NIELSEN, L. E. 1967. Models for the permeability of filled polymer systems. *Journal of Macromolecular Science-Chemistry,* 1**,** 929-942.

NOBILE, M. R., RAIMONDO, M., LAFDI, K., FIERRO, A., ROSOLIA, S. & GUADAGNO, L. 2015. Relationships between nanofiller morphology and viscoelastic properties in CNF/epoxy resins. *Polymer Composites,* 36**,** 1152-1160.

OPALIČKI, M., KENNY, J. M. & NICOLAIS, L. 1996. Cure kinetics of neat and carbon-fiber-reinforced TGDDM/DDS epoxy systems. *Journal of Applied Polymer Science,* 61**,** 1025-1037.

OSMAN, M. A., MITTAL, V., MORBIDELLI, M. & SUTER, U. W. 2003. Polyurethane adhesive nanocomposites as gas permeation barrier. *Macromolecules,* 36**,** 9851-9858.

PATEL, S., BANDYOPADHYAY, A., GANGULY, A. & BHOWMICK, A. K. 2006. Synthesis and properties of nanocomposite adhesives. *Journal of adhesion science and technology,* 20**,** 371-385.

PEARSON, R. & YEE, A. 1989. Toughening mechanisms in elastomer-modified epoxies. *Journal of materials science,* 24**,** 2571-2580.

PETROV, N., HADDAD, A., GRIFFITHS, H. & WATERS, R. Lightning strikes to aircraft radome: Electric field shielding simulation. 2008 17th International Conference on Gas Discharges and Their Applications, 2008.

PILATO, L. A. & MICHNO, M. J. 1994. Analysis/Testing. *Advanced Composite Materials.* Springer.

PLYUSHCH, A., MACUTKEVIC, J., KUZHIR, P., BANYS, J., BYCHANOK, D., LAMBIN, P., BISTARELLI, S., CATALDO, A., MICCIULLA, F. & BELLUCCI, S. 2016. Electromagnetic properties of graphene nanoplatelets/epoxy composites. *Composites Science and Technology,* 128**,** 75-83.

POGANY, G. 1970. Gamma relaxation in epoxy resins and related polymers. *Polymer,* 11**,** 66-78.

POLITI, R. 1985. Recent developments in polyimide and bismaleimide adhesives.
PROLONGO, S., GUDE, M., SANCHEZ, J. & URENA, A. 2009a. Nanoreinforced epoxy adhesives for aerospace industry. *The Journal of Adhesion,* 85**,** 180-199.
PROLONGO, S., GUDE, M., SANCHEZ, J. & UREÑA, A. 2009b. Nanoreinforced epoxy adhesives for aerospace industry. *The Journal of Adhesion,* 85**,** 180-199.
PROLONGO, S., GUDE, M. & UREÑA, A. 2010a. Rheological behaviour of nanoreinforced epoxy adhesives of low electrical resistivity for joining carbon fiber/epoxy laminates. *Journal of Adhesion Science and Technology,* 24**,** 1097-1112.
PROLONGO, S. G., UREÑA, A. & GUDE, M. A. R. 2010b. *Nanoreinforced adhesives,* INTECH Open Access Publisher.
PROLONGO, S. G., UREÑA, A. & GUDE, M. R. 2010c. *Nanoreinforced adhesives,* INTECH Open Access Publisher.
PUGLIA, D., VALENTINI, L., ARMENTANO, I. & KENNY, J. 2003. Effects of single-walled carbon nanotube incorporation on the cure reaction of epoxy resin and its detection by Raman spectroscopy. *Diamond and related materials,* 12**,** 827-832.
QIAN, D., WAGNER, G. J., LIU, W. K., YU, M.-F. & RUOFF, R. S. 2002. Mechanics of carbon nanotubes. *Applied mechanics reviews,* 55**,** 495-533.
RABINOWITCH, E. 1937. Collision, co-ordination, diffusion and reaction velocity in condensed systems. *Transactions of the Faraday Society,* 33**,** 1225-1233.
RAMOS, V. R. D., DA COSTA, H. M., SOARES, V. L. & NASCIMENTO, R. S. 2005. Hybrid composites of epoxy resin modified with carboxyl terminated butadiene acrilonitrile copolymer and fly ash microspheres. *Polymer Testing,* 24**,** 219-226.
RATNA, D. 2001. Phase separation in liquid rubber modified epoxy mixture. Relationship between curing conditions, morphology and ultimate behavior. *Polymer,* 42**,** 4209-4218.
RATNA, D. 2009. *Handbook of thermoset resins,* ISmithers Shawbury, UK.
REICH, S., THOMSEN, C. & MAULTZSCH, J. 2008. *Carbon nanotubes: basic concepts and physical properties,* John Wiley & Sons.
REZAIFARD, A. H., HODD, K. A. & BARTON, J. M. 1993. Toughening epoxy resin with poly (methyl methacrylate)-grafted natural rubber. American Chemical Society, Washington, DC (United States).
RIEW, C. K. & KINLOCH, A. J. 1993. Toughened plastics I: science and engineering. American Chemical Society, Washington, DC (United States).

ROSCA, I. D. & HOA, S. V. 2011. Method for reducing contact resistivity of carbon nanotube-containing epoxy adhesives for aerospace applications. *Composites Science and Technology,* 71**,** 95-100.

ROŞU, D., CA□CAVAL, C., MUSTATĂ, F. & CIOBANU, C. 2002. Cure kinetics of epoxy resins studied by non-isothermal DSC data. *Thermochimica Acta,* 383**,** 119-127.

S, E. 2011. Adhesives for electronics. *In:* S, E. (ed.) *Handbook of adhesives and surface preparation.* William Andrew.

SAADATI, P., BAHARVAND, H., RAHIMI, A. & MORSHEDIAN, J. 2005. Effect of modified liquid rubber on increasing toughness of epoxy resins. *Iranian Polymer Journal,* 14**,** 637-646.

SADEGHIAN, R., GANGIREDDY, S., MINAIE, B. & HSIAO, K.-T. 2006. Manufacturing carbon nanofibers toughened polyester/glass fiber composites using vacuum assisted resin transfer molding for enhancing the mode-I delamination resistance. *Composites Part A: applied science and manufacturing,* 37**,** 1787-1795.

SAEED, M. & ZHAN, M.-S. 2007. Adhesive strength of nano-size particles filled thermoplastic polyimides. Part-I: Multi-walled carbon nano-tubes (MWNT)-polyimide composite films. *International Journal of Adhesion and Adhesives,* 27**,** 306-318.

SANCAKTAR, E. 1995. Laser ablation of aluminum and titanium surfaces for improved adhesion.

SANDLER, J., KIRK, J., KINLOCH, I., SHAFFER, M. & WINDLE, A. 2003. Ultra-low electrical percolation threshold in carbon-nanotube-epoxy composites. *Polymer,* 44**,** 5893-5899.

SANDLER, J., SHAFFER, M., PRASSE, T., BAUHOFER, W., SCHULTE, K. & WINDLE, A. 1999. Development of a dispersion process for carbon nanotubes in an epoxy matrix and the resulting electrical properties. *Polymer,* 40**,** 5967-5971.

SARATHI, R., SAHU, R. K. & RAJESHKUMAR, P. 2007. Understanding the thermal, mechanical and electrical properties of epoxy nanocomposites. *Materials Science and Engineering: A,* 445**,** 567-578.

SARTI, G. C. 1979. Solvent osmotic stresses and the prediction of Case II transport kinetics. *Polymer,* 20**,** 827-832.

SARTI, G. C. & APICELLA, A. 1980. Non-equilibrium glassy properties and their relevance in case II transport kinetics. *Polymer,* 21**,** 1031-1036.

SBIRRAZZUOLI, N., GIRAULT, Y. & ELÉGANT, L. 1997. Simulations for evaluation of kinetic methods in differential scanning calorimetry. Part 3-Peak maximum evolution methods and isoconversional methods. *Thermochimica Acta,* 293**,** 25-37.

SBIRRAZZUOLI, N., VINCENT, L. & VYAZOVKIN, S. 2000. Comparison of several computational procedures for evaluating the kinetics of

thermally stimulated condensed phase reactions. *Chemometrics and Intelligent Laboratory Systems,* 54**,** 53-60.

SBIRRAZZUOLI, N., VYAZOVKIN, S., MITITELU, A., SLADIC, C. & VINCENT, L. 2003. A Study of Epoxy-Amine Cure Kinetics by Combining Isoconversional Analysis with Temperature Modulated DSC and Dynamic Rheometry. *Macromolecular Chemistry and Physics,* 204**,** 1815-1821.

SCELSI, L., BONNER, M., HODZIC, A., SOUTIS, C., WILSON, C., SCAIFE, R. & RIDGWAY, K. 2011. Potential emissions savings of lightweight composite aircraft components evaluated through life cycle assessment. *Express Polymer Letters,* 5**,** 209-217.

SCHADLER, L., GIANNARIS, S. & AJAYAN, P. 1998. Load transfer in carbon nanotube epoxy composites. *Applied physics letters,* 73**,** 3842-3844.

SCHERILLO, G., LAVORGNA, M., BUONOCORE, G. G., ZHAN, Y. H., XIA, H. S., MENSITIERI, G. & AMBROSIO, L. 2014. Tailoring assembly of reduced graphene oxide nanosheets to control gas barrier properties of natural rubber nanocomposites. *ACS applied materials & interfaces,* 6**,** 2230-2234.

SCHWEIZER, K. S. & CURRO, J. G. 1987. Integral-equation theory of the structure of polymer melts. *Physical review letters,* 58**,** 246.

SEYHAN, A., SUN, Z., DEITZEL, J., TANOGLU, M. & HEIDER, D. 2009. Cure kinetics of vapor grown carbon nanofiber (VGCNF) modified epoxy resin suspensions and fracture toughness of their resulting nanocomposites. *Materials Chemistry and Physics,* 118**,** 234-242.

SHAHID, M. & HASHIM, S. 2002. Effect of surface roughness on the strength of cleavage joints. *International journal of adhesion and adhesives,* 22**,** 235-244.

SHANAHAN, M. E. 2000. Diffusion effects in the wetting of a contaminated surface. *Journal of colloid and interface science,* 229**,** 168-173.

SHEHZAD, K., DANG, Z.-M., AHMAD, M. N., SAGAR, R. U. R., BUTT, S., FAROOQ, M. U. & WANG, T.-B. 2013. Effects of carbon nanotubes aspect ratio on the qualitative and quantitative aspects of frequency response of electrical conductivity and dielectric permittivity in the carbon nanotube/polymer composites. *Carbon,* 54**,** 105-112.

SHIELDS, J. 2013. *Adhesives handbook*, Elsevier.

SHIEU, F. 1997. Prediction of the critical particle size for toughening a glassy polymer. *Polymer,* 38**,** 3135-3137.

SHUKLA, S. K. & SRIVASTAVA, D. 2006. Blends of modified epoxy resin and carboxyl-terminated polybutadiene. I. *Journal of applied polymer science,* 100**,** 1802-1808.

SIMON, S. L. & GILLHAM, J. 1993. Cure kinetics of a thermosetting liquid dicyanate ester monomer/high-Tg polycyanurate material. *Journal of applied polymer science,* 47**,** 461-485.

SKORDOS, A. & PARTRIDGE, I. 2001. Cure kinetics modeling of epoxy resins using a non-parametric numerical procedure. *Polymer Engineering & Science,* 41**,** 793-805.

SOLES, C. L. & YEE, A. F. 2000. A discussion of the molecular mechanisms of moisture transport in epoxy resins. *Journal of Polymer Science Part B: Polymer Physics,* 38**,** 792-802.

SONG, Y. S. & YOUN, J. R. 2005. Influence of dispersion states of carbon nanotubes on physical properties of epoxy nanocomposites. *Carbon,* 43**,** 1378-1385.

ŠPITALSKÝ, Z., KRONTIRAS, C. A., GEORGA, S. N. & GALIOTIS, C. 2009. Effect of oxidation treatment of multiwalled carbon nanotubes on the mechanical and electrical properties of their epoxy composites. *Composites Part A: Applied Science and Manufacturing,* 40**,** 778-783.

SRIVASTAVA, V. 2011. Effect of carbon nanotubes on the strength of adhesive lap joints of C/C and C/C-SiC ceramic fibre composites. *International Journal of Adhesion and Adhesives,* 31**,** 486-489.

STEWART, I., CHAMBERS, A. & GORDON, T. 2007. The cohesive mechanical properties of a toughened epoxy adhesive as a function of cure level. *International journal of adhesion and adhesives,* 27**,** 277-287.

STRONG, A. B. 2008. *Fundamentals of composites manufacturing: materials, methods and applications,* Society of Manufacturing Engineers.

SU, C. C. & WOO, E. M. 1995. Cure kinetics and morphology of amine-cured tetraglycidyl-4, 4'-diaminodiphenylmethane epoxy blends with poly (ether imide). *Polymer,* 36**,** 2883-2894.

SU, C. C. & WOO, E. M. 1997. Diffusion-controlled reaction mechanisms during cure in polycarbonate-modified epoxy networks. *Journal of Polymer Science Part B: Polymer Physics,* 35**,** 2141-2150.

SULTAN, J. N., LAIBLE, R. & MCGARRY, F. J. Microstructure of two-phase polymers. Appl Polym Symp, 1971. 127-36.

SULTAN, J. N. & MCGARRY, F. J. 1973. Effect of rubber particle size on deformation mechanisms in glassy epoxy. *Polymer Engineering & Science,* 13**,** 29-34.

SUO, Z. 2001. Fracture in thin films. *Encyclopedia of Materials: Science and Technology***,** 3290-3296.

THAKKAR, J. R., PATEL, R. D., PATEL, R. G. & PATEL, V. S. 1990. Glass fibre reinforced composites of triglycidyl-p-aminophenol. *British polymer journal,* 22**,** 143-146.

THOMAS, N. & WINDLE, A. 1980. A deformation model for case II diffusion. *Polymer,* 21**,** 613-619.

TRIPATHI, G. & SRIVASTAVA, D. 2007. Effect of carboxyl-terminated poly (butadiene-co-acrylonitrile)(CTBN) concentration on thermal and mechanical properties of binary blends of diglycidyl ether of bisphenol-A (DGEBA) epoxy resin. *Materials Science and Engineering: A,* 443**,** 262-269.

TSAI, H. C., AROCHO, A. M. & GAUSE, L. W. 1990. Prediction of fiber-matrix interphase properties and their influence on interface stress, displacement and fracture toughness of composite material. *Materials Science and Engineering: A,* 126**,** 295-304.

TSAI, M. & MORTON, J. 1994. An evaluation of analytical and numerical solutions to the single-lap joint. *International Journal of Solids and Structures,* 31**,** 2537-2563.

TURI, E. 2012. *Thermal characterization of polymeric materials*, Elsevier.

VAKIL, U. & MARTIN, G. 1992. Crosslinked epoxies: network structure characterization and physical-mechanical properties. *Journal of applied polymer science,* 46**,** 2089-2099.

VENABLES, J. 1984. Adhesion and durability of metal-polymer bonds. *Journal of Materials Science,* 19**,** 2431-2453.

VERCHERE, D., PASCAULT, J., SAUTEREAU, H., MOSCHIAR, S., RICCARDI, C. & WILLIAMS, R. 1991a. Rubber-modified epoxies. II. Influence of the cure schedule and rubber concentration on the generated morphology. *Journal of applied polymer science,* 42**,** 701-716.

VERCHERE, D., PASCAULT, J., SAUTEREAU, H., MOSCHIAR, S., RICCARDI, C. & WILLIAMS, R. 1991b. Rubber-Modified epoxies. IV. Influence of morphology on mechanical properties. *Journal of applied polymer science,* 43**,** 293-304.

VERCHERE, D., SAUTEREAU, H., PASCAULT, J., MOSCHIAR, S., RICCARDI, C. & WILLIAMS, R. 1990a. Rubber-modified epoxies. I. Influence of carboxy-terminated butadiene-acrylonitrile random copolymers (CTBN) on the polymerization and phase separation processes. *Journal of Applied Polymer Science,* 41**,** 467-485.

VERCHERE, D., SAUTEREAU, H., PASCAULT, J., MOSCHIAR, S., RICCARDI, C. & WILLIAMS, R. 1990b. Rubber-modified epoxies. I. Influence of carboxyl-terminated butadiene-acrylonitrile random copolymers (CTBN) on the polymerization and phase separation processes. *Journal of Applied Polymer Science,* 41**,** 467-485.

VERTUCCIO, L., RUSSO, S., RAIMONDO, M., LAFDI, K. & GUADAGNO, L. 2015. Influence of carbon nanofillers on the curing kinetics of epoxy-amine resin. *RSC Advances,* 5**,** 90437-90450.

VIETRI, U., GUADAGNO, L., RAIMONDO, M., VERTUCCIO, L. & LAFDI, K. 2014. Nanofilled epoxy adhesive for structural aeronautic materials. *Composites Part B: Engineering,* 61**,** 73-83.

VYAZOVKIN, S. 1997. Evaluation of activation energy of thermally stimulated solidق│ ‖state reactions under arbitrary variation of temperature. *Journal of computational chemistry,* 18**,** 393-402.

VYAZOVKIN, S. 2001. Modification of the integral isoconversional method to account for variation in the activation energy. *Journal of Computational Chemistry,* 22**,** 178-183.

VYAZOVKIN, S. & SBIRRAZZUOLI, N. 1996. Mechanism and kinetics of epoxy-amine cure studied by differential scanning calorimetry. *Macromolecules,* 29**,** 1867-1873.

VYAZOVKIN, S. & SBIRRAZZUOLI, N. 1999a. Isoconversional method to explore the mechanism and kinetics of multi-step epoxy cures. *Macromolecular rapid communications,* 20**,** 387-389.

VYAZOVKIN, S. & SBIRRAZZUOLI, N. 1999b. Kinetic methods to study isothermal and nonisothermal epoxy-anhydride cure. *Macromolecular Chemistry and Physics,* 200**,** 2294-2303.

WAKE, W. C. 1987. *Synthetic adhesives and sealants,* John Wiley & Son Ltd.

WANG, S., LIANG, Z., GONNET, P., LIAO, Y. H., WANG, B. & ZHANG, C. 2007. Effect of nanotube functionalization on the coefficient of thermal expansion of nanocomposites. *Advanced functional materials,* 17**,** 87-92.

WANG, T., LEI, C.-H., DALTON, A. B., CRETON, C., LIN, Y., FERNANDO, K. S., SUN, Y.-P., MANEA, M., ASUA, J. M. & KEDDIE, J. L. 2006. Waterborne, nanocomposite pressure-sensitive adhesives with high tack energy, optical transparency, and electrical conductivity. *Advanced Materials,* 18**,** 2730-2734.

WHATLEY, W. & WAWNER, F. 1985. Kinetics of the reaction between SiC (SCS-6) filaments and Ti (6 Al-4 V) matrix. *Journal of materials science letters,* 4**,** 173-175.

WILLIAMS, R., BORRAJO, J., ADABBO, H. & ROJAS, A. 1983. A model for phase separation during a thermoset polymerization. *Rubber-Modified Thermoset Resins***,** 195-213.

WISANRAKKIT, G. & GILLHAM, J. 1990. The glass transition temperature (Tg) as an index of chemical conversion for a high-Tg amine/epoxy system: chemical and diffusion-controlled reaction kinetics. *Journal of Applied Polymer Science,* 41**,** 2885-2929.

WISE, C., COOK, W. & GOODWIN, A. 2000. CTBN rubber phase precipitation in model epoxy resins. *Polymer,* 41**,** 4625-4633.

WOERDEMAN, D. L., EMERSON, J. A. & GIUNTA, R. K. 2002. JKR contact mechanics for evaluating surface contamination on inorganic

substrates. *International journal of adhesion and adhesives,* 22**,** 257-264.

WON, Y.-G., GALY, J., GÎLRARD, J.-F. O., PASCAULT, J.-P., BELLENGER, V. R. & VERDU, J. 1990. Internal antiplasticization in copolymer and terpolymer networks based on diepoxides, diamines and monoamines. *Polymer,* 31**,** 1787-1792.

WU, J. & CHUNG, D. 2004. Calorimetric study of the effect of carbon fillers on the curing of epoxy. *Carbon,* 42**,** 3039-3042.

XIE, H., LIU, B., SUN, Q., YUAN, Z., SHEN, J. & CHENG, R. 2005. Cure kinetic study of carbon nanofibers/epoxy composites by isothermal DSC. *Journal of applied polymer science,* 96**,** 329-335.

XIE, H., LIU, B., YUAN, Z., SHEN, J. & CHENG, R. 2004. Cure kinetics of carbon nanotube/tetrafunctional epoxy nanocomposites by isothermal differential scanning calorimetry. *Journal of Polymer Science Part B: Polymer Physics,* 42**,** 3701-3712.

XU, L. R., LI, L., LUKEHART, C. M. & KUAI, H. 2007. Mechanical characterization of nanofiber-reinforced composite adhesives. *Journal of nanoscience and nanotechnology,* 7**,** 2546-2548.

YAKOBSON, B. I. & AVOURIS, P. 2001. Mechanical properties of carbon nanotubes. *Carbon nanotubes.* Springer.

YAN, N., BUONOCORE, G., LAVORGNA, M., KACIULIS, S., BALIJEPALLI, S. K., ZHAN, Y., XIA, H. & AMBROSIO, L. 2014. The role of reduced graphene oxide on chemical, mechanical and barrier properties of natural rubber composites. *Composites Science and Technology,* 102**,** 74-81.

YASMIN, A. & DANIEL, I. M. 2004. Mechanical and thermal properties of graphite platelet/epoxy composites. *Polymer,* 45**,** 8211-8219.

YU, H.-Y., QIN, Z.-Y., SUN, B., YANG, X.-G. & YAO, J.-M. 2014. Reinforcement of transparent poly (3-hydroxybutyrate-co-3-hydroxyvalerate) by incorporation of functionalized carbon nanotubes as a novel bionanocomposite for food packaging. *Composites Science and Technology,* 94**,** 96-104.

YU, S., TONG, M. N. & CRITCHLOW, G. 2009. Wedge test of carbon-nanotube-reinforced epoxy adhesive joints. *Journal of Applied Polymer Science,* 111**,** 2957-2962.

ZHAI, L., LING, G., LI, J. & WANG, Y. 2006. The effect of nanoparticles on the adhesion of epoxy adhesive. *Materials Letters,* 60**,** 3031-3033.

ZHAI, L., LING, G. & WANG, Y. 2008. Effect of nano-Al 2 O 3 on adhesion strength of epoxy adhesive and steel. *International Journal of Adhesion and Adhesives,* 28**,** 23-28.

ZHANG, J., LUO, R. & YANG, C. 2012. A multi-wall carbon nanotube-reinforced high-temperature resistant adhesive for bonding carbon/carbon composites. *Carbon,* 50**,** 4922-4925.

ZHOU, T., WANG, X., LIU, X. & XIONG, D. 2009. Influence of multi-walled carbon nanotubes on the cure behavior of epoxy-imidazole system. *Carbon,* 47**,** 1112-1118.

ZHOU, Y., WU, P., CHENG, Z., INGRAM, J. & JEELANI, S. 2008. Improvement in electrical, thermal and mechanical properties of epoxy by filling carbon nanotube. *Express polymer letters,* 2**,** 40-48.

ZVETKOV, V. 2001. Comparative DSC kinetics of the reaction of DGEBA with aromatic diamines.: I. Non-isothermal kinetic study of the reaction of DGEBA with m-phenylene diamine. *Polymer,* 42**,** 6687-6697.